AD_____

Award Number: W81XWH-07-1-0FÎ€

TITLE: ŒÞ/Øl ÊÃŒÁÞ[ç^|ÁT^åãæ{¦Á¬Áó@¬ÁŒ;æà|&ÁŒ&ą}•Á¬ÁÚVPÁ{}ÁÓ[}^

PRINCIPAL INVESTIGATOR: Ö¦ÉÁŐˇ[: @ÁÝãæ{

CONTRACTING ORGANIZATION: W}ãç^¦•ãĉÁ¬ÁÚãœà¨¦*@
                           ÁÚãœà¨¦*@ÊÁÚŒÁFÍGÎ€Á

REPORT DATE: Julˆ ÁG€FF

TYPE OF REPORT: Øã}æ|

PREPARED FOR: U.S. Army Medical Research and Materiel Command
               Fort Detrick, Maryland 21702-5012

DISTRIBUTION STATEMENT: Approved for public release; distribution unlimited

The views, opinions and/or findings contained in this report are those of the author(s) and should not be construed as an official Department of the Army position, policy or decision unless so designated by other documentation.

REPORT DOCUMENTATION PAGE

Form Approved
OMB No. 0704-0188

Public reporting burden for this collection of information is estimated to average 1 hour per response, including the time for reviewing instructions, searching existing data sources, gathering and maintaining the data needed, and completing and reviewing this collection of information. Send comments regarding this burden estimate or any other aspect of this collection of information, including suggestions for reducing this burden to Department of Defense, Washington Headquarters Services, Directorate for Information Operations and Reports (0704-0188), 1215 Jefferson Davis Highway, Suite 1204, Arlington, VA 22202-4302. Respondents should be aware that notwithstanding any other provision of law, no person shall be subject to any penalty for failing to comply with a collection of information if it does not display a currently valid OMB control number. **PLEASE DO NOT RETURN YOUR FORM TO THE ABOVE ADDRESS.**

1. REPORT DATE (DD-MM-YYYY)	2. REPORT TYPE	3. DATES COVERED (From - To)
01-07-2011	Final	1 JUL 2007 - 30 JUN 2011

4. TITLE AND SUBTITLE

ATF4, A Novel Mediator of the Anabolic Actions of PTH on Bone

5a. CONTRACT NUMBER

5b. GRANT NUMBER
W81XWH-07-1-0160

5c. PROGRAM ELEMENT NUMBER

6. AUTHOR(S)

Dr. Guozhi Xiao

E-Mail: xiaog@upmc.edu

5d. PROJECT NUMBER

5e. TASK NUMBER

5f. WORK UNIT NUMBER

7. PERFORMING ORGANIZATION NAME(S) AND ADDRESS(ES)

University of Pittsburgh
Pittsburgh, PA 15260

8. PERFORMING ORGANIZATION REPORT NUMBER

9. SPONSORING / MONITORING AGENCY NAME(S) AND ADDRESS(ES)
U.S. Army Medical Research and Materiel Command
Fort Detrick, Maryland 21702-5012

10. SPONSOR/MONITOR'S ACRONYM(S)

11. SPONSOR/MONITOR'S REPORT NUMBER(S)

12. DISTRIBUTION / AVAILABILITY STATEMENT
Approved for Public Release; Distribution Unlimited

13. SUPPLEMENTARY NOTES

14. ABSTRACT

In this study, we have successfully demonstrated that ATF4 plays a critical role in mediating the anabolic effects of intermittent PTH on bones. ATF4 is important for intermittent PTH to stimulate bone formation in mice. ATF4 favors bone formation through, at least in part, upregulation of osteoblasst proliferation and survival. Additionally, ATF4 increases osteoblast differentiation probably via osterix. At molecular level, ATF4 increases osteocalcin gene expression by cooperative interactions with TFIIAγ and Runx2. ATF4 increases the expression of cyclin D1, a key factor for cell cycle progression. We have identified and functionally characterized Erk/MAPK phosphorylation sites in Runx2, an ATF4-interacting factor. We have demonstrated that ATF4 is essential for osteoclast differentiation and bone resorption, which is increased by intermittent PTH.

15. SUBJECT TERMS
ATF4, Runx2, PTH, anabolism, proliferation, apoptosis

16. SECURITY CLASSIFICATION OF:

a. REPORT	b. ABSTRACT	c. THIS PAGE	17. LIMITATION OF ABSTRACT	18. NUMBER OF PAGES	19a. NAME OF RESPONSIBLE PERSON USAMRMC
U	U	U	UU	105	19b. TELEPHONE NUMBER (include area code)

Standard Form 298 (Rev. 8-98)
Prescribed by ANSI Std. Z39.18

Table of Contents

This progress report covers research from the period 07/01/07-06/30/11

Introduction

Osteoporosis, or reduced bone mass, is a metabolic bone disease that affects millions of people including many of our service women and men now in the Armed Forces and VA patients in the United States. It causes a significant amount of morbidity and mortality in patients and is often diagnosed after a fracture occurs. Reducing the risk of osteoporotic and associated fractures of these patients will greatly improve their life quality and survival. Parathyroid hormone (PTH) is the most potent anabolic treatment of osteoporosis currently available. It not only dramatically improves bone mass, but also restores bone microarchitecture and increases bone diameter. All of these mechanisms contribute to increasing bone strength and reducing the risk for fractures. However, the molecular mechanisms whereby PTH increases bone mass are not well understood and are the focus of the experiments of this proposal. This study was designed to (1) determine the mechanism whereby PTH regulates ATF4 transcriptional activity (2) establish whether the anabolic actions of PTH require ATF4 *in vivo*. Studies determine if ATF4 is required for the anabolic actions of PTH *in vivo* using ATF4-deficient mice. PTH anabolic activity is evaluated in wild type and *Atf4$^{-/-}$* mice. PTH effects are measured using standard biochemical and histomorphometric criteria.

Body

Task 1: To determine the mechanism by which PTH regulates ATF4 transcriptional activity (1-36 months).

1) Establish that ATF4 is a novel downstream target of PTH actions in cultured osteoblasts (P1).

In order to determine the role of ATF4 in PTH actions in osteoblasts, we examined effects of PTH on ATF4 expression and activity as well as the requirement for ATF4 in the regulation of *Ocn* by PTH (see P1). PTH elevated levels of ATF4 mRNA and protein in a dose and time-dependent manner (P1-Fig. 1A-C). This PTH regulation requires transcriptional activity, but not *de novo* protein synthesis (P1-Fig. 2A and B). PTH also increased binding of nuclear extracts to OSE1 DNA (P1-Fig. 4A-C). PTH stimulated ATF4-dependent transcriptional activity mainly through PKA with a lesser requirement for PKC and MAPK/ERK pathways (P1-Fig. 5A-C). PTH stimulation of *Ocn* expression was lost by siRNA downregulation of ATF4 in MC-4 cells (P1-Fig. 6A and C) and in *Atf4$^{-/-}$* bone marrow stromal cells (BMSCs) (P1-Fig. 7C). Collectively, these studies for the first time demonstrate that PTH increases ATF4 expression and activity and that ATF4 is required for PTH induction of *Ocn* expression in osteoblasts. Thus, ATF4 is a novel downstream target of PTH actions in osteoblasts.

2) Define a novel molecular mechanism through which ATF4 activates osteocalcin gene expression in osteoblasts (P2).

We defined a novel molecular mechanism mediating ATF4-Runx2 interactions (see P2). We identified general transcription factor IIAγ (TFIIAγ) as a Runx2-interacting factor in a yeast two-hybrid screen. Immunoprecipitation assays confirmed that TFIIAγ interacted with Runx2 in osteoblasts and when coexpressed in COS-7 cell or using purified GST-fusion proteins (P2-Fig. 1A-C). Chromatin immunoprecipitation (ChIP) assay of MC3T3-E1 (clone MC-4) preosteoblast cells showed that in intact cells TFIIAγ was recruited to the region of the *osteocalcin* promoter previously shown to bind Runx2 and ATF4 (P2-Fig. 2). A small region of Runx2 (aa 258-286) was found to be required for TFIIAγ binding (P2-Fig. 1D). While TFIIAγ interacted with Runx2, it did not activate Runx2 (P2-Fig. 3A and B). Instead, TFIIAγ bound to and activates ATF4 (P2-Fig. 3C-H). Further, TFIIAγ together with ATF4 and Runx2 stimulated *osteocalcin* promoter activity (P2-Fig. 5B) and endogenous mRNA expression (P2-Fig. 5A). siRNA silencing of TFIIAγ markedly reduced levels of endogenous ATF4 protein and *Ocn* mRNA in osteoblastic cells (P2-Fig. 6). Overexpression of TFIIAγ increased levels of ATF4 protein (P2-Fig. 7). TFIIAγ significantly prevented ATF4 degradation (P2-Fig. 8). Thus, TFIIAγ functions as a bridging protein linking ATF4 and Runx2. Interestingly, our preliminary studies (not shown) show that PTH increases ATF4-Runx2 interaction as measured co-immunoprecipitation assays.

1) Establish a role for ATF4 in regulating osteoblast proliferation and survival in vitro and in bones (P3 and P5).

In order to determine the mechanism where ATF4 regulates osteoblast activity, we examined the effects of ATF4 on osteoblast proliferation and survival (see P3 and P5). As shown in P3-Fig. 1B, the number of osteoblast precursor colonies (i.e., CFU-OBs) was significantly decreased in *Atf4$^{-/-}$* mice compared to wt mice. This decrease could be explained by a cell-autonomous defect in proliferation and/or survival or could be secondary to an impaired bone microenvironment due to ATF4 deficiency. To differentiate these possibilities, we conducted MTS and [^{3}H] thymidine incorporation assays. Results from MTS assay showed that ATF4-deficient cells grew at significantly reduced rates compared to wt cells (P3-Fig. 1C). This result was further confirmed by the [^{3}H] thymidine incorporation assays showing that [^{3}H] thymidine incorporation into the DNA of *Atf4$^{-/-}$* bone marrow stromal cells (BMSCs) was decreased by 4-fold compared to values in wt cells (P3-Fig. 1D). We next determined if ATF4 is required for osteoblast proliferation *in vivo* using 6-wk-old wt and *Atf4$^{-/-}$* mice that were injected with bromodeoxyuridine (BrdU)/fluorodeoxyuridine (FdU) 4 h before sacrifice. 10-µm sections of calvariae were obtained, and proliferating cells from the periosteal surface were counted and normalized to total cells from the same area. In wt calvariae, periosteal osteoblasts proliferated very actively with 60% of the total cells being BrdU-positive (P3-Fig. 2A). In contrast, the percent BrdU-positive osteoblasts were significantly reduced in *Atf4$^{-/-}$* calvariae (P3-Fig. 2 B and C). Thus, ATF4 is required for the proliferation of BMSCs or osteoblasts both *in vitro* and *in vivo*. As shown in P3-Fig. 3, ATF4-deficient cells showed a significant decrease in the cell distribution into both S and G2/M phases (32% and 45% change, respectively) when compared with values of wt control cells. In contrast, the fraction of the cells in G1 was not reduced by ATF4 deficiency. The protein level of cyclin D1 was markedly decreased in *Atf4$^{-/-}$* cells relative to wt control (P3-Fig. 4A). Quantitative real-time RT/PCR analysis shows that the level of *cyclin D1* mRNA was reduced by 52% in *Atf4$^{-/-}$* cells compared to values in wt controls (P3-Fig. 4B). ATF4 is also required for the proliferation of the pre-osteoblast cell line (MC-4 cells) as demonstrated by siRNA experiments (P3-Fig. 5). Furthermore, overexpression of ATF4 significantly increased the level of cyclin D1 protein as well as cell proliferation (P3-Fig. 6 and 7). Taken together, these results clearly establish that ATF4 increases cell proliferation probably via promoting the expression of cyclin D1 and cell cycle progression.

We also found that ATF4 is critical for osteoblast survival. The numbers of apoptotic cells including those with shrinking cytoplasm and chromatin condensation (early apoptosis) and DNA fragmentation (late apoptosis) were increased greater than 5-fold in *Atf4$^{-/-}$* BMSCs compared to wt cells (P3-8A-C). To confirm this finding, wt and *Atf4$^{-/-}$* BMSCs were stained using the ApopTag Peroxidase *In Situ* Apoptosis Detection Kit, a modified TUNEL staining that measures DNA fragmentation *in situ*. As shown in P3-Fig. 8D-F, the percent apoptotic cells in *Atf4$^{-/-}$* BMSCs were increased by 1.6-fold when compared to wt cells. To determine if ATF4 deficiency increases osteoblast apoptosis *in vivo*, 10-µm calvarial sections from wt and *Atf4$^{-/-}$* mice were obtained and stained using the same kit. Apoptotic cells that stained brown on the periosteal surface of calvariae were counted and normalized to total cells of the same periosteal surface. As shown in P3-Fig. 8G-I, a significant increase in apoptosis was found in *Atf4$^{-/-}$* mice compared to wt controls. Thus, ATF4 protects osteoblasts from apoptosis under physiological condition.

To define the mechanism whereby ATF4 regulates osteoblast function and bone formation, we further determined whether ATF4 plays a role in PTH regulation of osteoblast proliferation in the presence and absence of PTH in vivo. Sections of tibiae and calvariae from wt and *Atf4$^{-/-}$* mice treated with and without intermittent PTH were analyzed for in vivo cell proliferation using a Zymed BrdU immunostaining kit. As shown in Fig 4A, B, and E (P5), in wt mice, PTH increased the percentage of proliferating osteoblasts/preosteoblasts of tibial trabeculae by 2.8-fold relative to vehicle-treated control. Ablation of the *Atf4* gene resulted in a 50% decline in basal proliferation. In addition, the PTH-stimulated increase in proliferation was decreased by 40 percent (Fig 4C-E, P5). Similarly, PTH-induced proliferation in calvarial periosteal osteoblasts was also significantly reduced by ATF4 deficiency (Fig 4F-J, P5). Therefore, ATF4 is critical for both basal and PTH-stimulated proliferation of osteoblasts/preosteoblasts in vivo.

Mature osteoblasts synthesize and deposit a mineralizing extracellular matrix and become osteocytes. Both osteoblasts and osteocytes can be lost through apoptosis. PTH signaling increases the survival of osteoblasts and osteocytes by reducing apoptosis. ATF4 is anti-apoptotic in osteoblasts as described above. To determine whether ATF4 plays a role in PTH-mediated anti-apoptosis, sections of tibiae were stained with TUNEL and apoptotic cells were assessed. As shown in Fig 4K and L (P5), ATF4 deficiency significantly increased the basal levels of apoptosis. As expected, PTH dramatically reduced apoptotic death of tibial trabecular osteoblasts/osteocytes by 48 percent. Importantly, the PTH-stimulated decrease in apoptotic death was completely abolished in *Atf4$^{-/-}$* trabeculae (Fig 4M-

O, P5). ATF4 was similarly required for PTH to inhibit apoptosis in cortical osteocytes of tibiae (Fig 4P, P5). Collectively, ATF4 is essential for PTH-mediated inhibition of apoptosis in osteoblasts/osteocytes in vivo.

4) ATF4 is essential for PTH to increase osteoblast differentiation in vivo (P5).

We determined the effects of ATF4 deficiency on PTH induction of osteoblast differentiation markers in vivo. Total RNA was isolated from tibiae of *wt* and *Atf4*$^{-/-}$ mice treated with and without PTH for 28 d and expression levels of osteoblast differentiation marker genes were measured by quantitative real-time PCR analysis. As shown in Fig 5A (P5), PTH dramatically increased the expression of genes known to be associated with osteoblast differentiation including *osteocalcin* (*Ocn*), *bone sialoprotein* (*Bsp*), *alkaline phosphatase* (*Alp*), *α1(I) collagen* (*Col1(I)*), *osteopontin* (*Opn*), and *osterix* (*Osx*). Importantly, this PTH regulation was either dramatically reduced or completely abolished in *Atf4*$^{-/-}$ tibiae. In contrast, c-Fos and c-Jun, both early PTH-induced genes, were not induced by PTH in either wt or *Atf4*$^{-/-}$ tibiae.

5) ATF4 is a novel upstream transcriptional activator of osterix (Osx), a key factor for osteoblast differentiation and bone formation (P5).

To address the molecular mechanism whereby PTH promotes osteoblast differentiation, we measured the expression of Osterix (Osx) and Runx2 proteins, two critical transcription factors that regulate osteoblast differentiation. We used immunohistochemistry (IHC) to measure Osx in the tibiae and calvariae of wt and *Atf4*$^{-/-}$ mice with or without 28 d anabolic PTH treatment. As shown in Fig 6 (P5), in wt-vehicle-treated tibiae, Osx-positive osteoblasts were only identified in the trabeculae and cortical endosteum close to the growth plate (Fig 6A1, B1, and D1, P5) and were almost undetectable in the same regions close to the marrow (Fig 6C1, P5), indicating that cells in these areas are still in the immature (preosteoblast) state. In contrast, in the wt-PTH group, Osx-positive osteoblasts were identified on all surfaces of trabeculae and endosteum throughout the tibia. PTH increased the total number of Osx-positive cells per tibial section by 3.2-fold in wt mice (Panel 2). ATF4 deficiency reduced the numbers of Osx-positive cells by 50 percent (Panel 3). Strikingly, PTH failed to elevate the numbers of Osx-positive cells in *Atf4*$^{-/-}$ tibiae. Similar results were obtained in calvariae (Fig 6E, P6). The IHC staining was highly specific since no signal was detected in the IgG control group (Panel 5), in which Osx antibody was omitted.

To define the mechanism whereby ATF4 regulates Osx, we examined the effect of ATF4 overexpression on the expression of Osx, a key transcription factor for osteoblast differentiation, in MC-4 preosteoblast cells. As shown in Fig 7A (P5), ATF4 dose-dependently increased levels of Osx protein (top) and mRNA (bottom). We next examined whether ATF4 up-regulates Osx by increasing gene transcription by using a -1003/+68 mouse Osx promoter (Fig 7B, P5). Using COS-7 cells, which lack detectable Runx2, ATF4 had comparable activity to Runx2 in terms of its ability to activate promoter activity (approx. 1.8-fold). Together, ATF4 and Runx2 maximally activated the *Osx* promoter (3.2-fold induction). To further define the region of the Osx promoter necessary for ATF4 responsiveness, several constructs containing various deletion mutants of the mouse *Osx* promoter were transiently transfected into COS-7 cells with and without an ATF4 expression plasmid. Results showed that luciferase activity of both control and ATF4-transfected groups decreased with progressively larger 5' deletions. However, ATF4 stimulation was abrogated when a 132-bp region between bp -215 to -83 was deleted (Fig 7C, P5). A putative ATF4-binding sequence (CTTCCTCA) at -201/-194 bp was identified in this region by using a TRANSFAC retrieval program. Introduction of a 3-bp substitution mutation to this core sequence (from CTTCCTCA to CTTgtaCA) completely abolished ATF4 activation (Fig 7D, P5). As shown in Fig 7E (P5), a DNA oligo probe from the Osx promoter that contains the TTACATCA core sequence bound to a factor(s) in nuclear extracts from COS-7 cells transfected with an ATF4 expression vector. Importantly, this binding (see arrow) was dramatically reduced by the addition of a specific antibody against ATF4 but not by normal control IgG or antibodies against cFos (an AP1 family member) or ATF2.

6) Identification and characterization of Erk/MAPK phosphorylation sites in Runx2 (P4).

We used a combination of in vitro and in vivo phosphorylation analysis, mass spectroscopy and functional assays to identify two sites at S301 and S319 within the proline/serine/threonine domain of Runx2 that are required for MAPK regulation. These sites are phosphorylated by activated Erk1 in vitro and in cell culture. In addition to confirming Erk-dependent phosphorylation at S319, mass spectroscopy identified two other Erk-phosphorylated sites

at S43 and S510. Furthermore, introduction of S301,319A mutations rendered Runx2 resistant to MAPK-dependent activation and reduced its ability to stimulate osteoblast-specific gene expression and differentiation after transfection into Runx2-null calvarial cells and mesenchymal cells. In contrast, S301,319E Runx2 mutants had enhanced transcriptional activity that was minimally dependent on MAPK signaling, consistent with the addition of a negative charge mimicking serine phosphorylation. These results emphasize the important role played by Runx2 phosphorylation in the control of osteoblast gene expression and provide a mechanism to explain how physiological signals acting on bone through the ERK/MAPK pathway can stimulate osteoblast-specific gene expression. Similar approaches are being used to identify and characterize potential PTH-responsive phosphorylation sites in ATF4 molecule.

Task 2: To establish whether the anabolic actions of PTH require ATF4 (6-48 months).

1) The anabolic effects of PTH on bone are severely impaired in growing Atf4-deficient mice (P5).

We first evaluated our hypothesis that ATF4 mediates the anabolic actions of PTH in bone using a relatively simple "growing mouse" model system, that has been widely used for studying the anabolic actions of PTH, PTHrP, FGF2, and IGF-1 in bone (1-6). The advantages of this system are that it is less time consuming and costly versus adult ovarectomized mouse models. Furthermore, because young growing animals have relatively high osteoblast activity, they are more sensitive to PTH than adults (6-14). Mice were treated with vehicle or PTH and sacrificed 24 h after the last PTH injection. PTH-dependent anabolic activity was evaluated in these mice using standard biochemical and histomorphometric criteria. $Atf4^{-/-}$ mice grew more slowly than wild type (wt) animals. The growth rate was slightly but significantly increased by PTH treatment during d 6-18 in wt but not $Atf4^{-/-}$ animals (Fig S1A, P5). $Atf4^{-/-}$ femurs were also shorter than *wt* or $Atf4^{+/-}$ femurs. PTH did not alter the length of femurs (Fig S1B, P5). However, it did significantly increase the dry ash weight per femur in wt and $Atf4^{+/-}$ but not in $Atf4^{-/-}$ mice (Fig S1C, P5). Serum Pi and calcium concentration (Fig S1D and E, P5) were not markedly affected by PTH or ATF4 deficiency. Faxitron X-ray analysis of femurs revealed that *wt* and $Atf4^{+/-}$ mice responded to PTH with markedly increased radiopacity throughout the whole femur, with the most dramatic increase in the metaphyseal region (Fig S2, top and middle, P5). In contrast, PTH only slightly increased the radiopacity in the same region of $Atf4^{-/-}$ femurs (Fig S2, bottom, P5). As shown in Fig 1 (P5), quantitative μCT analysis of femur histomorphometric parameters showed that $Atf4^{-/-}$ mice had a significant reduction in bone volume/tissue volume (BV/TV), trabecular number (Tb.N), and cortical thickness (Cort.Th) and a marked increase in trabecular space (Tb.Sp) compared with the *wt* or $Atf4^{+/-}$ littermates. These data confirmed an essential role of ATF4 in bone that was previously demonstrated by the Karsenty group. As expected, in *wt* femurs, intermittent PTH increased BV/TV, Tb.N, and Tb.Th by 5.4-fold, 2.7-fold, and 1.5-fold, respectively, and decreased Tb.Sp by 60 percent. Similar effects were also seen in $Atf4^{+/-}$ mice (Fig 1B, P5). In contrast, the PTH response was greatly attenuated in $Atf4^{-/-}$ mice where the following PTH responses were observed; BV/TV, 2.2-fold increase; Tb.N, 1.7-fold increase; Tb.Th, 1.1-fold increase; Tb.Sp, 36 percent decrease. In all cases, the magnitude of PTH-stimulated changes on BV/TV, Tb.N, Tb.Sp was dramatically reduced in $Atf4^{-/-}$ mice relative to *wt* or $Atf4^{+/-}$ mice (P<0.05, PTH/veh-wt vs. PTH/veh-$Atf4^{-/-}$). Furthermore, PTH-stimulated increases in Cort.Th and Tb.Th were completely lost in $Atf4^{-/-}$ femurs. Because PTH similarly affected all trabecular and cortical parameters in $Atf4^{+/+}$ and $Atf4^{+/-}$ mice, subsequent experiments compared the PTH effects on bone only between *wt* and $Atf4^{-/-}$ mice.

We next measured effects of *Atf4* gene ablation on PTH stimulation of tibiae, vertebrae, and calvariae. The anabolic effect of PTH on wt tibiae was so dramatic that the majority of the bone marrow cavity was replaced by newly formed bone (Fig 2A and B, P5). In $Atf4^{-/-}$ tibiae, while PTH still induced a small increase in trabecular area, the magnitude of stimulation was significantly reduced (5-fold in wt vs. 2.2-fold in $Atf4^{-/-}$)(P<0.05, PTH/veh-wt vs. PTH/veh-$Atf4^{-/-}$)(Fig 2C-E, P5). Likewise, the PTH-stimulated increase in the trabeculae of vertebrae (L5) was markedly reduced in $Atf4^{-/-}$ mice (3-fold in wt vs. 2-fold in $Atf4^{-/-}$) (P<0.05, PTH/veh-wt vs. PTH/veh-$Atf4^{-/-}$)(Fig 2F-J). When histological sections of calvariae were compared, PTH increased the width of the calvariae by 1.8-fold in *wt* mice, a response that was abolished in $Atf4^{-/-}$ animals (Fig 2K-O, P5).

2) Ablation of the Atf4 gene impairs PTH stimulation of trabecular, but not cortical bone in 7-month-old ovariectomized (OVX) mice (P5).

The experiments described above established a critical role of ATF4 in the anabolic effects of PTH on long bones, vertebrae, and calvariae in rapidly growing mice. However, it is possible that results obtained from growing animals may be different from those in adults due to possible effects of PTH and/or ATF4 on animal growth or influences of animal growth on the anabolic response to PTH, either of which could complicate the interpretation of the results. In contrast, adult mice have a mature skeleton in which these possible complications can be avoided. Furthermore, the OVX mouse provides a model that may be more relevant to the clinical applications of PTH in the treatment of osteoporosis. For these reasons, we evaluated whether ATF4 is required for the anabolic response to PTH in 7-month-old OVX mice. OVX surgery was successful as demonstrated by significant reduction in BV/TV (65 percent), Tb.N (27 percent), and Tb.Th (18 percent) and increased Tb.Sp (37 percent) relative to sham surgery (P<0.05, wt-sham vs. wt-OVX) . OVX surgery did not reduce Cort.Th, which is consistent with results from rats, As shown in Fig 3 A-C (P5), similar to results from growing mice, ablation of the *Atf4* gene significantly decreased BV/TV and Tb.N and increased Tb.Sp in adult OVX mice. In further agreement with results in young mice, *Atf4*^{-/-} animals exhibited a clearly attenuated response to PTH. For example, while PTH increased BV/TV by 7.8-fold in wt mice, this value was only increased 4.2-fold in *Atf4*^{-/-} animals. Similarly, while PTH still stimulated formation of trabecular bone in *Atf4*^{-/-} trabeculae, the magnitude of this response was significantly reduced compared to wt control (P<0.05, PTH/veh-wt vs. PTH/veh-*Atf4*^{-/-}). In contrast to result from growing mice, Cort.Th was not reduced by ablation of the *Atf4* gene in adult OVX mice (0.21±0.01 mm in wt vs. 0.19±0.02 mm in *Atf4*^{-/-}, P>0.05 wt vs. *Atf4*^{-/-}). Also, PTH was much less effective in stimulating Cort.Th in adult OVX mice (24%) than in growing mice (95%) (Figs 1 and 3, P5). Furthermore, no difference in stimulation of cortical thickness by PTH was observed when wt and *Atf4*^{-/-} groups were compared (24% wt vs. 21% *Atf4*^{-/-})(P>0.05, PTH/veh-wt vs. PTH/veh-*Atf4*^{-/-}).

3) ATF4 is critical for PTH to increase bone formation in vivo (P5).

To determine if ATF4 is required for PTH to increase bone formation in vivo, we performed calcein double labeling experiments. As shown in Fig 3 A and B (P5), results from calcein double labeling of 7-month old OVX wt and *Atf4*^{-/-} tibia revealed that the PTH-stimulated increase in mineral apposition rate (MAR), an indicator of osteoblast function, was significantly reduced by ATF4 deficiency (P<0.05, PTH/veh-wt vs. PTH/veh-*Atf4*^{-/-}).

4) ATF4-deficient mice display a resistance to OVX-induced bone (P5).

Interestingly, as shown in Fig S3 (P5), OVX surgery significantly reduced bone mass in wt mice. This reduction was completely abolished in *Atf4*^{-/-} animals (P>0.05, *Atf4*^{-/-} -sham vs. *Atf4*^{-/-} -OVX). This result suggests that ATF4 may play an important role in OVX induction of bone loss. Current study in the project laboratory is to define the molecular mechanism underlying this important finding.

5) ATF4 is critical for OCL differentiation in vitro and in vivo (P6).

Our results revealed that TRAP activity (an OCL marker) was dramatically decreased in *Atf4*^{-/-} tibiae compared to wt tibiae (Figure 1C, P6). OCL surface/bone surface (Oc.S/BS) and OCL number/bone perimeter (Oc.Nb/BPm) were reduced similarly in both primary and secondary spongiosa in *Atf4*^{-/-} tibiae relative to wt tibiae (Figure 1D, P6). TRAP-positive MNCs (≥3 nuclei/cell) in BMM cultures from *Atf4*^{-/-} mice were dramatically reduced compared to that from wt mice (Figure 1E-F, P6). Furthermore, the number of nuclei per MNC was decreased by 75 percent in *Atf4*^{-/-} BMM cultures compared to wt cultures (Figure 1G, P6), and the MNCs that formed in *Atf4*^{-/-} BMM cultures were much smaller than those formed in wt cultures. Furthermore, the resorption pit area on dentin slices was dramatically reduced in *Atf4*^{-/-} BMM cultures compared to wt cultures (Figure 1H-I, P6). Co-culture experiments showed that wt osteoblasts failed to rescue the defective OCL formation of *Atf4*^{-/-} BMMs (Figure 2C-D, P6). Taken together, these experiments suggest that ATF4 deficiency impairs osteoclastogenesis in a cell autonomous manner. We developed transgenic mice in which the *Atf4* transgene is driven by an 1846-bp mouse Trap promoter that selectively expresses ATF4 in OCLs (Figure 3A, top, P6). Transgenic ATF4 dramatically increased the protein levels of NFATc1/A but not of PU.1 or c-Fms proteins in differentiated BMM cultures. The levels of OCL differentiation marker gene mRNAs (Trap, Rank, Cat K, and Mmp9) were all dramatically elevated in differentiated BMM cultures from *Trap-Atf4-tg* mice compared to those from wt mice. OCL-targeted overexpression of ATF4 dramatically increased the numbers of TRAP-positive MNCs in vitro (Figure 3D, P6). We found a similar effect of transgenic

ATF4 expression in vivo. The TRAP activity was markedly increased in *Trap-Atf4-tg* tibiae compared to wt tibiae (Figure 3E, P6). As shown in Figure 3F (P6), Oc.S/BS Oc.Nb/BPm in both primary and secondary spongiosa of tibiae were dramatically increased in *Trap-Atf4-tg* mice compared to wt controls. Quantitative μCT analysis of femur histomorphometric parameters showed that *Trap-Atf4-tg* mice had a significant reduction in bone volume/tissue volume (BV/TV) and trabecular number (Tb.N) and a marked increase in trabecular space (Tb.Sp) compared with the wt littermates (Figure 3G, P6). Because osteoclast activity was recently shown to be critical for the anabolic actions in bone, our finding that ATF4 regulates osteoclast differentiation and bone resorption has added a new layer to the molecular mechanisms underlying the PTH actions in osteoblasts and bone.

Key Research Accomplishments

- We have demonstrated that ATF4 is a novel downstream target of PTH signaling in osteoblasts (P1).
- We have demonstrated that TFIIAγ increases osteoblast-specific osteocalcin gene expression by facilitating ATF4-Runx2 interactions (P2).
- We have demonstrated that ATF4 increases the expression of cyclin D1, a key factor for cell cycle progression, and promotes osteoblast proliferation in vitro and in vivo (P3 and P5).
- We have demonstrated that ATF4 is critical for PTH to increase osteoblast differentiation in bone (P5).
- We have demonstrated that ATF4 is a novel upstream transcriptional activator of Osx, a key factor for osteoblast differentiation and bone formation (P5).
- We have demonstrated that ATF4 is important for intermittent PTH to stimulate osteoblast-mediated bone formation in vivo (P5).
- We have identified and functionally characterized Erk/MAPK phosphorylation sites in Runx2, an ATF4-interacting factor identified by the project laboratory (P4).
- We have demonstrated that ATF4 is required for the anabolic actions of PTH in bone in rapidly growing mice (P5).
- We have demonstrated that ATF4 is required for the anabolic actions of PTH in bone in adult OVX mice (P5).
- We have demonstrated that ATF4 is essential for OVX induction of bone loss in vivo (P5).
- We have demonstrated that ATF4 is essential for osteoclast differentiation and bone resorption, which is modulated by PTH (P6).

Reportable Outcomes

Peer-reviewed paper:
P1. Yu S, Franceschi RT, Luo M, Zhang X, Jiang D, Lai Y, Jiang Y, Zhang J, **Xiao G**. Parathyroid hormone increases activating transcription factor 4 expression and activity in osteoblasts: requirement for *osteocalcin* gene expression. ***Endocrinology*,** 2008; 149(4): 1960-8. PMCID: PMC2276723.
P2. Yu S, Jiang Y, Galson DL, Luo M, Lai Y, Lu Y, Ouyang HJ, Zhang J, **Xiao G**. General transcription factor IIA-gamma increases osteoblast-specific osteocalcin gene expression via activating transcription factor 4 and runt-related transcription factor 2. ***J Biol Chem***, 2008; 283(9): 5542-53. PMCID: PMC2736298.
P3. Zhang X, Yu S, Galson, DL, Luo M, Fan J, Zhang J, Guan Y, **Xiao G**. Activating transcription factor 4 is critical for proliferation and survival in primary bone marrow stromal cells and calvarial osteoblasts. ***J Cell Biochem***, 2008; 105(3): 885-95. PMCID: PMC2704124.
P4. Ge C, **Xiao G** (**co-first author**), Jiang D, Yang Q, Hatch NE, and Franceschi RT. Identification and functional characterization of extracellular-regulated kinase/MAPK phosphorylation sites in the Runx2 transcription factor. ***J Biol Chem***, 2009; 284(47):32533-43. PMCID: PMC2781667.
P5. Yu S, Franceschi RT, Luo M, Fan J, Jiang D, Cao H, Lai Y, Zhang J, Patrene K, Hankenson KD, Roodman GD, **Xiao G**. Critical role of activating transcription factor 4 in the anabolic actions of PTH in bone. ***PLoS One***. 2009, Oct 23;4(10):e7583. PMCID: PMC2762317. (This paper was listed as the No. 1 "**Not to be Missed**" paper in the November (2009) issue of the IBMS BoneKEy, BoneKEy is published by the International Bone & Mineral Society, link: http://www.bonekey-ibms.org/).

P6. Cao H, Yu S, Yao Z, Galson DL, Jiang Y, Zhang X, Fan J, Lu B, Guan Y, Luo M, Lai Y, Zhu, Y, Kurihara N, Patrene K, Roodman GD, **Xiao G**. Activating transcription factor 4 regulates osteoclast differentiation in mice. *J Clin Invest.* 2010 Aug 2;120(8):2755-66. PMCID: PMC2912190.

Abstracts:
A1. Yu S, Luo M, Franceschi RT, Jiang D, Zhang J, Patrene K, Hankenson KD, Roodman GD, Xiao G. ATF4 Is Required for the Anabolic Actions of PTH on Bone in vivo. ASBMR annual meeting-2007 (Oral Presentation)
A2. Yu S, Jiang Y, Luo M, Lu Y, Zhang J, Roodman GD, G. **Xiao G**. TFIIA, ATF4, and Runx2 Synergistically Activate Osteoblast-specific Osteocalcin Gene Expression. ASBMR annual meeting-2007 (poster)
A3. Zhang X, Yu S, Galson DL, Luo M, Fan J, Zhang J, Guan G, **Xiao G**. Role of ATF4 in osteoblast proliferation and survival, ASBMR annual meeting-2008 (poster).
A4. Yu S, Franceschi RT, Luo M, Fan J, Jiang D, Cao H, Lai Y, Zhang J, Patrene K, Hankenson K, Roodman GD, **Xiao G**. Activating transcription factor 4 mediates the anabolic actions of parathyroid hormone in bone ASBMR annual meeting-2009 (poster)
A5. Xiao G. Critical role of activating transcription factor 4 in parathyroid hormone-mediated bone formation. Military Health Research Forum (MHRF)-2009. (Oral Presentation)
A6. Cao H, Yu S, Yao Z, Galson DL, Jiang Y, Zhang X, Fan J, Lu B, Guan Y, Luo M, Lai Y, Kurihara N, Patrene K, Roodman GD, **Xiao G**. Critical role of ATF4 in regulating osteoclast differentiation and bone resorption. ASBMR annual meeting-2011 (Oral Presentation)
A7. Yang S, Xu H, Shibing Yu1, Cao H, Jie Fan, Ge C, Fransceschi RT, Dong HH, **Xiao G**. Foxo1 mediates IGF1/Insulin regulation of osteocalcin expression by antagonizing Runx2 in osteoblasts. ASBMR annual meeting-2011 (poster).

Conclusion

During the last four years of support, our studies establish that: i) ATF4 is essential for intermittent PTH to increase bone mass in both young and adult OVX mice. ii) ATF4 increases osteoblast proliferation in vitro and in bone probably via upregulation of cyclin D1; iii) ATF4 promotes osteoblast differentiation at least in part via upregulation of Osx, a key osteoblast differentiation transcription factor; iv) ATF4 is critical for PTH to increase bone formation in vivo; v) ATF4 plays a critical role in OVX induction of bone loss; and vi) Erk/MAPK, which is known to be activated by PTH signaling in osteoblasts, phosphorylates and activates Runx2; vii) ATF4 is critical for osteoclast differentiation and bone resorption; and xiii) ATF4 activates osteocalcin gene expression via cooperation with Runx2, a master regulator of osteoblast differentiation and bone formation. Collectively, the knowledge obtained from these studies will significantly enhance our understanding of the molecular mechanism underlying the actions of PTH in osteoblasts and bone and define new potential therapeutic targets for improved treatment of osteoporosis and other metabolic bone diseases.

References

1.   Hock JM, Gera I, Fonseca J, Raisz LG 1988 Human parathyroid hormone-(1-34) increases bone mass in ovariectomized and orchidectomized rats. Endocrinology 122(6):2899-904.
2.   Demiralp B, Chen HL, Koh AJ, Keller ET, McCauley LK 2002 Anabolic actions of parathyroid hormone during bone growth are dependent on c-fos. Endocrinology 143(10):4038-47.
3.   Tanaka S, Sakai A, Tanaka M, Otomo H, Okimoto N, Sakata T, Nakamura T 2004 Skeletal unloading alleviates the anabolic action of intermittent PTH(1-34) in mouse tibia in association with inhibition of PTH-induced increase in c-fos mRNA in bone marrow cells. J Bone Miner Res 19(11):1813-20.
4.   Hurley MM, Okada Y, Xiao L, Tanaka Y, Ito M, Okimoto N, Nakamura T, Rosen CJ, Doetschman T, Coffin JD 2006 Impaired bone anabolic response to parathyroid hormone in Fgf2-/- and Fgf2+/- mice. Biochem Biophys Res Commun 341(4):989-94.

5.   Iida-Klein A, Zhou H, Lu SS, Levine LR, Ducayen-Knowles M, Dempster DW, Nieves J, Lindsay R 2002 Anabolic action of parathyroid hormone is skeletal site specific at the tissue and cellular levels in mice. J Bone Miner Res 17(5):808-16.

6.   Miao D, He B, Karaplis AC, Goltzman D 2002 Parathyroid hormone is essential for normal fetal bone formation. J Clin Invest 109(9):1173-82.

7.   Cole JA 1999 Parathyroid hormone activates mitogen-activated protein kinase in opossum kidney cells. Endocrinology 140(12):5771-9.

8.   Pearman AT, Chou WY, Bergman KD, Pulumati MR, Partridge NC 1996 Parathyroid hormone induces c-fos promoter activity in osteoblastic cells through phosphorylated cAMP response element (CRE)-binding protein binding to the major CRE. J Biol Chem 271(41):25715-21.

9.   Swarthout JT, D'Alonzo RC, Selvamurugan N, Partridge NC 2002 Parathyroid hormone-dependent signaling pathways regulating genes in bone cells. Gene 282(1-2):1-17.

10.   Dempster DW, Cosman F, Parisien M, Shen V, Lindsay R 1993 Anabolic actions of parathyroid hormone on bone. Endocr Rev 14(6):690-709.

11.   Bellido T, Ali AA, Plotkin LI, Fu Q, Gubrij I, Roberson PK, Weinstein RS, O'Brien CA, Manolagas SC, Jilka RL 2003 Proteasomal Degradation of Runx2 Shortens Parathyroid Hormone-induced Anti-apoptotic Signaling in Osteoblasts: A PUTATIVE EXPLANATION FOR WHY INTERMITTENT ADMINISTRATION IS NEEDED FOR BONE ANABOLISM. J Biol Chem 278(50):50259-72.

12.   Chen HL, Demiralp B, Schneider A, Koh AJ, Silve C, Wang CY, McCauley LK 2002 Parathyroid hormone and parathyroid hormone-related protein exert both pro- and anti-apoptotic effects in mesenchymal cells. J Biol Chem 277(22):19374-81.

13.   Calvi LM, Sims NA, Hunzelman JL, Knight MC, Giovannetti A, Saxton JM, Kronenberg HM, Baron R, Schipani E 2001 Activated parathyroid hormone/parathyroid hormone-related protein receptor in osteoblastic cells differentially affects cortical and trabecular bone. J Clin Invest 107(3):277-86.

14.   Calvi LM, Adams GB, Weibrecht KW, Weber JM, Olson DP, Knight MC, Martin RP, Schipani E, Divieti P, Bringhurst FR, Milner LA, Kronenberg HM, Scadden DT 2003 Osteoblastic cells regulate the haematopoietic stem cell niche. Nature 425(6960):841-6.

Appendices

Six peer-reviewed research papers: P1-6
Seven national meeting abstracts: A1-7

Parathyroid Hormone Increases Activating Transcription Factor 4 Expression and Activity in Osteoblasts: Requirement for *Osteocalcin* Gene Expression

Shibing Yu, Renny T. Franceschi, Min Luo, Xiaoyan Zhang, Di Jiang, Yumei Lai, Yu Jiang, Jian Zhang, and Guozhi Xiao

Departments of Medicine (S.Y., M.L., X.Z., Y.L., J.Z., G.X.) and Pharmacology (Y.J.), University of Pittsburgh, Pittsburgh, Pennsylvania 15240; and Departments of Periodontics and Oral Medicine (R.T.F., D.J.), School of Dentistry, and Department of Biological Chemistry (R.T.F.), School of Medicine, University of Michigan, Ann Arbor, Michigan 48109

PTH is an important peptide hormone regulator of calcium homeostasis and osteoblast function. However, its mechanism of action in osteoblasts is poorly understood. Our previous study demonstrated that PTH activates mouse *osteocalcin* (*Ocn*) gene 2 promoter through the osteoblast-specific element 1 site, a recently identified activating transcription factor-4 (ATF4) -binding element. In the present study, we examined effects of PTH on ATF4 expression and activity as well as the requirement for ATF4 in the regulation of *Ocn* by PTH. Results show that PTH elevated levels of ATF4 mRNA and protein in a dose- and time-dependent manner. This PTH regulation requires transcriptional activity but not *de novo* pro-

tein synthesis. PTH also increased binding of nuclear extracts to osteoblast-specific element 1 DNA. PTH stimulated ATF4-dependent transcriptional activity mainly through protein kinase A with a lesser requirement for protein kinase C and MAPK/ERK pathways. Lastly, PTH stimulation of *Ocn* expression was lost by small interfering RNA down-regulation of ATF4 in MC-4 cells and *Atf4*−/− bone marrow stromal cells. Collectively, these studies for the first time demonstrate that PTH increases ATF4 expression and activity and that ATF4 is required for PTH induction of *Ocn* expression in osteoblasts. (*Endocrinology* 149: 1960–1968, 2008)

PTH IS A MAJOR regulator of osteoblast activity and skeletal homeostasis. PTH has both catabolic and anabolic effects on osteoblasts and bone that depend on the temporal pattern of administration; continuous administration decreases bone mass, whereas intermittent administration increases bone mass (1–3). At the molecular level, PTH binds to the PTH-1 receptor (PTH1R), a G protein-coupled receptor that is expressed in osteoblasts (4–6) and activates multiple intracellular signaling pathways that involve cAMP, inositol phosphates, intracellular Ca^{2+}, protein kinases A and C (7), and the ERK/MAPK pathway (8, 9). The ability of PTH to regulate gene expression is largely dependent on activation of specific transcription factors such as cAMP response element binding protein (CREB) (10, 11), activator protein-1 family members (12–15), pituitary-specific transcription factor-1 (16), and Runt-related transcription factor-2 (Runx2) (12, 17). A better understanding of the

downstream PTH signaling events is essential to understand the mechanistic basis for the anabolic and catabolic actions of this hormone on bone.

The *osteocalcin* (*Ocn*) promoter has been the major paradigm for unraveling the mechanisms mediating osteoblast-specific gene expression and defining a number of transcription factors and cofactors (18–29). Because *Ocn* gene is regulated by PTH (30–32), we considered it a good model for identifying new transcriptional mediators of PTH action. Using this system, we recently showed that the osteoblast-specific element (OSE)-1 in the proximal mouse (*Ocn*) gene 2 (mOG2) promoter (19) is necessary and sufficient for PTH induction of this gene (33). Immediately after publication of this study, the OSE1 was identified as a binding site for activating transcription factor-4 (ATF4) (34).

ATF4, also known as CREB2 (35) and tax-responsive enhancer element B67 (36), is a member of the ATF/CREB family of leucine-zipper factors that also includes CREB, cAMP response element modulator, ATF1, ATF2, ATF3, and ATF4 (37–41). These proteins bind to DNA via their basic region and dimerize via their leucine domain to form a large variety of homodimers and/or heterodimers that allow the cell to coordinate signals from multiple pathways (37–41). An *in vivo* role for ATF4 in bone development was established using *Atf4*-deficient mice (29). ATF4 is required for expression of *Ocn* and *bone sialoprotein* as demonstrated by the dramatic reduction of their mRNAs in *Atf4*−/− bone (29). ATF4 activates *Ocn* transcription through direct binding to the OSE1 site as well as interactions with Runx2 through

---

cooperative interactions with OSE1 and OSE2 (also known as nuclear matrix protein 2 binding site) sites in the promoter (19, 20, 25). ATF4 activity is negatively regulated by factor inhibiting activating transcription factor-4-mediated transcription (42). Factor inhibiting activating transcription factor binds to ATF4 and represses its activity and bone formation *in vivo*. Although *Atf4* mRNA is ubiquitously expressed, ATF4 protein preferentially accumulates in osteoblasts (34). This accumulation is explained by a selective reduction of proteasomal degradation in osteoblasts.

The purpose of this study was to determine the effects of PTH on ATF4 expression and activity and evaluate whether ATF4 mediates PTH induction of *Ocn* expression in osteoblasts.

Materials and Methods

Reagents

Tissue culture media and fetal bovine serum were obtained from HyClone (Logan, UT). γ-[^{32}P]ATP (3000 Ci/mmol) and α-[^{32}P]dCTP (3000 Ci/mmol) were purchased from GE Healthcare (Piscataway, NJ). Other reagents were obtained from the following sources: H89, forskolin (FSK), GF109203X, phorbol 12-myristate 13-acetate (PMA), cycloheximide (CHX), actinomycin D (ActD), and mouse monoclonal antibody against β-actin from Sigma (St. Louis, MO); U0126 from Promega (Madison, WI); and U0124 from Calbiochem (La Jolla, CA), PTH (1–34) from Bachem (Torrance, CA), antibodies against ATF4, Runx2, and horseradish peroxidase-conjugated mouse or goat IgG from Santa Cruz (Santa Cruz, CA). All other chemicals were of analytical grade.

Cell cultures

Mouse MC3T3-E1 subclone 4 (MC-4) cells were described previously (43, 44) and maintained in ascorbic acid-free α-MEM, 10% fetal bovine serum (FBS), and 1% penicillin/streptomycin and were not used beyond passage 15. Rat osteoblast-like UMR106-01 cells (45) were maintained in DMEM and 10% FBS. Isolation of mouse primary bone marrow stromal cells (BMSCs) was described previously (33). Briefly, 6-wk-old male C57BL/6 mice were killed by cervical dislocation. Tibiae and femurs were isolated and the epiphyses were cut. Marrow was flushed with DMEM containing 20% FBS, 1% penicillin/streptomycin, and 10^{-8} M dexamethasone into a 60-mm dish, and the cell suspension was aspirated up and down with a 20-gauge needle to break clumps of marrow. The cell suspension (marrow from two mice/flask) was then cultured in a T75 flask in the same medium. After 10 d, cells reach confluency and are ready for experiments.

DNA constructs and transfection

Wild-type and mutant p4OSE1-luc plasmids were described previously (25, 33). Cells were plated on 35-mm dishes at a density of 5×10^4 cells/cm^2. After 24 h, cells were transfected with lipofectAMINE 2000 (Invitrogen, Carlsbad, CA) according to the manufacturer's instructions. Each transfection contained 0.5 μg of the indicated plasmid plus 0.05 μg of pRL-SV40, containing a cDNA for Renilla reformis luciferase to control for transfection efficiency. Cells were harvested and assayed using the dual luciferase assay kit (Promega) on a Monolight 2010 luminometer (BD Biosciences, San Diego, CA).

Preparation of nuclear extracts and gel mobility shift assay (GMSA)

Nuclear extracts were prepared and GMSAs were conducted as previously described (43). Each reaction contained 1 μg of nuclear extracts. The DNA sequences of OSE1 oligonucleotides used for GMSA were as follows: wild-type (wt): TGC TTA CAT CAG AGA GCA); mutant (mt): TGC TTA gta CAG AGA GCA.

Western blot analysis

Twenty micrograms of nuclear extracts were fractionated on a 10% SDS-PAGE gel and transferred onto nitrocellulose membranes (Schleicher & Schuell, Keene, NH). The membrane was blocked in 5% nonfat milk in Tris-buffered saline/Tween 20 buffer; probed with antibodies against ATF4 (1:1000) followed by incubation with secondary antibodies conjugated with horseradish peroxidase (1:5000); and visualized using an enhanced chemiluminescence kit (Pierce, Rockford, IL). Finally, blots were stripped two times in buffer containing 65 mM Tris Cl (pH 6.8), 2% sodium dodecyl sulfate, and 0.7% (vol/vol) β-mercaptoethanol at 65 C for 15 min and reprobed with β-actin antibody (1:5000) for normalization.

RNA isolation and reverse transcription

Total RNA was isolated using TRIzol reagent (Invitrogen Life Technologies, Gaithersburg, MD) according to the manufacturer's protocol. Reverse transcription was performed using 2 μg of denatured RNA and 100 pmol of random hexamers (Applied Biosystems, Foster, CA) in a total volume of 25 μl containing 12.5 U MultiScribe reverse transcriptase (Applied Biosystems) according to the manufacturer's instructions.

Quantitative real-time PCR

Quantitative real-time PCR was performed on an iCycler (Bio-Rad, Minneapolis, MN) using a SYBR Green PCR core kit (Applied Biosystems) and cDNA equivalent to 10 ng RNA in a 50-μl reaction according to the manufacturer's instructions. The DNA sequences of mouse primers used for real-time PCR were: *Atf4*, 5'-GAG CTT CCT GAA CAG CGA AGT G-3' (forward), 5'-TGG CCA CCT CCA GAT AGT CAT C-3' (reverse); *Ocn*, 5'-TAG TGA ACA GAC TCC GGC GCT A-3' (forward), 5'-TGT AGG CGG TCT TCA AGC CAT-3' (reverse); *Pth1r*, 5'-GAT GCG GAC GAT GTC TTT ACC-3' (forward), 5'-GGC GGT CAA ATA CCT CC-3' (reverse); *Col1(I)*, 5'-AGA TTG AGA ACA TCC GCA GCC-3' (forward), 5'-TCC AGT ACT CTC CGC TCT TCC A-3' (reverse); *Opn*, 5'-CCA ATG AAA GCC ATG ACC ACA-3', (forward), 5'-CGT CAG ATT CAT CCG AGT CCA C-3' (reverse); *Gapdh*, 5'-CAG TGC CAG CCT CGT CCC GTA GA-3' (forward), 5'-CTG CAA ATG GCA GCC CTG GTG AC-3' (reverse). For all primers the amplification was performed as follows: initial denaturation at 95 C for 10 min followed by 40 cycles of 95 C for 15 sec and 60 C for 60 sec. Melting curve analysis was used to confirm the specificity of the PCR products. Six samples were run for each primer set. The levels of mRNA were calculated by the ΔCT (the difference between the threshold cycles) method (46). *Atf4*, *Ocn*, *Col1(I)*, *Pth1r*, and *Opn* mRNAs were normalized to *Gapdh* mRNA.

Northern blot

Twenty micrograms of total RNA was fractionated on 1.0% agarose-formaldehyde gels and blotted onto nitrocellulose paper. The mouse *Atf4* cDNA inserts were excised from plasmid DNA with the appropriate restriction enzymes and purified by agarose gel electrophoresis before labeling with α-[^{32}P]dCTP using a random primer kit (Roche Molecular Biochemicals, Indianapolis, IN). Hybridizations were performed as previously described using a Bellco Autoblot hybridization oven (47). Same blots were reprobed with [^{32}P]-labeled cDNA to *18S* rRNA for loading (48).

Small interfering RNA (siRNA)-MC-4 cells, which contain high levels of *Atf4* mRNA, were seeded at a density of 25,000 cells/cm^2. After 24 h, cells were transfected with mouse *Atf4* siRNA (sense: 5'-GAG CAU UCC UUU AGU UUA GUU-3'; antisense: 5'-CUA AAC UAA AGG AAU GCU CUU-3') (49) or negative control siRNA (low GC, catalog no. 12935–200; Invitrogen) using LipofectAMINE 2000 (Invitrogen). After 48 h, cells from three identically treated dishes were pooled and harvested for total RNA, followed by quantitative real-time RT-PCR analyses for *Atf4*, *Ocn*, and *Col1(I)* mRNAs. A second set of mouse *Atf4* siRNAs was purchased from Ambion (Austin, TX; catalog no. AM16704, ID 160775 and 160776) and used to confirm the results using the first set of *Atf4* siRNA.

Atf4-deficient mice

Breeding pairs of mice heterozygous for ATF4 (Swiss Black mouse background) were obtained from Dr. Randal J. Kaufman (the Howard
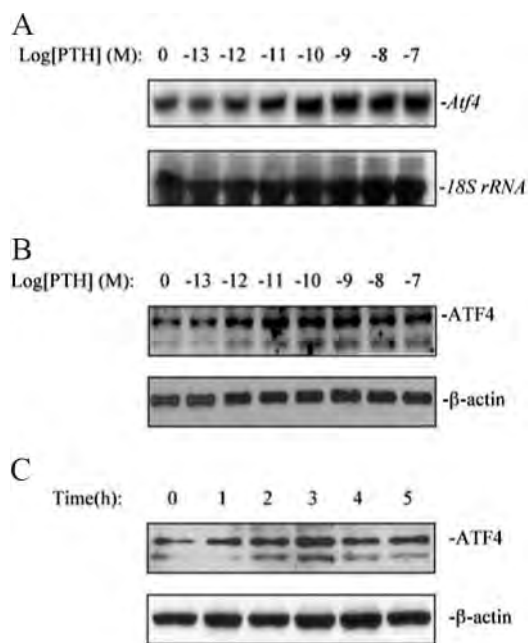
FIG. 1. PTH increases levels of ATF4 expression in osteoblasts. A, Effect of PTH on *Atf4* mRNA. MC-4 cells were seeded at a density of 50,000 cells/cm^2 in 35-mm dishes and cultured in 10% FBS medium overnight. Cells were then treated with various concentration of PTH for 6 h. For each group, total RNA (20 μg/lane) was loaded for Northern hybridization using cDNA probes for mouse *Atf4* mRNA and 18S rRNAs (for normalization). B, Effect of PTH on ATF4 proteins (dose response). MC-4 cells were treated with indicated concentrations of PTH for 6 h and nuclear extracts were prepared for Western blot analysis for ATF4. C, Effect of PTH on ATF4 proteins (time course). MC-4 cells were treated with 10^{-7} M PTH for indicated time (h). Experiments were repeated three to four times, and qualitatively identical results were obtained.

Hughes Medical Institute and the University of Michigan School of Medicine). These mice were originally developed by Dr. Tim M. Townes (University of Alabama at Birmingham) and were used to generate *Atf4* wild-type (*Atf4$^{+/+}$*), heterozygous (*Atf4$^{+/-}$*), and homozygous mutant (*Atf4$^{-/-}$*) embryos/pups for this study. Original reports describing the phenotype of *Atf4* homozygote-null mutants used the identical strain of mice (50). PCR genotyping was performed on tail DNA using a cocktail of three primers (TOWNES-1: 5'-AGC AAA ACA AGA CAG CAG CCA CTA-3'; TOWNES-2: 5'-GTT TCT ACA GCT TCC TCC ACT CTT-3', and
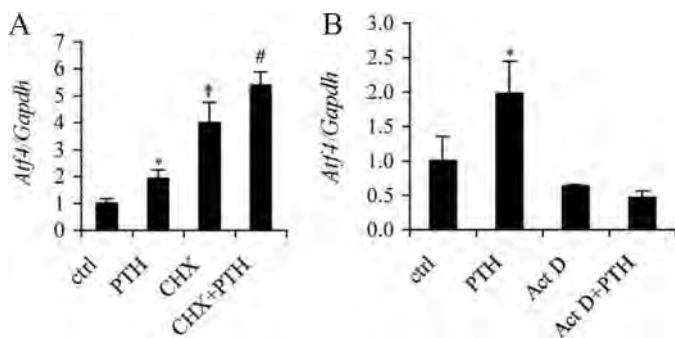
TOWNES-3: 5'-ATA TTG CTG AAG AGC TTG GCGGC-3') obtained from the laboratories of Dr. Randal J. Kaufman. A 700-bp DNA PCR product was amplified from *Atf4$^{-/-}$* mouse tail DNA and a 900-bp product from wild-type mice (see Fig. 7A). The genotype of each mouse established by PCR of tail genomic DNA was confirmed by Western blotting of calvaria cell lysates and anti-ATF4 antibody. A breeding colony was established using heterozygote mice to provide littermate controls. All animal studies were approved by the Animal Care Committee of the Veterans Affairs Pittsburgh Healthcare System.
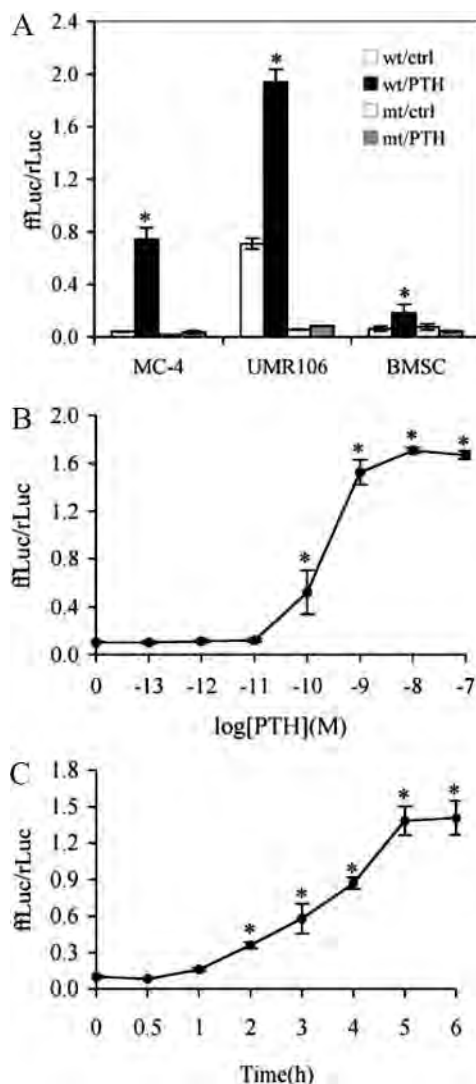

FIG. 3. PTH increases ATF4-dependent transcriptional activity in MC-4 cells. A, Target cell specificity. Cells (MC-4, UMR106–01, and primary BMSCs) were transiently transfected with p4OSE1-luc and renilla luciferase normalization plasmid and treated with 10^{-7} M PTH for 6 h before being harvested and assayed for dual-luciferase activity. Firefly luciferase activity was normalized to renilla luciferase activity (for transfection efficiency). B, Dose dependence. MC-4 cells were transiently transfected as in Fig. 2A and treated with indicated concentration of PTH (from 10^{-11} to 10^{-7} M) for 6 h followed by dual-luciferase assay. C, Time course. MC-4 cells were transiently transfected as in Fig. 2A and treated with 10^{-7} M PTH for indicated times. Data represent mean ± SD. Experiments were repeated three to four times and qualitatively identical results were obtained. *, $P < 0.05$ [control (ctrl) *vs.* PTH].

FIG. 2. Effects of CHX/ActD treatment on PTH induction of *Atf4* mRNA. MC-4 cells were treated with vehicle or 10 μg/ml CHX (A) or ActD (B) in the absence or presence of PTH for 6 h. *Atf4* and *Gapdh* mRNAs were determined by quantitative real-time RT-PCR analysis. Experiments were repeated three times, and qualitatively identical results were obtained. *, $P < 0.05$ [control (ctrl) *vs.* PTH]; #, $P < 0.05$ (CHX *vs.* CHX/PTH); †, < 0.05 (control *vs.* CHX).
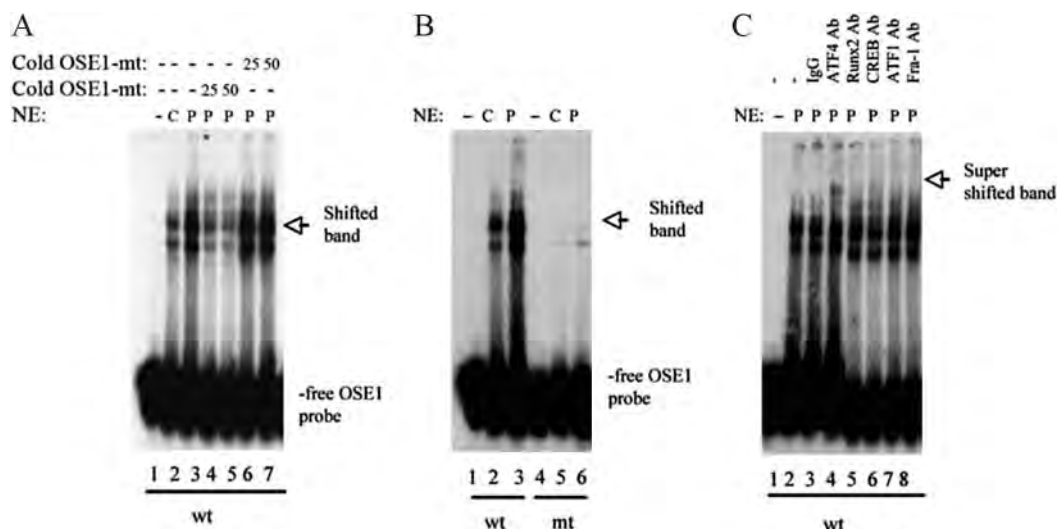
FIG. 4. PTH increases binding of ATF4 to OSE1 DNA. A, PTH increases binding of osteoblast nuclear extracts (NE) to OSE1. Nuclear extracts were prepared from MC-4 cells with (P) (lanes 3–7) or without (C) (lane 2) PTH treatment for 6 h. One microgram of each nuclear extract was incubated with end-labeled double-stranded OSE1 (TGC TTA CAT CAG AGA GCA) and analyzed by electrophoresis on 4% polyacrylamide gels. DNA binding to labeled wild-type OSE1 probe was analyzed in the presence of 25- to 50-fold molar excesses of cold wt (lanes 6 and 7) or mt (lanes 4 and 5) OSE1 (TGC TTA gta CAG AGA GCA) by GMSA using 1 μg of nuclear extracts from PTH-treated MC-4 cells. B, Binding site specificity. Labeled wt (lanes 1–3) and mt (lanes 4–6) OSE1 probes were incubated with 1 μg nuclear extracts from MC-4 cells with and without PTH treatment. C, The nuclear complex binding OSE1 contains ATF4. Labeled wild-type OSE1 probe was incubated with 1 μg nuclear extracts from PTH-treated MC-4 cells in the presence of normal control IgG (lane 3), ATF4 antibody (lane 4), Runx2 antibody (lane 5), CREB antibody (lane 6), ATF1 antibody (lane 7), and Fra-1 antibody (lane 8). Experiments were repeated three to four times, and qualitatively identical results were obtained.

Statistical analysis

Data were analyzed with GraphPad Prism software (GraphPad, San Diego, CA). A one-way ANOVA analysis was used followed by the Dunnett's test (see Fig. 3, B and C). Student's' *t* test was used to test for differences between two groups of data. Differences with a $P < 0.05$ was considered as statistically significant. Results were expressed as means $\pm$ SD.

Results

PTH increases ATF4 expression in MC-4 cells

To determine the effect of PTH on *Atf4* mRNA expression, MC-4 cells were treated with increasing concentrations of PTH (from 10^{-13} to 10^{-7} M) for 6 h, and total RNA was isolated for Northern blot analysis. As shown in Fig. 1A, PTH dose-dependently increased levels of *Atf4* mRNAs with a significant stimulatory effect first detected at a concentration of 10^{-10} M. Western blot analyses using nuclear extracts from MC-4 cells with and without PTH treatment show that PTH also dose-dependently elevated the levels of ATF4 protein with maximal stimulation at 10^{-10} M. Measurable stimulation of ATF4 protein was observed 1 h after PTH addition with maximal induction occurring at 3 h and lasting for at least 5 h (Fig. 1, B and C). PTH similarly increased *Atf4* and *Ocn* mRNA expression in mouse primary bone marrow stromal cells (BMSCs) (see Fig. 7, B and C). To assess the molecular mechanisms of PTH stimulation of *Atf4* mRNA expression, MC-4 cells were treated with and without inhibitors of transcription and translation in the presence and absence of PTH (10^{-7} M) for 6 h. As shown in Fig. 2A, the protein synthesis inhibitor CHX alone induced *Atf4* mRNA by 4-fold, which is typically observed in immediate early response genes such as *Fra-2* (15). The PTH-stimulation of

Atf4 mRNA was not blocked by CHX treatment, suggesting that *de novo* protein synthesis is not necessary for the PTH regulation. In contrast, the transcription inhibitor ActD completely abolished the PTH-stimulated *Atf4* mRNA induction (Fig. 2B), suggesting that the PTH effect requires transcription.

PTH increases ATF4-dependent transcriptional activity in osteoblasts

The effect of PTH on ATF4-dependent transcriptional activity was evaluated in two osteoblast cell lines and primary mouse bone marrow stromal cells. Cells were transiently transfected with wt or mt p4OSE1-luc, an artificial promoter containing four copies of wt or mt OSE1 (a specific ATF4-binding element) fused to a -34 to $+13$ minimal mOG2 promoter, and pRL-SV40, a renilla luciferase normalization plasmid. After 42 h, cells were treated with PTH (10^{-7} M) for 6 h followed by dual-luciferase assay. Firefly luciferase activity was normalized to renilla luciferase activity as a control for transfection efficiency. As shown in Fig. 3A, PTH stimulated ATF4-dependent OSE1 activity by 17-, 2.7-, and 2.8-fold in MC-4, UMR106-01, and primary BMSCs ($P < 0.05$, control *vs.* PTH), respectively. This PTH response was completely lost with the introduction of a 3-bp point mutation in the OSE1 core sequence (from TTA*CAT*CA to TTA*GTA*CA). (Note that there are no additional OSE1 sites in the upstream region of the mOG2 promoter.) Figure 3B shows that PTH stimulated ATF4-dependent transcriptional activity in a dose-dependent manner with a significant stimulatory effect first detected at a concentration of 10^{-10} M. This is consistent with our previous study that examined effects of PTH on endogenous *Ocn* mRNA (33). Time-course studies revealed

that the earliest effect of PTH stimulation was seen within 1 h and peaked at 5–6 h (Fig. 3C).

PTH increases ATF4 binding to OSE1 DNA

To determine whether PTH increases ATF4 binding to OSE1 DNA, we performed GMSA using nuclear extracts from MC-4 cells with and without 10^{-7} M PTH for 6 h. Consistent with our previous observation (33), nuclear extracts from PTH-treated MC-4 cells exhibited increased binding to intact OSE1 oligonucleotides (Fig. 4A, lanes 2 and 3), and this binding was significantly reduced by the addition of 25- and 50-fold molar excesses of unlabeled wt OSE1 oligonucleotides (Fig. 4A, lanes 4 and 5) but not by unlabeled mt OSE1 oligonucleotides (Fig. 4A, lane 6 and 7). In contrast, GMSA using labeled mt OSE1 oligonucleotides as probes showed that both basal and PTH-induced binding activity was abolished by the same 3-bp point mutation (Fig. 4B, lanes 4–6). The same mutation also abolished PTH activation of 647- and 116-bp mOG2 promoter fragments and 4OSE1 (33) (Fig. 3A). Importantly, PTH-increased binding to OSE1 was supershifted with an anti-ATF4 antibody (Fig. 4C, lanes 4). In contrast, normal IgG or antibodies against Runx2, CREB, ATF1, and Fra-1 did not significantly supershift the PTH-stimulated band (Fig 4C, lanes 3–8). Taken together, these studies demonstrate that ATF4 is a component of the PTH-stimulated DNA-protein complex associating with OSE1. [Note that PTH treatment did not alter binding of Runx2 to OSE2 DNA in the mOG2 promoter in GMSA (33).]

Protein kinase A (PKA) is the major signaling pathway mediating the PTH response

To identify signaling pathways mediating PTH activation of ATF4 transcriptional activity, we examined the effects of various inhibitors or activators. As shown in Fig. 5A, H89, a selective inhibitor of the PKA pathway, completely abolished PTH-stimulated ATF4 transcriptional activity ($P > 0.05$, control *vs.* PTH). GF109203X, a specific inhibitor of the protein kinase C (PKC) pathway, significantly decreased the PTH stimulation. U0126, a specific inhibitor of MAPK, partially suppressed PTH stimulation. As shown in Fig. 5B, FSK, a well-known activator of PKA, increased ATF4 activity in the absence of PTH in a dose-dependent manner. In combination with PTH, the effect of FSK was not additive, indicating that the PKA pathway was maximally stimulated. PMA, a PKC activator, did not significantly affect the PTH-induced ATF4 activity at a concentration range of 0.1–5 μM. A higher concentration of PMA (20 μM) slightly increased PTH-stimulated ATF4 activity without changing the basal activity (Fig. 5C). Taken together, these results indicate that PKA is the major pathway mediating PTH activation of ATF4 in osteoblasts with PKC and MAPK/ERK pathways playing lesser roles in the PTH response. The concentrations of the inhibitors or activators used in this study are in the range reported to selectively affect the relevant pathways (33, 51–53). We found no evidence of toxicity; compounds did not reduce cell DNA or protein under the current condition (data not shown).

FIG. 5. PKA is the major signaling pathway mediating the PTH response. A, Effects of inhibitors/activators on PTH-induced ATF4 transcriptional activity. MC-4 cells were transiently transfected with p4OSE1-luc and renilla luciferase normalization plasmid. After 42 h, cells were treated with 10 μM inhibitors/activators in the absence or presence of 10^{-7} M PTH for 6 h followed by dual-luciferase assay. Compounds used were: H89, a PKA inhibitor; FSK, a PKA activator; GF109203X, a PKC inhibitor; PMA, a PKC activator; U0126, a MAPK inhibitor; and U0124, an inactive analog of U0126. B and C, Dose-response of FSK (B) and PMA (C) on PTH stimulation of ATF4 transcriptional activity. MC-4 cells were transiently transfected as in Fig. 5A and treated with indicated concentration of respective activator for 6 h in the absence and presence of 10^{-7} M PTH followed by dual-luciferase assay. Data represent mean ± SD. Experiments were repeated three times and qualitatively identical results were obtained. *, $P < 0.05$ [control (ctrl) *vs.* PTH].
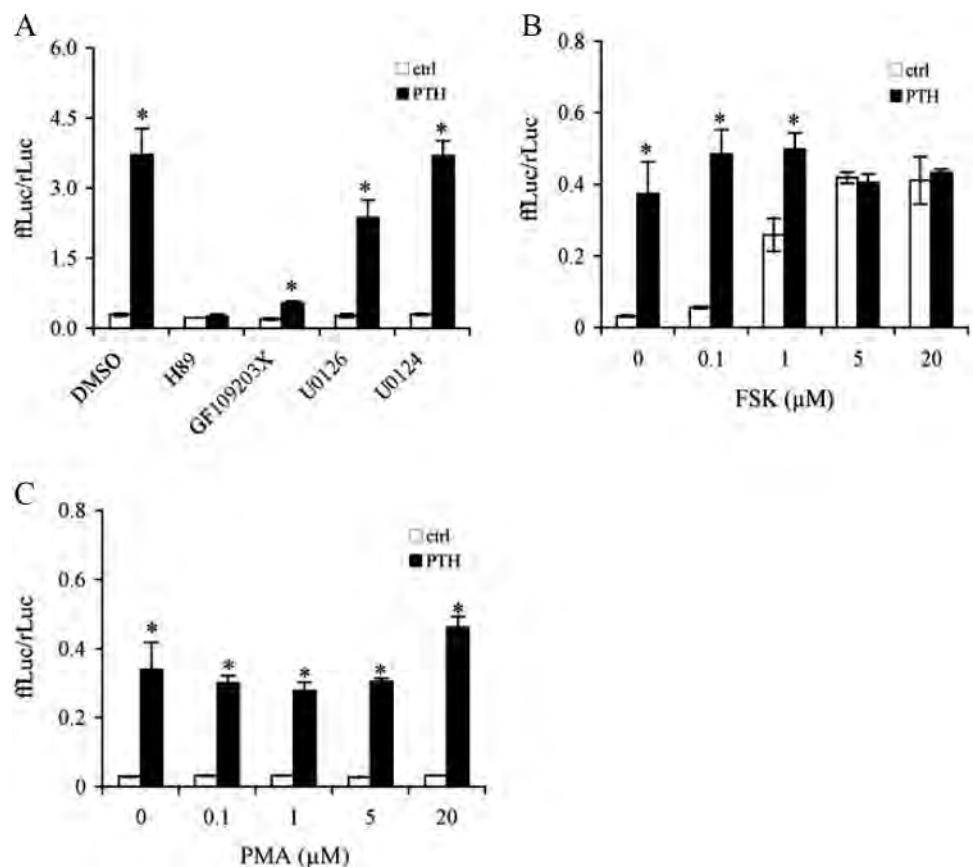
PTH-dependent induction of Ocn gene expression requires ATF4

We used two separate approaches to establish the requirements for ATF4 in the regulation of *Ocn* gene expression by PTH. First, we examined whether ATF4 is necessary for PTH induction of *Ocn* mRNA expression in osteoblasts by knocking down endogenous *Atf4* transcripts using siRNA. MC-4 cells, which express high levels of *Atf4* mRNA, were transiently transfected with ATF4 siRNA or negative control siRNA (Invitrogen) using LipofectAMINE 2000 according to the manufacturer's instructions. This siRNA specifically targets mouse *Atf4* (49). As shown in Fig. 6A, quantitative real-time RT-PCR analysis showed that ATF4 siRNA (20 and 40 nM) efficiently reduced the levels of *Atf4* mRNA by 57 and 71%, respectively. In contrast, the negative control siRNA did not reduce the *Atf4* mRNA (Fig. 6B). As shown in Fig. 6C, the basal level of *Ocn* mRNA was reduced greater than 70% by ATF4 siRNA ($P < 0.05$, control *vs.* ATF4 siRNA). Importantly, PTH-stimulated *Ocn* mRNA was completely abolished in ATF4 siRNA group relative to the control siRNA group. Conversely, *Col1(I)* mRNA was not altered by ATF4 siRNA or PTH (Fig. 6D). Similar results were obtained when a different set of ATF4 siRNAs was used in MC-4 cells (data not shown).

To further establish the requirement for ATF4 in the PTH response, primary BMSCs were isolated from *wt* and *Atf4^{-/-}* mice (Fig. 7A) and treated with or without PTH (10^{-7} M) for 6 h followed by RNA preparation and quantitative real-time PCR analysis. As shown in Fig. 7B, minimal *Atf4* mRNA was detected by real-time RT/PCR in the *Atf4^{-/-}* BMSCs. Consistent with the results of experiments with MC-4 cells, PTH

significantly stimulated *Atf4* mRNA in wt BMSCs ($P < 0.05$, control *vs.* PTH), but this induction was completely lost in cells from *Atf4^{-/-}* mice (Fig. 7B). As shown in Fig. 7C, PTH significantly increased *Ocn* mRNA in wt BMSCs, which was abolished in *Atf4^{-/-}* BMSCs ($P > 0.05$, control *vs.* PTH). The basal level of *Ocn* mRNA was also significantly reduced in *Atf4^{-/-}* BMSCs relative to wt cells ($P < 0.05$, wt *vs.* mt). In contrast, PTH did not increase *Opn* mRNA in wt or mt BMSCs ($P > 0.05$, control *vs.* PTH) (Fig. 7D). However, the level of *Opn* mRNA was increased in *Atf4^{-/-}* cells ($P < 0.05$, wt *vs.* mt), indicating that ATF4 may function as a negative regulator of *Opn* expression (Fig. 7D). In addition, the levels of *Pth1r* mRNA were not significantly changed by either ATF4 deficiency or PTH, suggesting that PTH signaling is intact in the absence of ATF4 (Fig. 7E). Taken together, these data clearly establish that ATF4 is required for PTH induction of *Ocn* mRNA in primary BMSCs.

Discussion

This study examined actions of PTH on ATF4 expression and activity in osteoblasts. Using the *Ocn* gene as a model system for studying PTH-dependent transcription, we found the following: 1) PTH rapidly induces *Atf4* expression in MC-4 cells and mouse primary bone marrow stromal cells in a time- and dose-dependent manners; 2) PTH increases *in vitro* binding of ATF4 to OSE1 DNA; 3) PTH dramatically activates ATF4 transcriptional activity mainly through the PKA pathway; 4) PTH stimulation of *Ocn* gene expression requires ATF4 because it is abolished by ATF4 siRNA in MC-4 cells and is not seen in ATF4-deficeint BMSCs. Col-

FIG. 6. ATF4 siRNA blocks PTH stimulation of *Ocn* expression. A and B, MC-4 cells were transiently transfected with *Atf4* siRNA (A) or negative control (Ctrl) siRNA (B). After 48 h, total RNA was prepared for quantitative real-time RT-PCR analyses for *Atf4* mRNA, which was normalized to *Gapdh* mRNA. C and D, MC-4 cells were transiently transfected with 40 nM *Atf4* siRNA or negative control siRNAs. After 42 h, cells were treated with and without 10^{-7} M PTH for 6 h followed by RNA preparation and quantitative real-time RT-PCR analyses for *Ocn* and *Col1(I)* mRNAs, which were normalized to the *Gapdh* mRNAs. *, $P < 0.05$ (ctrl *vs.* PTH); #, $P < 0.05$ (ctrl siRNA *vs.* ATF4 siRNA). Data represent mean ± SD. Experiments were repeated three times, and qualitatively identical results were obtained.
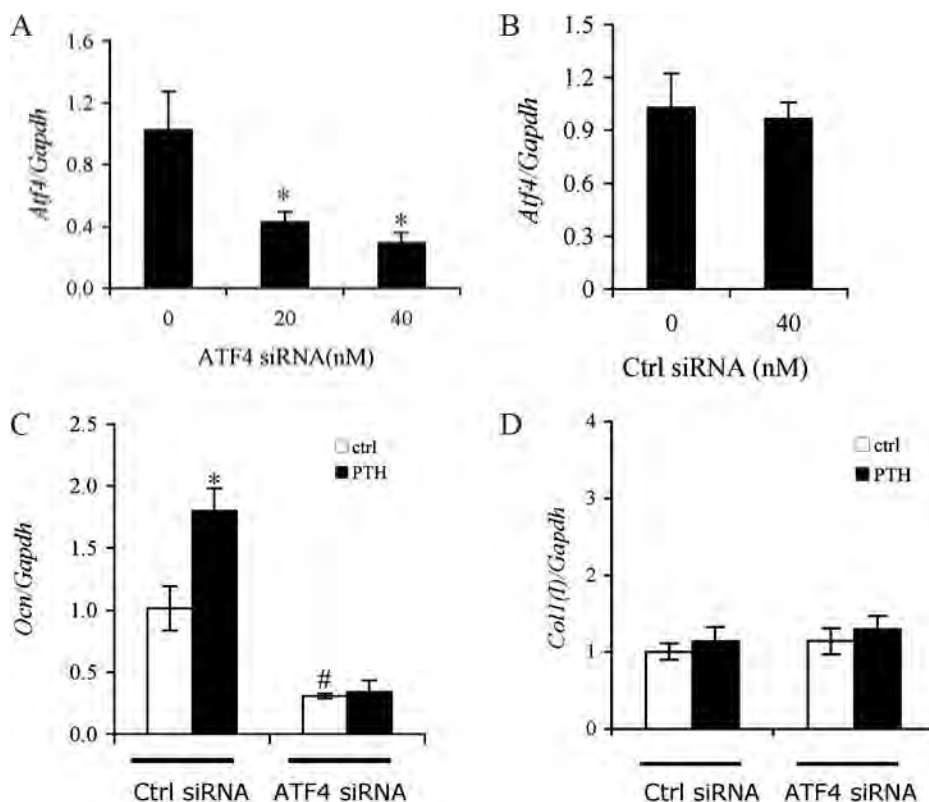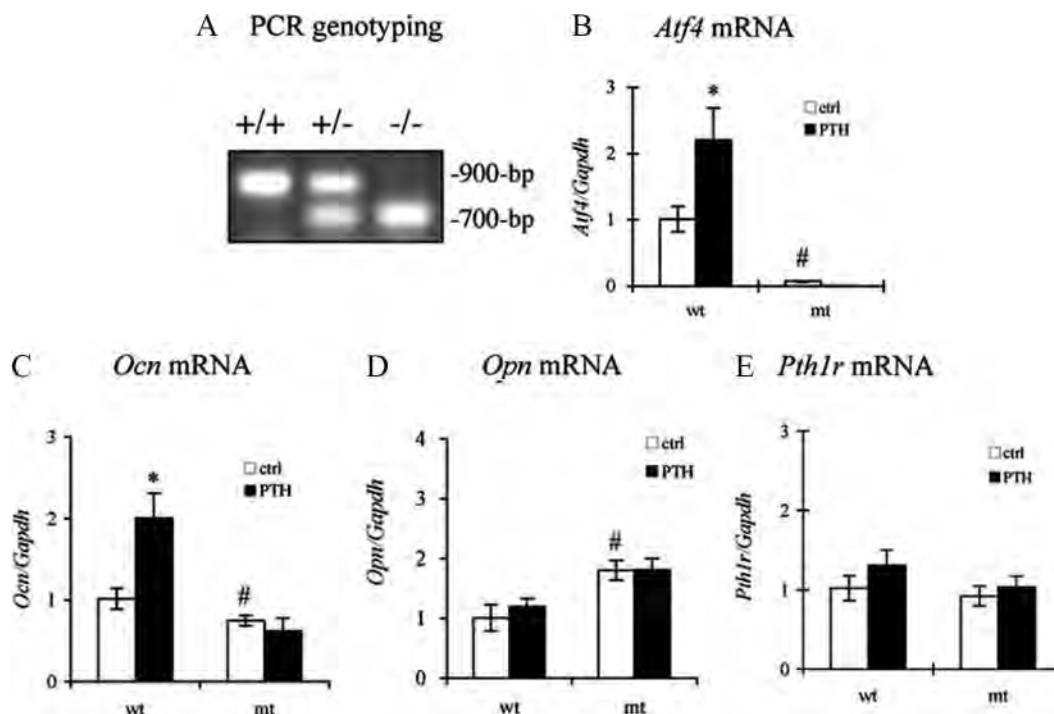
FIG. 7. PTH stimulation of *Ocn* expression is lost in *Atf4$^{-/-}$* BMSCs. A, PCR genotyping was performed on tail DNA using a cocktail of three primers (see *Materials and Methods*). A 700-bp DNA PCR product is amplified from *Atf4$^{-/-}$* mouse tail DNA and a 900-bp product from wild-type mice. B–E, Effects of ATF4 deficiency on PTH stimulation of *Atf4* (B), *Ocn* (C), *Opn* (D), and *Pth1r* (E) expression in BMSCs. Primary BMSCs were seeded at a density of 50,000 cells/cm^2 in 35-mm dishes and cultured in 10% FBS medium overnight. Cells were then treated with 10^{-7} M PTH for 6 h followed by RNA preparation and quantitative real-time RT/PCR for *Atf4* (B), *Ocn* (C), *Opn* (D), and *Pth1r* (E) mRNA, which were normalized to the *Gapdh* mRNAs. *, $P < 0.05$ (ctrl *vs.* PTH); #, $P < 0.05$ (wt *vs.* mt). Data represent mean ± SD. Experiments were repeated three times, and qualitatively identical results were obtained.

lectively, this study establishes that ATF4 is a novel downstream target of PTH actions in osteoblasts.

It is well documented that PTH signals mainly through the PKA pathway. In the present study, we show that PKA inhibition completely blocked PTH stimulation of ATF4 activity. Furthermore, activation of the PKA pathway by FSK dramatically increased ATF4 activity in the absence of PTH. However, when combined with PTH, the effect of FSK was not additive. These results strongly suggest that PKA is the major pathway for PTH to activate ATF4 because each agent (*i.e.* FSK or PTH) maximally stimulates the same pathway, making additional ATF4 activation impossible. Inhibition of the PKC pathway also resulted in a significant reduction in PTH-induced ATF4 activity (data not shown), but PKC activation by PMA failed to activate both basal or PTH-induced ATF4 activity. Thus, PKC is partially required for PTH activation of ATF4. Lastly, inhibition of the MAPK/ERK pathway led to partial inhibition of the PTH stimulation. These three pathways are also required for PTH induction of both *Ocn* mRNA and 1.3-kb *mOG2* promoter activity as previously described (33), further supporting our hypothesis that ATF4 mediates PTH induction of *Ocn* gene expression.

A recent study showed that ATF4 mediates β-adrenergic induction of *Rankl* mRNA expression via direct binding to the upstream OSE1 site in the *Rankl* promoter in osteoblasts (54). However, PTH stimulation of *Rankl* expression was not reduced in the absence of ATF4, suggesting that this catabolic action of PTH is independent of this transcription factor.

Phosphorylation seems to be critical for ATF4 to elicit its function in osteoblasts and bone. A PKA phosphorylation site (serine 254) within the ATF4 molecule was recently shown to mediate β-adrenergic induction of *Rankl* mRNA expression in osteoblasts (54). In addition, ATF4 is phosphorylated at serine 251 by ribosomal kinase 2 (RSK2), the kinase inactivated in Coffin-Lowry syndrome, an X-linked mental retardation disorder associated with skeletal manifestations (29). Because RSK2 is an immediate downstream target of MAPK/ERK that is activated by PTH signaling (8, 9), PTH may in part activate ATF4 via the MAPK/ERK/RSK2 pathway. It remains to be determined whether the PKA and/or RSK2 phosphorylation sites are involved in the PTH activation of ATF4.

One of the major downstream factors for PTH signaling is CREB, the cAMP response element binding protein. Actions of CREB are mediated through cAMP response elements (CREs) in the regulatory regions of target genes. PTH phosphorylates CREB at serine 133. This phosphorylation event stimulates the binding of CREB to the CRE and is required for CREB to activate transcription of target genes. Through this classical pathway, PTH rapidly induces transcription of immediate-early response genes including those encoding activator protein-1 family members such as c-Fos, c-Jun, Fra-1, Fra-2, and FosB (10, 14, 15, 52, 55–57). Although CREB was shown to binding to the OSE1 site (29), overexpression of CREB was unable to activate OSE1-dependent transcription activity of the mOG2 promoter *in vitro* (29), suggesting

that this site is not a major functional site for CREB. Furthermore, the OSE1 binding activity stimulated by PTH was not supershifted by an anti-CREB antibody. Instead, this complex clearly contains ATF4 protein (Fig. 4C). Thus, we were unable to obtain any evidence for the involvement of CREB in the PTH response. However, our results do not exclude the possibility that PTH/CREB activates *Atf4* mRNA transcription via CREB binding to potential CRE sites in the *Atf4* promoter.

PTH induction of immediate-early response genes occurs very rapidly (minutes to hours) and lasts for several hours. This PTH response is usually independent upon the presence of *de novo* protein synthesis but requires active cellular transcription. The time-course experiments in the present study indicate that PTH induction of *Atf4* occurs within 1 h of PTH addition and peaks after 3–6 h. Furthermore, this regulation depends on active cellular transcription and does not require *de novo* protein synthesis. Therefore, ATF4 may be considered as an additional PTH early response gene.

ATF4-deficeint mice as well as humans with mutations in RSK2, an ATF4 activating kinase, exhibit striking deficits in bone formation and osteoblast activity. Because ATF4 is required for osteoblast function and bone formation *in vivo*, and as shown herein, ATF4 is a novel downstream target of PTH in osteoblasts, it will be important to determine whether ATF4 is also required for the anabolic actions of PTH in bone.

Acknowledgments

References

1. **Neer RM, Arnaud CD, Zanchetta JR, Prince R, Gaich GA, Reginster JY, Hodsman AB, Eriksen EF, Ish-Shalom S, Genant HK, Wang O, Mitlak BH** 2001 Effect of parathyroid hormone (1–34) on fractures and bone mineral density in postmenopausal women with osteoporosis. N Engl J Med 344:1434–1441
2. **Miao D, He B, Karaplis AC, Goltzman D** 2002 Parathyroid hormone is essential for normal fetal bone formation. J Clin Invest 109:1173–1182
3. **Demiralp B, Chen HL, Koh AJ, Keller ET, McCauley LK** 2002 Anabolic actions of parathyroid hormone during bone growth are dependent on c-*fos*. Endocrinology 143:4038–4047
4. **Partridge NC, Alcorn D, Michelangeli VP, Kemp BE, Ryan GB, Martin TJ** 1981 Functional properties of hormonally responsive cultured normal and malignant rat osteoblastic cells. Endocrinology 108:213–219
5. **McCauley LK, Koh AJ, Beecher CA, Cui Y, Decker JD, Franceschi RT** 1995 Effects of differentiation and transforming growth factor β1 on PTH/PTHrP receptor mRNA levels in MC3T3-E1 cells. J Bone Miner Res 10:1243–1255
6. **McCauley LK, Koh AJ, Beecher CA, Cui Y, Rosol TJ, Franceschi RT** 1996 PTH/PTHrP receptor is temporally regulated during osteoblast differentiation and is associated with collagen synthesis. J Cell Biochem 61:638–647
7. **Swarthout JT, D'Alonzo RC, Selvamurugan N, Partridge NC** 2002 Parathyroid hormone-dependent signaling pathways regulating genes in bone cells. Gene 282:1–17
8. **Carpio L, Gladu J, Goltzman D, Rabbani SA** 2001 Induction of osteoblast

9. **Swarthout JT, Doggett TA, Lemker JL, Partridge NC** 2001 Stimulation of extracellular signal-regulated kinases and proliferation in rat osteoblastic cells by parathyroid hormone is protein kinase C-dependent. J Biol Chem 276:7586–7592
10. **Pearman AT, Chou WY, Bergman KD, Pulumati MR, Partridge NC** 1996 Parathyroid hormone induces c-*fos* promoter activity in osteoblastic cells through phosphorylated cAMP response element (CRE)-binding protein binding to the major CRE. J Biol Chem 271:25715–25721
11. **Gonzalez GA, Montminy MR** 1989 Cyclic AMP stimulates somatostatin gene transcription by phosphorylation of CREB at serine 133. Cell 59:675–680
12. **Selvamurugan N, Chou WY, Pearman AT, Pulumati MR, Partridge NC** 1998 Parathyroid hormone regulates the rat collagenase-3 promoter in osteoblastic cells through the cooperative interaction of the activator protein-1 site and the runt domain binding sequence. J Biol Chem 273:10647–10657
13. **D'Alonzo RC, Kowalski AJ, Denhardt DT, Nickols GA, Partridge NC** 2002 Regulation of collagenase-3 and osteocalcin gene expression by collagen and osteopontin in differentiating MC3T3-E1 cells. J Biol Chem 277:24788–24798
14. **McCauley LK, Koh AJ, Beecher CA, Rosol TJ** 1997 Proto-oncogene c-*fos* is transcriptionally regulated by parathyroid hormone (PTH) and PTH-related protein in a cyclic adenosine monophosphate-dependent manner in osteoblastic cells. Endocrinology 138:5427–5433
15. **McCauley LK, Koh-Paige AJ, Chen H, Chen C, Ontiveros C, Irwin R, McCabe LR** 2001 Parathyroid hormone stimulates fra-2 expression in osteoblastic cells *in vitro* and *in vivo*. Endocrinology 142:1975–1981
16. **Ogata Y, Nakao S, Kim RH, Li JJ, Furuyama S, Sugiya H, Sodek J** 2000 Parathyroid hormone regulation of bone sialoprotein (BSP) gene transcription is mediated through a pituitary-specific transcription factor-1 (Pit-1) motif in the rat BSP gene promoter. Matrix Biol 19:395–407
17. **Krishnan V, Moore TL, Ma YL, Helvering LM, Frolik CA, Valasek KM, Ducy P, Geiser AG** 2003 Parathyroid hormone bone anabolic action requires cbfa1/runx2-dependent signaling. Mol Endocrinol 17:423–435
18. **Ducy P, Zhang R, Geoffroy V, Ridall AL, Karsenty G** 1997 Osf2/Cbfa1: a transcriptional activator of osteoblast differentiation. Cell 89:747–754
19. **Ducy P, Karsenty G** 1995 Two distinct osteoblast-specific *cis*-acting elements control expression of a mouse osteocalcin gene. Mol Cell Biol 15:1858–1869
20. **Merriman HL, van Wijnen AJ, Hiebert S, Bidwell JP, Fey E, Lian J, Stein J, Stein GS** 1995 The tissue-specific nuclear matrix protein, NMP-2, is a member of the AML/CBF/PEBP2/runt domain transcription factor family: interactions with the osteocalcin gene promoter. Biochemistry 34:13125–13132
21. **Stein GS, Lian JB, van Wijnen AJ, Stein JL** 1997 The osteocalcin gene: a model for multiple parameters of skeletal-specific transcriptional control. Mol Biol Rep 24:185–196
22. **Banerjee C, McCabe LR, Choi JY, Hiebert SW, Stein JL, Stein GS, Lian JB** 1997 Runt homology domain proteins in osteoblast differentiation: AML3/CBFA1 is a major component of a bone-specific complex. J Cell Biochem 66:1–8
23. **Banerjee C, Hiebert SW, Stein JL, Lian JB, Stein GS** 1996 An AML-1 consensus sequence binds an osteoblast-specific complex and transcriptionally activates the osteocalcin gene. Proc Natl Acad Sci USA 93:4968–4973
24. **Lian JB, Stein GS** 2003 Runx2/Cbfa1: a multifunctional regulator of bone formation. Curr Pharm Des 9:2677–2685
25. **Xiao G, Jiang D, Ge C, Zhao Z, Lai Y, Boules H, Phimphilai M, Yang X, Karsenty G, Franceschi RT** 2005 Cooperative Interactions between activating transcription factor 4 and Runx2/Cbfa1 stimulate osteoblast-specific osteocalcin gene expression. J Biol Chem 280:30689–30696
26. **Stein GS, Lian JB, Stein JL, van Wijnen AJ, Frankel B, Montecino M** 1996 Mechanisms regulating osteoblast proliferation and differentiation. In: Bilezikian JP, Raise LG, Rodon GA, eds. Principles of bone biology. San Diego: Academic Press; 69–86
27. **Lian JB, Stein GS, Stein JL, Van Wijnen A, McCabe L, Banerjee C, Hoffmann H** 1996 The osteocalcin gene promoter provides a molecular blueprint for regulatory mechanisms controlling bone tissue formation: role of transcription factors involved in development. Connect Tissue Res 35:15–21
28. **Ducy P, Karsenty, G** 1999 Transcriptional control of osteoblast differentiation. Endocrinologist 9:32–35
29. **Yang X, Matsuda K, Bialek P, Jacquot S, Masuoka HC, Schinke T, Li L, Brancorsini S, Sassone-Corsi P, Townes TM, Hanauer A, Karsenty G** 2004 ATF4 Is a substrate of RSK2 and an essential regulator of osteoblast biology: implication for Coffin-Lowry syndrome. Cell 117:387–398
30. **Boguslawski G, Hale LV, Yu XP, Miles RR, Onyia JE, Santerre RF, Chandrasekhar S** 2000 Activation of osteocalcin transcription involves interaction of protein kinase A- and protein kinase C-dependent pathways. J Biol Chem 275:999–1006
31. **Yu XP, Chandrasekhar S** 1997 Parathyroid hormone (PTH 1–34) regulation of rat osteocalcin gene transcription. Endocrinology 138:3085–3092
32. **Boudreaux JM, Towler DA** 1996 Synergistic induction of osteocalcin gene expression: identification of a bipartite element conferring fibroblast growth factor 2 and cyclic AMP responsiveness in the rat osteocalcin promoter. J Biol Chem 271:7508–7515
33. **Jiang D, Franceschi RT, Boules H, Xiao G** 2004 Parathyroid hormone induction of the osteocalcin gene: requirement for an osteoblast-specific element 1

sequence in the promoter and involvement of multiple signaling pathways. J Biol Chem 279:5329–5337

34. **Yang X, Karsenty G** 2004 ATF4, the osteoblast accumulation of which is determined post-translationally, can induce osteoblast-specific gene expression in non-osteoblastic cells. J Biol Chem 279:47109–47114

35. **Karpinski BA, Morle GD, Huggenvik J, Uhler MD, Leiden JM** 1992 Molecular cloning of human CREB-2: an ATF/CREB transcription factor that can negatively regulate transcription from the cAMP response element. Proc Natl Acad Sci USA 89:4820–4824

36. **Tsujimoto A, Nyunoya H, Morita T, Sato T, Shimotohno K** 1991 Isolation of cDNAs for DNA-binding proteins which specifically bind to a tax-responsive enhancer element in the long terminal repeat of human T-cell leukemia virus type I. J Virol 65:1420–1426

37. **Brindle PK, Montminy MR** 1992 The CREB family of transcription activators. Curr Opin Genet Dev 2:199–204

38. **Hai T, Wolfgang CD, Marsee DK, Allen AE, Sivaprasad U** 1999 ATF3 and stress responses. Gene Expr 7:321–335

39. **Meyer TE, Habener JF** 1993 Cyclic adenosine 3′,5′-monophosphate response element binding protein (CREB) and related transcription-activating deoxyribonucleic acid-binding proteins. Endocr Rev 14:269–290

40. **Sassone-Corsi P** 1994 Goals for signal transduction pathways: linking up with transcriptional regulation. EMBO J 13:4717–4728

41. **Ziff EB** 1990 Transcription factors: a new family gathers at the cAMP response site. Trends Genet 6:69–72

42. **Yu VW, Ambartsoumian G, Verlinden L, Moir JM, Prud'homme J, Gauthier C, Roughley PJ, St. Arnaud R** 2005 FIAT represses ATF4-mediated transcription to regulate bone mass in transgenic mice. J Cell Biol 169:591–601

43. **Xiao G, Cui Y, Ducy P, Karsenty G, Franceschi RT** 1997 Ascorbic acid-dependent activation of the osteocalcin promoter in MC3T3-E1 preosteoblasts: requirement for collagen matrix synthesis and the presence of an intact OSE2 sequence. Mol Endocrinol 11:1103–1113

44. **Wang D, Christensen K, Chawla K, Xiao G, Krebsbach PH, Franceschi RT** 1999 Isolation and characterization of MC3T3-E1 preosteoblast subclones with distinct *in vitro* and *in vivo* differentiation/mineralization potential. J Bone Miner Res 14:893–903

45. **Benson MD, Bargeon JL, Xiao G, Thomas PE, Kim A, Cui Y, Franceschi RT** 2000 Identification of a homeodomain binding element in the bone sialoprotein gene promoter that is required for its osteoblast-selective expression. J Biol Chem 275:13907–13917

46. **Wang J, Xi L, Hunt JL, Gooding W, Whiteside TL, Chen Z, Godfrey TE, Ferris RL** 2004 Expression pattern of chemokine receptor 6 (CCR6) and CCR7 in squamous cell carcinoma of the head and neck identifies a novel metastatic phenotype. Cancer Res 64:1861–1866

47. **Franceschi RT, Iyer BS, Cui Y** 1994 Effects of ascorbic acid on collagen matrix formation and osteoblast differentiation in murine MC3T3-E1 cells. J Bone Miner Res 9:843–854

48. **Renkawitz R, Gerbi SA, Glatzer KH** 1979 Ribosomal DNA of fly *Sciara coprophila* has a very small and homogeneous repeat unit. Mol Gen Genet 173:1–13

49. **Adams CM** 2007 Role of the transcription factor ATF4 in the anabolic actions of insulin and the anti-anabolic actions of glucocorticoids. J Biol Chem 282:16744–16753

50. **Masuoka HC, Townes TM** 2002 Targeted disruption of the activating transcription factor 4 gene results in severe fetal anemia in mice. Blood 99:736–745

51. **Xiao G, Gopalakrishnan R, Jiang D, Reith E, Benson MD, Franceschi RT** 2002 Bone morphogenetic proteins, extracellular matrix, and mitogen-activated protein kinase signaling pathways are required for osteoblast-specific gene expression and differentiation in MC3T3-E1 cells. J Bone Miner Res 17:101–110

52. **Selvamurugan N, Pulumati MR, Tyson DR, Partridge NC** 2000 Parathyroid hormone regulation of the rat collagenase-3 promoter by protein kinase A-dependent transactivation of core binding factor α1. J Biol Chem 275:5037–5042

53. **Ouyang H, Franceschi R, McCauley L, Wang D, Somerman M** 2000 Parathyroid hormone-related protein downregulates bone sialoprotein gene expression in cementoblasts: role of the protein kinase A pathway. Endocrinology 141:4671–4680

54. **Elefteriou F, Ahn JD, Takeda S, Starbuck M, Yang X, Liu X, Kondo H, Richards WG, Bannon TW, Noda M, Clement K, Vaisse C, Karsenty G** 2005 Leptin regulation of bone resorption by the sympathetic nervous system and CART. Nature 434:514–520

55. **Porte D, Tuckermann J, Becker M, Baumann B, Teurich S, Higgins T, Owen MJ, Schorpp-Kistner M, Angel P** 1999 Both AP-1 and Cbfa1-like factors are required for the induction of interstitial collagenase by parathyroid hormone. Oncogene 18:667–678

56. **Tyson DR, Swarthout JT, Partridge NC** 1999 Increased osteoblastic *c-fos* expression by parathyroid hormone requires protein kinase A phosphorylation of the cyclic adenosine 3′,5′-monophosphate response element-binding protein at serine 133. Endocrinology 140:1255–1261

57. **Koe RC, Clohisy JC, Tyson DR, Pulumati MR, Cook TF, Partridge NC** 1997 Parathyroid hormone versus phorbol ester stimulation of activator protein-1 gene family members in rat osteosarcoma cells. Calcif Tissue Int 61:52–58

Endocrinology **is published monthly by The Endocrine Society (http://www.endo-society.org), the foremost professional society serving the endocrine community.**

General Transcription Factor IIA-γ Increases Osteoblast-specific *Osteocalcin* Gene Expression via Activating Transcription Factor 4 and Runt-related Transcription Factor 2*[S]

Shibing Yu[‡], Yu Jiang[§], Deborah L. Galson[‡], Min Luo[‡], Yumei Lai[‡], Yi Lu[‡], Hong-Jiao Ouyang[‡], Jian Zhang[‡], and Guozhi Xiao[‡1]

From the Departments of [‡]Medicine and [§]Pharmacology, University of Pittsburgh, Pittsburgh, Pennsylvania 15240

ATF4 (activating transcription factor 4) is an osteoblast-enriched transcription factor that regulates terminal osteoblast differentiation and bone formation. ATF4 knock-out mice have reduced bone mass (severe osteoporosis) throughout life. Runx2 (runt-related transcription factor 2) is a runt domain-containing transcription factor that is essential for bone formation during embryogenesis and postnatal life. In this study, we identified general transcription factor IIAγ (TFIIAγ) as a Runx2-interacting factor in a yeast two-hybrid screen. Immunoprecipitation assays confirmed that TFIIAγ interacts with Runx2 in osteoblasts and when coexpressed in COS-7 cells or using purified glutathione S-transferase fusion proteins. Chromatin immunoprecipitation assay of MC3T3-E1 (clone MC-4) preosteoblast cells showed that in intact cells TFIIAγ is recruited to the region of the *osteocalcin* promoter previously shown to bind Runx2 and ATF4. A small region of Runx2 (amino acids 258–286) was found to be required for TFIIAγ binding. Although TFIIAγ interacts with Runx2, it does not activate Runx2. Instead, TFIIAγ binds to and activates ATF4. Furthermore, TFIIAγ together with ATF4 and Runx2 stimulates *osteocalcin* promoter activity and endogenous mRNA expression. Small interfering RNA silencing of *TFIIAγ* markedly reduces levels of endogenous ATF4 protein and *Ocn* mRNA in osteoblastic cells. Overexpression of TFIIAγ increases levels of ATF4 protein. Finally, TFIIAγ significantly prevents ATF4 degradation. This study shows that a general transcription factor, TFIIAγ, facilitates osteoblast-specific gene expression through interactions with two important bone transcription factors ATF4 and Runx2.

Skeletal integrity requires a balance between bone-forming cells (osteoblasts) and bone-resorbing cells or osteoclasts. Imbalance between bone formation and resorption results in metabolic bone diseases such as osteoporosis. Multipotential mesenchymal cells proliferate and differentiate into osteoblasts that synthesize and deposit the mineralizing extracellular matrix of bone. Osteoblast activity is regulated by a number of growth factors and hormones, including bone morphogenetic proteins, insulin-like growth factor 1, basic fibroblast growth factor 2, parathyroid hormone, tumor necrosis factor-α, and extracellular matrix signals (1–9). Runx2 is a runt domain-containing transcription factor identified as a transcriptional activator of osteoblast differentiation and the master gene for bone development *in vitro* and *in vivo* (10–14). Runx2 knock-out mice die at birth and completely lack both skeletal ossification and mature osteoblasts (10, 12). Runx2 haplo-insufficiency causes the skeletal disorder, cleidocranial dysplasia, a disease characterized by defective endochondral and intramembranous bone formation. Runx2 is expressed in mesenchymal condensations during early development at E11.5 and acts as an osteoblast differentiation factor (13).

ATF4 (a̲ctivating t̲ranscription f̲actor 4̲), also known as CREB2 (c̲AMP-r̲esponse e̲lement-b̲inding protein 2̲) (15) and Tax-responsive Enhancer Element B67 (TAXREB67) (16), is a member of the activating transcription factor cAMP-response element-binding protein family of leucine zipper factors that also includes cAMP-response element-binding protein, cAMP-response element modulator (CREM)[2] ATF1, ATF2, ATF3, and ATF4 (17–21). These proteins bind to DNA via their basic region and dimerize via their leucine domain to form a large variety of homodimers and/or heterodimers that allow the cell to coordinate signals from multiple pathways (17–21). An *in vivo* role for ATF4 in bone development was established using *Atf4*-deficient mice (22). ATF4 is required for expression of *osteocalcin* (*Ocn*) and *bone sialoprotein* (*Bsp*) as demonstrated by a dramatic reduction of their mRNAs in *Atf4^{−/−}* bone (22). ATF4 activates *Ocn* transcription through direct binding to the OSE1 site of the *mOG2* promoter. In addition, ATF4 interacts with Runx2 in osteoblasts or when coexpressed in COS-7 cells. ATF4 and Runx2 cooperatively regulate *Ocn* transcription through interactions with OSE1 (osteoblast-specific element 1)

---

and OSE2 (osteoblast-specific element 2, also known as nuclear matrix protein 2 or NMP2-binding site) sites in the promoter (23–25).

One of the most striking characteristics of ATF4 protein is its very short half-life (30–60 min) in many cell types (26). ATF4 is rapidly degraded via a ubiquitin/proteasomal pathway. This degradation requires the presence of the serine residue 219 in the context of DSG*XXX*S within the ATF4 molecule and its phosphorylation by an unknown kinase. This phosphorylation was shown to be required for subsequent recognition by the SCF$^{\beta TrCP}$ and degradation by the 26 S proteasome (27). Although *Atf4* mRNA is ubiquitously expressed, ATF4 protein preferentially accumulates in osteoblasts (28). This accumulation is explained by a selective reduction of proteasomal degradation in osteoblasts. Indeed, inhibition of the ubiquitin/proteasomal pathway by MG115, which blocks the N-terminal threonine in the active site of β-subunit of 26 S proteasomal complex (29, 30), led to ATF4 accumulation and induced *Ocn* mRNA expression in non-osteoblastic cells (28). These observations suggest that modulation of ATF4 stability constitutes an important step to control its protein level and activity and, ultimately, osteoblast-specific gene expression and bone formation.

Transcription factor IIA (TFIIA) is a general transcription factor consisting of three subunits designated TFIIAα, TFIIAβ, and TFIIAγ (31). TFIIA interacts with and stabilizes TFIID (also known as TBP, <u>T</u>ATA box-<u>b</u>inding protein) to DNA and activates transcription (32, 33). Although TFIIA was classified as a general transcription factor when it was first identified, more and more evidence shows that this elusive factor may play an important role in the regulation of tissue-specific gene expression via interactions with tissue- or cell type-specific transcription factors (34–36).

The *Ocn* promoter has been the major paradigm for unraveling the mechanisms mediating osteoblast-specific gene expression and defining a number of key transcription factors or cofactors (13, 14, 23–25, 37–41). However, very few studies have focused on how tissue-specific transcription factors interface with general transcriptional initiation factors in osteoblasts. In this study, by using a combination of a yeast two-hybrid system and pulldown assays as well as functional assays, we show that TFIIAγ, the smallest subunit (12 kDa) of TFIIA (42), interacts with both Runx2 and ATF4. TFIIAγ delays ATF4 protein degradation and increases its activity. Together with ATF4 and Runx2, TFIIAγ enhances osteoblast-specific *Ocn* gene expression.

EXPERIMENTAL PROCEDURES

Reagents—Tissue culture media were purchased from Invitrogen and fetal bovine serum from HyClone (Logan, UT). Other reagents were obtained from the following sources: antibodies against TFIIA-α, TFIIA-γ, ATF4, Runx2, and horseradish peroxidase-conjugated mouse or goat IgG from Santa Cruz Biotechnology (Santa Cruz, CA), mouse monoclonal antibody against β-actin from Sigma, and GST antibody from Amersham Biosciences. All other chemicals were of analytical grade.

Cell Cultures—Mouse MC3T3-E1 subclone 4 (MC-4) cells were described previously (43, 44) and maintained in ascorbic acid-free α-modified Eagle's medium, 10% fetal bovine serum (FBS), and 1% penicillin/streptomycin and were not used beyond passage 15. C2C12 myoblasts, a gift from Dr. Daniel Goldman (University of Michigan, Ann Arbor, MI), C3H10T1/2 fibroblasts (American Type Culture Collection), and 3T3-L1 mouse preadipocytes (American Type Culture Collection) were maintained in Dulbecco's modified Eagle's medium, 10% FBS. F9 teratocarcinoma cells (American Type Culture Collection) and rat ROS17/2.8 osteosarcoma cells (gift from Dr. Laurie McCauley, University of Michigan School of Dentistry) were grown in modified Eagle's medium, 10% FBS.

Yeast Two-hybrid Analysis—A yeast pLexA two-hybrid system (Clontech) was used to identify proteins that bind to mouse Runx2. A cDNA fragment encoding the aa-263–351 region of Runx2 was subcloned into the BamHI/XhoI sites of pLexA, creating an in-frame fusion with the DNA binding domain of the *LexA* gene that is controlled by the strong yeast *ADH1* promoter. The resultant plasmid pLexA-Runx2 (aa 263–351) was then transformed into a yeast reporter strain (YM4271), and the transformed cells (1×10^9) were mated for 24 h with cells (2.5×10^8) of a pretransformed two-hybrid library made from human brain cDNA. The resultant mating mixture was spread on $20 \times$ 10-cm plates to select for expression of the *LEU2* and *lacZ* reporter genes. Approximately 2×10^6 colonies were screened. Sixty four positive colonies were isolated. The prey plasmids were extracted from the positive colonies and the cDNA inserts in the plasmids were amplified by PCR and sequenced. Of the 64 positive colonies, 5 are the full-length *TFIIAγ* cDNAs, and the rest contained 16 different cDNAs.

DNA Constructs and Transfection—p657mOG2-luc, p657mOG2OSE1mt-luc, p657mOG2OSE2mt-luc, p657mOG2-(OSE1 + 2)mt-luc, p4OSE1-luc, p4OSE1mt-luc, p6OSE2-luc, p6OSE2mt-luc, pCMV/β-galactosidase, pCMV/ATF4, pCMV/Runx2, pCMV/FLAG-Runx2 and its deletion mutants (aa 1–330, aa 1–286, and aa-258), GST-Runx2 and GST-ATF4 fusion protein expression vectors were described previously (1, 13, 23, 25, 45). The full-length cDNA of human *TFIIA-γ* was cloned by an RT-PCR strategy using total RNA from human Saos2 osteoblastic cells as a template and specific primers (forward, 5′-ATG GCA TAT CAG TTA TAC AGA AA-3′, and reverse, 5′-TTC TGT AGT ATT GGA GCC AGT A-3′). Digested PCR products were purified and subcloned into the NotI/BamHI sites of the pFLAG-5a expression vector (Sigma). Addition of a C-terminal FLAG sequence into the *TFIIA-γ* cDNA facilitates monitoring of expression levels and immunoprecipitation using M2 antibody (Sigma). GST-TFIIAγ fusion protein expression plasmid was constructed by subcloning the full-length *TFIIAγ* cDNA into the glutathione *S*-transferase gene fusion vector pGEX-4T-1 (Amersham Biosciences) in correct reading frame. The accuracy of DNA sequences was verified by automatic sequencing. The size of expressed proteins was confirmed by Western blot analysis using specific antibodies. For expression and functional studies, cells were plated on 35-mm dishes at a density of 5×10^4 cells/cm^2. After 24 h, cells were transfected with the indicated plasmid DNAs (0.01 μg of pRL-SV40, 0.25 μg of test luciferase reporter, and 1.0 μg of expression plasmids balanced as necessary with β-galactosidase expression plasmid such that the total DNA was constant)

and Lipofectamine 2000 (Invitrogen) according to manufacturer's instructions. After 36 h, whole cell extracts were prepared and used for Western blot analysis or dual luciferase assay using the dual luciferase assay kit (Promega, Madison, WI) on a Veritas™ microplate luminometer (Turner Biosystem, Inc., Sunnyvale, CA). Firefly luciferase activity was normalized to *Renilla* luciferase activity for transfection efficiency.

RNA Isolation and Reverse Transcription (RT)—Total RNA was isolated using TRIzol reagent (Invitrogen) according to the manufacturer's protocol. RT was performed using 2 μg of denatured RNA and 100 pmol of random hexamers (Applied Biosystem, Foster, CA) in a total volume of 25 μl containing 12.5 units of MultiScribe reverse transcriptase (Applied Biosystem, Foster, CA) according to the manufacturer's instructions.

Regular PCR—Regular PCR was performed on a 2720 Thermal Cycler (Applied Biosystem, Foster, CA), using 2.5 μl of the cDNA (equivalent to 0.2 μg of RNA) and AmpliTaq DNA polymerase (Applied Biosystems, Foster City, CA) in a 25-μl reaction according to the manufacturer's instructions. The DNA sequences of primers used for PCR were as follows: mouse/rat *TFIIAγ*, 5′-ATG GCA TAT CAG TTA TAC AGA AAT ACA-3′ (forward), 5′-GGT ATT TTT ACC ATC ACA GGC T-3′(reverse); mouse/rat *Atf4*, 5′-ATG GCT TGG CCA GTG CCT CAG A-3′ (forward), 5′-GCT CTG GAG TGG AAG ACA GAA C-3′ (reverse); mouse/rat *Hprt*, 5′-GTT GAG AGA TCA TCT CCA CC-3′ (forward), 5′-AGC GAT GAT GAA CCA GGT TA-3′ (reverse). For all primers the amplification was performed as follows: initial denaturation at 95 °C for 30s followed by 31 cycles of 95 °C for 15 s, 60 °C for 30 s, 72 °C for 30 s and extension at 72 °C for 7 min. The amplified PCR products were run on a 1.2% agarose gel and visualized by ethidium bromide staining.

Quantitative Real Time PCR—Quantitative real time PCR was performed on an iCycler (Bio-Rad) using a SYBR® Green PCR core kit (Applied Biosystem, Foster, CA) and cDNA equivalent to 10 ng of RNA in a 50-μl reaction according to the manufacturer's instructions. The DNA sequences of primers used for real time PCR were as follows: mouse *Ocn*, 5′-TAG TGA ACA GAC TCC GGC GCT A-3′ (forward), 5′-TGT AGG CGG TCT TCA AGC CAT-3′ (reverse); mouse and rat *18 S rRNA*, 5′-CGT CTG CCC TAT CAA CTT TCG ATG GTA G-3′ (forward), 5′-GCC TGC TGC CTT CCT TGG ATG T-3′ (reverse); mouse and rat *TFIIAγ*, 5′-TGG GGA ACA GTC TTC AAG AGA GCC TT-3′ (forward); 5′-TTC CTG ACT CTC TGA GCC AAT GCT G-3′ (reverse); rat *Ocn*, 5′-TGG TGA ATA GAC TCC GGC GCT ACC T-3′ (forward), 5′-CCT GGA AGC CAA TGT GGT CCG-3′ (reverse); rat *Bsp*: 5′-GGC TGG AGA TGC AGA GGG CAA GGC-3′ (forward), 5′-TGG TGC TGG TGC CGT TGA CGA CCT-3′ (reverse); rat *Opn*, 5′-TGG TGA ATA GAC TCC GGC GCT ACC T-3′ (forward), 5′-CCT GGA AGC CAA TGT GGT CCG-3′ (reverse). For all primers the amplification was performed as follows: initial denaturation at 95 °C for 10 min followed by 40 cycles of 95 °C for 15 s and 60 °C for 60 s. Melting curve analysis was used to confirm the specificity of the PCR products. Six samples were run for each primer set. The levels of mRNA were calculated by the ΔCT method (46). *Ocn*, *Bsp*, *TFIIAγ*, osteopontin (*Opn*), and *Atf4* mRNAs were normalized to *18 S rRNA* mRNA.

Western Blot Analysis—Cells were washed with cold 1× phosphate-buffered saline and lysed in 1× Passive Buffer (Promega, Madison, WI) at room temperature for 20 min. Lysates were clarified by centrifugation (20 min, 13,000 × g, 4 °C). Protein concentrations were determined by the method developed by Bio-Rad. Twenty μg of total protein were fractionated on a 10% SDS-polyacrylamide gel and transferred onto nitrocellulose membranes (Schleicher & Schuell). The membrane was blocked in 5% nonfat milk in Tris-buffered saline/Tween 20 (TBST) buffer, probed with antibodies against TFIIA-γ (1:200), TFIIA-α (1:1000), ATF4 (1:1000), Runx2 (1:1000), Fra-1 (1:1000), GST (1:5000), or M2 (1:2000) followed by incubation with anti-goat-mouse or -rabbit antibodies conjugated with horseradish peroxidase (1:5000) and visualized using an enhanced chemiluminescence kit (Pierce). Finally, blots were stripped two times in buffer containing 65 mM Tris-Cl, pH 6.8, 2% SDS, and 0.7% (v/v) β-mercaptoethanol at 65 °C for 15 min and re-probed with β-actin antibody (1:5000) for normalization.

Immunoprecipitation—GST, GST-TFIIAγ, GST-ATF4, and GST-Runx2 fusion proteins were purified using the Bulk GST purification module kit (Amersham Biosciences) according the manufacturer's instructions. Whole cell extracts (500 μg), nuclear extracts (200 μg), or GST fusion proteins (1.0 μg) were pre-cleaned twice with 50 μl of protein A/G-agarose beads (Stratagene, La Jolla, CA) for 30 min followed by pelleting of beads. The protein A/G-agarose beads were blocked with 10 μg/ml bovine serum albumin in 1× phosphate-buffered saline for 1 h before use to reduce nonspecific binding of proteins. Five μg of respective antibody was added and incubated for 2 h at 4 °C with gentle rocking. The immune complexes were collected by addition of 30 μl of protein A/G-agarose beads and incubation for 1 h at 4 °C followed by centrifugation. Precipitates were washed five times with 1× washing buffer (20 mM HEPES, pH 7.6, 50 mM KCl, 1 mM dithiothreitol, 0.25% Nonidet P-40, 5 mM NaF, 1 mM EGTA, 5 mM MgCl$_2$, 0.25 mM phenylmethylsulfonyl fluoride), and the immunoprecipitated complexes were suspended in SDS sample buffer and analyzed by SDS-PAGE followed by Western blot analysis using the indicated antibodies.

ChIP Assays—ChIP assays were performed as described previously (41) using a protocol kindly provided by Dr. Dwight Towler (Washington University) (47). After sonication, the amount of chromatin was quantified using the PicoGreen double-stranded DNA quantitation assay (Molecular Probes) according to the manufacturer's instructions. The equivalent of 10 μg of DNA was used as starting material (input) in each ChIP reaction with 2 μg of the appropriate antibody (TFIIAγ, or control rabbit IgG). Fractions of the purified ChIP DNA (5%) or inputs (0.02–0.05%) were used for PCR analysis. The reaction was performed with AmpliTaq Gold DNA polymerase (Applied Biosystems) for 35 cycles of 60 s at 95 °C, 90 s at 58 °C, and 120 s at 68 °C. PCR primer pairs were generated to detect DNA segments located near the Runx2-binding site at −137/−131 (primers P1 and P2), ATF4-binding site at −55/−48 (primers P3 and P4) in mouse *osteocalcin* gene 2 (*mOG2*) proximal promoter, or the Runx2-binding site located between −370 and −42 in the proximal mouse *Runx2* promoter region (primers
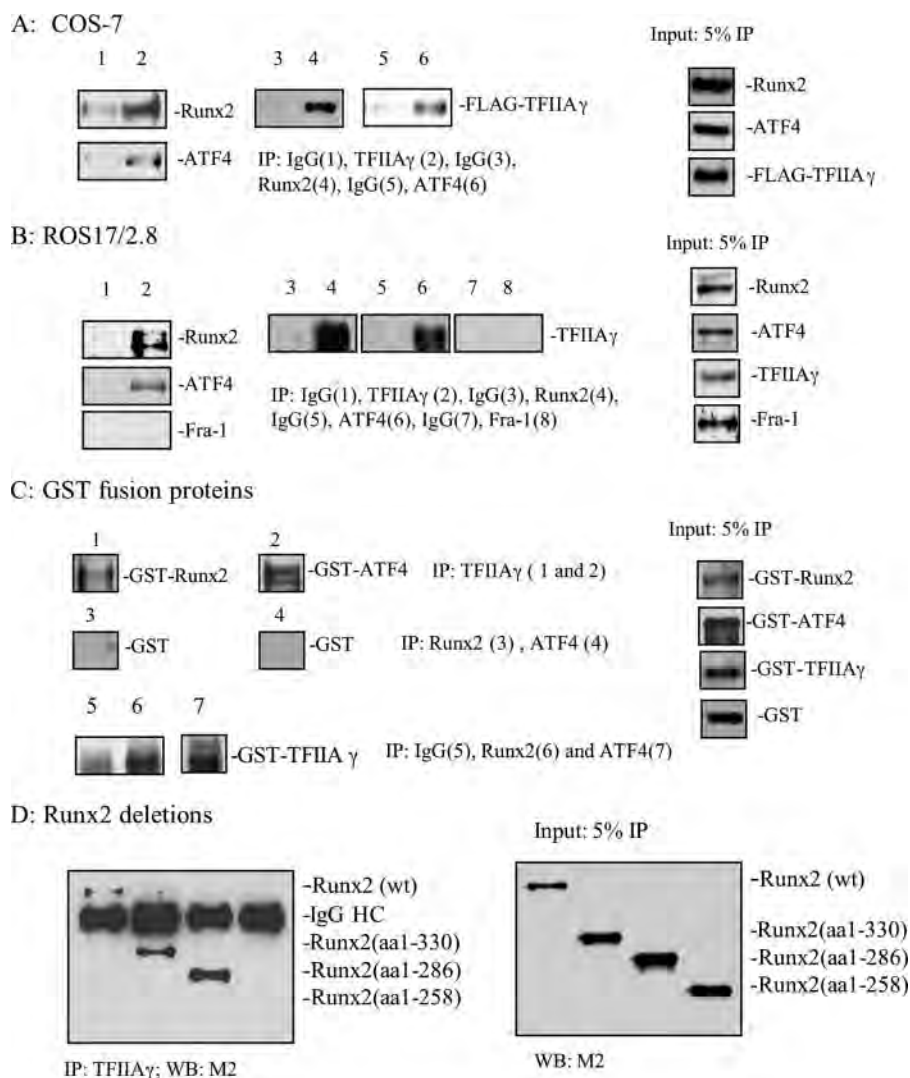
FIGURE 1. **Protein-protein interactions among TFIIAγ, Runx2, and ATF4.** *A,* whole cell extracts from COS-7 cells overexpressing pFLAG-TFIIAγ, pCMV-Runx2, and pCMV-ATF4 were immunoprecipitated (*IP*) with normal IgG (*lane 1*) or TFIIAγ antibody (*lane 2*) followed by Western blot (*WB*) analysis using Runx2 or ATF4 antibodies. In reciprocal IPs, the same extracts were immunoprecipitated with normal IgG (*lanes 3* and *5*), Runx2 antibody (*lane 4*), or ATF4 antibody (*lane 6*) followed by WB using M2 antibody. *B,* nuclear extracts from ROS17/2.8 cells were immunoprecipitated with normal IgG (*lane 1*) or TFIIAγ antibody (*lane 2*) followed by WB using Runx2, ATF4, or Fra-1 antibodies. In reciprocal IPs, the same extracts were immunoprecipitated with normal IgG (*lanes 3, 5* and *7*), Runx2 antibody (*lane 4*), ATF4 antibody (*lane 6*), or Fra-1 antibody (*lane 8*) followed by WB using TFIIAγ antibody. *C,* mixture of purified GST-TFIIAγ and GST-Runx2 was immunoprecipitated by TFIIAγ antibody followed by WB for Runx2 (*lane 1*). A mixture of purified GST-TFIIAγ and GST-ATF4 was immunoprecipitated by TFIIAγ antibody followed by WB for ATF4 (*lane 2*). A mixture of purified GST and GST-Runx2 was immunoprecipitated by Runx2 antibody followed by WB for GST (*lane 3*). A mixture of purified GST and GST-ATF4 was immunoprecipitated by ATF4 antibody followed by WB for GST (*lane 4*). In reciprocal IPs, a mixture of purified GST-TFIIAγ and GST-Runx2 was immunoprecipitated by normal IgG (*lane 5*) or Runx2 antibody (*lane 6*) followed by WB for TFIIAγ. A mixture of purified GST-TFIIAγ and GST-ATF4 was immunoprecipitated by ATF4 antibody (*lane 7*) followed by WB for TFIIAγ. *D,* nuclear extracts from ROS17/2.8 cells were mixed with equal amount of nuclear extracts from COS-7 cells overexpressing FLAG-Runx2(wt), FLAG-Runx2 (aa 1–330), FLAG-Runx2 (aa 1–286), and FLAG-Runx2 (aa 1–258), and immunoprecipitated with TFIIAγ antibody followed by WB for Runx2 (M2 antibody). Experiments were repeated 2–3 times, and qualitatively identical results were obtained.

control siRNA(low GC, catalog number 12935-200, Invitrogen) using Lipofectamine 2000 (Invitrogen) according the manufacturer's instruction. After 36 h, total RNA was harvested for quantitative real time RT-PCR analysis for *TFIIAγ, Ocn, Bsp, Opn (osteopontin),* and *Atf4* mRNAs. A second set of mouse *TFIIAγ* siRNAs (sense, AUG ACA ACA CUG UGC UAU AUU; antisense, UAU AGC ACA GUG UUG UCA UUU) was designed in the project laboratory and used to confirm the results using the first set of *TFIIAγ* siRNA.

Statistical Analysis—Results were expressed as means ± S.D. Students' *t* test was used to test for differences between two groups. Differences with a $p < 0.05$ was considered as statistically significant.

RESULTS

TFIIAγ Interacts with Runx2 and ATF4—A yeast pLexA two-hybrid system (Clontech) was used to identify proteins that bind to mouse Runx2. cDNA fragments encoding several C-terminal regions of Runx2 were subcloned into the BamHI/XhoI sites of pLexA, creating in-frame fusions with the DNA binding domain of the *LexA* gene that is controlled by the strong yeast *ADH1* promoter. Preliminary experiments using relatively larger regions of Runx2 (aa 232–391, aa 232– 428, and aa 232–517) as baits were not successful because of their ability to autoactivate the *lacZ* reporter gene in yeast. In contrast, by using the aa 263–351 region of Runx2 as a bait, we identified TFIIAγ, a general transcriptional factor involved in the initiation step of eukaryotic transcription, as a Runx2-interacting factor. A diagram and a picture of a positive colony are shown in Fig. S1.

To verify the TFIIAγ-Runx2 interaction identified by yeast two-hybrid system, we conducted pulldown assays. COS-7 cells were transiently transfected with expression vectors for FLAG-TFIIAγ, Runx2, and ATF4 (a recently identified Runx2-interacting factor). After 36 h, whole cell extracts were prepared for immunoprecipitation (IP) assay using a TFIIAγ antibody followed by Western blot analysis for Runx2 and ATF4. As seen in Fig. 1*A* (*lane 2*), Runx2 protein was present in a TFIIAγ anti-

P5 and P6) (48), and the *mOG2* gene region (+177/+311) (primers P7 and P8) (see Fig. 2*A* and Table 1). The PCR products were separated on 3% agarose gels and visualized with ultraviolet light. All ChIP assays were repeated at least three times.

siRNA—ROS17/2.8 osteoblast-like cells, which contain high levels of TFIIAγ protein, were transfected with mouse *TFIIAγ* siRNA kit (Santa Cruz Biotechnology) or negative
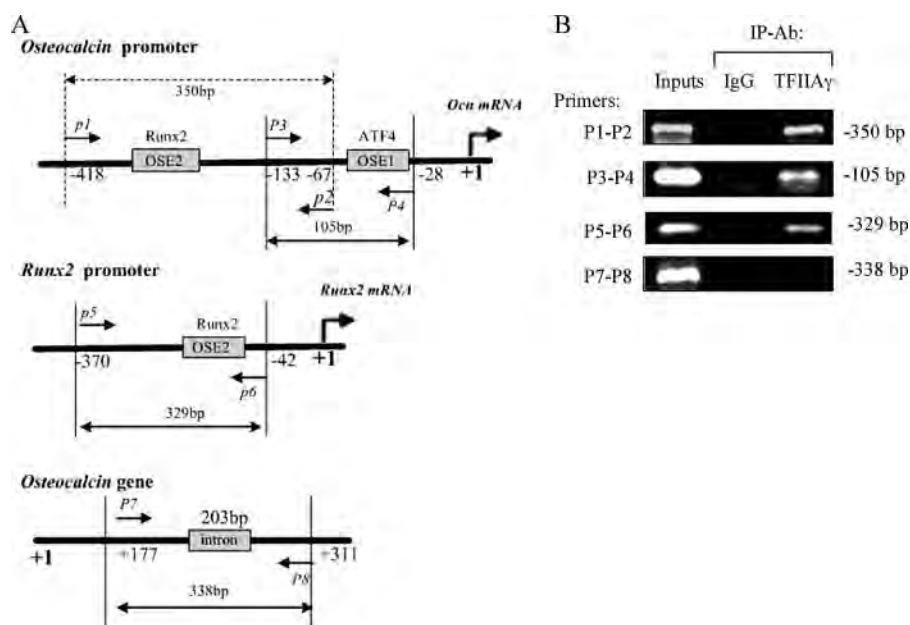
FIGURE 2. ChIP analysis of TFIIAγ interaction with Runx2/ATF4 binding sites-containing chromatin fragments of *mOG2* promoter in MC-4 cells. *A,* schematic representation of relevant regions of the *mOG2* promoter, mouse *Runx2* promoter, and *mOG2* gene. P1, P2, P3, P4, P5, P6, P7, and P8 indicate PCR primers used to analyze ChIP DNAs. The positions of these primers and the size of the fragments they amplify are indicated at the top or bottom of the figure. *B,* MC-4 cells were seeded at a density of 50,000 cells/cm² in 35-mm dishes, cultured in 10% FBS medium overnight, and cross-linked with formaldehyde for ChIP assays. IPs were conducted with TFIIAγ antibody (*Ab*) or normal control IgG. PCR products were run on 3% agarose gel and stained with ethidium bromide. Purified input chromatin was used to perform parallel PCRs with the respective primer pairs. Experiments were repeated three times with similar results.

TABLE 1
PCR primers used in ChIP assay

Oligonucleotide name	Sequence
P1	CCGCTCTCAGGGGCAGAC
P2	AGGGGATGCTGCCAGGACTAAT
P3	CACAGCATCCTTTGGGTTTGAC
P4	TATCGGCTACTCTGTGCTCTCTGA
P5	GCTATA ACCTTCTT AATGCCAG
P6	AGCACTATTACTGGAGAGACAGAATC
P7	TAGTGAACAGACTCCGGCGCTA
P8	TGTAGGCGGTCTTCA AGCCAT

body immunoprecipitate. Interestingly, anti-TFIIAγ antibody also immunoprecipitated ATF4. Reciprocal IPs showed that both Runx2 and ATF4 antibodies immunoprecipitated the FLAG-tagged TFIIAγ (Fig. 1*A*, lanes 4 and 6). To determine whether TFIIAγ can interact with Runx2 and ATF4 in osteoblasts, nuclear extracts from ROS17/2.8 cells that express high levels of Runx2, ATF4, and TFIIAγ were immunoprecipitated with anti-TFIIAγ antibody followed by Western blot analysis for Runx2, ATF4, or Fra-1 (a member of AP1 family). Results show that both Runx2 and ATF4 but not Fra-1 proteins were present in anti-TFIIAγ immunoprecipitates (Fig. 1*B*, lane 2). Reciprocal IPs showed that antibodies against Runx2 or ATF4 but not Fra-1 immunoprecipitated TFIIAγ in ROS17/2.8 cells (Fig. 1*B*, lanes 4, 6, and 8). Normal control IgG failed to significantly pull down Runx2, ATF4, or TFIIAγ in either COS-7 cells or osteoblasts. Taken together, these studies confirm that TFIIAγ interacts with Runx2 and ATF4 in osteoblasts or when coexpressed in COS-7 cells.

Although Runx2 and ATF4 interact in osteoblasts, IP assays using purified GST fusion proteins failed to show a direct phys-

ical interaction between ATF4 and Runx2 (25), suggesting that accessory factors may be involved in their interactions. To determine whether TFIIAγ can directly interact with Runx2 or ATF4 in the absence of other nuclear proteins, we mixed GST or GST-TFIIAγ with GST-ATF4 or GST-Runx2 fusion proteins purified from *Escherichia coli*, followed by IP and Western blot analysis. As shown in Fig. 1*C*, both GST-Runx2 and GST-ATF4 proteins mixed with GST-TFIIAγ were immunoprecipitated by anti-TFIIAγ antibody (*lanes 1* and *2*). Anti-Runx2 or anti-ATF4 antibody was unable to immunoprecipitate GST protein mixed with GST-Runx2 (Fig. 1*C*, *lane 3*) or GST-ATF4 (*lane 4*). Reciprocal IPs show that GST-TFIIAγ was immunoprecipitated by both anti-Runx2 or anti-ATF4 antibodies (Fig. 1*C*, *lanes 6* and *7*) but not by normal control IgG (*lane 5*). These results demonstrate that TFIIAγ directly binds to both Runx2 and ATF4.

As a first step to identify the TFIIAγ-binding domain, FLAG-Runx2 deletion mutant expression vectors (wild type aa 1–528, aa 1–330, aa 1–286, and aa 1–258) were transfected into COS-7 cells because of the high transfection efficiency. Nuclear extracts were prepared 36 h later, mixed with equal amounts of nuclear extracts of ROS17/2.8 (which contain large amounts of endogenous TFIIAγ), and immunoprecipitated using anti-TFIIAγ antibody followed by Western blot analysis for Runx2 (M2 antibody). As shown in Fig. 1*D*, deletion of Runx2 from aa 528 to aa 286 did not reduce TFIIAγ binding. However, further deletion from aa 286 to aa 258 completely abrogated TFIIAγ-Runx2 complex formation. These data clearly demonstrate the following: (i) endogenous TFIIAγ can interact with overexpressed FLAG-Runx2 proteins *in vitro*; and (ii) the aa 258–286 region of Runx2 is required for TFIIAγ binding. Interestingly, this same region is required for ATF4-Runx2 interactions (25).

To determine whether, in intact cells, TFIIAγ is associated with the endogenous *osteocalcin* gene 2 (*mOG2*) promoter region that has been shown to bind Runx2 and ATF4, we performed the chromatin immunoprecipitation (ChIP) assay using MC3T3-E1 (clone MC-4) preosteoblast cells. After shearing, soluble chromatin was immunoprecipitated with either an antibody against TFIIAγ or control IgG. The positions and sequences of primers used for PCR analysis of ChIP DNAs are shown in Fig. 2*A* and Table 1. As shown in Fig. 2*B*, the PCR bands amplified with primers P1/P2 and P3/P4 and corresponding to ChIP DNAs immunoprecipitated with TFIIAγ antibody revealed that TFIIAγ specifically interacts with chromatin fragments of the proximal *mOG2* promoter that contain Runx2- or ATF4-binding sites. Furthermore, TFIIAγ antibody
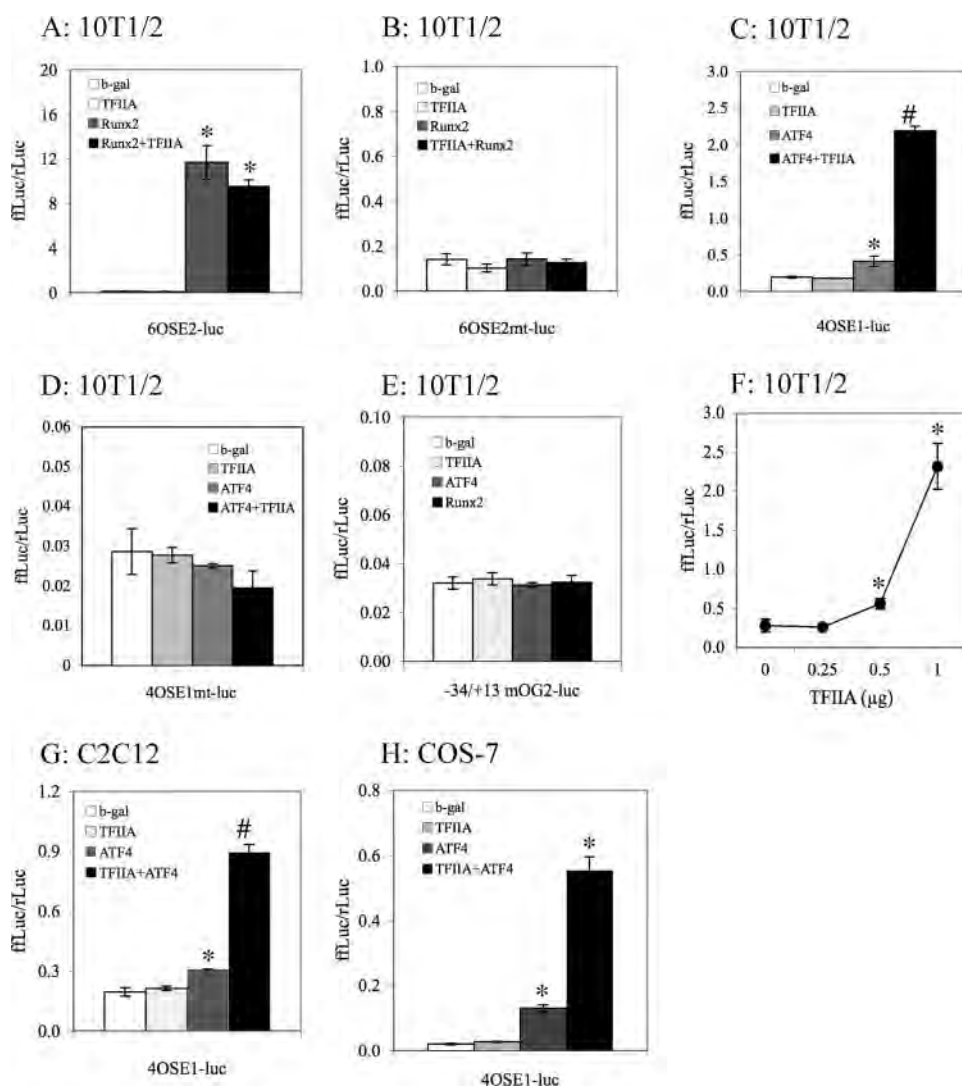
FIGURE 3. **TFIIAγ increases ATF4 but not Runx2 transcriptional activity.** *A* and *B*, 10T1/2 cells were transiently transfected with p6OSE2-luc (*A*) or p6OSE2mt-luc (*B*) and pRL-SV40 (for normalization) and expression plasmids for β-galactosidase, TFIIAγ, Runx2, or Runx2 plus TFIIAγ. After 36 h, cells were harvested for dual luciferase assay. Firefly luciferase was normalized to *Rotylenchulus reniformis* luciferase to control the transfection efficiency (*, $p < 0.01$ (β-galactosidase *versus* Runx2 or Runx2+TFIIAγ). *C* and *D*, 10T1/2 cells were transiently transfected with p4OSE2-luc (*C*) or p4OSE1mt-luc (*D*) and pRL-SV40 and expression plasmids for β-galactosidase, TFIIAγ, ATF4, or ATF4 plus TFIIAγ. *, $p < 0.01$ (β-galactosidase *versus* ATF4 or ATF4+TFIIAγ); #, $p < 0.01$(ATF4 *versus* ATF4+TFIIAγ). *E*, 10T1/2 cells were transiently transfected with −34/+13 mOG2-luc and pRL-SV40 and expression plasmids for β-galactosidase, TFIIAγ, ATF4, or Runx2. *F*, dose-response experiment, 10T1/2 cells were transiently transfected with p4OSE1-luc and pRL-SV40 and ATF4 expression plasmid and increasing amounts of TFIIAγ plasmid. *, $p < 0.01$ (β-galactosidase *versus* TFIIAγ). *G* and *H*, C2C12 (*G*) and COS-7 cells (*H*) were transiently transfected with p4OSE2-luc and pRL-SV40 and expression plasmids for β-galactosidase, TFIIAγ, ATF4, or ATF4 plus TFIIAγ. *, $p < 0.01$ (β-galactosidase *versus* ATF4 or ATF4+TFIIAγ). Data represent mean ± S.D. Experiments were repeated three times and qualitatively identical results were obtained. Note the expanded scale for the mutant reporters (*B*, *D*, and *E*) because of low basal activity to enable visualization of any potential differences as a consequence of cotransfection with the expression vectors noted above.

also immunoprecipitated a Runx2-binding site-containing chromatin fragment of the proximal *Runx2* promoter (primers P5/P6). In contrast, TFIIAγ antibody failed to immunoprecipitate a chromatin fragment of *mOG2* gene that contains no Runx2- or ATF4-binding sites (primers P7/P8). Taken together, these data show that TFIIAγ is recruited to a chromatin fragment of the *mOG2* promoter that was previously demonstrated to be bound by Runx2 and ATF4 in osteoblasts (13, 22).

TFIIAγ Increases ATF4 but Not Runx2-dependent Transcriptional Activity—To determine whether *TFIIAγ* increases Runx2- and ATF4-dependent transcriptional activity, we measured the ability of TFIIAγ to stimulate transcription of p6OSE2-luc, a reporter plasmid containing 6 copies of the Runx2-binding element OSE2 upstream of a minimal 34-bp *mOG2* promoter (13, 43, 49) or p4OSE1-luc, a reporter plasmid that contains four copies of OSE1 (a specific ATF4-binding element) upstream of a minimal 34-bp *mOG2* promoter (22, 25). For these studies, we used C3H10T1/2 fibroblasts because they contain undetectable levels of both endogenous Runx2 and ATF4 proteins (28, 49). As shown in Fig. 3*A*, as expected, Runx2 alone increased OSE2 transcriptional activity by 11-fold. This stimulation was abolished in the 6OSE2mt-luc in which the OSE2 core sequence was mutated (25) (Fig. 3*B*). Although we have shown above that TFIIAγ interacts with Runx2, TFIIAγ transfection did not activate basal or Runx2-dependent OSE2 transcription (Fig. 3*A*). As shown in Fig. 3*C*, ATF4 activated OSE1 activity about 2-fold ($p < 0.01$, β-galactosidase *versus* ATF4). Although TFIIAγ alone was unable to activate OSE1 activity, unexpectedly, when coexpressed with ATF4, it dramatically increased OSE1 activity 5-fold above ATF4 alone. This stimulation was abolished in 4OSE1mt-luc, in which the OSE1 core sequence was mutated from TTA<u>CAT</u>CA to TTA<u>GTA</u>CA in the reporter plasmid (45) (Fig. 3*D*). Note: TFIIAγ, Runx2, or ATF4 failed to activate a minimal 34-bp *mOG2* promoter that contains a TATA box (23, 50) (Fig. 3*E*). Fig. 3*F* shows that TFIIAγ activated ATF4 transcription activity in a dose-dependent manner in C3H10T1/2 cells. TFIIAγ similarly stimulated ATF4-directed OSE1 activity in C2C12 myoblasts (3-fold) and COS-7 cells (4.3-fold) (Fig. 3, *G* and *H*).

TFIIAγ Expression in Different Cell Lines—The levels of *TFIIAγ* mRNAs and proteins were determined in different cell lines by RT-PCR and Western blot analysis, respectively. As shown in Fig. 4, Western blot analysis shows that TFIIAγ protein was expressed at high levels in osteoblastic cells (MC-4

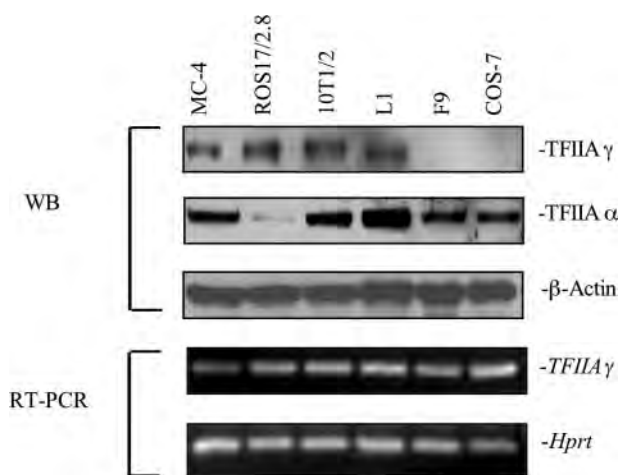FIGURE 4. **TFIIAγ expression in different cell lines.** Total RNAs or whole cell extracts were prepared from MC-4, ROS17/2.8, 10T1/2, L1, F9, and COS-7 cells and used for RT-PCR and Western blot analysis for levels of TFIIAα and TFIIAγ mRNAs and proteins. Experiments were repeated three times with similar results.

cells and ROS17/2.8), C3H10T1/2 fibroblasts, and L1 preadipocytes. In contrast, levels of TFIIAγ protein were undetectable in F9 teratocarcinoma cells and COS-7 (transformed African green monkey kidney fibroblasts). Interestingly, *TFIIAγ* mRNA was ubiquitously expressed in these cell lines. In addition, TFIIAα proteins were present in all these cell lines except for ROS17/2.8 cells, which contain a low level of TFIIAα protein.

TFIIAγ Stimulation of Endogenous Ocn mRNA Expression and the 657-bp mOG2 Promoter Activity Is Dependent upon the Presence of ATF4 and Runx2—ATF4 is an osteoblast-enriched protein that is required for late osteoblast differentiation (*i.e.* *Ocn* and *Bsp* mRNA expression) and bone formation *in vivo*. Our recent study demonstrated that ATF4 activation of *mOG2* promoter activity and *Ocn* mRNA expression was dependent upon the presence of Runx2 via a mechanism involving protein-protein interactions (25). To determine the effects of TFIIAγ on endogenous *Ocn* mRNA expression, C3H10T1/2 cells were transiently transfected with expression vectors for β-galactosidase, TFIIAγ, ATF4, Runx2, ATF4/Runx2, TFIIAγ/Runx2, TFIIAγ/ATF4, and ATF4/Runx2/TFIIAγ. After 36 h, cells were harvested for RNA preparation and quantitative real time RT-PCR detection of *Ocn* mRNA. As shown in Fig. 5*A*, consistent with its role as a master gene of osteoblast differentiation, Runx2 alone increased endogenous *Ocn* expression by 3.3-fold ($p < 0.01$; β-galactosidase *versus* Runx2). TFIIAγ alone, ATF4 alone, and TFIIAγ/ATF4 were all not sufficient for activation of endogenous *Ocn* mRNA expression. TFIIAγ alone did not enhance Runx2-dependent *Ocn* expression. As demonstrated previously (25), ATF4 dramatically stimulated Runx2-dependent *Ocn* mRNA expression by 10-fold ($p < 0.01$, Runx2 *versus* Runx2/ATF4). Importantly, TFIIAγ further augmented *Ocn* mRNA expression 4.2-fold in the presence of ATF4 and Runx2 ($p < 0.01$, ATF4/Runx2 *versus* ATF4/Runx2/TFIIAγ). TFIIAγ similarly enhanced ATF4/Runx2-dependent 657-bp *mOG2* promoter activity in C3H0T1/2 cells (3.6-fold) (Fig. 5*B*) ($p < 0.01$, ATF4/Runx2 *versus* ATF4/Runx2/TFIIAγ). This stimulation was completely abolished by point mutations in the OSE1 and/or OSE2 core sequences.

Silencing of TFIIAγ Markedly Reduces Levels of Endogenous Ocn and Bsp mRNAs and ATF4 Protein in Osteoblasts—To determine whether TFIIAγ is required for the endogenous *Ocn* mRNA expression in osteoblasts, we knocked down the endogenous *TFIIAγ* transcripts by siRNA. ROS17/2.8 osteoblast-like cells, which express high levels of *TFIIAγ* and *Ocn* and *Bsp* mRNAs, were transiently transfected with *TFIIAγ* siRNA reagent from Santa Cruz Biotechnology according to the manufacturer's instructions. This siRNA is a pool of three specific 20–25-nucleotide siRNA targeting both mouse and rat *TFIIAγ*. As shown in Fig. 6*A*, quantitative real time RT-PCR analysis showed that levels of *TFIIAγ* mRNA were efficiently reduced by *TFIIAγ* siRNA in a dose-dependent manner. The level of *Ocn* mRNA was reduced greater than 50% by *TFIIAγ* siRNA ($p < 0.01$, control *versus* *TFIIAγ* siRNA). Interestingly, *Bsp* mRNA, another ATF4 downstream target gene (22), was also reduced by 50% ($p < 0.01$, control *versus* *TFIIAγ* siRNA). This inhibition was specific because levels of *Opn* and *Atf4* mRNAs were not reduced by *TFIIAγ* siRNA. In contrast, as shown in Fig. 6*B*, levels of all these mRNAs were not reduced by the negative control siRNA (Invitrogen). Although *Atf4* mRNA was not altered by *TFIIAγ* siRNA, the level of endogenous ATF4 protein was significantly reduced by silencing *TFIIAγ* in osteoblasts (Fig. 6*C*). Similar results were obtained when a different set of *TFIIAγ* siRNA was used (Fig. S2).

Overexpression of TFIIAγ Increases the Levels of ATF4 Protein—The above studies clearly demonstrated that TFIIAγ increased ATF4-dependent transcription activity and *Ocn* gene expression probably by targeting ATF4 protein. To further study the mechanism of this regulation, we determined the effect of TFIIAγ overexpression on the levels of ATF4 protein. C3H10T1/2 cells, which express undetectable level of endogenous ATF4 protein (28), were transiently transfected with 1.0 µg of ATF4 expression plasmid and increasing amounts of TFIIAγ expression plasmid (0, 0.5, 1, and 2 µg). After 36 h, cells were harvested for Western blot analysis. As shown in Fig. 7*A*, overexpression of TFIIAγ in C3H10T1/2 cells increased the levels of ATF4 protein in a dose-dependent manner. This increase in ATF4 protein was specific because levels of Runx2 were not altered by TFIIAγ. TFIIAγ similarly elevated levels of ATF4 protein in COS-7 cells (Fig. 7*B*). Next, we determined if TFIIAγ could increase the levels of endogenous ATF4 proteins in osteoblasts. ROS17/2.8 cells were transiently transfected with indicated amount of TFIIAγ expression vector. Western blot analysis shows that TFIIAγ dose-dependently increased levels of endogenous ATF4 protein in ROS17/2.8 cells (Fig. 7*C*). Similar results were obtained in MC-4 cells (Fig. 7*D*). Interestingly, overexpression of TFIIAγ did not increase the levels of *Atf4* mRNA in all these cells examined (*bottom*, Fig. 7, *A–D*). Taken collectively, TFIIAγ markedly increased levels of ATF4 proteins in osteoblasts and non-osteoblasts.

TFIIAγ Increases ATF4 Protein Stability—Lassot *et al.* (51) recently showed that acetylase p300 markedly increased the levels of ATF4 protein and ATF4-dependent transcriptional activity by inhibiting ATF4 protein degradation via a proteasomal ubiquitin pathway. As an initial step to determine whether TFIIAγ alters ATF4 protein stability, C3H10T1/2 cells were
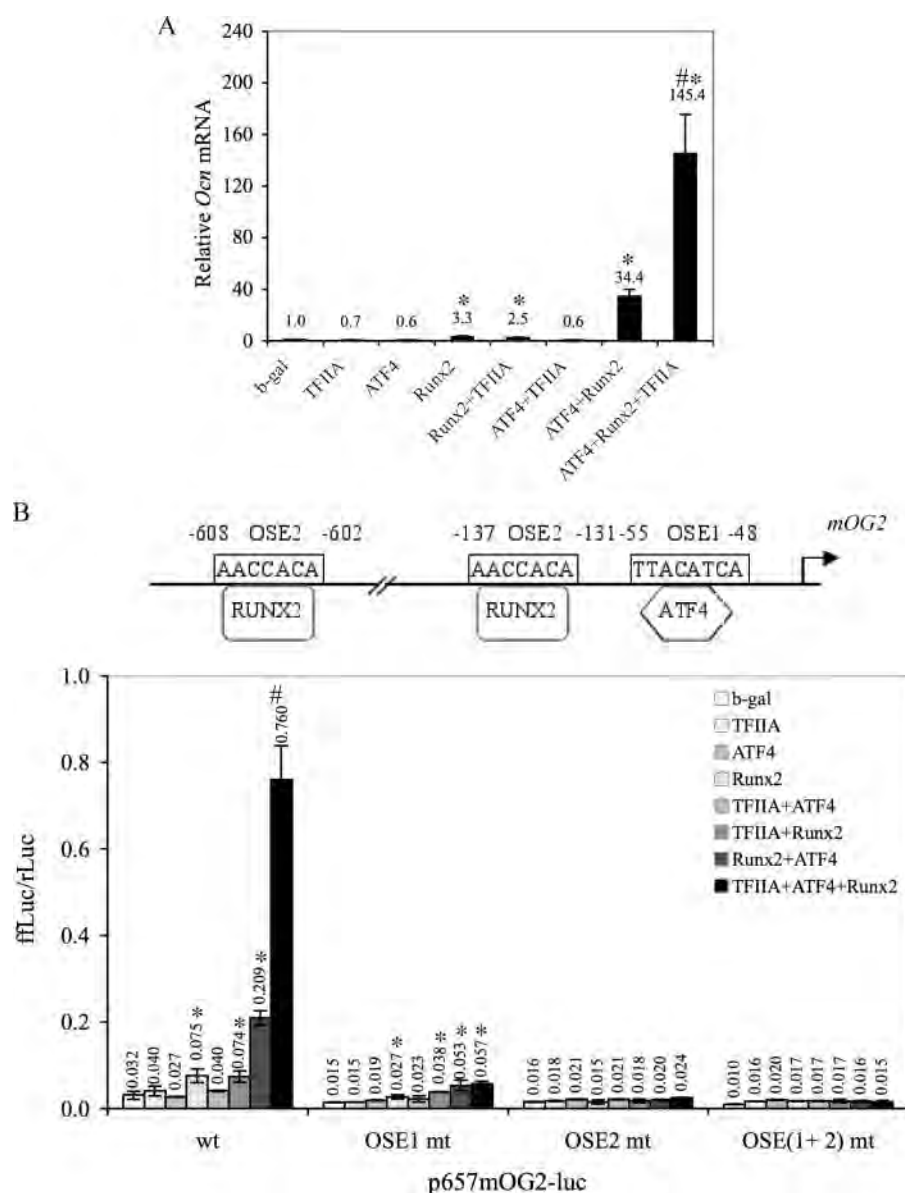
FIGURE 5. **TFIIAγ activates endogenous *Ocn* gene expression and 0.657-kb *mOG2* promoter activity in the presence of ATF4 and Runx2.** *A,* 10T1/2 cells were transfected with expression plasmids for β-galactosidase (β-gal), TFIIAγ, ATF4, Runx2, Runx2/TFIIAγ, ATF4/TFIIAγ, ATF4/Runx2, or ATF4/TFIIAγ/Runx2. After 36 h, the cells were harvested for RNA isolation and quantitative real time RT/PCR analysis for *Ocn* mRNA. *B,* 10T1/2 cells were transfected with p657mOG2-luc or p657mOG2OSE1mt-luc or p657mOG2OSE2mt-luc or p657mOG2OSE(1 + 2)mt-luc, pRL-SV40, and expression plasmids for β-galactosidase, TFIIAγ, ATF4, Runx2, Runx2/TFIIAγ, ATF4/TFIIAγ, ATF4/Runx2, or ATF4/TFIIAγ/Runx2. After 36 h, the cells were harvested for dual luciferase assay. *, $p < 0.01$ (β-galactosidase *versus* Runx2, or ATF4+Runx2 or ATF4+Runx2+TFIIAγ); #, $p < 0.01$ (ATF4+Runx2 *versus* ATF4+Runx2+TFIIAγ). Data represent mean ± S.D. Experiments were repeated 3–4 times and qualitatively identical results were obtained.

transiently transfected with ATF4 expression vector in the presence of β-galactosidase, TFIIAγ, or Runx2 expression vectors. After 36 h, cells were treated with 50 μg/ml of protein synthesis inhibitor cycloheximide (CHX) (*i.e.* to completely block *de novo* protein synthesis) and harvested at different time points of CHX addition (0, 0.5, 1, and 3 h) followed by Western blot analysis for ATF4 and Runx2. This technique has been widely used to study protein stability (51). As shown in Fig. 8*A,* in the absence of TFIIAγ overexpression, ATF4 protein was rapidly degraded and almost undetectable on Western blot by 3 h after CHX addition, which is consistent with a

previous study (51). However, overexpression of TFIIAγ greatly delayed the degradation process with the levels of ATF4 protein only slightly reduced by 3 h after CHX addition. In contrast, levels of Runx2 protein were not affected by TFIIAγ (Fig. 8*B*).

DISCUSSION

This study identifies TFIIAγ as a bridging molecule between Runx2, ATF4, and the transcription machinery in osteoblasts. Although Runx2 and ATF4 interact in osteoblasts or when coexpressed in COS-7 cells, IPs using purified GST fusion proteins were unable to demonstrate a direct physical interaction between ATF4 and Runx2 (25). Thus, accessory factors are likely involved in bridging these two molecules. Several lines of evidence support that TFIIAγ may be a factor linking Runx2 and ATF4. (i) TFIIAγ forms complexes with both Runx2 and ATF4 in osteoblasts and when coexpressed in COS-7 cells. (ii) The same region of Runx2 (*i.e.* aa 258–286) is required for both TFIIAγ-Runx2 and ATF4-Runx2 interactions. (iii) Purified GST-TFIIAγ fusion protein directly binds to both purified GST-Runx2 and GST-ATF4 fusion proteins. (iv) Overexpression of TFIIAγ in 10T1/2 cells dramatically enhances endogenous *Ocn* gene expression and the 657-bp *mOG2* promoter activity in the presence of ATF4 and Runx2. (v) siRNA knockdown of *TFIIAγ* mRNA markedly reduces osteoblast-specific *Ocn* and *Bsp* expression.

Accumulating evidence establishes that ubiquitin-proteasome pathways control osteoblast differentiation and bone formation. For example, the proteasome inhibitors epoxomicin and proteasome inhibitor-1, when administered systemically to mice, strongly stimulated bone volume and bone formation rates by greater than 70% after only 5 days of treatment (52). Although the mechanism of this regulation remains unclear, critical bone transcription factors seem to be targets for the ubiquitin-proteasomal pathway. Zhao and co-workers (52, 53) recently showed that Smurf1, an E3 ubiquitin-protein isopeptide ligase, accelerated Runx2 ubiquitin-proteasomal degradation and inhibited osteoblast differentiation and bone forma-
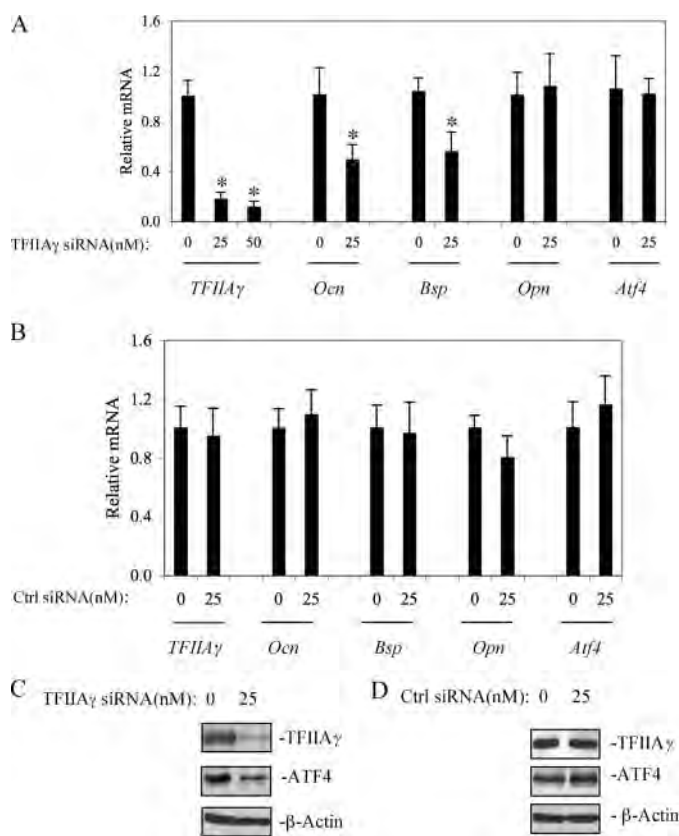
FIGURE 6. **TFIIAγ siRNA blocks endogenous *Ocn* mRNA expression in osteoblastic cells.** ROS17/2.8 osteoblast-like cells were transiently transfected with *TFIIAγ* siRNA (*A*) or negative control (*Ctrl*) siRNAs (*B*). After 36 h, total RNA or whole cell extracts were prepared for quantitative real time RT-PCR analysis for *TFIIAγ*, *Ocn*, *Bsp*, *Opn*, and *Atf4* mRNAs which were normalized to the *18 S rRNA* mRNAs or Western blot analysis for ATF4, TFIIAγ, and β-actin (*C* and *D*). *, $p < 0.01$ (control *versus* siRNA). Data represent mean ± S.D. Experiments were repeated three times with similar results.

tion *in vitro* and *in vivo*. Although *Atf4* mRNA is ubiquitously expressed, in most cells ATF4 proteins are rapidly degraded via the ubiquitin-proteasome pathway with a half-life of 30–60 min. However, this degradation pathway is less active in osteoblasts, thereby allowing ATF4 accumulation (28). Indeed, inhibition of the ubiquitin/proteasomal pathway by MG115, which blocks the N-terminal threonine in the active site of β-subunit of 26 S proteasomal complex (29, 30), led to ATF4 accumulation and induced *Ocn* mRNA expression in non-osteoblastic cells (28). Similarly, silencing of *β-TrCP1*, an E3 ubiquitin-protein isopeptide ligase that interacts with ATF4, by RNA interference, resulted in ATF4 accumulation and increased *Ocn* expression. Thus, ATF4 is a major target of the uquibitin-proteasome pathway, and modulation of ATF4 stability may play a critical role in the regulation of osteoblast-specific gene expression. Because *β-TrCP1* is present in osteoblasts (28), other factor(s) must be present in these cells to protect ATF4 from the proteasomal degradation that occurs in other cell types. Experiments from this study show that overexpression of TFIIAγ dose-dependently increases ATF4 protein in osteoblasts (ROS17/2.8 and MC-4 cells) and non-osteoblasts (C3H10T1/2 and COS-7 cells) without altering *Atf4* mRNA. Experiments using the protein synthesis inhibitor CHX further demonstrate that TFIIAγ greatly inhibits ATF4 degradation. TFIIAγ siRNA

decreases ATF4 stability in osteoblasts. Lassot *et al.* (51) recently found that ATF4 is similarly stabilized by cofactor p300, a histone acetyltransferase. p300 inhibits ATF4 ubiquitination and degradation through interaction with the ATF4 N terminus. Interestingly, this stabilization does not require either the acetyltransferase activity of p300 or the serine residue 219 in the context of DSG*XXX*S within ATF4 molecule that is known to be required for ATF4 degradation via the SCF$^{\beta TrCP}$ and the 26 S proteasome (51).

TFIIAγ stimulation of *Ocn* gene transcription is dependent on the presence of both ATF4 and Runx2. As a master regulator of osteoblast differentiation, Runx2 alone is sufficient to activate expression of many osteoblast-specific genes, including *Ocn* and *Bsp*, by direct binding to their promoters (13). In contrast, although ATF4 directly binds to the OSE1 site of the mouse *Ocn* gene and activates OSE1, it alone is not sufficient for activation of the endogenous *Ocn* gene or the 657-bp *mOG2* promoter which contains sufficient information for the bone-specific expression of *Ocn in vivo* (54). Instead, ATF4 stimulation of *Ocn* is dependent on the presence of Runx2 as demonstrated by our recent study (25). ATF4 interacts with Runx2 and activates Runx2-dependent transcriptional activity. A recent study shows that SATB2, a nuclear matrix protein that directly interacts with both ATF4 and Runx2, activates osteoblast differentiation and controls craniofacial patterning *in vivo* (55). This study shows that although TFIIAγ interacts with Runx2, it does not directly activate Runx2. Like ATF4, TFIIAγ alone is not sufficient to activate transcription from either the *Ocn* gene or the 657-bp *mOG2* promoter. In fact, even TFIIAγ and ATF4 together are not sufficient for *Ocn* gene expression without the presence of Runx2 (Fig. 5). However, in the presence of both ATF4 and Runx2, TFIIAγ greatly activates *Ocn* gene expression.

General transcription factors were originally defined as such because they were thought to be universally required for transcription. In eukaryotic cells, initiation of transcription is a complex process, which requires RNA polymerase II and many other basal transcription factors and/or cofactors, including TFIIA, TFIIB, TFIID (TBP or <u>T</u>ATA box-<u>b</u>inding <u>p</u>rotein), TFIIE, TFIIF, and TFIIH (56–59). Binding of TBP to the TATA box is the first step, which is regulated by TFIIA. TFIIA enhances transcription by interacting with TBP and stabilizing its binding to DNA (32, 33). More and more evidence shows that general transcription factors play unique roles in the regulation of tissue-specific gene expression under physiological and pathological conditions. For example, the androgen receptor , via its N-terminal AF1 domain, interacts with basal transcription factors TBP and TFIIF and activates tissue-specific transcription in target tissues and cells (60). Likewise, TAFII$_{17}$ (a component of the TFIID complex), via specific protein-protein interactions with the vitamin D receptor (VDR), increases osteoclast formation from osteoclast precursors in response to 1,25-dihydroxyvitamin D$_3$ in patients with Paget disease (61). In osteoblasts, bone transcription factors such as Runx2 and ATF4 directly bind to specific DNA sequences in their target gene promoters (*i.e.* OSE2 or NMP2 and OSE1, respectively) and activate osteoblast-specific gene expression, osteoblast differentiation, and bone formation (1, 10–14, 24, 43). Obviously,
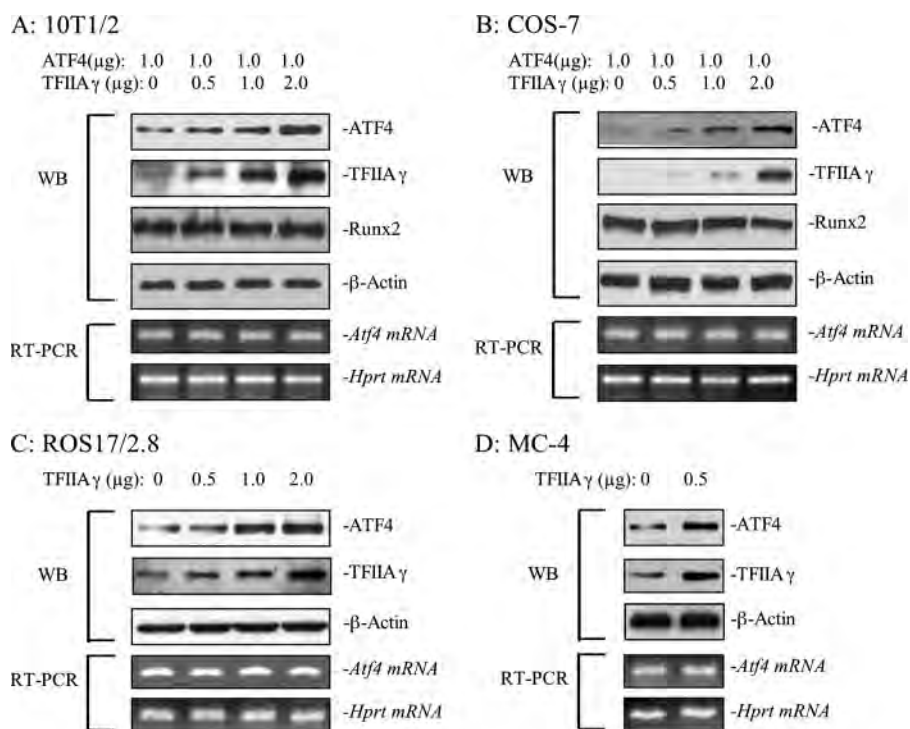
FIGURE 7. **TFIIAγ increases the levels of ATF4 protein.** C3H10T1/2 (*A*) and COS-7 (*B*) cells were transfected with 1 μg of pCMV/ATF4 or pCMV/Runx2 and increasing amounts of FLAG-TFIIAγ expression vector (0, 0.5 1, 2 μg) followed by Western blotting for ATF4, TFIIAγ, Runx2, and β-actin (*top*) or RNA preparation and RT-PCR for *Atf4* and *Hprt* mRNA (*bottom*). ROS17/2.8 (*C*) and MC-4 (*D*) cells were transfected with increasing amounts of FLAG-TFIIAγ expression vector (0, 0.5, 1, and 2 μg). Experiments were repeated three times with similar results.
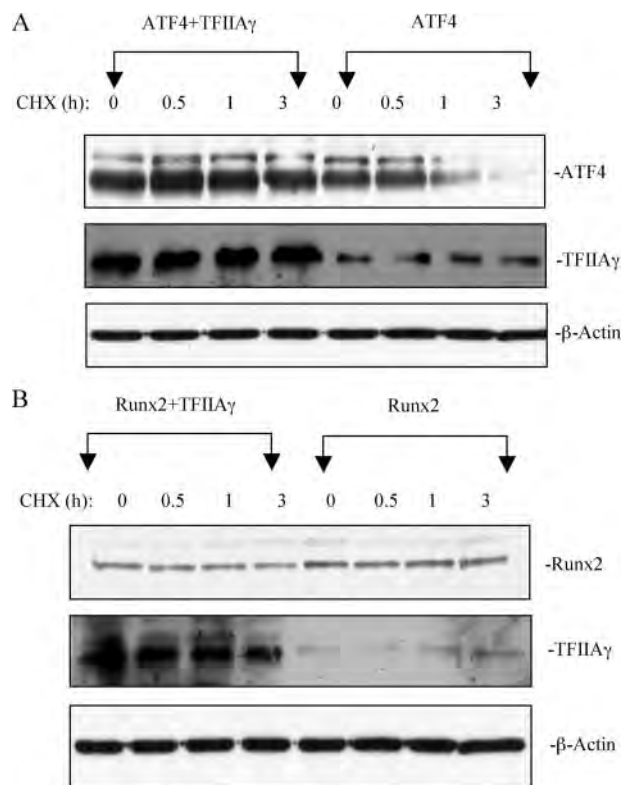
FIGURE 8. **TFIIAγ increases ATF4 protein stability.** C3H10T1/2 cells were transfected with 1.0 μg ATF4 (*A*) or Runx2 (*B*) expression vector with and without 1.0 μg of TFIIA expression vector. After 36 h, cells were treated with 50 μg/ml of protein synthesis inhibitor cycloheximide (*CHX*) and harvested at different time points (0, 1, and 3 h) followed by Western blot analysis for ATF4 and Runx2. Experiments were repeated three times with similar results.

cooperative interactions between osteoblast-specific transcription factors and basal (general) transcriptional machinery are essential for achieving maximal transcription of osteoblast-specific genes. However, little is known about these interactions. Experiments from this study demonstrate that TFIIAγ, which is expressed at high level in osteoblasts, facilitates osteoblast-specific gene expression via two mechanisms. 1) TFIIAγ stabilizes ATF4 and increases the levels of ATF4 proteins. The increased levels of ATF4 further activate Runx2 activity and *Ocn* transcription (25). 2) Through its ability to directly interact with both ATF4 and Runx2, TFIIAγ could recruit these two critical bone transcription factors to the basal transcriptional machinery and greatly enhance osteoblast-specific gene expression. In support of our observation, Guo and Stein (62) showed that Yin Yang-1 (YY1) regulates vitamin D enhancement of *Ocn* gene transcription by interfering with interactions of the VDR with both the VDR element and TFIIB. TFIIB interacts with both VDR and YY1 (63). Likewise, Newberry *et al.* (64) showed that TFIIF (RAP74 and RAP30) mediates Msx2 (a homeobox transcription factor required for craniofacial development) inhibition of *Ocn* promoter activity. Finally, a recent study showed that TFIIB could directly bind to the transactivation domain of Osterix, another important osteoblast transcription factor (65).

TFIIA consists of three subunits designated TFIIAα, TFIIAβ, and TFIIAγ. TFIIAα and TFIIAβ are produced by a specific proteolytic cleavage of the αβ polypeptide that is encoded by *TFIIA-L* (31, 33). TFIIAγ is the smallest subunit with a molecular mass of 12 kDa (42). Although it is encoded by a distinct gene (*TFIIAγ*), TFIIAγ shares a high degree of homology with TFIIAα and TFIIAβ. Interestingly, TFIIAα activates testis-specific gene expression via interactions with a tissue-specific partner, ACT (activator of CREM in testis) and CREM (34). Likewise, TFIIAα enhances human T-cell lymphotropic virus type 1 gene activation through interactions with the Tax protein, a factor associated with adult enhances human T-cell lymphotropic virus type 1 (*HTLV-1*) (35, 66). It remains to be determined whether TFIIAα and TFIIAβ can also interact with ATF4 and Runx2 and similarly activate osteoblast-specific gene expression.

It should be noted that although TFIIAγ belongs to the family of general transcription factors, its expression seems to show some tissue or cell specificity. Osteoblastic cells (MC-4 cells and ROS17/2.8), C3H10T1/2 fibroblasts, and L1 preadipocytes express high levels of TFIIAγ proteins. In contrast, the levels of TFIIAγ protein were undetectable in F9 teratocarcinoma cells
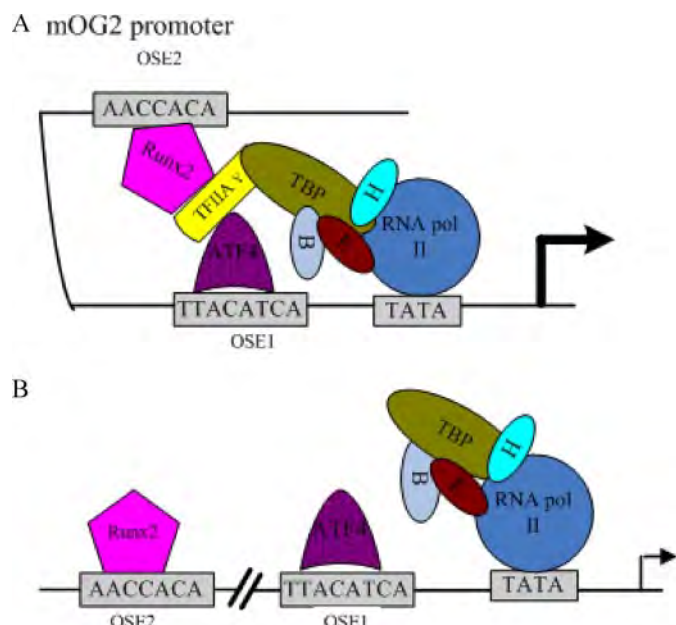
A mOG2 promoter

B

FIGURE 9. Role of TFIIAγ in osteoblast-specific *Ocn* gene expression. In osteoblasts, when the level of TFIIAγ is high (*A*), ATF4 and Runx2 are recruited to the transcriptional initiation complex of the *mOG2* promoter through direct binding to TFIIAγ, which in complex with RNA polymerase II and many other basal transcription factors and/or cofactors, including TFIIA, TFIIB, TBP (TFIID), TFIIE, TFIIF, and TFIIH, leads to an increase in transcription. In contrast, when the level of TFIIAγ is low (*B*), ATF4 and Runx2 are not recruited to the basal transcriptional machinery, resulting in a decrease in transcription. Level of TFIIAγ can be regulated by factors to be defined.

and COS-7 on Western blots. The meaning of this observation remains unknown.

These findings suggest that TFIIAγ is a critical factor regulating ATF4 stability and functions as a molecular linker between ATF4 and Runx2 and the basal transcriptional machinery. TFIIAγ may play a unique role in the regulation of osteoblast-specific gene expression and ultimately osteoblast differentiation and bone formation. A working model is proposed in Fig. 9, which summarizes the role of TFIIAγ in osteoblast-specific *mOG2* gene expression. Future study aimed at identifying factors that affect levels and activity of TFIIAγ will allow us to address the functional significance of TFIIAγ in osteoblast function in greater detail.

REFERENCES

1. Yang, S., Wei, D., Wang, D., Phimphilai, M., Krebsbach, P. H., and Franceschi, R. T. (2003) *J. Bone Miner. Res.* **18,** 705–715
2. Xiao, G., Jiang, D., Gopalakrishnan, R., and Franceschi, R. T. (2002) *J. Biol. Chem.* **277,** 36181–36187
3. Gilbert, L., He, X., Farmer, P., Rubin, J., Drissi, H., van Wijnen, A. J., Lian, J. B., Stein, G. S., and Nanes, M. S. (2002) *J. Biol. Chem.* **277,** 2695–2701
4. Krishnan, V., Moore, T. L., Ma, Y. L., Helvering, L. M., Frolik, C. A., Valasek, K. M., Ducy, P., and Geiser, A. G. (2003) *Mol. Endocrinol.* **17,** 423–435
5. Xiao, G., Gopalakrishnan, R., Jiang, D., Reith, E., Benson, M. D., and Franceschi, R. T. (2002) *J. Bone Miner. Res.* **17,** 101–110
6. Zhang, X., Sobue, T., and Hurley, M. M. (2002) *Biochem. Biophys. Res. Commun.* **290,** 526–531
7. Hurley, M. M., Tetradis, S., Huang, Y. F., Hock, J., Kream, B. E., Raisz, L. G., and Sabbieti, M. G. (1999) *J. Bone Miner. Res.* **14,** 776–783
8. Montero, A., Okada, Y., Tomita, M., Ito, M., Tsurukami, H., Nakamura, T., Doetschman, T., Coffin, J. D., and Hurley, M. M. (2000) *J. Clin. Investig.* **105,** 1085–1093
9. Yakar, S., Rosen, C. J., Beamer, W. G., Ackert-Bicknell, C. L., Wu, Y., Liu, J. L., Ooi, G. T., Setser, J., Frystyk, J., Boisclair, Y. R., and LeRoith, D. (2002) *J. Clin. Investig.* **110,** 771–781
10. Komori, T., Yagi, H., Nomura, S., Yamaguchi, A., Sasaki, K., Deguchi, K., Shimizu, Y., Bronson, R. T., Gao, Y. H., Inada, M., Sato, M., Okamoto, R., Kitamura, Y., Yoshiki, S., and Kishimoto, T. (1997) *Cell* **89,** 755–764
11. Otto, F., Thornell, A. P., Crompton, T., Denzel, A., Gilmour, K. C., Rosewell, I. R., Stamp, G. W., Beddington, R. S., Mundlos, S., Olsen, B. R., Selby, P. B., and Owen, M. J. (1997) *Cell* **89,** 765–771
12. Mundlos, S., Otto, F., Mundlos, C., Mulliken, J. B., Aylsworth, A. S., Albright, S., Lindhout, D., Cole, W. G., Henn, W., Knoll, J. H., Owen, M. J., Mertelsmann, R., Zabel, B. U., and Olsen, B. R. (1997) *Cell* **89,** 773–779
13. Ducy, P., Zhang, R., Geoffroy, V., Ridall, A. L., and Karsenty, G. (1997) *Cell* **89,** 747–754
14. Banerjee, C., McCabe, L. R., Choi, J. Y., Hiebert, S. W., Stein, J. L., Stein, G. S., and Lian, J. B. (1997) *J. Cell. Biochem.* **66,** 1–8
15. Karpinski, B. A., Morle, G. D., Huggenvik, J., Uhler, M. D., and Leiden, J. M. (1992) *Proc. Natl. Acad. Sci. U. S. A.* **89,** 4820–4824
16. Tsujimoto, A., Nyunoya, H., Morita, T., Sato, T., and Shimotohno, K. (1991) *J. Virol.* **65,** 1420–1426
17. Brindle, P. K., and Montminy, M. R. (1992) *Curr. Opin. Genet. Dev.* **2,** 199–204
18. Hai, T., Wolfgang, C. D., Marsee, D. K., Allen, A. E., and Sivaprasad, U. (1999) *Gene Expr.* **7,** 321–335
19. Meyer, T. E., and Habener, J. F. (1993) *Endocr. Rev.* **14,** 269–290
20. Sassone-Corsi, P. (1994) *EMBO J.* **13,** 4717–4728
21. Ziff, E. B. (1990) *Trends Genet.* **6,** 69–72
22. Yang, X., Matsuda, K., Bialek, P., Jacquot, S., Masuoka, H. C., Schinke, T., Li, L., Brancorsini, S., Sassone-Corsi, P., Townes, T. M., Hanauer, A., and Karsenty, G. (2004) *Cell* **117,** 387–398
23. Ducy, P., and Karsenty, G. (1995) *Mol. Cell. Biol.* **15,** 1858–1869
24. Merriman, H. L., van Wijnen, A. J., Hiebert, S., Bidwell, J. P., Fey, E., Lian, J., Stein, J., and Stein, G. S. (1995) *Biochemistry* **34,** 13125–13132
25. Xiao, G., Jiang, D., Ge, C., Zhao, Z., Lai, Y., Boules, H., Phimphilai, M., Yang, X., Karsenty, G., and Franceschi, R. T. (2005) *J. Biol. Chem.* **280,** 30689–30696
26. Hai, T., and Hartman, M. G. (2001) *Gene (Amst.)* **273,** 1–11
27. Lassot, I., Segeral, E., Berlioz-Torrent, C., Durand, H., Groussin, L., Hai, T., Benarous, R., and Margottin-Goguet, F. (2001) *Mol. Cell. Biol.* **21,** 2192–2202
28. Yang, X., and Karsenty, G. (2004) *J. Biol. Chem.* **279,** 47109–47114
29. Lee, D. H., and Goldberg, A. L. (1996) *J. Biol. Chem.* **271,** 27280–27284
30. Rock, K. L., Gramm, C., Rothstein, L., Clark, K., Stein, R., Dick, L., Hwang, D., and Goldberg, A. L. (1994) *Cell* **78,** 761–771
31. Hoiby, T., Zhou, H., Mitsiou, D. J., and Stunnenberg, H. G. (2007) *Biochim. Biophys. Acta* **1769,** 429–436
32. Zhou, H., Spicuglia, S., Hsieh, J. J., Mitsiou, D. J., Hoiby, T., Veenstra, G. J., Korsmeyer, S. J., and Stunnenberg, H. G. (2006) *Mol. Cell. Biol.* **26,** 2728–2735
33. Hoiby, T., Mitsiou, D. J., Zhou, H., Erdjument-Bromage, H., Tempst, P., and Stunnenberg, H. G. (2004) *EMBO J.* **23,** 3083–3091
34. De Cesare, D., Fimia, G. M., Brancorsini, S., Parvinen, M., and Sassone-Corsi, P. (2003) *Mol. Endocrinol.* **17,** 2554–2565
35. Duvall, J. F., Kashanchi, F., Cvekl, A., Radonovich, M. F., Piras, G., and Brady, J. N. (1995) *J. Virol.* **69,** 5077–5086
36. Zhao, C., Irie, N., Takada, Y., Shimoda, K., Miyamoto, T., Nishiwaki, T., Suda, T., and Matsuo, K. (2006) *Cell Metab.* **4,** 111–121
37. Geoffroy, V., Ducy, P., and Karsenty, G. (1995) *J. Biol. Chem.* **270,** 30973–30979
38. Stein, G. S., Lian, J. B., van Wijnen, A. J., and Stein, J. L. (1997) *Mol. Biol. Rep.* **24,** 185–196
39. Banerjee, C., Hiebert, S. W., Stein, J. L., Lian, J. B., and Stein, G. S. (1996)

Proc. Natl. Acad. Sci. U. S. A. **93,** 4968–4973

40. Lian, J. B., and Stein, G. S. (2003) *Curr. Pharm. Des.* **9,** 2677–2685
41. Roca, H., Phimphilai, M., Gopalakrishnan, R., Xiao, G., and Franceschi, R. T. (2005) *J. Biol. Chem.* **280,** 30845–30855
42. DeJong, J., Bernstein, R., and Roeder, R. G. (1995) *Proc. Natl. Acad. Sci. U. S. A.* **92,** 3313–3317
43. Xiao, G., Cui, Y., Ducy, P., Karsenty, G., and Franceschi, R. T. (1997) *Mol. Endocrinol.* **11,** 1103–1113
44. Wang, D., Christensen, K., Chawla, K., Xiao, G., Krebsbach, P. H., and Franceschi, R. T. (1999) *J. Bone Miner. Res.* **14,** 893–903
45. Jiang, D., Franceschi, R. T., Boules, H., and Xiao, G. (2004) *J. Biol. Chem.* **279,** 5329–5337
46. Wang, J., Xi, L., Hunt, J. L., Gooding, W., Whiteside, T. L., Chen, Z., Godfrey, T. E., and Ferris, R. L. (2004) *Cancer Res.* **64,** 1861–1866
47. Willis, D. M., Loewy, A. P., Charlton-Kachigian, N., Shao, J. S., Ornitz, D. M., and Towler, D. A. (2002) *J. Biol. Chem.* **277,** 37280–37291
48. Xiao, Z. S., Liu, S. G., Hinson, T. K., and Quarles, L. D. (2001) *J. Cell. Biochem.* **82,** 647–659
49. Xiao, G., Jiang, D., Thomas, P., Benson, M. D., Guan, K., Karsenty, G., and Franceschi, R. T. (2000) *J. Biol. Chem.* **275,** 4453–4459
50. Meyer, T., Carlstedt-Duke, J., and Starr, D. B. (1997) *J. Biol. Chem.* **272,** 30709–30714
51. Lassot, I., Estrabaud, E., Emiliani, S., Benkirane, M., Benarous, R., and Margottin-Goguet, F. (2005) *J. Biol. Chem.* **280,** 41537–41545
52. Garrett, I. R., Chen, D., Gutierrez, G., Zhao, M., Escobedo, A., Rossini, G., Harris, S. E., Gallwitz, W., Kim, K. B., Hu, S., Crews, C. M., and Mundy, G. R. (2003) *J. Clin. Investig.* **111,** 1771–1782
53. Zhao, M., Qiao, M., Harris, S. E., Oyajobi, B. O., Mundy, G. R., and Chen, D. (2004) *J. Biol. Chem.* **279,** 12854–12859
54. Frendo, J. L., Xiao, G., Fuchs, S., Franceschi, R. T., Karsenty, G., and Ducy, P. (1998) *J. Biol. Chem.* **273,** 30509–30516
55. Dobreva, G., Chahrour, M., Dautzenberg, M., Chirivella, L., Kanzler, B., Farinas, I., Karsenty, G., and Grosschedl, R. (2006) *Cell* **125,** 971–986
56. Nakajima, N., Horikoshi, M., and Roeder, R. G. (1988) *Mol. Cell. Biol.* **8,** 4028–4040
57. Buratowski, S., Hahn, S., Guarente, L., and Sharp, P. A. (1989) *Cell* **56,** 549–561
58. Conaway, R. C., and Conaway, J. W. (1989) *Proc. Natl. Acad. Sci. U. S. A.* **86,** 7356–7360
59. Maldonado, E., Ha, I., Cortes, P., Weis, L., and Reinberg, D. (1990) *Mol. Cell. Biol.* **10,** 6335–6347
60. Lavery, D. N., and McEwan, I. J. (2006) *Biochem. Soc. Trans.* **34,** 1054–1057
61. Kurihara, N., Reddy, S. V., Araki, N., Ishizuka, S., Ozono, K., Cornish, J., Cundy, T., Singer, F. R., and Roodman, G. D. (2004) *J. Bone Miner. Res.* **19,** 1154–1164
62. Guo, B., Aslam, F., van Wijnen, A. J., Roberts, S. G., Frenkel, B., Green, M. R., DeLuca, H., Lian, J. B., Stein, G. S., and Stein, J. L. (1997) *Proc. Natl. Acad. Sci. U. S. A.* **94,** 121–126
63. Jurutka, P. W., Hsieh, J. C., Remus, L. S., Whitfield, G. K., Thompson, P. D., Haussler, C. A., Blanco, J. C., Ozato, K., and Haussler, M. R. (1997) *J. Biol. Chem.* **272,** 14592–14599
64. Newberry, E. P., Latifi, T., Battaile, J. T., and Towler, D. A. (1997) *Biochemistry* **36,** 10451–10462
65. Hatta, M., Yoshimura, Y., Deyama, Y., Fukamizu, A., and Suzuki, K. (2006) *Int. J. Mol. Med.* **17,** 425–430
66. Clemens, K. E., Piras, G., Radonovich, M. F., Choi, K. S., Duvall, J. F., DeJong, J., Roeder, R., and Brady, J. N. (1996) *Mol. Cell. Biol.* **16,** 4656–4664

ARTICLE

Activating Transcription Factor 4 Is Critical for Proliferation and Survival in Primary Bone Marrow Stromal Cells and Calvarial Osteoblasts

Xiaoyan Zhang,[1,2] Shibing Yu,[1] Deborah L. Galson,[1] Min Luo,[1] Jie Fan,[3] Jian Zhang,[1] Youfei Guan,[2] and Guozhi Xiao[1]*

[1]*Department of Medicine, University of Pittsburgh, Pittsburgh, Pennsylvania 15240*

[2]*Department of Physiology and Pathophysiology, Peking (Beijing) University Health Science Center, Beijing 100083, China*

[3]*Department of Surgery, University of Pittsburgh, Pittsburgh, Pennsylvania 15240*

ABSTRACT

Activating transcription factor 4 (ATF4) is essential for bone formation. However, the mechanism of its actions in bone is poorly understood. The present study examined the role for ATF4 in the regulation of proliferation and survival of primary mouse bone marrow stromal cells (BMSCs) and osteoblasts. Results showed that $Atf4^{-/-}$ cells display a severe proliferative defect as measured by multiple cell proliferation assays. Cell cycle progression of $Atf4^{-/-}$ BMSCs was largely delayed with significant G1 arrest. Expression of cyclin D1 was decreased both at the mRNA and protein level. A similar proliferation defect was observed in $Atf4^{-/-}$ calvarial periosteal osteoblasts when compared with wt control. Knocking down $Atf4$ mRNA by small interfering RNA in MC3T3-E1 subclone 4 preosteoblasts markedly reduced expression of cyclin D1 and cell proliferation. In contrast, overexpression of ATF4 increased cyclin D1 expression as well as cell proliferation in $Atf4^{-/-}$ BMSCs. In addition, apoptosis was significantly increased in $Atf4^{-/-}$ BMSCs and calvarial periosteal osteoblasts relative to wt controls. Taken together, these results for the first time demonstrate that ATF4 is a critical regulator of proliferation and survival in BMSCs and osteoblasts in vitro and in vivo. J. Cell. Biochem. 105: 885–895, 2008. © 2008 Wiley-Liss, Inc.

KEY WORDS: ATF4; OSTEOBLASTS; PROLIFERATION; APOPTOSIS; CELL CYCLE; CYCLIN D1

Activating transcription factor 4 (ATF4), also known as cAMP-response element-binding protein 2 (CREB2) [Karpinski et al., 1992] and Tax-responsive enhancer element B67 (TAXREB67) [Tsujimoto et al., 1991], is a ubiquitous basic leucine-zipper transcription factor that is a member of the ATF/CREB protein family. This family includes cAMP-response element-binding protein (CREB), cAMP-response element modulator (CREM), ATF1, ATF2, ATF3, and ATF4 [Ziff, 1990; Brindle and Montminy, 1992; Meyer and Habener, 1993; Sassone-Corsi, 1994; Hai et al., 1999]. ATF4 functions as both transcriptional repressor and activator by forming homodimers and heterodimers with members of the AP-1 and C/EBP family of protein, or interacting with many other partners, such as human T-cell lymphotropic virus type 1, granulocyte colony-stimulating factor promoter element 1-binding protein, insulin-like growth factor-binding protein-1, NF-E2-related factor 2, c-maf, p300, Zhangfei, factor inhibiting ATF4-mediated transcription, special AT-rich sequence binding protein 2, transcription factor IIAγ, and runt-related transcription factor 2 [Hai and Curran, 1991; Chevray and Nathans, 1992; Nishizawa and Nagata, 1992; Vallejo et al., 1993; Vinson et al., 1993; Motohashi et al., 1997; Reddy et al., 1997; He et al., 2001; Lassot et al., 2005; Xiao et al., 2005; Yu et al., 2005, 2008b; Dobreva et al., 2006; Hogan et al., 2006]. ATF4 expression is up-regulated by several factors/stressors, including oxygen deprivation, endoplasmic reticulum stress, oxidative stress [Ameri et al., 2004; Blais et al., 2004; Roybal et al., 2005].

A role for ATF4 in bone development was established using *Atf4*-deficient mice [Yang et al., 2004]. *Atf4*$^{-/-}$ mice have a dramatically reduced bone formation rate and bone mineral density (severe osteoporosis) that persists throughout life. The expression of both *osteocalcin* (*Ocn*) and *bone sialoprotein* (*Bsp*), both markers for terminally differentiated osteoblasts, was markedly reduced in *Atf4*-deficient osteoblasts, suggesting a critical role for ATF4 in osteoblast differentiation. The *Atf4*$^{-/-}$ skeleton is much smaller relative to its wild-type (wt) control littermate, suggesting reduced numbers of bone cells. However, it is not known if ATF4 regulates osteoblast proliferation.

Cell cycle progression is a complex process that regulates cell proliferation. Cell cycle consists of several phases including G1 (from the end of the previous M phase till the beginning of DNA synthesis), S (DNA synthesis), G2 (significant protein synthesis occurs during this phase), and M phase (cell splits itself into two distinct cells) [Sherr and Roberts, 2004]. In addition, quiescent cells are in G0 phase. Cell cycle progression is a highly regulated process in that DNA replication occurs only once in each cycle. Transition from one phase to another is regulated by distinct cyclin-dependent kinases (CDKs) that are regulated by various cyclins, CDK inhibitors, and phosphorylations. Distinct cyclins and appropriate CDKs form complexes that function at different points of the cell cycle [Sherr and Roberts, 2004]. For example, formation of cyclin D1-CDK4/6 complex in early to mid G1 phase activates the kinases that phosphorylate and inactivate the tumor suppressor Rb, a critical step that is necessary for the transition from G1 to S phase [Kato et al., 1994; Sherr, 1994; Zhao et al., 2001]. The activity of cyclin E-CDK2 is periodic and maximal at the G1 to S phase transition [Roberts et al., 1994; Ohtsubo et al., 1995]. Cyclin A1 activates CDK2 and is essential at the G1/S boundary and throughout S phase [Pagano et al., 1992]. In addition, cyclin-CDK complexes also have a noncatalytic role in G1 phase by sequestering proteins of the cip/kip family, including p27^{kip} and p21^{cip}, both CDK2 inhibitors (CDKIs) that negatively regulate cell cycle progression [Hofmann and Livingston, 1996].

Apoptosis is a form of cell death in which a programmed sequence of events leads to the destruction of cells. It occurs in both physiological and pathological conditions when the body needs to eliminate aged cells, unnecessary cells, and unhealthy cells. The caspase family, a set of cysteine proteases that cleave a variety of substrates, plays a crucial role in apoptosis. Caspases are divided into two groups: "initiator" caspases such as caspase-8 and -9 and "executioner" caspases including caspase-3, -6, and -7 [Shi, 2002]. During apoptosis, after being activated by various forms of stress such as inadequate growth factor support and different types of intracellular damage, initiator caspases proteolytically cleave executioner caspases that cause cell death events such as cytoplasm shrinkage, chromatin condensation, and DNA fragmentation. B-cell lymphoma 2 (Bcl-2) is the prototype for a family of mammalian genes encoding the proteins that control mitochondrial outer membrane permeabilization (MOMP) and can be either pro-apoptotic (Bax, BAD, Bak, and Bok) or anti-apoptotic (including Bcl-2, Bcl-xL, and Bcl-w) [Adams, 2003]. *Atf4*$^{-/-}$ mice are blind due to excessive apoptosis of cells in the lens epithelium [Kato et al., 1994; Sherr and Roberts, 2004], suggesting a critical role for ATF4 in protecting these cells from apoptosis under physiological condition.

The aim of this study was to determine the effects of ATF4 in the regulation of proliferation and apoptosis in primary BMSCs and osteoblasts.

MATERIALS AND METHODS

REAGENTS

Tissue culture media were purchased from Invitrogen (Carlsbad, CA) and fetal bovine serum from HyClone (Logan, UT). Other reagents were obtained from the following sources: Antibodies against cyclins D1, D3, p21, p27, CDK2, and horseradish peroxidase-conjugated mouse or goat IgG from Santa Cruz (Santa Cruz, CA), mouse monoclonal antibody against β-actin from Sigma (St. Louis, MO), BrdU immunostaining kit (Zymed Laboratories Inc., San Francisco, CA) from Invitrogen, ApopTag Peroxidase In Situ Apoptosis Detection Kit from Chemicon (Temecula, CA). Hoechst staining reagent was kindly provided by Dr. Rentian Feng of the University of Pittsburgh. All other chemicals were of analytical grade.

Atf4–DEFICIENT MICE

Breeding pairs of ATF4 heterozygous mice were described previously [Yu et al., 2008a] and used to generate *Atf4* wild-type (wt) (*Atf4*$^{+/+}$), heterozygous (*Atf4*$^{+/-}$) and homozygous mutant (*Atf4*$^{-/-}$) mice for this study. All research protocols were approved by the Institutional Animal Care and Use Committee of the VA Pittsburgh Healthcare System, where this study was conducted.

HISTOLOGICAL EVALUATION

Six-week-old wt and *Atf4*$^{-/-}$ mice were euthanized and calvariae were fixed in 10% formalin at 4°C for 24 h, decalcified in 10% EDTA (pH 7.4) for 10 days, and embedded in paraffin. Calvariae were then bisected perpendicular to the sagittal suture through the central portion of the parietal bones, parallel to lamboidal and coronal sutures, and embedded in paraffin to obtain sections of a standard area according to the method described by Zhao et al. [2000].

CELL CULTURES AND ISOLATION OF PRIMARY BMSCs

Mouse MC3T3-E1 subclone 4 (MC-4) preosteoblasts were described previously [Xiao et al., 1997; Wang et al., 1999] and maintained in ascorbic acid-free alpha-modified Eagle's medium (alpha-MEM), 10% fetal bovine serum (FBS), and 1% penicillin/streptomycin (proliferation medium). Isolation of mouse primary BMSCs was described previously [Xiao et al., 2002]. Briefly, 6-week-old male wt and *Atf4*$^{-/-}$ mice were euthanized. Femurs and tibias were isolated and the epiphyses were cut. Marrow was flushed with alpha-MEM containing 20% FBS and 1% penicillin/streptomycin into a 100-mm dish and the cell suspension was aspirated up and down with a 20-gauge needle in order to break clumps of marrow. The cell suspension was then cultured in a T75 flask in the same medium. After 10 days, cells reached confluency and were ready for experiments.

ELECTROPORATION

Primary BMSCs were transfected using an Amaxa Nucleofector device (Cologne, Germany) as described by Nakashima et al. [2005]. Briefly, 2×10^6 BMSCs were suspended in 100 μl solution from Cell Line Nucleofector Kit V (Amaxa Biosystems, Cologne, Germany) and mixed with indicated plasmid DNAs. Cells were electroporated using the Program A-23 of the Amaxa Nucleofector device. Immediately after electroporation, cells were seeded for experiments.

MTS ASSAY

MTS assay was described previously [Singha et al., 2007]. Briefly, 1×10^4 cells/well were planted in a 96-well plate in 100 μl proliferation medium. Cells were incubated at 37°C for 24 h to allow attachment. The medium was changed every 48 h. At different time points, 20 μl of CellTitre96AQ solution reagent (Promega, Madison, WI) was added into each well and incubated for 2 h. Finally, the absorbance was recorded at 490 nm using a 96-well plate reader.

[³H] THYMIDINE INCORPORATION

Cells were plated in 12-well plates at 5×10^4 cells/well in proliferation medium for 24 h and switched to 0.1% FBS alpha-MEM for another 24 h and [³H] thymidine was then added to a final concentration of 5 μCi/ml and incubated at 37°C for 1 h in proliferation medium. Medium was removed by aspiration, and cells were washed twice with ice-cold serum-free alpha-MEM. Cell were extracted twice with 10% trichloroacetic acid (TCA) on ice for 5 min. TCA precipitates were solubilized by adding 10% SDS for 2 min at room temperature. Cells were harvested, and the amount of radioactivity was measured by liquid scintillation counting (Beckman Instruments, Inc., Fullerton, CA).

BROMODEOXYURIDINE (BrdU) INCORPORATION ASSAY

BrdU labeling reagent was purchased from Invitrogen. BrdU staining was performed using cells cultured in 8-well culture chambers (Nalgene Nunc, NY) or 10-μm sections of calvariae from wt and $Atf4^{-/-}$ mice. Cells were cultured in 8-well chamber at a density of 10^5 cells/well in 400 μl proliferation medium. After 4 days, cells from four identically treated wells per group were labeled with BrdU (1:100 dilution) overnight in the same medium. For calvarial sections, wt and $Atf4^{-/-}$ mice (6/group) were injected intraperitoneally with 100 μg bromodeoxyuridine (BrdU)/12 μg fluorodeoxyuridine (FdU) per gram of body weight 4 h before sacrifice. After sacrifice, 10-μm sections of calvariae were obtained as described previously [Demiralp et al., 2002]. To identify actively proliferating cells, nuclei that have incorporated BrdU were detected using a Zymed BrdU immunostaining kit according to the manufacturer's instruction. BrdU-positive cells on the periosteal surface of calvariae were counted and normalized to the total periosteal cell numbers in the same area [Zhao et al., 2004].

FLOW CYTOMETRIC ANALYSIS

Primary BMSCs from wt and $Atf4^{-/-}$ mice were cultured in proliferation medium for 4 days and harvested. 5×10^5 cells were suspended in 1 ml proliferation medium and Vybrant violent dye (Invitrogen) was added to a final concentration of 5 μM and incubated at 37°C for 30 min. The distribution of BMSCs throughout the cell cycle was assessed by flow cytometry using 405 nm excitation and 440 nm emission. The fraction of the population in each phase was determined as a function of DNA content using an FACS with software.

ApopTag PEROXIDASE IN SITU APOPTOSIS DETECTION

This method is based on the classical TUNEL assay to examine apoptosis by detecting DNA fragmentation. Primary BMSCs from wt and $Atf4^{-/-}$ mice were cultured in proliferation medium for 4 days and stained using the ApopTag Peroxidase In Situ Apoptosis Detection Kit according to the manufacturer's instruction. Cells were counterstained with Hematoxylin. Sections of wt and $Atf4^{-/-}$ calvariae (6/group) were prepared and stained using the same kit. Negative controls were made by omitting the terminal deoxynucleotidyl transferase (TdT). All positive (brown) and negative (blue) nuclei were counted. Apoptotic cells on the periosteal surface were counted and normalized to the total cells from the same area.

RNA ISOLATION AND REVERSE TRANSCRIPTION (RT)

Tibias (6/group) were isolated and soft tissues were removed. Tibias were frozen in liquid nitrogen and ground into powder using a mortar and pestle and total RNAs from each group were isolated using the Trizol reagent (Invitrogen) following the manufacturer's protocol. Reverse transcription (RT) was performed using 1 μg of denatured RNA and 100 pmol of random hexamers (Applied Biosystem, Foster, CA) in a total volume of 25 μl containing 12.5 U MultiScribe reverse transcriptase (Applied Biosystem).

QUANTITATIVE REAL–TIME PCR

Quantitative real-time PCR was performed on an iCycler (BIO-RAD, Minneapolis, MN) using a SYBR® Green PCR Core Kit (Applied Biosystem) and cDNA equivalent to 10 ng RNA in a 50 microliter reaction according to the manufacturer's instructions. The DNA sequences of mouse primers used for real-time PCR were: *cyclin D1* (GenBank Accession number-NM-007631), 5′ GAG GAG GGG GAA GTG GAG GA 3′ (forward, +1,049-bp), 5′ CCT CTT TGC GGG TGC CAC TA 3′ (reverse, +1,170-bp); *Foxo1*(GenBank Accession number-NM-019739), 5′ AGA GGC TCA CCC TGT CGC AGA 3′ (forward, +955-bp), 5′ GTG AAG GGA CAG ATT GTG GCG A 3′ (reverse, +1,080-bp); *Gapdh* (GenBank Accession number-NM-001001303), 5′-CAG TGC CAG CCT CGT CCC GTA GA-3′ (forward, +32-bp), 5′-CTG CAA ATG GCA GCC CTG GTG AC-3′ (reverse, +127-bp). For all primers the amplification was performed as follows: initial denaturation at 95°C for 10 min followed by 40 cycles of 95°C for 15 s and 60°C for 60 s. Melting curve analysis was used to confirm the specificity of the PCR products. Six samples were run for each primer set. The levels of mRNA were calculated by the ΔCT (the difference between the threshold cycles) method [Wang et al., 2004]. The mRNA level of each gene was normalized to *Gapdh* mRNA.

WESTERN BLOT ANALYSIS

Cells were washed with cold 1× PBS and lysed in 1× Passive Buffer (Promega) at RT for 20 min. Lysates were clarified by centrifugation (20 min, 13,000g, 4°C). For bone tissues, wt and $Atf4^{-/-}$ tibias (6/group) were frozen in liquid nitrogen and ground into powder

with a mortar and pestle. Samples were solubilized with 1× Passive Buffer for 20 min on ice and sonicated on ice (3 times, 5 s each) and lysates were then clarified by centrifugation (20 min, 13,000g, 4°C). Protein concentrations were determined by the method developed by Bio-Rad Laboratories, Inc. (Hercules, CA). Twenty-five microgram of total protein were fractionated on a 10% SDS–PAGE gel and transferred onto nitrocellulose membranes (Whatman). The membrane was blocked in 5% nonfat milk in Tris-buffered saline/ Tween-20 (TBST) buffer, probed with antibodies (1:1,000) against cyclins D1, D3, CDK2, p21, and p27 followed by incubation with anti-rabbit or anti-mouse antibodies conjugated with horseradish peroxidase (1:5,000) and visualized using an enhanced chemiluminescence kit (Pierce, Rockford, IL). Finally, blots were striped 2 times in buffer containing 65 mM Tris–Cl (pH 6.8), 2% SDS, and 0.7% (v/v) β-mercaptoethanol at 65°C for 15 min and re-probed with β-actin antibody (1:2,000) for normalization.

SMALL INTERFERING RNA (siRNA)

MC-4 cells, which contain high levels of *Atf4* mRNA, were seeded at a density of 25,000 cells/cm^2. After 24 h, cells were transfected with mouse *Atf4* siRNA (sense: 5′-GAG CAU UCC UUU AGU UUA GUU-3′; antisense: 5′-CUA AAC UAA AGG AAU GCU CUU-3′) or negative control siRNA (low GC, Cat #: 12935-200, Invitrogen) [Adams, 2007; Yu et al., 2008a] using LipofectAMINE 2000 (Invitrogen). After 48 h, cells from three identically treated dishes were pooled

and harvested for total RNA, followed by quantitative real-time RT-PCR analysis for *Atf4*, *cyclin D1* and *Foxo1* mRNAs. A second set of mouse *Atf4* siRNAs was purchased from Ambion (Cat #: AM16704, ID#: 160775 and 160776) and used to confirm the results using the first set of *Atf4* siRNA.

STATISTICAL ANALYSIS

Data was analyzed with GraphPad Prism software. Students' *t*-test was used to test for differences between two groups. A one-way ANOVA analysis was used followed by the Dunnett's test for Figures 1C, 5A–D, 6A–C, and 7A,B. Differences with a $P < 0.05$ were considered as statistically significant. All experiments were repeated a minimum of 3 times with triplicate samples.

RESULTS

ATF4 DEFICIENCY REDUCES CELL PROLIFERATION IN PRIMARY BMSCs and CALVARIAL PERIOSTEAL OSTEOBLASTS

To determine if ATF4 plays a role in the regulation of osteoblast proliferation, we performed several experiments. We first determined the effects of ATF4 deficiency on the numbers of total nucleated bone marrow cells, bone marrow from 6-week-old male wt and $Atf4^{-/-}$ mice (6/group) were isolated. After lysing the red blood cells (RBCs) using the RBC lysis buffer (Sigma), the remaining nucleated bone marrow cells were directly counted using a
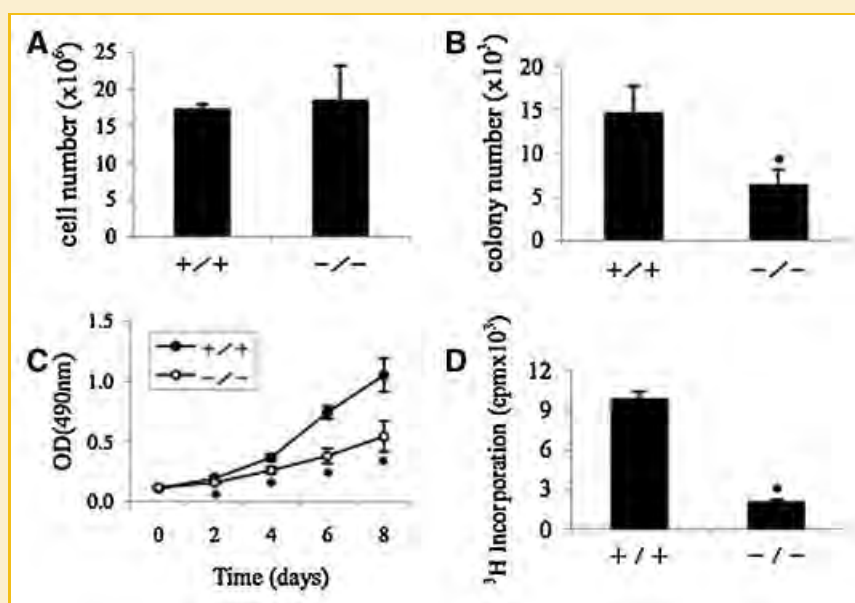

Fig. 1. ATF4 is required for primary BMSC proliferation. A: Total nucleated bone marrow cells. Long bones (two femurs and two tibias) from 6–week–old male wt and Atf4−/− mice (6 mice per group) were isolated. Bone marrow was flushed out and red blood cells (RBC) were lysed using the RBC lysis buffer. Total nucleated bone marrow cells were counted using a hemacytometer. B: Colony numbers in bone marrow. After lysing the RBCs, the remaining total nucleated bone marrow cells from each mouse (two femurs and two tibias, 6 mice/group) were diluted (1:2,000) and cultured in proliferation medium. 24 h later, the non–adhering cells were removed by washing the cells 3 times with 1× PBS. Cells were then cultured in proliferation medium for 10 days. The numbers of colonies were then counted using a microscope. C: MTS assay. Wt and $Atf4^{-/-}$ BMSCs were seeded at a density of 10^4 cells/well in 96–well plate and cultured in proliferation medium for 0, 2, 4, 6, and 8 days followed by incubation with 20 μl of CellTitre96AQ solution reagent for 2 h. The absorbance was recorded at 490 nm using a 96–well plate reader. D: [^{3}H] thymidine incorporation. wt and $Atf4^{-/-}$ BMSCs were plated in 12–well plates at 5 × 10^4 cells/well in proliferation medium for 24 h and switched to 0.1% FBS alpha–MEM for 24 h and [^{3}H] thymidine was then added to the culture (proliferation medium) to a final concentration of 5 μCi/ml and incubated at 37°C for 1 h. *$P < 0.05$ (wt vs. $Atf4^{-/-}$), Data represent mean ± SD. Experiments were repeated 3 times and qualitatively identical results were obtained.

hemacytometer. As shown in Figure 1A, although the long bones of $Atf4^{-/-}$ mice were significantly shorter and thinner than those of wt mice, surprisingly, we found no significant difference in the numbers of total nucleated bone marrow cells between wt and $Atf4^{-/-}$ mice. This might be accounted by the relatively larger marrow cavity associated with the reduced cortical and trabecular bone volume observed in the $Atf4^{-/-}$ mice. We next determined whether ATF4 deficiency affects the numbers of total bone marrow stromal cells (BMSCs). After lysing the RBCs as described above, the remaining total nucleated bone marrow cells from each mouse (two femurs and two tibias, 6 mice/group) were diluted (1:2,000) and cultured in proliferation medium. Twenty-four hours later, the non-adhering cells were removed by washing the cells 3 times with $1\times$ PBS. Cells were then cultured in proliferation medium for 10 days. The numbers of colonies from each dish were then counted using a microscope. As shown in Figure 1B, the number of BMSC colonies per mouse (from two femurs and two tibias) was significantly reduced in $Atf4^{-/-}$ group compared to values in the wt group ($P < 0.05$, wt vs. $Atf4^{-/-}$). This decrease could be explained by a cell-autonomous defect in proliferation and/or survival or could be secondary to an impaired bone microenvironment due to ATF4 deficiency. To differentiate these possibilities, we conducted MTS and [^{3}H] thymidine incorporation assays. For the MTS assay, 10^4 cells/well of wt and $Atf4^{-/-}$ BMSCs were seeded in 96-well plate and were cultured in proliferation medium for 0, 2, 4, 6, and 8 days. Cell numbers were then measured as described previously [Singha et al., 2007]. As shown in Figure 1C, ATF4-deficient cells grew at significantly reduced rates compared to wt cells. For the [^{3}H] thymidine incorporation assays, wt and $Atf4^{-/-}$ BMSCs were cultured in proliferation medium for 4 days and labeled with [^{3}H] thymidine for 1 h before harvesting. As shown in Figure 1D, [^{3}H] thymidine incorporation into the DNA of $Atf4^{-/-}$ BMSCs was decreased by fourfold compared to values in wt cells ($P < 0.05$, wt vs. $Atf4^{-/-}$). It should be noted that the adherent murine BMSC population is contaminated with macrophages, however, macrophages and their precursors would be less proliferative under the culture conditions used, consequently, the proliferation measured is primarily that of BMSCs. To determine if ATF4 is required for osteoblast proliferation in vivo, 6-week-old wt and $Atf4^{-/-}$ mice were injected with bromodeoxyuridine (BrdU)/fluorodeoxyuridine (FdU) 4 h before sacrifice, 10-μm sections of calvariae were obtained, and proliferating cells from the periosteal surface were counted and normalized to total cells from the same area. As shown in Figure 2A, in wt calvariae, periosteal osteoblasts proliferated very actively with 60% of the total cells being BrdU-positive. In contrast, the percent BrdU-positive osteoblasts were significantly reduced in $Atf4^{-/-}$ calvariae ($P < 0.05$, wt vs. $Atf4^{-/-}$) (Fig. 2B,C). It should be noted that very few osteocytes (mature osteoblasts) that permeate the bone matrix were stained BrdU-positive in both wt and $Atf4^{-/-}$ calvariae. Thus, ATF4 is required for the proliferation of BMSCs or osteoblasts both in vitro and in vivo.

ATF4 IS REQUIRED FOR CELL CYCLE PROGRESSION AND CYCLIN D1 EXPRESSION

To determine whether ATF4 is required for cell cycle progression, we performed flow cytometric analysis to compare the cell distribution
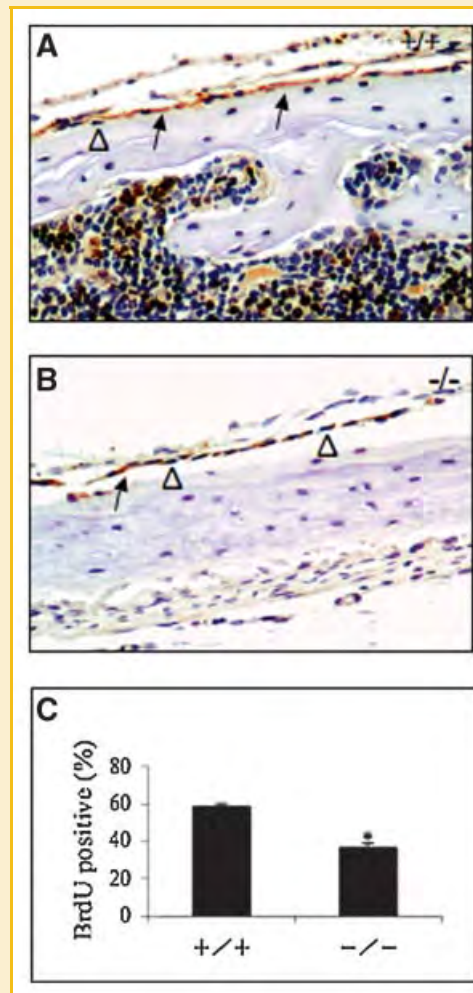

Fig. 2. ATF4 is required for proliferation of calvarial periosteal osteoblasts in vivo. Six-week-old male wt (A) and $Atf4^{-/-}$ (B) mice (6 mice per group) were injected intraperitoneally with 100 μg bromodeoxyuridine (BrdU)/12 μg fluorodeoxyuridine (FdU) per gram of body weight 4 h before sacrifice. After sacrifice, sections of calvariae were obtained. C: BrdU positive cells on the periosteal surface of calvariae were counted and normalized to the total cells from the same area. $^*P < 0.05$ (wt vs. $Atf4^{-/-}$). Data represent mean $\pm$ SD. Arrows indicate BrdU-positive (proliferating) cells and Δ indicates BrdU-negative (nonproliferating) cells. [Color figure can be viewed in the online issue, which is available at www.interscience.wiley.com.]

across different phases of the cell cycle between wt and $Atf4^{-/-}$ BMSCs. As shown in Figure 3, ATF4-deficient cells showed a significant decrease in the cell distribution into both S and G2/M phases (32% and 45% change, respectively) when compared with values of wt control cells ($P < 0.05$, wt vs. $Atf4^{-/-}$). In contrast, the fraction of the cells in G1 was not reduced by ATF4 deficiency ($P > 0.05$, wt vs. $Atf4^{-/-}$). Cell-cycle progression from one phase to another is controlled by cyclin-dependent kinases (CDKs) whose activity is mainly regulated by distinct cyclins and cyclin-dependent kinase inhibitors (CDKIs). We examined the effects of ATF4 deficiency on the expression levels of critical cyclin D1, a major regulator of cell cycle progression and cell proliferation, and CDKIs. Wt and $Atf4^{-/-}$ BMSCs were cultured in proliferation medium for
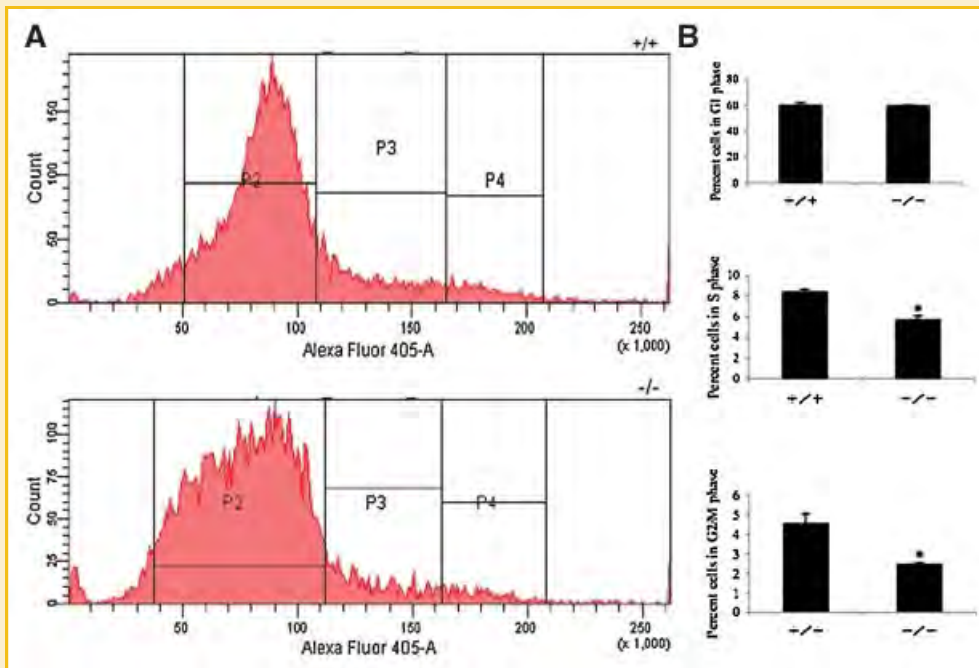
Fig. 3. ATF4 deficiency attenuates cell cycle progression. 5×10^5 wt (A, top) and Atf4−/− (A, bottom) BMSCs were suspended in 1.0 ml proliferation medium and labeled using the Vybrant DyeCycle Violet Stain Kit according to the manufacturer's instruction (Invitrogen). Cell population of different cell cycle phases was then measured by flow cytometry using 405 nm excitation and 440 nm emission. Quantitative data are presented in panel B. $^*P < 0.05$ (wt vs. Atf4$^{-/-}$). Data represent mean $\pm$ SD. Experiments were repeated 3 times and qualitatively identical results were obtained. P2, P3, and P4 represent cell population of G1, S and G2/M phases, respectively. It should be noted that scales are different from +/+ and −/−. [Color figure can be viewed in the online issue, which is available at www.interscience.wiley.com.]

4 days followed by Western blot analysis for cyclin D1, CDK2, p21, and p27. As shown in Figure 4A, the protein level of cyclin D1 was markedly decreased in $Atf4^{-/-}$ cells relative to wt control. In contrast, the level of p21 protein was slightly increased in $Atf4^{-/-}$ cells. Levels of both p27 and CDK2 proteins were low in BMSCs and their relative abundance did not display any significant difference between wt and $Atf4^{-/-}$ cells. Quantitative real-time RT/PCR analysis shows that the level of *cyclin D1* mRNA was reduced by 52% in $Atf4^{-/-}$ cells compared to values in wt controls ($P < 0.05$, wt vs. $Atf4^{-/-}$) (Fig. 4B). Note: as expected, minimal *Atf4* mRNA was detected by real-time RT/PCR in $Atf4^{-/-}$ cells (Fig. 4B, top).

To determine whether ATF4 is required for proliferation of the pre-osteoblast cell line, MC-4, which expresses high levels of *Atf4* mRNA and protein, the cells were transiently transfected with the indicated concentrations of *Atf4* siRNA or negative control siRNA (Invitrogen). This siRNA specifically targets mouse *Atf4* mRNA [Adams, 2007; Yu et al., 2008a]. As shown in Figure 5A, levels of *Atf4* mRNA were efficiently reduced by *Atf4* siRNA in a dose-dependent manner. In contrast, the negative control (40 nM) did not reduce *Atf4* mRNA. Importantly, the level of *cyclin D1* mRNA was significantly reduced by *Atf4* siRNA in a dose-dependent manner (Fig. 5B). Conversely, the level of *Foxo1* mRNA, a factor of the forkhead transcription factor family, was not reduced by *Atf4* siRNA (Fig. 5C). Furthermore, knocking-down *Atf4* mRNA markedly reduced MC-4 proliferation as measured by both MTS (Fig. 5D) and BrdU incorporation assays (Fig. 5E–G) ($P < 0.05$, ctrl siRNA vs. *Atf4* siRNA). Similar results were obtained when a different set of *Atf4* siRNAs was used in MC-4 cells (data not shown).

OVEREXPRESSING ATF4 RESCUES THE DEFECT IN CELL PROLIFERATION IN $Atf4^{-/-}$ BMSCs

We next determined whether overexpression of ATF4 could increase cell proliferation in BMSCs. To this end, we used a Cell Line
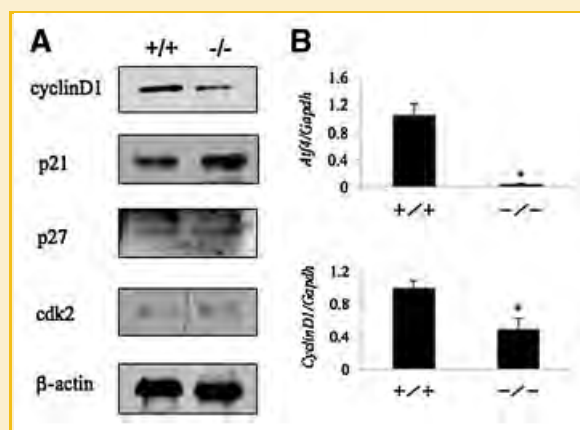

Fig. 4. ATF4 deficiency decreases cyclins D1 expression in primary BMSCs. A: Western blot analysis. wt and $Atf4^{-/-}$ BMSCs were seeded at a density of 5×10^4 cells/cm^2 in 35-mm dish and cultured in proliferation medium for 4 days. Whole cell extracts were used for Western blot analysis for cyclin D1, p21, p27, CDK2, and beta-actin (for loading). B: Quantitative real-time RT/PCR. wt and $Atf4^{-/-}$ BMSCs were treated as in (A) and harvested for RNA isolation and quantitative real-time RT/PCR analysis for cyclin D1 and Atf4 mRNAs that were normalized to Gapdh mRNA. $^*P < 0.05$ (wt vs. $Atf4^{-/-}$). Experiments were repeated 3 times and qualitatively identical results were obtained.
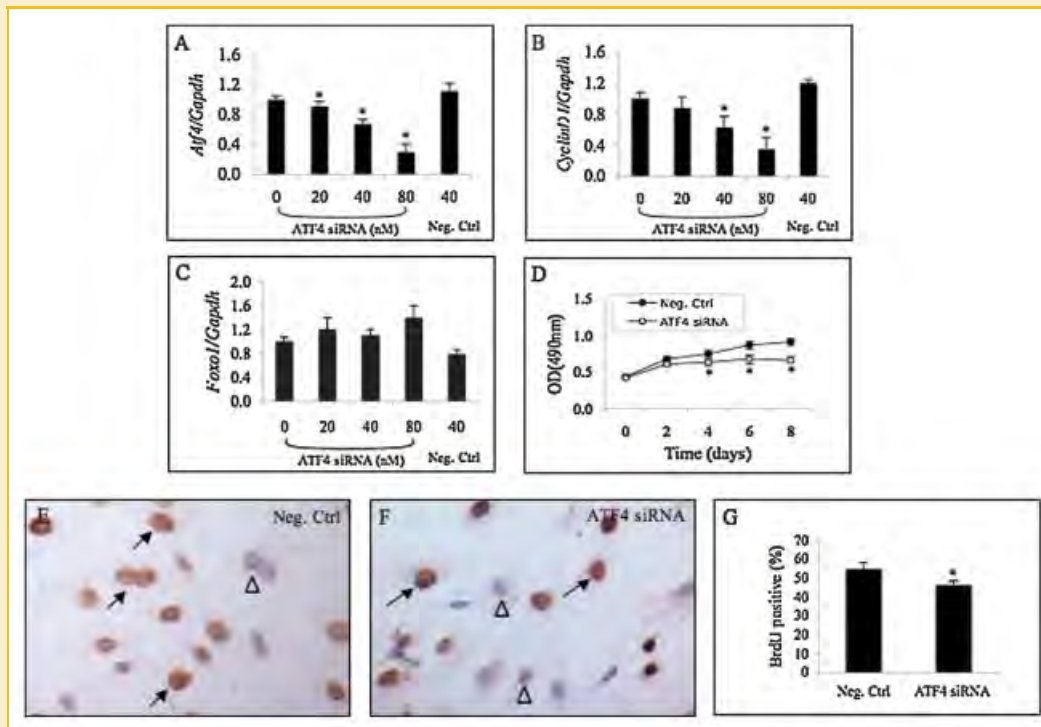
Fig. 5. ATF4 siRNA blocks endogenous cyclin D1 expression and inhibits cell proliferation in MC-4 Cells. A–C: Quantitative real-time RT/PCR. MC-4 cells were seeded at a density of 5×10^4 cells/cm^2 in 35-mm dish and transiently transfected with ATF4 siRNA (0, 20, 40, 80 nM) or negative control siRNA (40 nM). After 48 h, total RNA was prepared for quantitative real-time RT-PCR analysis for Atf4, cyclin D1 and Foxo1 mRNAs that were normalized to Gapdh mRNA. D: MTS assay. MC-4 cells were first seeded at a density of 5×10^4 cells/cm^2 in 100-mm dish and transiently transfected with 40 nM ATF4 siRNA or negative control siRNA. After 24 h, cells were re-seeded at 10^4 cells/well in 96-well plate in proliferation medium for indicated times followed by MTS assay. E–G: BrdU staining. MC-4 cells were seeded at 10^5 cells/well in 8-well chamber and transiently transfected with 40 nM ATF4 siRNA or negative control siRNA and cultured in proliferation medium for 4 days followed by BrdU staining. $^*P < 0.05$ (control siRNA vs. ATF4 siRNA). Data represent mean ± SD. Experiments were repeated at least 3 times and qualitatively identical results were obtained. Arrows indicate BrdU-positive (proliferating) cells and Δ indicates BrdU-negative (non-proliferating) cells. [Color figure can be viewed in the online issue, which is available at www.interscience.wiley.com.]

Nucleofector Kit V and a Nucleofector Device from Amaxa Biosystem (Cologne, Germany) because primary mouse BMSCs were transfected with higher than 40% efficiency by using this method (data not shown). To determine the effects of ATF4 overexpression on cyclins expression, $Atf4^{-/-}$ BMSCs were electroporated with increasing amounts of FLAG-ATF4-YFP expression vector (0, 0.5, 1, and 2 μg) [Xiao et al., 2005]. Thirty hours later, cells were harvested for the preparation of total RNA or protein. In addition, as shown in Figure 6A, Atf4 mRNA was efficiently expressed in primary BMSCs in a dose-dependent manner. As shown in Figure 6B,D, ATF4 dose-dependently stimulated cyclin D1 expression both at the mRNA and protein level. In contrast, overexpressing ATF4 failed to elevate the level of cyclin D3 mRNA and protein (Fig. 6C,D). As shown in Figure 7, ATF4 overexpression significantly increased the rate of proliferation in $Atf4^{-/-}$ BMSC as measured by direct cell count, MTS assay, and BrdU staining ($P < 0.05$, ctrl vs. ATF4). Overexpressing ATF4 similarly increased cyclin D1 expression and cell proliferation in wt BMSCs (data not shown).

Taken together, these results clearly establish that ATF4 increases cell proliferation probably via promoting expression of cyclin D1 and cell cycle progression.

ATF4 DEFICIENCY INCREASES CELL APOPTOSIS

ATF4 is known to prevent lens epithelium from apoptosis [Tanaka et al., 1998; Hettmann et al., 2000]. As an initial step to determine if ATF4 regulates apoptosis in BMSCs, wt and $Atf4^{-/-}$ cells were cultured in proliferation media for 4 days and stained by the Hoechst method [Yamanaka et al., 2003]. As shown in Figure 8A–C, the numbers of apoptotic cells including those with shrinking cytoplasm and chromatin condensation (early apoptosis) and DNA fragmentation (late apoptosis) were increased greater than fivefold in $Atf4^{-/-}$ BMSCs compared to wt cells ($P < 0.05$, wt vs. $Atf4^{-/-}$). To confirm this finding, wt and $Atf4^{-/-}$ BMSCs were stained using the ApopTag Peroxidase In Situ Apoptosis Detection Kit, a modified TUNEL staining that measures DNA fragmentation in situ. As shown in Figure 8D–F, the percent apoptotic cells in $Atf4^{-/-}$ BMSCs were increased by 1.6-fold when compared to wt cells ($P < 0.05$, wt vs. $Atf4^{-/-}$). To determine if ATF4 deficiency increases osteoblast apoptosis in vivo, 10-μm calvarial sections from wt and $Atf4^{-/-}$ mice were obtained and stained using the same kit. Apoptotic cells that stained brown on the periosteal surface of calvariae were counted and normalized to total cells of the same periosteal surface. As shown in Figure 8G–I, a significant increase in apoptosis was found in $Atf4^{-/-}$ mice compared to wt controls ($P < 0.05$, wt vs.
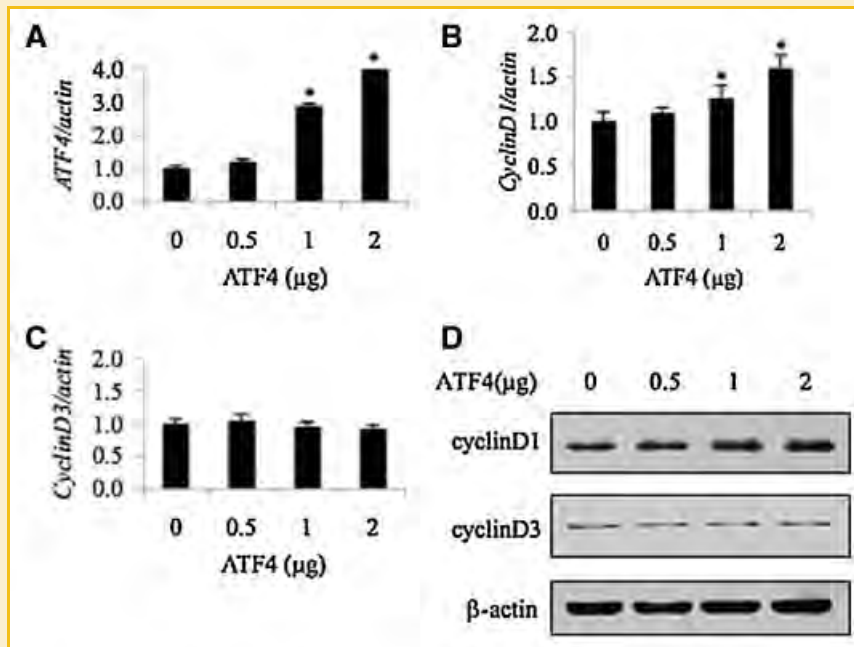
Fig. 6. Overexpression of ATF4 increases cyclin D1 expression. A–C: Quantitative real-time-RT/PCR. $Atf4^{-/-}$ BMSCs (2×10^6 cells/group) were electroporated with increasing amounts of FLAG–ATF4–YFP expression vector (0, 0.5, 1, and 2 μg). The amount of plasmid DNAs was balanced as necessary with beta–galactosidase expression plasmid such that the total DNA was constant in each group. Thirty hours later, cells were harvested for the preparation of total RNA and quantitative real–time RT/PCR analysis. D: Western blot analysis. Cells were treated as in (A) and harvested for whole cell extracts preparation and Western blot analysis. $^*P < 0.05$ (beta–gal vs. ATF4). Data represent mean ± SD. Experiments were repeated at least 3 times and qualitatively identical results were obtained.

$Atf4^{-/-}$). Thus, ATF4 protects osteoblasts from apoptosis under physiological condition.

DISCUSSION

In this study, we used two complementary approaches to establish the requirement for ATF4 in the regulation of proliferation in primary BMSCs and a preosteoblast cell line (MC-4 cells): (i) loss-of-function studies using $Atf4^{-/-}$ or $Atf4$ siRNA-treated cells demonstrate that cell proliferation is significantly reduced in the absence of ATF4; and (ii) gain-of-function experiments via overexpression of ATF4 show that ATF4 enhances osteoblast proliferation in both wt and $Atf4^{-/-}$ BMSCs. In addition, this study reveals that ATF4 protects osteoblasts against apoptosis. Thus, the reduced bone mass
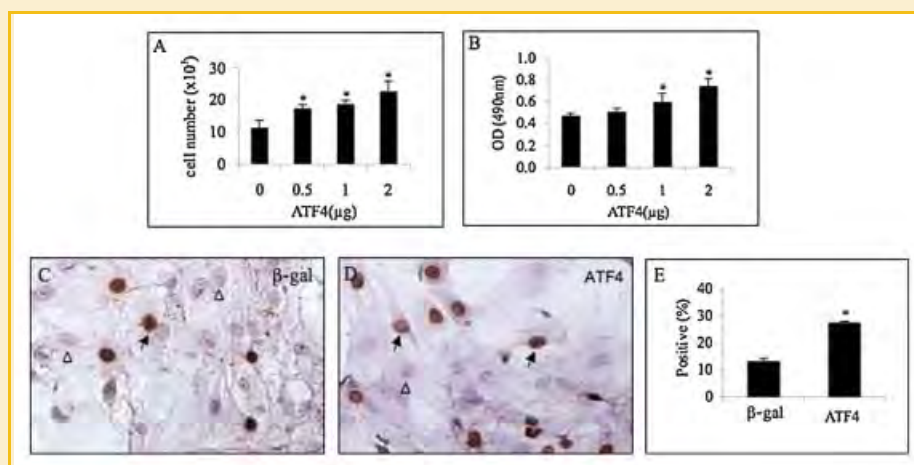

Fig. 7. Overexpression of ATF4 increases BMSC proliferation. A: Direct cell count. $Atf4^{-/-}$ BMSCs were electroporated as in Figure 6A. 5×10^3 cells/well were seeded in 96-well plates in proliferation medium for 4 days followed by direct cell count using a hemacytometer. B: MTS assay. Cells were electroporated as in Figure 6A. After electroporation, cells were used for the MTS assay as in Figure 1C. C–E: BrdU staining. Cells were electroporated as in Figure 6A. After electroporation, cells were used for the BrdU staining. $^*P < 0.05$ (beta–gal vs. ATF4). Data represent mean ± SD. Experiments were repeated at least 3 times and qualitatively identical results were obtained. Arrows indicate BrdU–positive (proliferating) cells and Δ indicates BrdU–negative (nonproliferating) cells. [Color figure can be viewed in the online issue, which is available at www.interscience.wiley.com.]
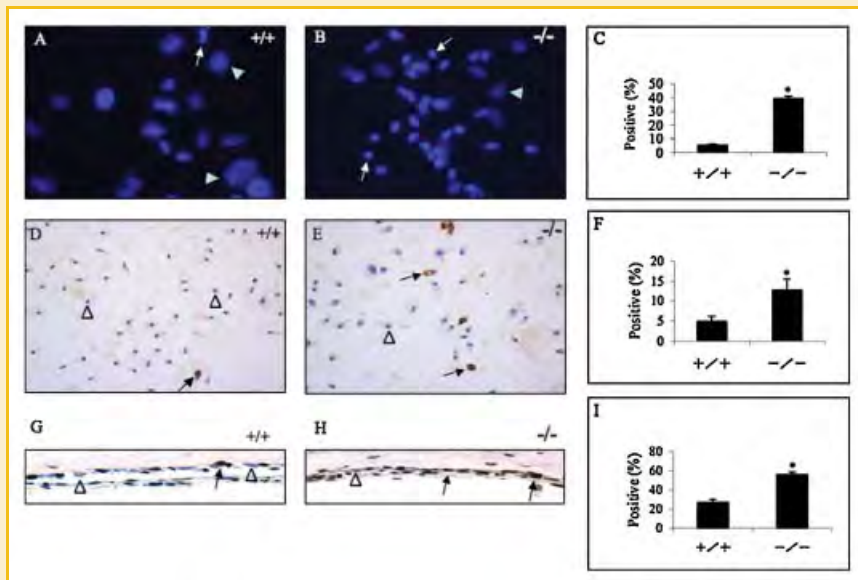
Fig. 8. ATF4 deficiency increases apoptosis in osteoblasts. A–C: Hoechst staining. wt and $Atf4^{-/-}$ BMSCs were seeded at a density of 5×10^4 cells/cm^2 in 35-mm dishes, cultured in proliferation medium for 4 days, and incubated with 1 μl of Hoechst dye at 37°C for 30 min. Cell images were obtained under UV light using a microscope (Olympus IX70). D–F: Apoptosis assay in BMSCs. wt and $Atf4^{-/-}$ BMSCs were seeded at 10^5 cells/well in 8-well chamber, cultured in proliferation medium for 4 days, and stained using the ApopTag Peroxidase In Situ Apoptosis Detection Kit according the manufacturer's instruction. G–I: Apoptosis assay in calvarial sections. Sections of calvariae from 6-week-old male wt and $Atf4^{-/-}$ mice (6 mice per group) were stained using the same kit. $P < 0.05$ (wt vs. $Atf4^{-/-}$). Data represent mean $\pm$ SD. Arrows indicate apoptotic cells and indicates nonapoptotic cells. [Color figure can be viewed in the online issue, which is available at www.interscience.wiley.com.]

and bone mineral density observed in ATF4 knock-out mice could be at least in part caused by decreased proliferation and increased apoptosis of $Atf4^{-/-}$ osteoprogenitors and osteoblasts.

While our results clearly show that the proliferation rate was significantly decreased in $Atf4^{-/-}$ BMSCs or $Atf4$ siRNA-treated MC-4 cells (Figs. 1C and 5D), the magnitude of inhibition of cell proliferation by $Atf4$ siRNA in MC-4 cells was markedly lower compared to that in $Atf4^{-/-}$ BMSCs. This discrepancy is likely due to our observation that the control siRNA treatment of MC-4 cells non-specifically reduces cell proliferation, which could mask the inhibitory effect of the $Atf4$ siRNA on cell proliferation. In addition, the $Atf4$ siRNA may not completely knock down the $Atf4$ mRNA in MC-4 cells.

Previous studies established that ATF4 is critical for osteoblast differentiation as demonstrated by dramatically reduced expression of osteocalcin and bone sialoprotein mRNA in ATF4-deficient mice [Yang et al., 2004]. The present study demonstrates an essential role for ATF4 in the regulation of BMSC and osteoblast proliferation. $Atf4^{-/-}$ BMSCs and osteoblasts proliferate at a dramatically reduced rate compared to wt cells both in vitro and in vivo. Overexpressing ATF4 in $Atf4^{-/-}$ BMSCs rescues the proliferative defect. Expression of cyclin D1 is highly dependent upon the presence of ATF4 as demonstrated by the dramatic reduction in its mRNA and protein in $Atf4^{-/-}$ BMSCs. Reduced expression of cyclin D1 and possibly other cyclins in $Atf4^{-/-}$ cells leads to a lack of progression from G1 into the S and G2/M phases of the cell cycle. Since the percentage of the population in G1 is not affected by ATF4 deficiency, there must be concomitantly an increase in the percentage of G0 cells (quiescent cells) and/or cells undergoing cell death, thereby reducing overall cell proliferation.

Cyclin D1 is a key sensor and integrator of extracellular signals of cells and plays a critical role in cell cycle progression and proliferation [Stacey, 2003]. The expression level of cyclin D1 has been shown to be rate-limiting in cell proliferation induced by a variety of stimuli [Zhao et al., 2001]. Our results show that ATF4 is a key regulator of cyclin D1 expression in BMSCs or osteoblasts. Levels of cyclin D1 mRNA and protein are significantly reduced in the absence of ATF4. Forced expression of ATF4 efficiently augmented the level of cyclin D1 mRNA as well as cell proliferation in both wt and $Atf4^{-/-}$ cells. Mechanisms whereby ATF4 increases cyclin D1 mRNA remain to be determined. An ATF/CRE site located in the proximal region of cyclin D1 promoter was reported to bind to CREB and AP1 proteins and mediate active transcription of the gene [Sabbah et al., 1999; Nagata et al., 2001; Datta et al., 2007]. It is likely that ATF4 directly binds to this ATF/CRE site and activates transcription. It is also probable that ATF4 activates the cyclin D1 promoter through interactions with CREB and AP1 proteins. Finally, ATF4 can stabilize cyclin D1 mRNA through post-transcriptional mechanisms. Future study will differentiate these possibilities.

The periosteal surface of calvariae is mainly occupied by four cell types: osteoblasts or osteoprogenitors, bone lining cells, and osteoclasts. In rapidly growing animals, osteoblasts or osteoprogenitors are the major cells that cover the surface. In contrast, bone lining cells occupy the majority of the surface in adult or aged bones that have reached peak bone mass. Calvaria, which does not involve endochondral bone formation, has a relatively simple structure relative to other bones such as long bones and vertebrae. In addition, it is easy to histologically localize the osteoprogenitors/osteoblasts on the periosteal surface of calvaria. Therefore, it provides a unique model system for studying the functions of osteoblasts in vivo.

Using this model system, we found that osteoblasts from wt 6-week-old mice proliferate very actively on the periosteal surface (Fig. 2A). Conversely, proliferation of $Atf4^{-/-}$ osteoblasts is significantly reduced (Fig. 2B,C). Thus, an in vivo role for ATF4 in osteoblast proliferation is established. In support of our findings, Masuoka and Townes [2002] showed that $Atf4^{-/-}$ mice have severe fetal anemia due to impaired fetal-liver definitive hematopoiesis associated with a proliferative defect in fetal-liver cells. Furthermore, primary murine embryonic fibroblasts (MEFs) from $Atf4^{-/-}$ mice also display a defect in proliferation [Masuoka and Townes, 2002]. Lastly, transgenic overexpression of ATF4 in the developing lens results in hyperproliferation of lens fiber cells [Hettmann et al., 2000]. These results suggest that ATF4 is critical for proliferation of rapidly growing cells (i.e., BMSCs, osteoblasts, fetal-liver cells, MEFs, and lens fiber cells). Consistent with this notion, ATF4 is usually expressed at high level in rapidly growing tissues or cells [Tanaka et al., 1998; Hettmann et al., 2000; Masuoka and Townes, 2002; Yang et al., 2004].

The numbers of osteoblasts are eventually determined by the relative rate of cell proliferation and death by apoptosis. Experiments from this study establish that ATF4 is anti-apoptotic in BMSCs and osteoblasts. Nevertheless, ATF4 is not a global anti-apoptotic factor since no increase in apoptosis has been observed in $Atf4^{-/-}$ fetal liver cells although the ability of these cells to proliferate is impaired. ATF4 may elicit its anti-apoptotic function in combination with other factors in specific tissue and cells types. Thus, ATF4 deficiency increases apoptosis in lens fiber cells in a p53-dependent manner. The embryonic lens in double homozygous $p53/Atf4^{-/-}$ mice does not undergo apoptosis [Tanaka et al., 1998; Hettmann et al., 2000]. Interestingly, ATF4 expression is usually induced by oxygen deprivation, endoplasmic reticulum stress, and the oxidative stressor arsenite, all of which are known to induce cell apoptosis [Ameri et al., 2004; Blais et al., 2004; Roybal et al., 2005]. Therefore, it is reasonable to speculate that expression of ATF4 induced by apoptosis-inducing factors in fact provides a protection mechanism for cells to antagonize apoptosis. The molecular mechanism whereby ATF4 regulates apoptosis in osteoblasts remains to be determined in future study.

In summary, this study for the first time establishes that ATF4 is essential for cell proliferation and anti-apoptosis in BMSCs and osteoblasts.

ACKNOWLEDGMENTS

REFERENCES

Adams JM. 2003. Ways of dying: Multiple pathways to apoptosis. Genes Dev 17:2481–2495.

Adams CM. 2007. Role of the transcription factor ATF4 in the anabolic actions of insulin and the anti-anabolic actions of glucocorticoids. J Biol Chem 282:16744–16753.

Ameri K, Lewis CE, Raida M, Sowter H, Hai T, Harris AL. 2004. Anoxic induction of ATF-4 through HIF-1-independent pathways of protein stabilization in human cancer cells. Blood 103:1876–1882.

Blais JD, Filipenko V, Bi M, Harding HP, Ron D, Koumenis C, Wouters BG, Bell JC. 2004. Activating transcription factor 4 is translationally regulated by hypoxic stress. Mol Cell Biol 24:7469–7482.

Brindle PK, Montminy MR. 1992. The CREB family of transcription activators. Curr Opin Genet Dev 2:199–204.

Chevray PM, Nathans D. 1992. Protein interaction cloning in yeast: Identification of mammalian proteins that react with the leucine zipper of Jun. Proc Natl Acad Sci USA 89:5789–5793.

Datta NS, Pettway GJ, Chen C, Koh AJ, McCauley LK. 2007. Cyclin D1 as a target for the proliferative effects of PTH and PTHrP in early osteoblastic cells. J Bone Miner Res 22:951–964.

Demiralp B, Chen HL, Koh AJ, Keller ET, McCauley LK. 2002. Anabolic actions of parathyroid hormone during bone growth are dependent on c-fos. Endocrinology 143:4038–4047.

Dobreva G, Chahrour M, Dautzenberg M, Chirivella L, Kanzler B, Farinas I, Karsenty G, Grosschedl R. 2006. SATB2 is a multifunctional determinant of craniofacial patterning and osteoblast differentiation. Cell 125:971–986.

Hai T, Curran T. 1991. Cross-family dimerization of transcription factors Fos/Jun and ATF/CREB alters DNA binding specificity. Proc Natl Acad Sci USA 88:3720–3724.

Hai T, Wolfgang CD, Marsee DK, Allen AE, Sivaprasad U. 1999. ATF3 and stress responses. Gene Expr 7:321–335.

He CH, Gong P, Hu B, Stewart D, Choi ME, Choi AM, Alam J. 2001. Identification of activating transcription factor 4 (ATF4) as an Nrf2-interacting protein. Implication for heme oxygenase-1 gene regulation. J Biol Chem 276:20858–20865.

Hettmann T, Barton K, Leiden JM. 2000. Microphthalmia due to p53-mediated apoptosis of anterior lens epithelial cells in mice lacking the CREB-2 transcription factor. Dev Biol 222:110–123.

Hofmann F, Livingston DM. 1996. Differential effects of cdk2 and cdk3 on the control of pRb and E2F function during G1 exit. Genes Dev 10:851–861.

Hogan MR, Cockram GP, Lu R. 2006. Cooperative interaction of Zhangfei and ATF4 in transactivation of the cyclic AMP response element. FEBS Lett 580:58–62.

Karpinski BA, Morle GD, Huggenvik J, Uhler MD, Leiden JM. 1992. Molecular cloning of human CREB-2: An ATF/CREB transcription factor that can negatively regulate transcription from the cAMP response element. Proc Natl Acad Sci USA 89:4820–4824.

Kato JY, Matsuoka M, Polyak K, Massague J, Sherr CJ. 1994. Cyclic AMP-induced G1 phase arrest mediated by an inhibitor (p27Kip1) of cyclin-dependent kinase 4 activation. Cell 79:487–496.

Lassot I, Estrabaud E, Emiliani S, Benkirane M, Benarous R, Margottin-Goguet F. 2005. p300 modulates ATF4 stability and transcriptional activity independently of its acetyltransferase domain. J Biol Chem 280:41537–41545.

Masuoka HC, Townes TM. 2002. Targeted disruption of the activating transcription factor 4 gene results in severe fetal anemia in mice. Blood 99:736–745.

Meyer TE, Habener JF. 1993. Cyclic adenosine 3′,5′-monophosphate response element binding protein (CREB) and related transcription-activating deoxyribonucleic acid-binding proteins. Endocr Rev 14:269–290.

Motohashi H, Shavit JA, Igarashi K, Yamamoto M, Engel JD. 1997. The world according to Maf. Nucleic Acids Res 25:2953–2959.

Nagata D, Suzuki E, Nishimatsu H, Satonaka H, Goto A, Omata M, Hirata Y. 2001. Transcriptional activation of the cyclin D1 gene is mediated by multiple cis-elements, including SP1 sites and a cAMP-responsive element in vascular endothelial cells. J Biol Chem 276:662–669.

Nakashima S, Matsuyama Y, Nitta A, Sakai Y, Ishiguro N. 2005. Highly efficient transfection of human marrow stromal cells by nucleofection. Transplant Proc 37:2290–2292.

Nishizawa M, Nagata S. 1992. cDNA clones encoding leucine-zipper proteins which interact with G-CSF gene promoter element 1-binding protein. FEBS Lett 299:36–38.

Ohtsubo M, Theodoras AM, Schumacher J, Roberts JM, Pagano M. 1995. Human cyclin E, a nuclear protein essential for the G1-to-S phase transition. Mol Cell Biol 15:2612–2624.

Pagano M, Pepperkok R, Verde F, Ansorge W, Draetta G. 1992. Cyclin A is required at two points in the human cell cycle. EMBO J 11:961–971.

Reddy TR, Tang H, Li X, Wong-Staal F. 1997. Functional interaction of the HTLV-1 transactivator Tax with activating transcription factor-4 (ATF4). Oncogene 14:2785–2792.

Roberts JM, Koff A, Polyak K, Firpo E, Collins S, Ohtsubo M, Massague J. 1994. Cyclins, Cdks, and cyclin kinase inhibitors. Cold Spring Harb Symp Quant Biol 59:31–38.

Roybal CN, Hunsaker LA, Barbash O, Vander Jagt DL, Abcouwer SF. 2005. The oxidative stressor arsenite activates vascular endothelial growth factor mRNA transcription by an ATF4-dependent mechanism. J Biol Chem 280: 20331–20339.

Sabbah M, Courilleau D, Mester J, Redeuilh G. 1999. Estrogen induction of the cyclin D1 promoter: Involvement of a cAMP response-like element. Proc Natl Acad Sci USA 96:11217–11222.

Sassone-Corsi P. 1994. Goals for signal transduction pathways: Linking up with transcriptional regulation. EMBO J 13:4717–4728.

Sherr CJ. 1994. G1 phase progression: Cycling on cue. Cell 79:551–555.

Sherr CJ, Roberts JM. 2004. Living with or without cyclins and cyclin-dependent kinases. Genes Dev 18:2699–2711.

Shi Y. 2002. Mechanisms of caspase activation and inhibition during apoptosis. Mol Cell 9:459–470.

Singha UK, Jiang Y, Yu S, Luo M, Lu Y, Zhang J, Xiao G. 2007. Rapamycin inhibits osteoblast proliferation and differentiation in MC3T3-E1 cells and primary mouse bone marrow stromal cells. J Cell Biochem 103:434–446.

Stacey DW. 2003. Cyclin D1 serves as a cell cycle regulatory switch in actively proliferating cells. Curr Opin Cell Biol 15:158–163.

Tanaka T, Tsujimura T, Takeda K, Sugihara A, Maekawa A, Terada N, Yoshida N, Akira S. 1998. Targeted disruption of ATF4 discloses its essential role in the formation of eye lens fibres. Genes Cells 3:801–810.

Tsujimoto A, Nyunoya H, Morita T, Sato T, Shimotohno K. 1991. Isolation of cDNAs for DNA-binding proteins which specifically bind to a tax-responsive enhancer element in the long terminal repeat of human T-cell leukemia virus type I. J Virol 65:1420–1426.

Vallejo M, Ron D, Miller CP, Habener JF. 1993. C/ATF, a member of the activating transcription factor family of DNA-binding proteins, dimerizes with CAAT/enhancer-binding proteins and directs their binding to cAMP response elements. Proc Natl Acad Sci USA 90:4679–4683.

Vinson CR, Hai T, Boyd SM. 1993. Dimerization specificity of the leucine zipper-containing bZIP motif on DNA binding: Prediction and rational design. Genes Dev 7:1047–1058.

Wang D, Christensen K, Chawla K, Xiao G, Krebsbach PH, Franceschi RT. 1999. Isolation and characterization of MC3T3-E1 preosteoblast subclones with distinct in vitro and in vivo differentiation/mineralization potential. J Bone Miner Res 14:893–903.

Wang J, Xi L, Hunt JL, Gooding W, Whiteside TL, Chen Z, Godfrey TE, Ferris RL. 2004. Expression pattern of chemokine receptor 6 (CCR6) and CCR7 in squamous cell carcinoma of the head and neck identifies a novel metastatic phenotype. Cancer Res 64:1861–1866.

Xiao G, Cui Y, Ducy P, Karsenty G, Franceschi RT. 1997. Ascorbic acid-dependent activation of the osteocalcin promoter in MC3T3-E1 preosteoblasts: Requirement for collagen matrix synthesis and the presence of an intact OSE2 sequence. Mol Endocrinol 11:1103–1113.

Xiao G, Jiang D, Gopalakrishnan R, Franceschi RT. 2002. Fibroblast growth factor 2 induction of the osteocalcin gene requires MAPK activity and phosphorylation of the osteoblast transcription factor, Cbfa1/Runx2. J Biol Chem 277:36181–36187.

Xiao G, Jiang D, Ge C, Zhao Z, Lai Y, Boules H, Phimphilai M, Yang X, Karsenty G, Franceschi RT. 2005. Cooperative interactions between activating transcription factor 4 and Runx2/Cbfa1 stimulate osteoblast-specific osteocalcin gene expression. J Biol Chem 280:30689–30696.

Yamanaka S, Tatsumi T, Shiraishi J, Mano A, Keira N, Matoba S, Asayama J, Fushiki S, Fliss H, Nakagawa M. 2003. Amlodipine inhibits doxorubicin-induced apoptosis in neonatal rat cardiac myocytes. J Am Coll Cardiol 41:870–878.

Yang X, Matsuda K, Bialek P, Jacquot S, Masuoka HC, Schinke T, Li L, Brancorsini S, Sassone-Corsi P, Townes TM, Hanauer A, Karsenty G. 2004. ATF4 is a substrate of RSK2 and an essential regulator of osteoblast biology; implication for Coffin-Lowry syndrome. Cell 117:387–398.

Yu VW, Ambartsoumian G, Verlinden L, Moir JM, Prud'homme J, Gauthier C, Roughley PJ, St-Arnaud R. 2005. FIAT represses ATF4-mediated transcription to regulate bone mass in transgenic mice. J Cell Biol 169:591–601.

Yu S, Franceschi RT, Luo M, Zhang X, Jiang D, Lai Y, Jiang Y, Zhang J, Xiao G. 2008a. Parathyroid hormone increases activating transcription factor 4 expression and activity in osteoblasts: Requirement for osteocalcin gene expression. Endocrinology 149:1960–1968.

Yu S, Jiang Y, Galson DL, Luo M, Lai Y, Lu Y, Ouyang HJ, Zhang J, Xiao G. 2008b. General transcription factor IIA-gamma increases osteoblast-specific osteocalcin gene expression via activating transcription factor 4 and runt-related transcription factor 2. J Biol Chem 283:5542–5553.

Zhao W, Byrne MH, Wang Y, Krane SM. 2000. Osteocyte and osteoblast apoptosis and excessive bone deposition accompany failure of collagenase cleavage of collagen. J Clin Invest 106:941–949.

Zhao J, Pestell R, Guan JL. 2001. Transcriptional activation of cyclin D1 promoter by FAK contributes to cell cycle progression. Mol Biol Cell 12: 4066–4077.

Zhao M, Qiao M, Harris SE, Oyajobi BO, Mundy GR, Chen D. 2004. Smurf1 inhibits osteoblast differentiation and bone formation in vitro and in vivo. J Biol Chem 279:12854–12859.

Ziff EB. 1990. Transcription factors: A new family gathers at the cAMP response site. Trends Genet 6:69–72.

Identification and Functional Characterization of ERK/MAPK Phosphorylation Sites in the Runx2 Transcription Factor*□S

Chunxi Ge[‡1], **Guozhi Xiao**[§1], **Di Jiang**[‡], **Qian Yang**[‡], **Nan E. Hatch**[‡], **Hernan Roca**[‡], and **Renny T. Franceschi**[‡¶12]

From the ‡Department of Periodontics and Oral Medicine, School of Dentistry, and ¶Department of Biological Chemistry, School of Medicine, University of Michigan, Ann Arbor, Michigan 48109-1078 and the §Department of Medicine, University of Pittsburgh, Pittsburgh, Pennsylvania 15240

The Runx2 transcription factor is required for commitment of mesenchymal cells to bone lineages and is a major regulator of osteoblast-specific gene expression. Runx2 is subject to a number of post-transcriptional controls including selective proteolysis and phosphorylation. We previously reported that Runx2 is phosphorylated and activated by the ERK/MAPK pathway (Xiao, G., Jiang, D., Thomas, P., Benson, M. D., Guan, K., Karsenty, G., and Franceschi, R. T. (2000) *J. Biol. Chem.* 275, 4453–4459). In this study, we used a combination of *in vitro* and *in vivo* phosphorylation analysis, mass spectroscopy, and functional assays to identify two sites at Ser^{301} and Ser^{319} within the proline/serine/threonine domain of Runx2 that are required for this regulation. These sites are phosphorylated by activated ERK1 *in vitro* and in cell culture. In addition to confirming ERK-dependent phosphorylation at Ser^{319}, mass spectroscopy identified two other ERK-phosphorylated sites at Ser^{43} and Ser^{510}. Furthermore, introduction of S301A,S319A mutations rendered Runx2 resistant to MAPK-dependent activation and reduced its ability to stimulate osteoblast-specific gene expression and differentiation after transfection into Runx2-null calvarial cells and mesenchymal cells. In contrast, S301E,S319E Runx2 mutants had enhanced transcriptional activity that was minimally dependent on MAPK signaling, consistent with the addition of a negative charge mimicking serine phosphorylation. These results emphasize the important role played by Runx2 phosphorylation in the control of osteoblast gene expression and provide a mechanism to explain how physiological signals acting on bone through the ERK/MAPK pathway can stimulate osteoblast-specific gene expression.

The bone cell lineage is controlled by a hierarchy of transcription factors that are expressed in a defined temporal sequence. Runx2, an essential factor for both hypertrophic cartilage and bone formation, is expressed very early in skeletal development, first appearing coincident with the formation of mesenchymal condensations (1). Subsequent development of the osteoblast lineage requires at least two additional factors; Osterix, which is essential for subsequent progression of the osteoblast lineage, and ATF4, which regulates osteoblast activity, particularly in postnatal animals (2, 3). Runx2 expression continues during the later stages of bone development and persists in regions of active bone remodeling throughout life. Skeletal development in Runx2-deficient mice fails to progress beyond the cartilage anlage stage, whereas dominant-negative suppression of Runx2 even in postnatal animals inhibits osteoblast activity and bone formation (4). Thus, Runx2 is required for both the initial formation of osteoblasts and hypertrophic chondrocytes during development and for sustained osteoblast differentiation during bone remodeling.

Consistent with its multiple roles in bone formation, Runx2 is highly regulated. In addition to transcriptional control by factors such as bone morphogenetic proteins (5), Runx2 activity is controlled both by its interaction with a number of accessory nuclear factors and by post-translational modifications, including phosphorylation. We have been particularly interested in this latter regulation and proposed that Runx2 is phosphorylated and activated by a ERK[3]/MAPK-dependent pathway initiated by the interaction of osteoprogenitors with a type I collagen-containing extracellular matrix (ECM) via $\alpha 2\beta 1$ integrins (6, 7). This collagen-integrin interaction is necessary for subsequent osteoblast-specific gene expression and differentiation (7–9). Consistent with this model, steady-state Runx2 phosphorylation and DNA binding activity increase with osteoblast differentiation, whereas pharmacological inhibition of the ERK/MAPK pathway rapidly inhibits ECM and BMP-induced gene expression (10–12). In related studies, FGF2 treatment of osteoblasts, which is known to stimulate both ERK/MAPK and protein kinase C pathways, increases Runx2 phosphorylation and *Ocn* expression in a MAPK-dependent manner (13). Furthermore, manipulation of the MAPK pathway by overexpression of constitutively active or dominant-negative mutants of MEK1, respectively, increases or decreases osteocalcin gene expression and Runx2 phosphorylation (6). ERK/MAPK signaling is also important for *in vivo* bone development. Transgenic overexpression of constitutively active or dominant-negative MEK1 in mouse osteoblasts, respectively, stimulates or inhibits Runx2 phosphorylation and skeletal maturation. Furthermore,

---

□S The on-line version of this article (available at http://www.jbc.org) contains supplemental Fig. S1.

[1] Both authors contributed equally to this study.

[2] To whom correspondence should be addressed: University of Michigan School of Dentistry, 1011 N. University Ave., Ann Arbor, MI 48109-1078. Fax: 734-763-5503; E-mail: rennyf@umich.edu.

[3] The abbreviations used are: ERK, extracellular signal-regulated kinase; MAPK, mitogen-activated protein kinase; ECM, extracellular matrix; MEK, mitogen-activated protein kinase/extracellular signal-regulated kinase kinase; OSE2, osteoblast-specific element 2; Mek(sp), constitutively active MEK1 mutant; FGF, fibroblast growth factor; HA, hemagglutinin; aa, amino acid; FBS, fetal bovine serum; MS, mass spectrometry.

the cleidocranial dysplasia phenotype of Runx2 heterozygous null mice can be partially rescued by crossing these animals with mice expressing constitutively active MEK1, consistent with the *in vivo* actions of the ERK/MAPK pathway being at least in part mediated by Runx2 (14).

In addition to the work from our laboratory cited above (6–14), a number of studies from other groups support the concept that ECM-integrin binding, MAPK activation, and Runx2 phosphorylation are important for osteoblast differentiation. The requirement for $\alpha1\beta1$ and $\alpha2\beta1$ collagen-binding integrins in osteoblast differentiation and BMP responsiveness was demonstrated by both *in vitro* and *in vivo* analysis (15–18). Also, ERK/MAPK signaling was shown to be necessary for differentiation of human osteoblasts and marrow stromal cells (19, 20). A number of groups also confirmed that Runx2 can be phosphorylated and activated by MAPK inducers. During the osteoblastic differentiation of human marrow stromal cells, Runx2 levels remain relatively unchanged, but DNA binding increases as does Runx2 phosphorylation (21). Also, mechanical loading of osteoblasts, mediated in part through $\alpha2\beta1$ integrins, induces MAPK activity (22, 23). Similarly, loading of periodontal ligament cells (osteoprogenitor-like cells) increases Runx2 phosphorylation and binding to OSE2 DNA via an ERK/MAPK-dependent process (24). In osteomimetic prostate cancer cells, differentiation is accompanied by ERK1/2 activation, increased Runx2-DNA binding, and *Ocn* expression, responses that were all blocked by MAPK inhibition (25). Last, insulin-like growth factor-1, which activates phosphatidylinositol 3-kinase and, subsequently, ERK/MAPK pathways, stimulates Runx2-OSE2 binding and phosphorylation in vascular endothelial cells (26) as well as differentiation of marrow stromal cells (27, 28). Thus, ERK/MAPK-dependent phosphorylation of Runx2 likely plays an important role in the response of osteoblasts to a variety of signals initiated by cell-ECM binding, hormone/growth factor signaling, and mechanical loading.

To further understand how the ERK/MAPK pathway regulates Runx2 transcriptional activity, in the present study we identify amino acid residues in Runx2 that are phosphorylated in a ERK/MAPK-dependent manner and show that these sites are necessary for osteoblast-specific gene expression and differentiation.

EXPERIMENTAL PROCEDURES

Reagents—The reagents used in this study were obtained from the following sources: tissue culture medium and fetal bovine serum from Invitrogen; U0126 from Calbiochem; mouse anti-Runx2 antibody from MBL; phosphoserine antibody from ABCam; and M2 and M2 horseradish peroxidase-conjugated antibody from Sigma.

DNA Constructs and Viral Expression Vectors—The 0.6-kb mouse osteocalcin gene 2-Luc reporter plasmid and a constitutively active MEK1 expression vector were previously described (29–31). A series of Runx2 expression plasmids encoding HA- or FLAG-tagged full-length type II Runx2 (N-terminal sequence: MASN) or several N- and C-terminal deletions were generated by PCR and subcloning into the pCMV5 expression vector. Serine mutants of full-length and aa 1–330 Runx2 were generated using the QuikChange site-directed mutagenesis kit

(Stratagene). A cDNA encoding Runx2 with a biotinylation tag was generated by adding the sequence, MASSLRQILDSQK-MEWRSNAGGS, to the N terminus of mouse Runx2. This sequence is specifically recognized by bacterial BirA biotin ligase (32). Plasmids containing cDNAs encoding the biotinylation tag and BirA were a generous gift from Dr. John Strouboulis (Alexander Fleming Biomedical Sciences Research Center, Athens, Greece). Adenoviruses encoding wild type and mutant Runx2, and biotinylation tagged Runx2, BirA, and Mek(sp) (constitutively active MEK1) were constructed by first subcloning the respective cDNA into pAdloxp and then generating viruses using Cre-Lox recombination as previously described (33).

Cell Culture—C3H10T1/2, COS7, and HEK293 cells were obtained from the American Type Culture Collection and maintained in Dulbecco's modified Eagle's medium containing 10% FBS and 1% antibiotics. An mTERT-immortalized calvarial cell line from Runx2$^{-/-}$ mice (34) was a generous gift from Drs. Jane Lian and Gary Stein (University of Massachusetts Medical Center, Worcester, MA) and maintained in minimal essential medium-α, 10% FBS. MC3T3-E1 clone 4 (MC-4) cells, previously developed in this laboratory (35), were also maintained in minimal essential medium-α, 10% FBS. To induce differentiation, C3H10T1/2, mTERT cells, and MC-4 cells were grown in minimal essential medium-α, 10% FBS containing 50 μg/ml ascorbic acid as previously described (12, 34, 36).

Transfections—COS7 cells were plated at a density of 5×10^4 cells/cm^2 on 35-mm dishes and transfected using Lipofectamine (Invitrogen). Each transfection contained 0.5 μg of the indicated plasmid and 0.05 μg of pRL-SV40 containing a cDNA for *Renilla reniformis* luciferase to control transfection efficiency. Cells were harvested and assayed using a dual luciferase assay kit (Promega) with a Monolight 2010 luminometer (Pharmingen). For mTERT cells, transfection was accomplished using FuGENE 6 reagent (Roche). For studies where effects of more sustained Runx2 expression were analyzed, C3H10T1/2 cells were transduced with adenovirus expression vectors as previously described (36).

Western Blot Analysis—Whole cell extracts were prepared by dissolving cell layers in SDS sample buffer. Samples were fractionated by SDS-PAGE on 4–12% precast minigels (Invitrogen) and electrophoretically transferred to nitrocellulose membranes (Schleicher & Schuell). Primary antibodies were used at the following dilutions (Runx2, 1:500; M2, 1:2000; phosphoserine, 1:500). Secondary antibody was used at a dilution of 1:10,000. Immunoreactivity was detected using ECL chemiluminescence reagents (Amersham Biosciences).

RNA Analysis—RNA was isolated using TRIzol reagent (Invitrogen) and further purified by DNase I treatment and an RNeasy kit (Qiagen). Reverse transcriptase reactions were conducted with 2 μg of total RNA, TaqMan reverse transcriptase reagents, and an oligo(dT) primer (Applied Biosystems)). PCR was performed using an ABI Prism 7700 sequence detection system. Glyceradehyde-3-phosphate dehydrogenase mRNA was used as an endogenous control.

Metabolic Labeling and Immunoprecipitation of Runx2—COS7 cells were transfected with Runx2 expression plasmids, cultured for 30 h, and preincubated in phosphate-free Dulbec-

co's modified Eagle's medium, 0.1% FBS for 12 h. Labeling was conducted for 4 h in phosphate-free Dulbecco's modified Eagle's medium containing 200 μCi/ml [^{32}P]orthophosphate (phosphorus-32 or [^{35}S]methionine/cysteine Tran^{35}S-label, Amersham Biosciences). Nuclear extracts were prepared as previously described (12) and precleared twice with 50 μl of protein A/G-agarose beads. Appropriate antibodies were added and incubated for 2 h at 4 °C with gentle rocking. Immune complexes were then collected by the addition 30 μl of protein A/G-agarose beads and incubation for 1 h at 4 °C followed by centrifugation. Precipitates were washed five times with 1× washing buffer (20 mM HEPES, pH 7.6, 50 mM KCl, 1 mM dithiothreitol, 0.25% Nonidet P-40, 5 mM sodium fluoride, 1 mM EGTA, 5 mM MgCl$_2$). The immunoprecipitated complexes were suspended in SDS sample buffer and analyzed by SDS-PAGE and autoradiography or Western blot analysis using the indicated antibodies. ^{32}P incorporation was measured using a Packard A2024 InstantImager.

In Vitro Phosphorylation—Synthetic peptides were prepared by the University of Michigan Protein Structure Facility. Each peptide (1 μg) was incubated with 10 μCi of [γ-^{32}P]ATP and 1 unit of activated MAPK (Calbiochem) in a buffer containing 25 mM Tris-HCl, pH 7.4, 10 mM MgCl$_2$, 1 mM dithiothreitol, 40 μM ATP, and 0.5 mM EGTA in a final volume of 25 μl. Samples were incubated at 25 °C for 30 min. Reactions were terminated by addition of 25 μl of 2× SDS sample buffer and samples were analyzed by electrophoresis on 15% SDS gels. For *in vitro* Runx2 phosphorylation, biotinylated Runx2 was purified on streptavidin beads as described below and directly phosphorylated by incubation of beads under the same conditions used for peptide phosphorylation, except that [γ-^{32}P]ATP was omitted.

Runx2 Purification and Identification of Phosphorylation Sites by Mass Spectroscopy—An adenovirus expression system for biotinylation tagging of Runx2 was developed (32). COS7 cells were transduced with adenovirus encoding Runx2 cDNA with an N-terminal biotinylation sequence and AdBirA (adenovirus expressing bacterial biotin protein ligase) with or without AdMek(sp). After 48 h, cell lysates were adsorbed to streptavidin magnetic beads and purified Runx2 was resolved by SDS-PAGE using a 4–12% gradient gel. The Runx2 gel band was alkylated with iodoacetamide and peptide fragments were generated by in-gel digestion with pepsin. Samples were analyzed by LC/MS/MS using a ThermoFisher LTQ Orbitrap XL (Next-GenSciences, Ann Arbor, MI). The Orbitrap MS scan was performed at 60,000 full-width at half-maximum resolution and searched using a local copy of Mascot. Phosphorylated peptides containing P-serine were then identified. In certain cases, product ion data were used to confirm identification of the phosphorylation site.

Statistical Analysis—All statistical analyses were performed using SPSS 16.0 Software. Unless indicated otherwise, each reported value is the mean ± S.D. of triplicate independent samples. Statistical significance was assessed using a one-way analysis of variance.

RESULTS

ERK/MAPK-dependent Phosphorylation and Activation of Runx2 Require a Specific Region of the C-terminal Pro/Ser/Thr
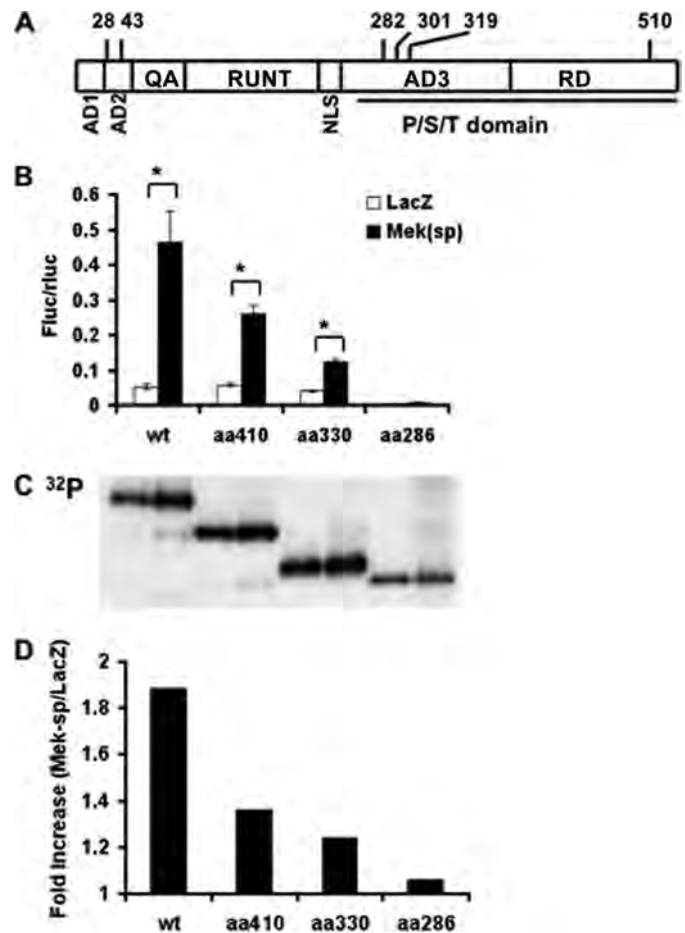

FIGURE 1. **Identification of a region in Runx2 necessary for ERK/MAPK-dependent transcriptional activation and phosphorylation.** *A*, schematic of the domain structure of Runx2 with relevant serine residues indicated. *AD1–3*, transcriptional activation domains; *QA*, glutamine/alanine-rich domain; *RUNT*, runt/DNA-binding domain; *NLS*, nuclear localization sequence; *P/S/T domain*, proline/serine/threonine-rich domain; *RD*, repressor domain (from Ref. 30). *B*, MAPK-dependent transcriptional activity. COS7 cells were transfected with wild type (*WT*) Runx2 or the indicated C-terminal deletions in the presence of control (LacZ) or Mek(sp) expression vectors and a 6OSE2-luc reporter as described under "Experimental Procedures." Firefly luciferase activity was normalized for transfection efficiency using a *R. reinformis* luciferase plasmid. *Asterisk*, significantly different from corresponding control, $p < 0.01$; *brackets* indicate comparisons made; *error bars*, ±S.D. *C* and *D*, Runx2 phosphorylation. COS7 cell cultures treated as in *B* were metabolically labeled with [^{32}P]orthophosphate or Tran^{35}S-label as described under "Experimental Procedures." Runx2 was immunoprecipitated (*C*) and ^{32}P incorporation was normalized to total ^{35}S-labeled protein in each group and expressed as fold-increase with Mek(sp) stimulation (*D*).

Domain—Fig. 1*A* shows a schematic of the domain structure of Runx2 with positions of potential phosphorylation sites to be discussed in this study. Activation of the ERK/MAPK pathway by overexpression of a constitutively active form of MEK1 or by treatment with FGF2 was previously shown to stimulate *Ocn* mRNA expression and promoter activity via a mechanism requiring Runx2 (6, 13). An initial deletion analysis of the Runx2 coding sequence showed that removal of the entire C-terminal proline/serine/threonine-rich (Pro/Ser/Thr) domain (contains AD3 and RD regions encompassing amino acid residues 258–528 in the mouse sequence) rendered Runx2 completely resistant to MAPK regulation and phosphorylation. In contrast, deletion of the N-terminal AD1, AD2, and QA-rich regions (amino acids 1–108) lowered basal transcriptional

MAPK Regulation of Runx2 Phosphorylation

activity without affecting MAPK-dependent activation (6). Similarly, deletion of the Pro/Ser/Thr domain also rendered Runx2 unresponsive to activation by FGF2 (13).

To more precisely define regions of Runx2 necessary for MAPK responsiveness, we carried out a more detailed deletion analysis of the Pro/Ser/Thr domain (Fig. 1, B–D). Wild type Runx2 or several C-terminal deletions (to residues 410, 330, and 286) were transfected into COS7 cells in the presence or absence of constitutively active MEK1 (Mek(sp)) and a p6OSE2-luc Runx2 reporter gene. Samples were either assayed for luciferase activity (*panel B*) or were metabolically labeled with [^{32}P]orthophosphate and assayed for Runx2 phosphorylation by immunoprecipitation and autoradiography (*panels C* and *D*). C-terminal Runx2 deletions gradually reduced MAPK activation of Runx2 transcriptional activity from ~9-fold with wild type Runx2 to ~3-fold with the amino acid 330 deletion. Mek(sp) stimulation was completely lost with deletion to residue 286. Similarly, Mek(sp) stimulated total ^{32}P incorporation into wild type Runx2 by ~2-fold (*panel C*). This stimulation gradually decreased in the 410 and 330 deletions and was completely lost after deletion to residue 286. These results indicate that the minimal region for MAPK phosphorylation and activation of Runx2 is between amino acids 286 and 330. Subsequent analysis was restricted to this region although it is possible that more C-terminal sites may also participate in this regulation.

Identification of Runx2 Phosphorylation Sites—Inspection of the Runx2 peptide sequence in the 286–330 region (Fig. 2A) identified two putative proline-directed serine phosphorylation sites at residues 301 and 319 and an adjacent site at residue 282. A similar proline-directed threonine site was also seen (Thr^{326}). Incubation of peptides spanning the 264 to 337 region with active ERK1 and [γ-^{32}P]ATP revealed that Ser^{282}, Ser^{301}, and Ser^{319} were all phosphorylated *in vitro*, whereas Ser/Ala substitution

at each site prevented phosphorylation. In contrast, Thr^{326} was not phosphorylated under these conditions (*i.e.* Introduction of an S319A mutation in the 316–337 peptide blocked phos-
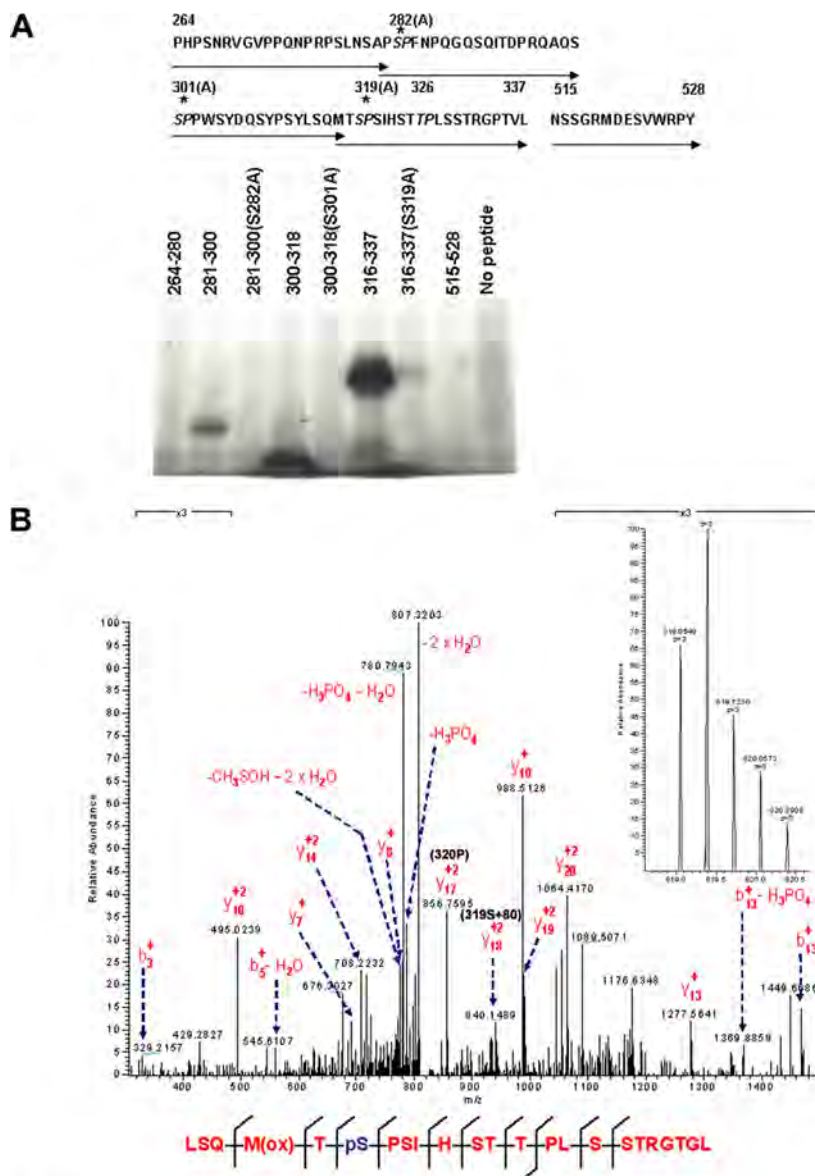
C

Measured Mass-groups	Residues from-to	Peptide sequence filtered by phosphate event	Correlation rate	Serine
In vivo Phophorylation	23-42	TSRRFSPPSSSLQPGKMSDV	95%	S28
	32-48	SSLQPGKMSDVSPVVAA	74%	S43
	276-292	LNSAPSPFNPQGQSOI	95%	S282
	313-337	YLSQMTSPSIHSTTPLSSTRGTGLP	95%	S319
	389-514	LLNPNLPNQNDGVDADGSHSSSPTVL	95%	S510
U0126 Treatment	23-43	SRRFSPPSSSLQPGKMSDVV	88%	S28
In vitro Phosphorylation	23-43	TSRRFSPPSSSLQPGKMSDVS	94%	S24, S28
	22-48	SRRFSPPSSSLQPGKMSDVSPVVAA	73%	S43
	313-337	YLSQMTSPSIHSTTPLSSTRGTGLP	94%	S319,S321
	337-356	LAITDVRPPISDDDTATSDF	77%	S347
	389-514	LLNPNLPNQNDGVDADGSHSSSPTVL	85%	S510

phorylation). Peptides containing residues 264–280 and 515–528 were also not phosphorylated.

More extensive analysis of Runx2 phosphorylation was conducted using mass spectroscopy. COS7 cells were transduced with adenovirus vectors expressing a biotinylation tagged Runx2, BirA (bacterial biotin protein ligase), and Mek(sp). Runx2 was then purified from cell lysates using streptavidin magnetic beads and LC/MS/MS analysis was carried out on pepsin-digested samples. As shown in Fig. 2B, five peptides were identified containing phosphoserine at residues 28, 43, 282, 319, and 510. The probability of a correct identification for each peptide was 95% with the exception of the peptide containing Ser[43], which had a correlation of 74%. In contrast, only phosphoserine 28 was identified in Runx2 purified from cells pretreated with the MAPK inhibitor, U0126. This indicates that other sites at Ser[43], Ser[282], Ser[319], and Ser[510] are directly or indirectly dependent on ERK/MAPK activity for phosphorylation. To identify direct MAPK targets, nondenatured Runx2 purified from U0126-treated cells was phosphorylated directly on streptavidin beads with activated P-ERK *in vitro* and MS was repeated. In this case, phosphate was detected on Ser[24], Ser[43], Ser[319], Ser[347], and Ser[510]. From this analysis, we conclude that the *in vivo* phosphorylation sites identified by MS, Ser[43], Ser[319], and Ser[510] are probably direct ERK substrates, whereas Ser[282] is likely phosphorylated by a second kinase activated by ERK. Because we also obtained functional evidence for the importance of Ser[319] in Runx2 regulation (below), more extensive confirmation that this site is phosphorylated was obtained by analyzing product ion data for the LSQMTpSPSIHST-TPLSSTRGTGL peptide (residues 313–337). Both $[M + 2H]^{2+}$ and $[M + 3H]^{3+}$ charge states were analyzed ($[M + 3H]^{3+}$ is shown in the *left panel* of Fig. 2C). Analysis of product ion data (Fig. 2C, *right*) confirmed that this peptide was phosphorylated at Ser[6] (Ser[319]) within a mass accuracy of 2 ppm.

Surprisingly, although MS analysis consistently identified peptides containing 56–69% of the entire Runx2 sequence (62–76% if the N-terminal Gln/Ala region is excluded), peptides were never identified spanning the Ser[301] region. Identified peptides contained 11 of the 12 proline-directed serine/threonine sites in Runx2, making Ser[301] the only site not included in our analysis. Similar results were obtained using alternative protease digestions (trypsin/AspN *versus* pepsin). This suggests that the Ser[301] region contains some abnormality in secondary structure, possibly due to post-translational modification, which prevents normal fragmentation and identification.

To further explore the possibility that the Ser[301] site is phosphorylated *in vivo*, we used an indirect approach that takes advantage of the observation that activation of MAPK signaling

stimulates a shift in the electrophoretic mobility of a truncated Runx2-(1–330) (Fig. 3A). For this experiment, wild type truncated Runx2-(1–330) or Runx2 containing an S301A mutation, an S319A mutation, or combined S301A,S319A mutations was transfected into COS7 cells with or without constitutively active Mek(sp) and ERK1 expression vectors and analyzed by SDS-PAGE. Activation of MAPK signaling clearly reduced the electrophoretic mobility of wild type Runx2-(1–330) and this mobility change was eliminated by treatment of samples with alkaline phosphatase. In contrast, no detectable MAPK-dependent change in mobility was seen with S301A, S319A mutations or the S301A,S319A double mutation. This is the result that would be expected if a detectable mobility shift requires phosphorylation on both Ser[301] and Ser[319].

Although the larger size of full-length Runx2 (528 amino acid residues) precluded conducting mobility shift analysis, we obtained additional evidence for Ser[301] and Ser[319] phosphorylation using immunoprecipitation/immunoblotting with Runx2 and Ser(P) antibodies (Fig. 3B). COS7 cells were transfected with FLAG-tagged wild type, S301A, S319A, or S301A,S319A full-length Runx2 mutants in the presence or absence of Mek(sp) expression vector or in the presence of the MAPK inhibitor, U0126. Samples were then either immunoprecipitated with a specific anti-Runx2 (M2) antibody followed by Western blotting with antiphosphoserine antibody or, alternatively, immunoprecipitated with antiphosphoserine followed by probing with anti-Runx2 antibody. Cells transfected with WT Runx2 displayed a strong Runx2-associated P-serine signal that was further increased by Mek(sp). S301A or S319A mutations each reduced the P-serine signal to a similar extent, whereas the combined S301A,S319A double mutant displayed even weaker P-serine immunoreactivity. MAPK inhibition (+U0126) greatly reduced the P-serine signal in all groups and eliminated differences between WT and mutant Runx2 as would be expected if Ser[301] and Ser[319] were both phosphorylated in a MAPK-dependent manner. However, the fact that the double mutant still displayed a Mek(sp)-dependent increase in P-serine indicates that Runx2 contains additional direct or indirect MAPK phosphorylation sites, in agreement with our MS data.

In summary, multiple phosphorylation sites were identified in Runx2 including two sites in the aa 286–330 region. Definitive identification of Ser[319] as a direct ERK substrate was established using a combination of *in vitro* peptide phosphorylation, MS/MS, and electrophoresis mobility shift analysis. Strong evidence was also obtained that Ser[301] is phosphorylated by ERK (*in vitro* peptide phosphorylation, electrophoresis mobility shift analysis, and Ser(P)/Runx2 co-precipitation). However, it

FIGURE 2. **Runx2 phosphorylation sites.** *A*, *in vitro* peptide phosphorylation. Synthetic peptides were prepared containing amino acid residues 264–337 of the Runx2 sequence (indicated by *arrows*) or the indicated amino acid substitutions (*top panel*). Peptides were labeled with [γ-³²P]ATP using activated ERK1 and resolved by SDS-PAGE as described under "Experimental Procedures" (*lower panel*). *B*, MS/MS analysis of ERK/MAPK-related phosphorylation sites. COS7 cells were transduced with adenoviruses encoding biotinylation-tagged Runx2, BirA biotin transferase, and Mek(sp) with (U0126 treatment) or without (*in vivo* phosphorylation) MAPK inhibitor. Runx2 as then purified as described under "Experimental Procedures" and subjected to MS/MS analysis. For *in vitro* phosphorylation, an aliquot of Runx2 purified from U0126-treated cells was incubated with the activated MAPK before MS/MS analysis. Phosphopeptides were identified using Mascot software. *Correlation rate* indicates the probability that the indicated peptide identification in the Runx2 sequence is correct. *C*, verification of Ser[319] phosphorylation. The peptic peptide LSQMTSPSIHSTTPLSSTRGRGL was selected to manually validate the phosphorylation event. Mascot search results indicated that acquired MS/MS spectra contain production ion data for both $[M + 2H]^{2+}$ and $[M + 3H]^{3+}$ charged states for this peptide. The full MS spectra of the $[M + 3H]^{3+}$ charged state is shown in the *left panel*. The *right panel* shows the annotated MS/MS spectra of *m/z* = 819.05 (+3). Diagnostic Y_{17}^{+2} and Y_{18}^{+2} ions are indicated with *m/z* values of 856.8 and 940.2, respectively, which confirms the presence of a phosphate on Ser[319].

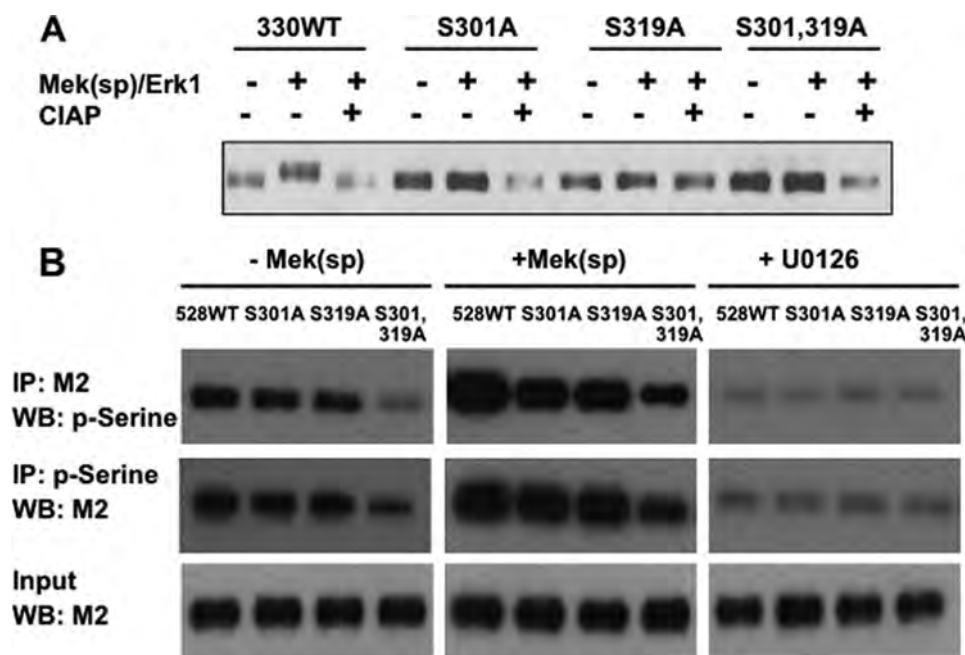## MAPK Regulation of Runx2 Phosphorylation

FIGURE 3. **Additional evidence for Runx2 phosphorylation at Ser[301].** *A*, analysis of electrophoretic mobility of wild type (*WT*) truncated Runx2-(1–330) and Ser[301] and Ser[319] mutants. The indicated truncated Runx2 mutants were expressed in COS7 cells in the presence or absence of Mek(sp) and ERK1 expression vectors. Cell lysates were analyzed by SDS-PAGE with or without prior treatment with calf intestinal alkaline phosphatase (*CIAP*). Runx2 was detected by Western blotting. *B*, anti-P-serine antibody reactivity with full-length Runx2. FLAG-tagged WT Runx2 or the indicated mutants were expressed in COS7 cells in the presence (+) or absence (−) of Mek(sp) or in the presence of the MAPK inhibitor (+*U0126*). Nuclear extracts were then either immuno-precipitated with M2 antibody and probed with an anti-P-serine monoclonal antibody or immunoprecipitated (*IP*) with anti-P-serine and probed with M2.

was not possible to detect peptide fragments containing the Ser[301] region in MS/MS, precluding its identification using this approach.

Identification of an ERK Binding Region in Runx2—Consistent with the concept that Runx2 is an ERK/MAPK substrate, ERK was shown to bind Runx2 in co-immunoprecipitation assays (Fig. 4). ERK-Runx2 complexes were detected in nuclear extracts from MC-4 cells that have high endogenous levels of both proteins (*panel A*) as well as in COS7 cells transfected with affinity-tagged Runx2 (*panels B–D*). To identify the Runx2 region responsible for ERK binding, COS7 cells were transfected with wild type HA-tagged Runx2, Runx2 with S301A,S319A mutations, or Runx2 with several N-terminal deletions and interactions with endogenous ERK1/2 were examined. Cell lysates were immunoprecipitated with an anti-ERK1/2 antibody and precipitates were probed on Western blots with an anti-HA antibody (Fig. 4*B*, *top*). Wild type Runx2 was clearly coprecipitated with the anti-ERK antibody. Of the N-terminal deletions examined, only the Δ97 fragment was precipitated, whereas Δ232 and 242 deletions failed to interact with ERK. The reciprocal experiment (immunoprecipitation with HA antibody and probing blots with anti-ERK antibody, Fig. 4*B*, *second panel* from *top*) gave equivalent results. Similarly, when C-terminal deletions were examined using FLAG-tagged Runx2 (Fig. 4*C*), Runx2-ERK binding was retained down to and including the Δ330 deletion. This indicates that the ERK binding site is in the runt domain of Runx2. Interestingly, the S301A,S319A mutant Runx2 bound ERK normally, indicating that this interaction does not require intact phosphorylation sites.

Inspection of the runt domain region of Runx2 revealed that it contains a consensus ERK docking "D" site (GKSFTLTITVFTNPP) at aa 201–215 (37). To confirm its role in ERK complex formation, this region of Runx2 was deleted, resulting in complete loss of ERK binding (Fig. 4*D*). The D site deletion also almost completely blocked the ability of Mek(sp) to stimulate Runx2-dependent transcription of a 6OSE2-luc reporter (supplemental Fig. S1).

Functional Analysis of Phosphorylation Sites—We initially assessed the functionality of the above phosphorylation sites in the context of the Runx2-(1–330) fragment because this contained the minimal sequence for MAPK responsiveness. Ser/Ala mutants described above or Ser/Glu mutations were generated at each site individually or in combination, and wild type or mutated expression plasmids were transfected into COS7 cells with 6OSE2-luc +/−Mek(sp). As shown in Fig. 5*A*, the ability of Mek(sp) to stimulate transcriptional activity of Runx2-(1–330) was totally blocked with the MEK1/2 inhibitor, U0126. However, individual Ser/Ala mutations at residues 301 or 319 only slightly inhibited MAPK stimulation, whereas the S282A mutation was without effect. On the other hand, introduction of a S301A,S319A double mutation completely eliminated MAPK responsiveness. In contrast, the S301E,S319E mutant exhibited high basal transcriptional activity in the absence of MAPK stimulation that was not affected by Mek(sp). This is consistent with previous studies showing that addition of the charged amino acid is able to mimic a phosphorylated serine residue (38).

To evaluate the role of phosphorylation sites in the context of the native Runx2 protein, S301A,S319A or S301E,S319E mutations were also introduced into full-length Runx2 and evaluated for Mek(sp) (Fig. 5*B*) or FGF2 responsiveness (Fig. 5*C*) using the same 6OSE2-luc reporter used above. As was the case with Runx2-(1–330), the Mek(sp)-dependent induction of luciferase activity was blocked with U0126, whereas the S301E,S319E mutation resulted in constitutive activation of reporter activity that was not further stimulated by Mek(sp). In contrast to the result obtained with Runx2-(1–330), S301A,S319A mutations only partially blocked the MAPK response (approximately 40% inhibition).

As noted above, FGF2 induction of *Ocn* expression also requires ERK/MAPK activity and is associated with Runx2 phosphorylation (13). A preliminary deletion analysis (not shown) also indicated that FGF2 responsiveness was lost after deletion of the aa 286–330 Runx2 region. To evaluate whether Ser[301] and Ser[319] are required for the FGF2 response, wild type
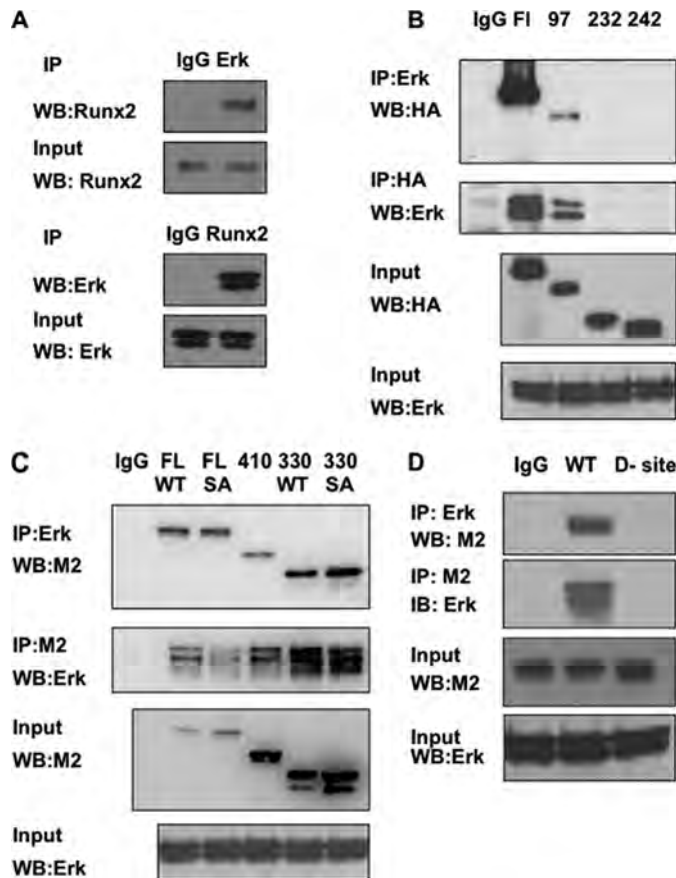
FIGURE 4. **Association of Runx2 with ERK.** *A*, co-immunoprecipitation of endogenous Runx2 and ERK. MC-4 cell nuclear extracts were immunoprecipitated with IgG, ERK, or Runx2 antibodies and blots were probed as indicated. *B–D*, identification of the ERK binding domain in Runx2. Wild type (*WT*) Runx2 or the indicated N-terminal (HA-tagged Runx2, *B*) or C-terminal Runx2 deletions (FLAG-tagged Runx2, *C*) were expressed in COS7 cells and immunoprecipitated (*IP*) with the indicated antibodies. Blots were then probed for Runx2 (HA or M2 antibodies) or total ERK. *Panel C* also shows immunoprecipitation results using either full-length or the 1–330 truncated Runx2 containing either wild type sequence (*WT*) or the S301A,S319A double mutation (*SA*). *Panel D* compares immunoprecipitation activity of WT Runx2 with an internal deletion containing a consensus ERK-binding D site (amino acid residues 201–215).

or S301A,S319A mutant Runx2 were transfected into COS7 cells together with 6OSE2-luc, and luciferase activity was measured after a 24-h treatment with FGF2. Consistent with our previous report (13), FGF2 stimulated 6OSE2-luc activity in a Runx2-dependent manner. However, growth factor activity was significantly reduced, although not eliminated, in cells transfected with the S301A,S319A mutant (Fig. 5*C*). Taken together, studies with full-length Runx2 indicate that Ser[301] and Ser[319] phosphorylation sites are important for MAPK responsiveness although more distal sites outside the 1–330 region may also be needed for full transcriptional activation.

Requirement for Ser[301] and Ser[319] Phosphorylation Sites for Osteoblast-specific Gene Expression and Differentiation—The studies shown in Fig. 5 demonstrated that S301A,S319A mutations in Runx2-(1–330) completely blocked Mek(sp)-dependent activation of transcriptional activity, whereas the same mutations in the context of the full-length Runx2 molecule only partially eliminated MAPK responsiveness. Because results from transcription assays using constitutively active kinases

and artificial reporter constructs often do not mimic those obtained with endogenous genes, we considered it important to show that these mutations also reduce the ability of Runx2 to stimulate endogenous osteoblast gene expression and differentiation. Two approaches were taken to address this issue. In the first, mTERT-immortalized calvarial cells from Runx2$^{-/-}$ mice (34) were transfected with wild type Runx2, S301A,S319A, or S301E,S319E mutants (Fig. 6). After 5 days of growth in ascorbic acid-containing medium to stimulate ECM-dependent differentiation, total RNA was isolated and levels of osteocalcin (*A*) and bone sialoprotein mRNAs (*B*) were measured by quantitative reverse transcription-PCR. As expected, wild type Runx2 transfection strongly induced both mRNAs and this induction was suppressed by the MAPK inhibitor, U0126. In contrast, the S301A,S319A mutant only weakly stimulated mRNA expression and its activity was resistant to further inhibition by U0126. The S301E,S319E mutant, on the other hand, induced *Ocn* and *Bsp* mRNAs to higher levels than those obtained with wild type Runx2 via a mechanism that was largely resistant to MAPK inhibition. As shown in *panel C*, these results cannot be explained by differences in expression levels of wild type and mutant Runx2 proteins.

To examine the requirement for Runx2 phosphorylation sites in osteoblast differentiation over a more prolonged time period, we used an adenovirus expression system in C3H10T1/2 cells. This mesenchymal cell line contains no detectable endogenous Runx2, but will undergo osteoblast differentiation after transduction with an adeno-Runx2 expression vector. Previous studies showed that AdRunx2 vectors continue to produce active transcription factors for at least 7–10 days in this system (36). Wild type and S301A,S319A Runx2 adenovirus were constructed and titered in C3H10T1/2 cells to produce equivalent amounts of Runx2 protein as measured on Western blots. As shown in Fig. 7, wild type Runx2 clearly induced osteoblast differentiation in this system. Sustained induction of alkaline phosphatase activity (*panel A*) as well as *Ocn* and *Bsp* mRNAs (*panels B* and *C*) was observed over a 12-day period. In contrast, cells expressing the Ser/Ala mutant had less than 25% the alkaline phosphatase activity of wild type at all times examined. Induction of *Ocn* and *Bsp* mRNAs was similarly attenuated. Western blot results revealed little or no differences in Runx2 protein levels in the two groups at all times examined, making it unlikely that differences in Runx2 expression or stability could explain these results.

DISCUSSION

In this study, we identified two phosphorylation sites in Runx2 at Ser[301] and Ser[319] that are required for MAPK-dependent activation of Runx2 transcriptional activity and osteoblast differentiation. These sites are phosphorylated in a MAPK-dependent manner in intact cells. As shown by MS/MS analysis, at least one, Ser[319], is a direct ERK1 substrate. Furthermore, Runx2 can bind ERK using a D site between amino acids 201 and 215 in the runt domain region. Consistent with Ser[301] and Ser[319] being important for osteoblast function, inactivating Ser to Ala mutations greatly reduced the ability of Runx2 to stimulate expression of *Ocn* and *Bsp* mRNAs in Runx2$^{-/-}$ calvarial cells and blocked Runx2-dependent induction of osteo-

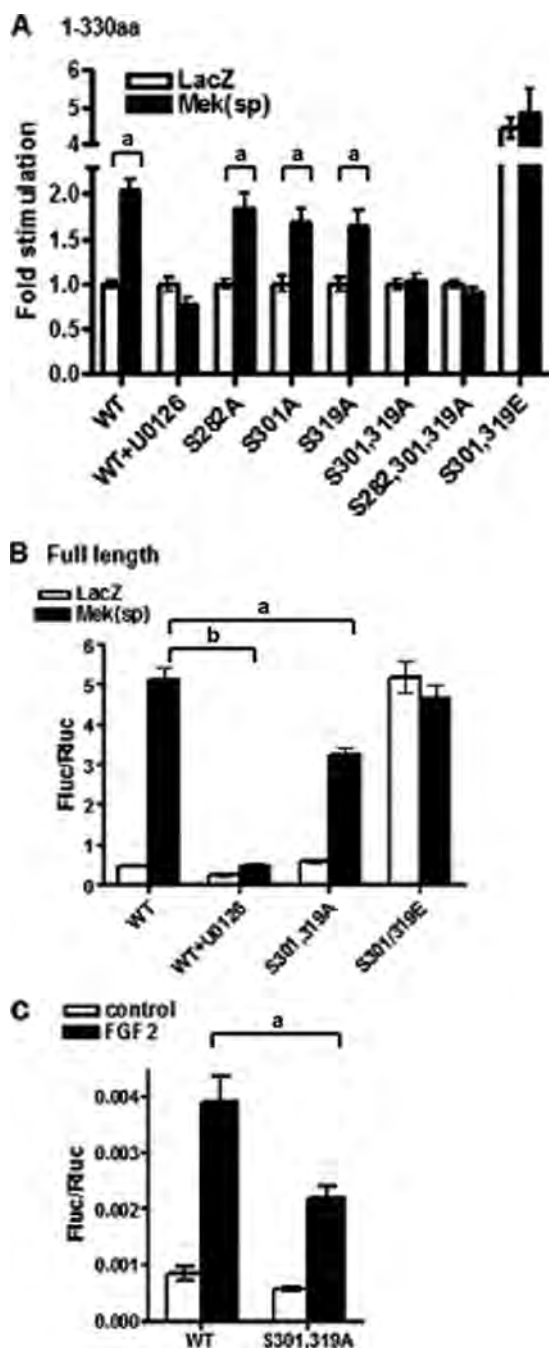## MAPK Regulation of Runx2 Phosphorylation

FIGURE 5. **Functional analysis of Runx2 phosphorylation sites.** *A*, identification of phosphorylation sites necessary for MAPK responsiveness using Runx2-(1–330). Specific mutations were created in Runx2-(1–330) to generate S282A, S301A, or S319A mutants or the indicated combinations as well as an S301E,S319E mutant. Runx2 expression plasmids were transfected into COS7 cells in the presence or absence of Mek(sp) vector and luciferase reporters as described in the legend to Fig. 1. *B*, evaluation of requirement for Ser[301] and Ser[319] sites in the context of full-length Runx2 protein. S301A,S319A or S301E,S319E mutations were generated in full-length Runx2 and evaluated for Mek(sp) responsiveness as in *panel A*. *C*, FGF2-responsiveness of wild type (*WT*) and mutant Runx2. COS7 cells were transfected with wild type full-length Runx2 or the S301A,S319A mutant. After 24 h, cells were treated for an additional 24 h with FGF2 (50 ηg/ml) before luciferase activity was measured. Statistically significant differences are indicated: *a*, $p < 0.05$; *b*, $p < 0.01$. *Error bars*, ±S.D.
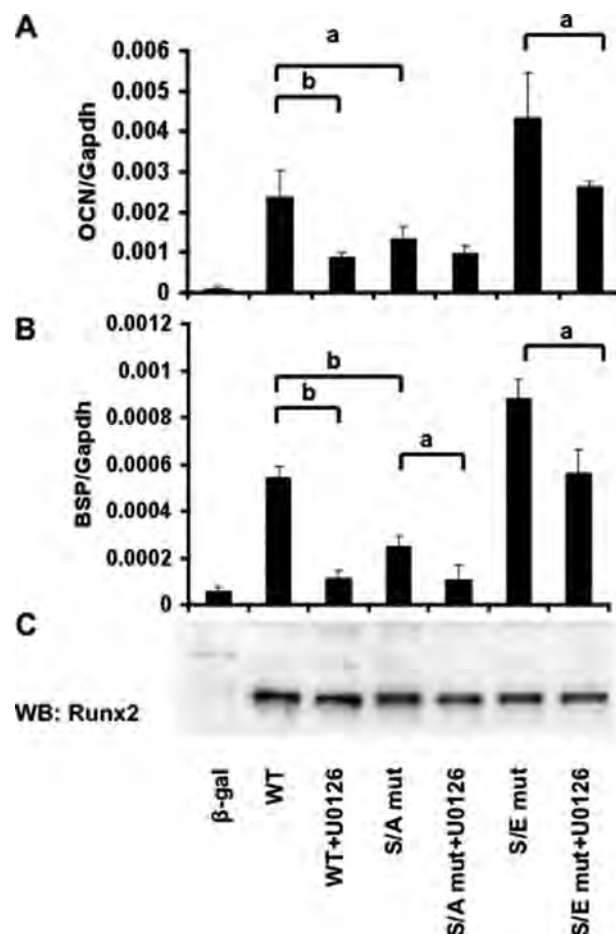
FIGURE 6. **Induction of osteoblast differentiation markers by wild type (WT) Runx2 and phosphorylation site mutants.** An mTERT-immortalized cell line derived from Runx2$^{-/-}$ calvaria was transfected with wild type and mutant Runx2 expression vectors and grown for 5 days in ascorbic acid-containing medium before measurement of *Ocn* (*A*) and *Bsp* (*B*) mRNAs by real-time reverse transcription-PCR. Indicated samples were also treated with U0126 12 h before harvest. The mRNA levels were normalized to glyceraldehyde-3-phosphate dehydrogenase (*Gapdh*) mRNA in each sample. Runx2 protein in each group was measured on Western blots (*WB*) (*C*). *S/A mut*, S301A,S319A mutant; *S/E mut*, S301E,S319E mutant. Statistically significant differences are indicated: *a*, $p < 0.05$; *b*, $p < 0.01$. *β-gal*, β-galactosidase. *Error bars*, ±S.D.

pendent transcription. Taken together, these studies emphasize the importance of MAPK-dependent phosphorylation as a means of controlling Runx2 transcriptional activity in bone.

As one of the major signal transduction pathways in bone, the ERK/MAPK pathway is able to integrate stimuli from growth/differentiation factor binding to receptor tyrosine kinases (39), ECM-integrin binding and focal adhesion kinase activation (40), certain non-genomic actions of estrogens (41), and mechanical stimulation mediated by FAK activation (42) and connexin 43 up-regulation (43). It also has important functions in the differentiation of post-mitotic mesenchymal and neuronal cells (44, 45) and regulates the activity of several tissue-specific transcription factors including MyoD (muscle (46)), Sox9 (cartilage (47)) and peroxisome proliferator-activated receptor γ (adipose (48)). Furthermore, as previously shown by this laboratory, *in vivo* transgenic stimulation of ERK/MAPK signaling in osteoblasts accelerates bone development and is able to partially rescue the cleidocranial dysplasia pheno-
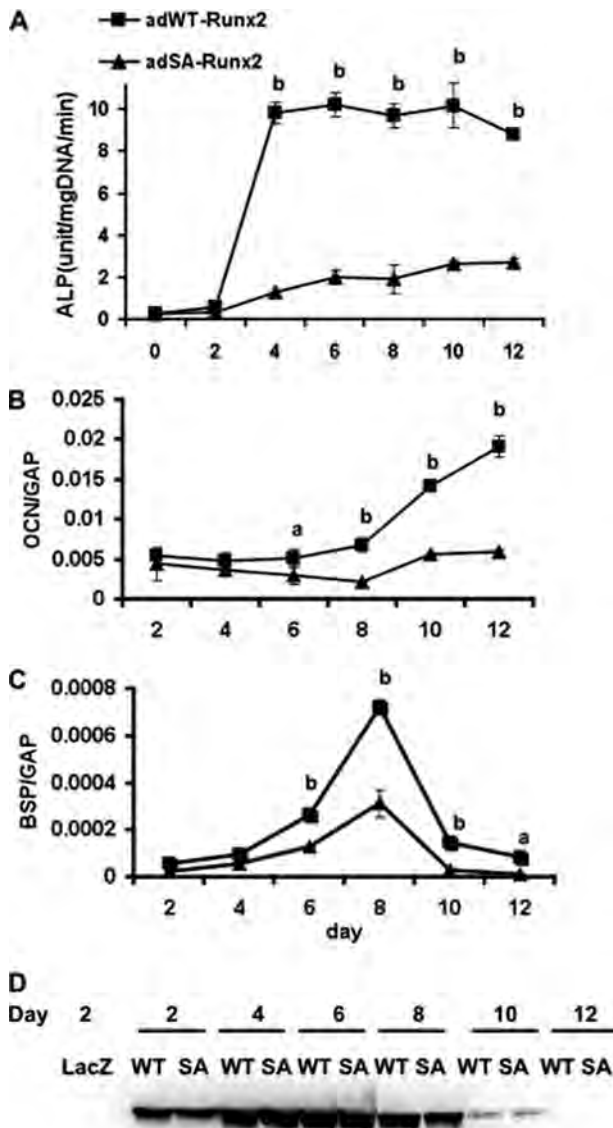
blast gene expression and differentiation in a mesenchymal cell line. In contrast, Ser to Glu mutations, which mimic the charge density of phosphorylated amino acids, activated Runx2-de-

FIGURE 7. **Induction of osteoblast differentiation by wild type Runx2 and the S301A,S319A phosphorylation site mutant.** Adenovirus expression vectors containing wild type and S301A,S319A Runx2 mutants (SA) were used to transduce C3H10T1/2 mesenchymal cells. Cells were then grown in differentiation medium for the indicated times before measurement of alkaline phosphatase activity (*ALP*; *A*) or *Ocn/Bsp* mRNA levels (*OCN* and *BSP*; normalized to glyceraldehyde-3-phosphate dehydrogenase (GAP); *C* and *D*). Runx2 protein in each sample was measured on Western blots (*D*). Statistically significant differences are indicated: *a*, $p < 0.05$; *b*, $p < 0.01$. *SA*, S301A,S319A mutant. *Error bars*, ±S.D.

type of Runx2 haploinsufficient mice (14). Based on this work, it is likely that the phosphorylation sites we identified at Ser[301] and Ser[319] are critical for regulating Runx2 activity *in vivo* and may function to integrate the osteogenic response to hormonal, mechanical, and environmental stimuli.

Although Ser[301] and Ser[319] are clearly very important for Runx2 transcriptional activity, it is possible that other sites also participate in the MAPK response. Specifically, progressively larger C-terminal deletions of Runx2 gradually reduced MAPK-dependent activation of the 6OSE2-luc reporter gene, with the truncated Runx2-(1–330) being the minimal Runx2 truncation that still retained MAPK responsiveness (Fig. 1). It is, therefore,

possible that phosphorylation sites in the region between residues 330 and 528 may also participate in the MAPK response, perhaps functioning as secondary sites after priming phosphorylations occur at Ser[301] and Ser[319]. Consistent with this idea, our MS/MS analysis, which identified peptides containing all proline-directed serines in Runx2 except Ser[301], detected two additional direct MAPK phosphorylation sites at Ser[43] and Ser[510] as well as an indirect MAPK site at Ser[282]. Also, the S301A,S319A mutant Runx2 still retained a MAPK-dependent increase in total P-serine on Western blots as would be expected if additional sites were present (Fig. 3). However, the observation that the high constitutive activity of the S301E,S319E Runx2 mutant was refractory to MAPK inhibition (Fig. 6) argues against these other sites being major contributors to the MAPK response because inhibiting their phosphorylation was not able to prevent the transcriptional activation seen when 301 and 319 sites were in an activated state.

MAPK-dependent phosphorylation of Runx2 is also clearly required for FGF2-dependent induction of *Ocn* expression (13). However, S301A,S319A mutations only partially blocked FGF2 activation of the 6OSE2-luc reporter (Fig. 5*C*). This partial inhibition may be explained by the involvement of additional MAPK sites as well as other kinase sites. In this regard, a recent study by Kim and co-workers (49) reported that FGF2 also activates Runx2 via phosphorylation by PKCγ at Ser[247]. Thus, it is possible that FGF2 activates Runx2 transcriptional activity by phosphorylating both ERK/MAPK and PKC sites.

Runx family members exhibit a high degree of amino acid sequence conservation, particularly in the DNA binding or Runt domain. Although the C-terminal Pro/Ser/Thr domain of Runx proteins is not highly conserved, the two phosphorylation sites we identified in Runx2 are also present in Runx1 (but not in Runx3). Interestingly, EGF and phorbol ester activation of the ERK/MAPK pathway can stimulate Runx1 transcriptional activity via phosphorylation on these sites (50, 51). Runx1 is essential for hematopoietic cell differentiation (52) and is also a frequent site for chromosomal translocations in acute myelogenous leukemia. Consistent with this oncogenic activity, transfection of Runx1 into fibroblasts stimulates anchorage-independent growth and transformation. Interestingly, Ser/Ala mutations at Ser[249] and Ser[266] in Runx1 (equivalent to Ser[301] and Ser[319] in Runx2) inhibit growth of NIH 3T3 fibroblasts in soft agar, a common assay for cell transformation (50). Runx2 can also function as an oncogene under certain conditions and has been associated with cell proliferation and migration of breast cancer cells (53, 54). It is, therefore, possible that ERK/MAPK-dependent phosphorylation of Runx2 at Ser[301] and Ser[319] could also be associated with this metastasis-related behavior.

It is not presently understood how phosphorylation of Runx2 stimulates transcription. We and others previously observed that the apparent affinity of Runx2 for OSE2-containing DNA increases with differentiation and this increase can be blocked with MAPK inhibition (12, 26, 55). However, it is not known if this is a direct consequence of Runx2 phosphorylation. Interestingly, using chromatin immunoprecipitation assays, we find Runx2 associated with *Ocn* and *Bsp* chromatin in both differentiated and undifferentiated MC3T3-E1 cells even in the pres-

ence of MAPK inhibition (56). Thus, Runx2 does not dissociate from its binding sites on chromatin even though its *in vitro* affinity for DNA may be lower in the unphosphorylated state. Runx2 is also known to serve as a docking site for many nuclear factors that can form active or inactive transcription complexes on chromatin (57). In this regard, we recently showed that the physical association of Runx2 with ERK reported in the present study can also be detected on the chromatin of Runx2 target genes *in vivo* (56). In this case, P-ERK binding to *Ocn* and *Bsp* chromatin required Runx2 and intact Runx2 binding sites in the DNA. Furthermore, this binding was dependent on the elevated MAPK activity associated with osteoblast differentiation. Runx2 can therefore be viewed as providing a docking site for P-ERK on the chromatin of target genes. In addition to phosphorylating Runx2, chromatin-bound P-ERK may also initiate subsequent events such as phosphorylation of other chromatin substrates or the recruitment of additional factors including histone acetyltransferases like p300/cAMP-response element-binding protein to modify chromatin structure, thereby allowing the initiation of transcription. Interestingly, the ERK/MAPK-dependent phosphorylation of Runx1 discussed above is associated with the dissociation of the histone deacetylase co-factor, mSin3a, from Runx1, thereby allowing subsequent increases in histone acetylation (58). Because Runx1 phosphorylation sites are conserved in Runx2, this observation provides a plausible mechanism for how ERK/MAPK phosphorylation could alter Runx2-dependent transcription. This possibility is currently being pursued by this laboratory. Last, Afzal and co-workers (59) showed that MAPK-mediated phosphorylation of Runx2 is also necessary for complex formation with Smads.

In addition to the ERK/MAPK-dependent regulation of Runx2 described herein, several other types of post-translational modifications have been described for this molecule. Phenylthiohydantoin/protein kinase A-mediated phosphorylation of a C-terminal Runx2 site was correlated with induction of MMP13 (60). More recently, Cdk4-mediated phosphorylation at Ser^{472} was shown to target Runx2 for ubiquitination and proteosomal degradation during the cell cycle (61), whereas cdc2 phosphorylation at Ser^{451} was shown to be necessary for cell cycle progression of endothelial cells (62). Also, glycogen synthase kinase 3β-dependent phosphorylation of Runx2 at Ser^{369}-Ser^{373}-Ser^{377} was shown to reduce transcriptional activity (63). Last, Runx2 can be acetylated on critical lysine residues by p300 acetyltransferase. This modification, which is stimulated by BMP2, increases transcription and stabilizes Runx2 against proteosomal degradation (64). Thus, post-translational modification appears to be a common mechanism for regulating Runx2 activity and stability.

In summary, phosphorylation of Runx2 at Ser^{301} and Ser^{319} clearly has an important regulatory role in Runx2-dependent transcription because mutation of these sites in the context of the intact Runx2 molecule severely attenuated the ability of Runx2 to stimulate osteoblast-specific gene expression during differentiation. Ongoing *in vivo* studies will be necessary to assess the full impact of Runx2 phosphorylation to the overall activity of this molecule during skeletal development and remodeling.

REFERENCES

1. Ducy, P., Zhang, R., Geoffroy, V., Ridall, A. L., and Karsenty, G. (1997) *Cell* **89,** 747–754
2. Nakashima, K., Zhou, X., Kunkel, G., Zhang, Z., Deng, J. M., Behringer, R. R., and de Crombrugghe, B. (2002) *Cell* **108,** 17–29
3. Yang, X., Matsuda, K., Bialek, P., Jacquot, S., Masuoka, H. C., Schinke, T., Li, L., Brancorsini, S., Sassone-Corsi, P., Townes, T. M., Hanauer, A., and Karsenty, G. (2004) *Cell* **117,** 387–398
4. Ducy, P., Starbuck, M., Priemel, M., Shen, J., Pinero, G., Geoffroy, V., Amling, M., and Karsenty, G. (1999) *Genes Dev.* **13,** 1025–1036
5. Tou, L., Quibria, N., and Alexander, J. M. (2003) *Mol. Cell Endocrinol.* **205,** 121–129
6. Xiao, G., Jiang, D., Thomas, P., Benson, M. D., Guan, K., Karsenty, G., and Franceschi, R. T. (2000) *J. Biol. Chem.* **275,** 4453–4459
7. Xiao, G., Wang, D., Benson, M. D., Karsenty, G., and Franceschi, R. T. (1998) *J. Biol. Chem.* **273,** 32988–32994
8. Franceschi, R. T., and Iyer, B. S. (1992) *J. Bone Miner. Res.* **7,** 235–246
9. Franceschi, R. T., Iyer, B. S., and Cui, Y. (1994) *J. Bone Miner. Res.* **9,** 843–854
10. Franceschi, R. T., Ge, C., Xiao, G., Roca, H., and Jiang, D. (2007) *Ann. N. Y. Acad. Sci.* **1116,** 196–207
11. Xiao, G., Gopalakrishnan, R., Jiang, D., Reith, E., Benson, M. D., and Franceschi, R. T. (2002) *J. Bone Miner. Res.* **17,** 101–110
12. Xiao, G., Cui, Y., Ducy, P., Karsenty, G., and Franceschi, R. T. (1997) *Mol. Endocrinol.* **11,** 1103–1113
13. Xiao, G., Jiang, D., Gopalakrishnan, R., and Franceschi, R. T. (2002) *J. Biol. Chem.* **277,** 36181–36187
14. Ge, C., Xiao, G., Jiang, D., and Franceschi, R. T. (2007) *J. Cell Biol.* **176,** 709–718
15. Zimmerman, D., Jin, F., Leboy, P., Hardy, S., and Damsky, C. (2000) *Dev. Biol.* **220,** 2–15
16. Takeuchi, Y., Nakayama, K., and Matsumoto, T. (1996) *J. Biol. Chem.* **271,** 3938–3944
17. Takeuchi, Y., Suzawa, M., Kikuchi, T., Nishida, E., Fujita, T., and Matsumoto, T. (1997) *J. Biol. Chem.* **272,** 29309–29316
18. Jikko, A., Harris, S. E., Chen, D., Mendrick, D. L., and Damsky, C. H. (1999) *J. Bone Miner. Res.* **14,** 1075–1083
19. Lai, C. F., Chaudhary, L., Fausto, A., Halstead, L. R., Ory, D. S., Avioli, L. V., and Cheng, S. L. (2001) *J. Biol. Chem.* **276,** 14443–14450
20. Jaiswal, R. K., Jaiswal, N., Bruder, S. P., Mbalaviele, G., Marshak, D. R., and Pittenger, M. F. (2000) *J. Biol. Chem.* **275,** 9645–9652
21. Shui, C., Spelsberg, T. C., Riggs, B. L., and Khosla, S. (2003) *J. Bone Miner. Res.* **18,** 213–221
22. Schmidt, C., Pommerenke, H., Dürr, F., Nebe, B., and Rychly, J. (1998) *J. Biol. Chem.* **273,** 5081–5085
23. Pavalko, F. M., Chen, N. X., Turner, C. H., Burr, D. B., Atkinson, S., Hsieh, Y. F., Qiu, J., and Duncan, R. L. (1998) *Am. J. Physiol. Cell Physiol.* **275,** C1591–C1601
24. Ziros, P. G., Gil, A. P., Georgakopoulos, T., Habeos, I., Kletsas, D., Basdra, E. K., and Papavassiliou, A. G. (2002) *J. Biol. Chem.* **277,** 23934–23941
25. Zayzafoon, M., Abdulkadir, S. A., and McDonald, J. M. (2004) *J. Biol. Chem.* **279,** 3662–3670
26. Qiao, M., Shapiro, P., Kumar, R., and Passaniti, A. (2004) *J. Biol. Chem.* **279,** 42709–42718
27. Celil, A. B., Hollinger, J. O., and Campbell, P. G. (2005) *J. Cell. Biochem.* **95,** 518–528
28. Celil, A. B., and Campbell, P. G. (2005) *J. Biol. Chem.* **280,** 31353–31359
29. Ducy, P., and Karsenty, G. (1995) *Mol. Cell. Biol.* **15,** 1858–1869
30. Thirunavukkarasu, K., Mahajan, M., McLarren, K. W., Stifani, S., and Karsenty, G. (1998) *Mol. Cell. Biol.* **18,** 4197–4208
31. Zheng, C. F., and Guan, K. L. (1993) *J. Biol. Chem.* **268,** 23933–23939
32. de Boer, E., Rodriguez, P., Bonte, E., Krijgsveld, J., Katsantoni, E., Heck, A., Grosveld, F., and Strouboulis, J. (2003) *Proc. Natl. Acad. Sci. U.S.A.* **100,** 7480–7485
33. Hardy, S., Kitamura, M., Harris-Stansil, T., Dai, Y., and Phipps, M. L. (1997) *J. Virol.* **71,** 1842–1849
34. Bae, J. S., Gutierrez, S., Narla, R., Pratap, J., Devados, R., van Wijnen, A. J.,

Stein, J. L., Stein, G. S., Lian, J. B., and Javed, A. (2007) *J. Cell. Biochem.* **100,** 434–449

35. Wang, D., Christensen, K., Chawla, K., Xiao, G., Krebsbach, P. H., and Franceschi, R. T. (1999) *J. Bone Miner. Res.* **14,** 893–903

36. Yang, S., Wei, D., Wang, D., Phimphilai, M., Krebsbach, P. H., and Franceschi, R. T. (2003) *J. Bone Miner. Res.* **18,** 705–715

37. Akella, R., Moon, T. M., and Goldsmith, E. J. (2008) *Biochim. Biophys. Acta* **1784,** 48–55

38. Mansour, S. J., Matten, W. T., Hermann, A. S., Candia, J. M., Rong, S., Fukasawa, K., Vande Woude, G. F., and Ahn, N. G. (1994) *Science* **265,** 966–970

39. Cobb, M. H., Boulton, T. G., and Robbins, D. J. (1991) *Cell Regul.* **2,** 965–978

40. Franceschi, R. T., and Xiao, G. (2003) *J. Cell. Biochem.* **88,** 446–454

41. Kousteni, S., Han, L., Chen, J. R., Almeida, M., Plotkin, L. I., Bellido, T., and Manolagas, S. C. (2003) *J. Clin. Invest.* **111,** 1651–1664

42. Moalli, M. R., Wang, S., Caldwell, N. J., Patil, P. V., and Maynard, C. R. (2001) *J. Appl. Physiol.* **91,** 912–918

43. Lecanda, F., Warlow, P. M., Sheikh, S., Furlan, F., Steinberg, T. H., and Civitelli, R. (2000) *J. Cell Biol.* **151,** 931–944

44. Yao, Y., Li, W., Wu, J., Germann, U. A., Su, M. S., Kuida, K., and Boucher, D. M. (2003) *Proc. Natl. Acad. Sci. U.S.A.* **100,** 12759–12764

45. Kao, S., Jaiswal, R. K., Kolch, W., and Landreth, G. E. (2001) *J. Biol. Chem.* **276,** 18169–18177

46. Zetser, A., Frank, D., and Bengal, E. (2001) *Dev. Biol.* **240,** 168–181

47. Murakami, S., Kan, M., McKeehan, W. L., and de Crombrugghe, B. (2000) *Proc. Natl. Acad. Sci. U.S.A.* **97,** 1113–1118

48. Adams, M., Reginato, M. J., Shao, D., Lazar, M. A., and Chatterjee, V. K. (1997) *J. Biol. Chem.* **272,** 5128–5132

49. Kim, B. G., Kim, H. J., Park, H. J., Kim, Y. J., Yoon, W. J., Lee, S. J., Ryoo, H. M., and Cho, J. Y. (2006) *Proteomics* **6,** 1166–1174

50. Tanaka, T., Kurokawa, M., Ueki, K., Tanaka, K., Imai, Y., Mitani, K., Okazaki, K., Sagata, N., Yazaki, Y., Shibata, Y., Kadowaki, T., and Hirai, H. (1996) *Mol. Cell. Biol.* **16,** 3967–3979

51. Zhang, Y., Biggs, J. R., and Kraft, A. S. (2004) *J. Biol. Chem.* **279,** 53116–53125

52. Tanaka, T., Tanaka, K., Ogawa, S., Kurokawa, M., Mitani, K., Nishida, J., Shibata, Y., Yazaki, Y., and Hirai, H. (1995) *EMBO J.* **14,** 341–350

53. Barnes, G. L., Hebert, K. E., Kamal, M., Javed, A., Einhorn, T. A., Lian, J. B., Stein, G. S., and Gerstenfeld, L. C. (2004) *Cancer Res.* **64,** 4506–4513

54. Pratap, J., Lian, J. B., Javed, A., Barnes, G. L., van Wijnen, A. J., Stein, J. L., and Stein, G. S. (2006) *Cancer Metastasis Rev.* **25,** 589–600

55. Fujita, T., Azuma, Y., Fukuyama, R., Hattori, Y., Yoshida, C., Koida, M., Ogita, K., and Komori, T. (2004) *J. Cell Biol.* **166,** 85–95

56. Li, Y., Ge, C., and Franceschi, R. (2009) *J. Bone Miner. Res.,* in press

57. Lian, J. B., Javed, A., Zaidi, S. K., Lengner, C., Montecino, M., van Wijnen, A. J., Stein, J. L., and Stein, G. S. (2004) *Crit. Rev. Eukaryot. Gene Expr.* **14,** 1–41

58. Imai, Y., Kurokawa, M., Yamaguchi, Y., Izutsu, K., Nitta, E., Mitani, K., Satake, M., Noda, T., Ito, Y., and Hirai, H. (2004) *Mol. Cell. Biol.* **24,** 1033–1043

59. Afzal, F., Pratap, J., Ito, K., Ito, Y., Stein, J. L., van Wijnen, A. J., Stein, G. S., Lian, J. B., and Javed, A. (2005) *J. Cell. Physiol.* **204,** 63–72

60. Selvamurugan, N., Pulumati, M. R., Tyson, D. R., and Partridge, N. C. (2000) *J. Biol. Chem.* **275,** 5037–5042

61. Shen, R., Wang, X., Drissi, H., Liu, F., O'Keefe, R. J., and Chen, D. (2006) *J. Biol. Chem.* **281,** 16347–16353

62. Qiao, M., Shapiro, P., Fosbrink, M., Rus, H., Kumar, R., and Passaniti, A. (2006) *J. Biol. Chem.* **281,** 7118–7128

63. Kugimiya, F., Kawaguchi, H., Ohba, S., Kawamura, N., Hirata, M., Chikuda, H., Azuma, Y., Woodgett, J. R., Nakamura, K., and Chung, U. I. (2007) *PLoS ONE* **2,** e837

64. Jeon, E. J., Lee, K. Y., Choi, N. S., Lee, M. H., Kim, H. N., Jin, Y. H., Ryoo, H. M., Choi, J. Y., Yoshida, M., Nishino, N., Oh, B. C., Lee, K. S., Lee, Y. H., and Bae, S. C. (2006) *J. Biol. Chem.* **281,** 16502–16511

IDENTIFICATION AND FUNCTIONAL CHARACTERIZATION OF EXTRACELLULAR-REGULATED KINASE/MAPK PHOSPHORYLATION SITES IN THE RUNX2 TRANSCRIPTION FACTOR

Chunxi Ge[1,4], Guozhi Xiao[3,4], Di Jiang[1], Qian Yang[1], Nan E. Hatch[1] and Renny T. Franceschi[1,2].
From Department of Periodontics and Oral Medicine, School of Dentistry[1] and Department of Biological Chemistry, School of Medicine[2], University of Michigan, Ann Arbor, MI 48109-1078, [3]Department of Medicine, University of Pittsburgh, Pittsburgh, PA 15240. [4]Both authors contributed equally to this study.

Supplementary Figure S1

Supplementary Figure Legend

Address Correspondence to : Renny T. Franceschi, Department of Periodontics and Oral Medicine, University of Michigan School of Dentistry, 1011 N. University Ave., Ann Arbor, MI 48109-1078; Tel. 734 763-7381; FAX 734 763-5503; email: rennyf@umich.edu

Supplementary Figure S1
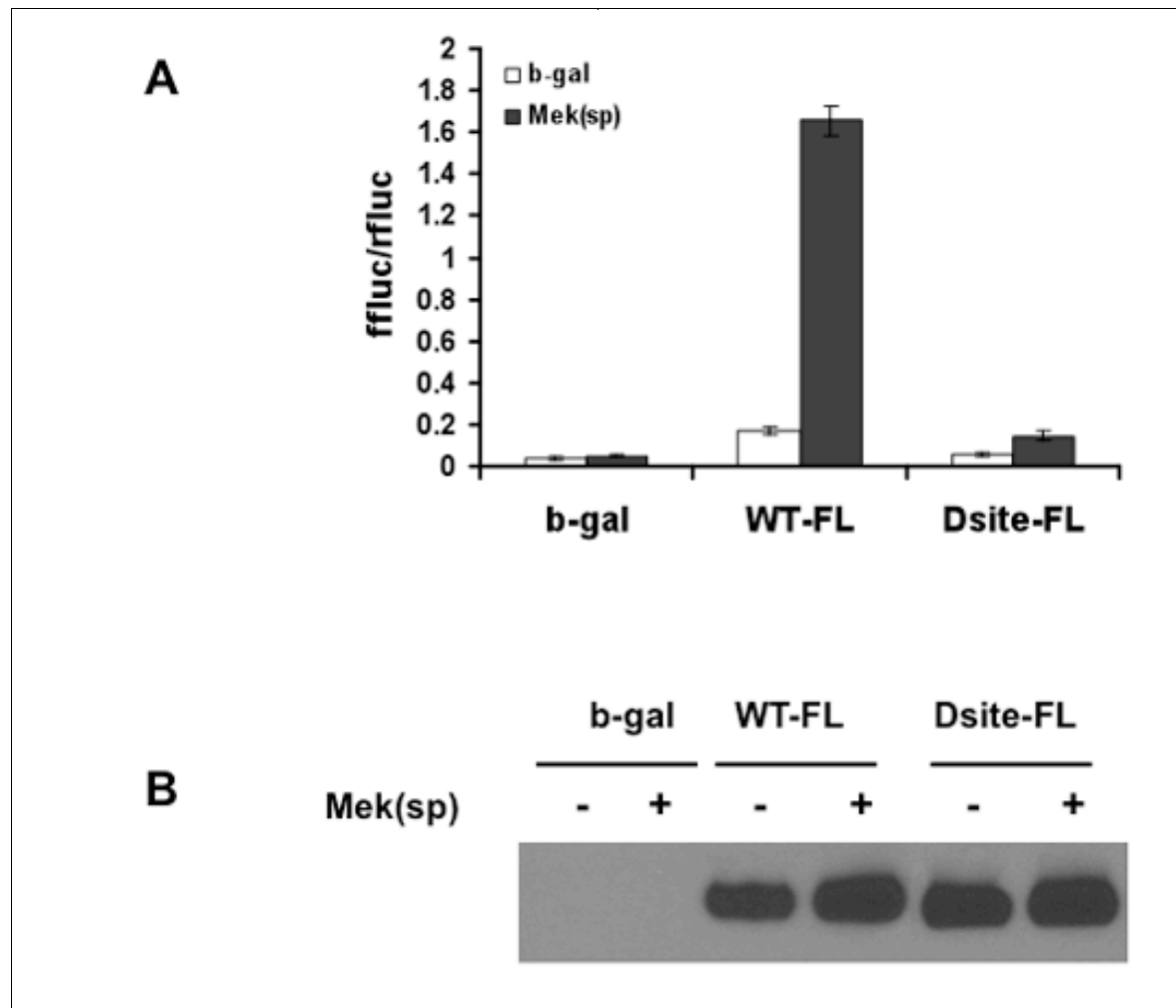
SUPPLEMENTARY FIGURE LEGEND

Supplementary Figure S1. Effect of D site deletion on MAPK-stimulated Runx2 transcriptional activity. Wild type full-length Runx2 (WT-FL) or Runx2 containing a 15 amino acid residue deletion (Δ201-215) spanning the Erk-binding D site (D site-FL) was transfected into COS7 cells with a 6OSE2-luc reporter and renilla normalization vector in the presence or absence of constitutively-active Mek1 (Meksp). After 48 h, cells were harvested for measurement of luciferase activity (A) or total transfected Runx2 protein as measured by immunoblotting (B).

PLoS one

Critical Role of Activating Transcription Factor 4 in the Anabolic Actions of Parathyroid Hormone in Bone

Shibing Yu[1], Renny T. Franceschi[4,5], Min Luo[1], Jie Fan[2], Di Jiang[4], Huiling Cao[1], Tae-Geon Kwon[7], Yumei Lai[3], Jian Zhang[6], Kenneth Patrene[1], Kurt Hankenson[8], G. David Roodman[1], Guozhi Xiao[1]*

1 Department of Medicine, University of Pittsburgh, Pittsburgh, Pennsylvania, United States of America, 2 Department of Surgery, University of Pittsburgh, Pittsburgh, Pennsylvania, United States of America, 3 Department of Pharmacology and Chemical Biology, University of Pittsburgh, Pittsburgh, Pennsylvania, United States of America, 4 Department of Periodontics and Oral Medicine, University of Michigan, Ann Arbor, Michigan, United States of America, 5 Department of Biological Chemistry, School of Dentistry, University of Michigan, Ann Arbor, Michigan, United States of America, 6 Department of Medicine, School of Medicine, University of Michigan, Ann Arbor, Michigan, United States of America, 7 Department of Oral and Maxillofacial Surgery, School of Dentistry, Kyungpook National University, Daegu, Korea, 8 Department of Animal Biology, School of Veterinary Medicine, University of Pennsylvania, Philadelphia, Pennsylvania, United States of America

Abstract

Parathyroid hormone (PTH) is a potent anabolic agent for the treatment of osteoporosis. However, its mechanism of action in osteoblast and bone is not well understood. In this study, we show that the anabolic actions of PTH in bone are severely impaired in both growing and adult ovariectomized mice lacking bone-related activating transcription factor 4 (ATF4). Our study demonstrates that ATF4 deficiency suppresses PTH-stimulated osteoblast proliferation and survival and abolishes PTH-induced osteoblast differentiation, which, together, compromise the anabolic response. We further demonstrate that the PTH-dependent increase in osteoblast differentiation is correlated with ATF4-dependent up-regulation of Osterix. This regulation involves interactions of ATF4 with a specific enhancer sequence in the Osterix promoter. Furthermore, actions of PTH on Osterix require this same element and are associated with increased binding of ATF4 to chromatin. Taken together these experiments establish a fundamental role for ATF4 in the anabolic actions of PTH on the skeleton.

Competing Interests: The authors have declared that no competing interests exist.

* E-mail: xiaog@upmc.edu

Introduction

Parathyroid hormone (PTH) is a major regulator of calcium homeostasis and has both catabolic and anabolic effects on osteoblasts and bone that depend on the temporal pattern of administration. Continuous administration of PTH decreases bone mass whereas intermittent administration increases bone mass [1–6]. The mechanism(s) responsible for these differing effects are poorly understood. The anabolic activity of PTH has been attributed to both direct actions of this hormone on osteoprogenitor cells as well as indirect effects mediated by the production of growth factors such as insulin-like growth factor-1 (IGF-1) and basic fibroblast growth factor-2 (FGF-2) [7,8]. Most cellular actions of PTH are mediated by the PTH-1 receptor, a G protein-coupled receptor that is expressed in osteoblasts [9,10]. Binding of PTH to its receptor activates multiple intracellular signaling pathways that involve cAMP, inositol phosphates, intracellular Ca^{2+}, protein kinases A and C [11], and the extracellular signal-related (ERK)/mitogen-activated protein kinase (MAPK) pathway [12,13]. Activation of these signal transduction pathways ultimately affects cellular behavior. In this regard, the anabolic actions of PTH on bone have been attributed to increased proliferation of osteopregenitors/osteoblasts [2,14,15] and/or decreased osteoblast apoptosis [6,16,17].

Although a number of transcription factors including cAMP response element binding protein (CREB) [18,19], AP1 family members [20–22], and Runx2 [20,23] have been implicated in the molecular actions of PTH in osteoblasts, genetic studies have not strongly linked any of these factors in the anabolic actions of this hormone. To better understand the anabolic actions of PTH, it is essential that the downstream signals induced by this hormone be identified and evaluated for possible roles in bone formation. The osteocalcin (Ocn) promoter has been an important tool for unraveling the mechanisms mediating osteoblast-specific gene expression and was used to identify a number of important transcription factors and cofactors involved in Ocn gene expression [24–28]. Because the Ocn gene is regulated by PTH [29,30], we have used it as a model system for identifying new transcriptional mediators of PTH action. We previously demonstrated that the OSE1 (osteoblast-specific element 1) in the proximal mOG2 promoter [24] is necessary and sufficient for PTH induction of this gene [31]. The OSE1 core sequence (TTACATCA) was subsequently identified as a DNA binding site for the ATF4 transcription factor. The critical role of ATF4 in osteoblast differentiation and bone development was established using Atf4-deficient mice [26]. At the cellular level, ATF4 is critical for proliferation and differentiation as well as survival in osteoblasts [32,33]. We recently showed that ATF4 is also required for PTH induction of Ocn expression in osteoblasts [34]. Specifically, PTH elevated levels of ATF4 mRNA and protein in a dose and time-dependent manner and increased binding of ATF4 to OSE1 DNA. Furthermore, PTH stimulation of Ocn expression was lost by siRNA downregulation of ATF4 in

MC-4 cells and in primary bone marrow stromal cells from $Atf4^{-/-}$ mice. Collectively, these studies demonstrate that ATF4 is a novel downstream mediator of PTH signaling.

Osterix (Osx, or Sp7), a zinc-finger-containing transcription factor of the sp family, is essential for osteoblast differentiation and bone formation [35]. Since Osx is not detected in mice lacking Runx2 [35], a master regulator of osteoblast differentiation [25,36–38], it functions downstream of Runx2. However, the molecular mechanisms whereby the Osx gene is transcriptionally regulated are not well understood.

In the present study, we used ATF4-deficient mice to determine whether ATF4 is more generally required for the in vivo anabolic actions of PTH in bone as well as explore the mechanism used by PTH to regulate ATF4 activity. As will be shown, loss of ATF4 greatly attenuated the anabolic effects of PTH. Furthermore, ATF4 may participate in the PTH response by regulating the expression of the Osterix transcription factor.

Results

The anabolic effects of PTH on bone are severely impaired in growing Atf4-deficient mice

We first evaluated our hypothesis that ATF4 mediates the anabolic actions of PTH in bone using a relatively simple "growing mouse" model system, that has been widely used for studying the anabolic actions of PTH, PTHrP, FGF2, and IGF-1 in bone [2–4,8,39,40]. The advantages of this system are that it is less time consuming and costly versus adult ovarectomized mouse models. Furthermore, because young growing animals have relatively high osteoblast activity, they are more sensitive to PTH than adults [2,11,14,16–18,41–43]. Mice were treated with vehicle or PTH and sacrificed 24 h after the last PTH injection. PTH-dependent anabolic activity was evaluated in these mice using standard biochemical and histomorphometric criteria. $Atf4^{-/-}$ mice grew more slowly than wild type (wt) animals. The growth rate was slightly but significantly increased by PTH treatment during d 6–18 in wt but not $Atf4^{-/-}$ animals (Fig. S1A). $Atf4^{-/-}$ femurs were also shorter than wt or $Atf4^{+/-}$ femurs. Consistent with results from a previous study [3], PTH did not alter the length of femurs (Fig. S1B). However, it did significantly increase the dry ash weight per femur in wt and $Atf4^{+/-}$ but not in $Atf4^{-/-}$ mice (Fig. S1C). Serum Pi and calcium concentration (Fig. S1D and E) were not markedly affected by PTH or ATF4 deficiency. Faxitron X-ray analysis of femurs revealed that wt and $Atf4^{+/-}$ mice responded to PTH with markedly increased radiopacity throughout the whole femur, with the most dramatic increase in the metaphyseal region (Fig. S2, top and middle). In contrast, PTH only slightly increased the radiopacity in the same region of $Atf4^{-/-}$ femurs (Fig. S2, bottom). As shown in Fig. 1, quantitative μCT analysis of femur histomorphometric parameters showed that $Atf4^{-/-}$ mice had a significant reduction in bone volume/tissue volume (BV/TV), trabecular number (Tb.N), and cortical thickness (Cort.Th) and a marked increase in trabecular space (Tb.Sp) compared with the wt or $Atf4^{+/-}$ littermates. These data confirmed an essential role of ATF4 in bone that was previously demonstrated by the Karsenty group [26]. As expected, in wt femurs, intermittent PTH increased BV/TV, Tb.N, and Tb.Th by 5.4-fold, 2.7-fold, and 1.5-fold, respectively, and decreased Tb.Sp by 60 percent. Similar effects were also seen in $Atf4^{+/-}$ mice (Fig. 1B). In contrast, the PTH response was greatly attenuated in $Atf4^{-/-}$ mice where the following PTH responses were observed; BV/TV, 2.2-fold increase; Tb.N, 1.7-fold increase; Tb.Th, 1.1-fold increase; Tb.Sp, 36 percent decrease. In all cases, the magnitude of PTH-stimulated changes on BV/TV, Tb.N, Tb.Sp was dramatically reduced in $Atf4^{-/-}$ mice relative to wt or $Atf4^{+/-}$ mice (P<0.05,

PTH/veh-wt vs. PTH/veh-$Atf4^{-/-}$). Furthermore, PTH-stimulated increases in Cort.Th and Tb.Th were completely lost in $Atf4^{-/-}$ femurs. Because PTH similarly affected all trabecular and cortical parameters in $Atf4^{+/+}$ and $Atf4^{+/-}$ mice, subsequent experiments compared the PTH effects on bone only between wt and $Atf4^{-/-}$ mice.

We next measured effects of $Atf4$ gene ablation on PTH stimulation of tibiae, vertebrae, and calvariae. The anabolic effect of PTH on wt tibiae was so dramatic that the majority of the bone marrow cavity was replaced by newly formed bone (Fig. 2A and B). In $Atf4^{-/-}$ tibiae, while PTH still induced a small increase in trabecular area, the magnitude of stimulation was significantly reduced (5-fold in wt vs. 2.2-fold in $Atf4^{-/-}$)(P<0.05, PTH/veh-wt vs. PTH/veh-$Atf4^{-/-}$)(Fig. 2C-E). Likewise, the PTH-stimulated increase in the trabeculae of vertebrae (L5) was markedly reduced in $Atf4^{-/-}$ mice (3-fold in wt vs. 2-fold in $Atf4^{-/-}$) (P<0.05, PTH/veh-wt vs. PTH/veh-$Atf4^{-/-}$)(Fig. 2F–J). When histological sections of calvariae were compared, PTH increased the width of the calvariae by 1.8-fold in wt mice, a response that was abolished in $Atf4^{-/-}$ animals (Fig. 2K–O).

Ablation of the Atf4 gene impairs PTH stimulation of trabecular, but not cortical bone in 7-month-old ovariectomized (OVX) mice

The experiments described above clearly establish a critical role of ATF4 in the anabolic effects of PTH on long bones, vertebrae, and calvariae in rapidly growing mice. However, it is possible that results obtained from growing animals may be different from those in adults due to possible effects of PTH and/or ATF4 on animal growth or influences of animal growth on the anabolic response to PTH, either of which could complicate the interpretation of the results. In contrast, adult mice have a mature skeleton in which these possible complications can be avoided. Furthermore, the OVX mouse provides a model that may be more relevant to the clinical applications of PTH in the treatment of osteoporosis. For these reasons, we next evaluated whether ATF4 is required for the anabolic response to PTH in 7-month-old OVX mice. OVX surgery was successful as demonstrated by significant reduction in BV/TV (65 percent), Tb.N (27 percent), and Tb.Th (18 percent) and increased Tb.Sp (37 percent) relative to sham surgery (P<0.05, wt-sham vs. wt-OVX) (Fig. S3). OVX surgery did not reduce Cort.Th, which is consistent with results from rats [44], Interestingly, OVX surgery did not significantly reduce bone parameters in $Atf4^{-/-}$ animals (P>0.05, $Atf4^{-/-}$-sham vs. $Atf4^{-/-}$-OVX). As shown in Fig. 3 A–C, similar to results from growing mice, ablation of the $Atf4$ gene significantly decreased BV/TV and Tb.N and increased Tb.Sp in adult OVX mice. In further agreement with results in young mice, $Atf4^{-/-}$ animals exhibited a clearly attenuated response to PTH. For example, while PTH increased BV/TV by 7.8-fold in wt mice, this value was only increased 4.2-fold in $Atf4^{-/-}$ animals. Similarly, while PTH still stimulated formation of trabecular bone in $Atf4^{-/-}$ trabeculae, the magnitude of this response was significantly reduced compared to wt control (P<0.05, PTH/veh-wt vs. PTH/veh-$Atf4^{-/-}$). In contrast to result from growing mice, Cort.Th was not reduced by ablation of the $Atf4$ gene in adult OVX mice (0.21±0.01 mm in wt vs. 0.19±0.02 mm in $Atf4^{-/-}$, P>0.05 wt vs. $Atf4^{-/-}$). Also, PTH was much less effective in stimulating Cort.Th in adult OVX mice (24%) than in growing mice (95%) (Figs. 1 and 3). Furthermore, no difference in stimulation of cortical thickness by PTH was observed when wt and $Atf4^{-/-}$ groups were compared (24% wt vs. 21% $Atf4^{-/-}$)(P>0.05, PTH/veh-wt vs. PTH/veh-$Atf4^{-/-}$). As shown in Fig. 3D and E, results from calcein double labeling of 7-month old OVX wt and $Atf4^{-/-}$ tibia revealed that the PTH-stimulated increase in mineral
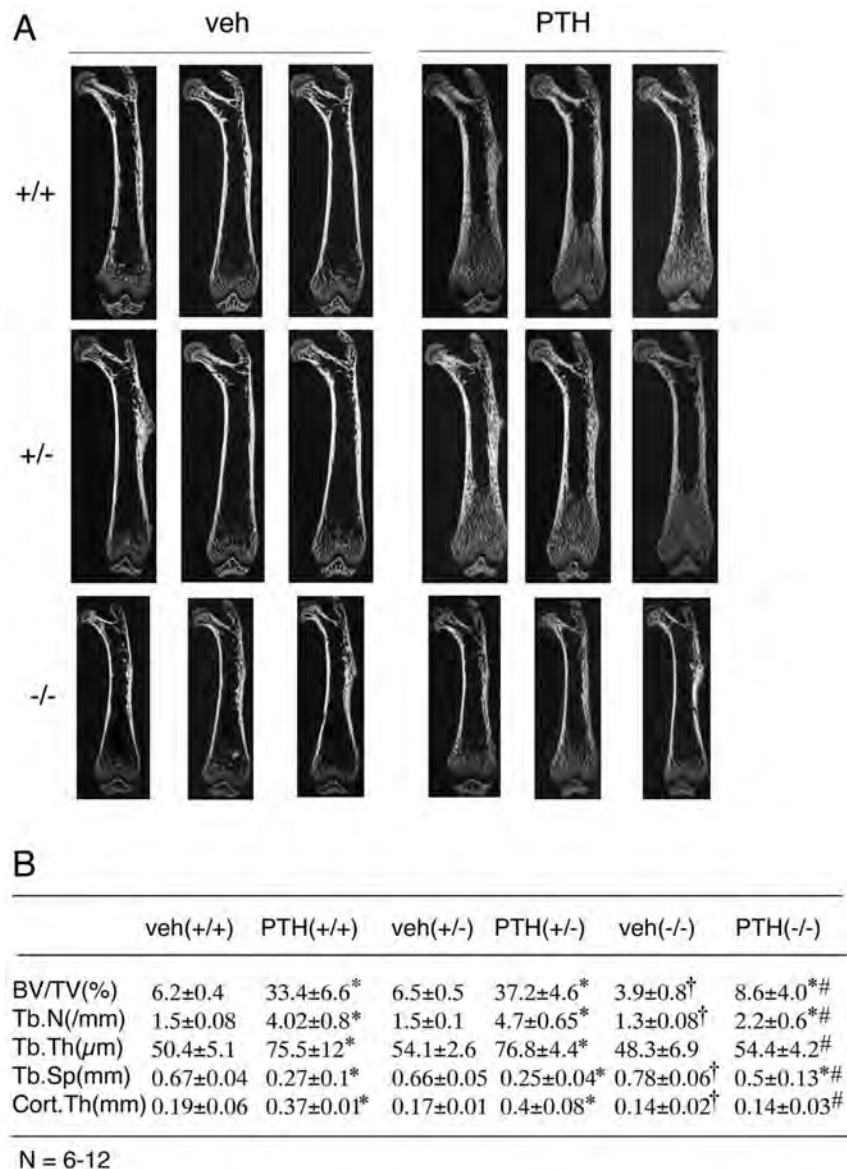
Figure 1. PTH-stimulated bone was significantly reduced or lost in Atf4$^{-/-}$ femurs. A, two-dimensional (2D) reconstruction from μCT scan of femurs from growing *wt*, *Atf4$^{+/-}$* and *Atf4$^{-/-}$* mice treated with and without intermittent PTH for 28 d. B, quantitative analysis of bone volume/tissue volume (BV/TV), trabecular number (Tb. N), trabecular thickness (Tb.Th), trabecular space (Tb.Sp), and cortical thickness (Cort. Th). *P<0.05 (veh vs. PTH), † P<0.05 (wt-veh vs. *Atf4$^{-/-}$*-veh), #P<0.05 (PTH/veh-wt vs. PTH/veh-*Atf4$^{-/-}$*).
doi:10.1371/journal.pone.0007583.g001

ATF4 deficiency significantly reduces basal and PTH-stimulated proliferation in osteoblasts/preosteoblasts

apposition rate (MAR), an indicator of osteoblast function, was significantly reduced by ATF4 deficiency (P<0.05, PTH/veh-wt vs. PTH/veh-*Atf4$^{-/-}$*).

PTH and PTHrP are both known to increase the proliferation and numbers of osteoblasts [14,15,17,45]. ATF4 is also a positive regulator of osteoblast proliferation and can be up-regulated by PTH in these cells [33,34]. To determine whether ATF4 plays a role in PTH regulation of osteoblast proliferation, sections of tibiae and calvariae from wt and *Atf4$^{-/-}$* mice treated with and without intermittent PTH were analyzed for in vivo cell proliferation using a Zymed BrdU immunostaining kit. As shown in Fig. 4A, B, and E, in wt mice, PTH increased the percentage of proliferating osteoblasts/preosteoblasts of tibial trabeculae by 2.8-fold relative to vehicle-

treated control. Ablation of the *Atf4* gene resulted in a 50% decline in basal proliferation. In addition, the PTH-stimulated increase in proliferation was decreased by 40 percent (Fig. 4C–E). Similarly, PTH-induced proliferation in calvarial periosteal osteoblasts was also significantly reduced by ATF4 deficiency (Fig. 4F–J). As expected, very few osteocytes were BrdU-positive in both tibiae and calvariae. Note: basal proliferation rate of calvarial periosteal osteoblasts was significantly higher than that of tibial trabecular osteoblasts (28% vs. 4%). Therefore, ATF4 is critical for basal and PTH-stimulated proliferation of osteoblasts/preosteoblasts in vivo.

PTH fails to reduce apoptotic death in Atf4$^{-/-}$ osteoblasts/osteocytes

Mature osteoblasts synthesize and deposit a mineralizing extracellular matrix and become osteocytes. Both osteoblasts and osteocytes can be lost through apoptosis. PTH signaling increases
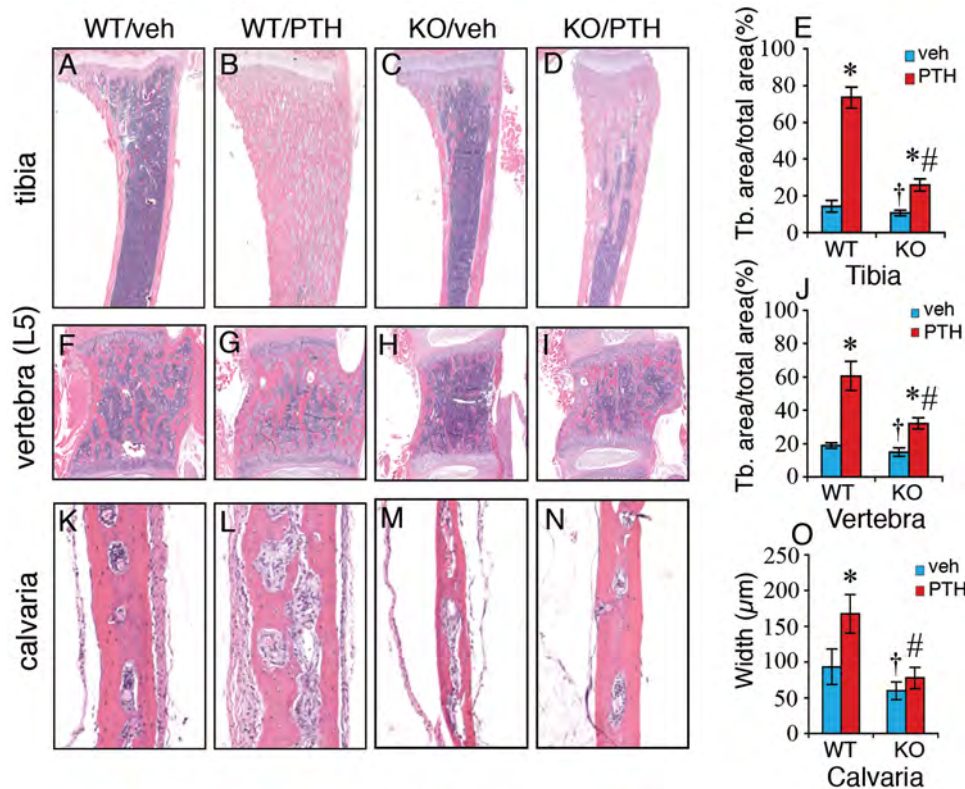
Figure 2. PTH-stimulated bone is severely impaired in Atf4$^{-/-}$ tibiae, vertebrae, and calvariae. Representative H&E stained sections of tibiae (A–E), vertebrae (L5) (F–J), and calvariae (K–O) are shown. Trabecular bone area versus total area of tibiae (E) and vertebrae (J) was measured using an Image Pro Plus 6.2 software. The calvarial width was obtained from 20 random measurements throughout the whole calvaria using a SPOT Advanced imaging software (O). *P<0.05 (veh vs. PTH), † P<0.05 (wt-veh vs. Atf4$^{-/-}$-veh), #P<0.05 (PTH/veh-wt vs. PTH/veh-Atf4$^{-/-}$).
doi:10.1371/journal.pone.0007583.g002

the survival of osteoblasts and osteocytes by reducing apoptosis [6,16,17,45]. Our recent study shows that ATF4 is anti-apoptotic in osteoblasts [33]. To determine whether ATF4 plays a role in PTH-mediated anti-apoptosis, sections of tibiae were stained with TUNEL and apoptotic cells were assessed. As shown in Fig. 4K and L, ATF4 deficiency significantly increased the basal levels of apoptosis. As expected, PTH dramatically reduced apoptotic death of tibial trabecular osteoblasts/osteocytes by 48 percent, which is consistent with results from previous studies [6,16,17,45]. Importantly, the PTH-stimulated decrease in apoptotic death was completely abolished in Atf4$^{-/-}$ trabeculae (Fig. 4M–O). ATF4 was similarly required for PTH to inhibit apoptosis in cortical osteocytes of tibiae (Fig. 4P). Collectively, ATF4 is essential for PTH-mediated inhibition of apoptosis in osteoblasts/osteocytes in vivo.

PTH-induced increase in expression of osteoblast differentiation marker genes is dramatically reduced or completely abolished in Atf4$^{-/-}$ animals

We next determined the effects of ATF4 deficiency on PTH induction of osteoblast differentiation markers in vivo. Total RNA was isolated from tibiae of wt and Atf4$^{-/-}$ mice treated with and without PTH for 28 d and expression levels of osteoblast differentiation marker genes were measured by quantitative real-time PCR analysis. As shown in Fig. 5A, PTH dramatically elevated the expression of genes known to be associated with osteoblast differentiation including osteocalcin (Ocn) (2.2-fold), bone sialoprotein (Bsp) (4.2-fold), alkaline phosphatase (Alp) (3.2-fold), α1(I) collagen (Col1(I))(4.7-fold), osteopontin (Opn) (4.6-fold), and osterix (Osx)

(4.1-fold). Importantly, this PTH regulation was either dramatically reduced or completely abolished in Atf4$^{-/-}$ tibiae. ATF4 deficiency also reduced basal Ocn and Osx mRNA levels. Consistent with our previous report [34], PTH increased Atf4 mRNA 2.2-fold in wt tibiae, while Atf4 was undetectable in Atf4$^{-/-}$ animals. In contrast, c-Fos and c-Jun, both early PTH-induced genes, were not induced by PTH in either wt or Atf4$^{-/-}$ tibiae. As shown in Fig. 5B, the levels of IGF-1 and FGF-2 which have both been implicated in the anabolic actions of PTH in bone [7,8] were markedly reduced in plasma from Atf4$^{-/-}$ mice compared to wt mice (P<0.05, wt vs. Atf4$^{-/-}$). However, their levels were not significantly elevated by the treatment of intermittent PTH in both wt or Atf4$^{-/-}$ animals (P>0.05, veh vs. PTH).

Intermittent PTH increases in vivo Osx expression in osteoblasts through a pathway requiring ATF4

Our above results demonstrate that ATF4 is essential for the major anabolic actions of PTH on bone and is also required for PTH-dependent induction of osteoblast differentiation. To begin to address the mechanism underlying this response, we measured the expression of Osterix (Osx) and Runx2 proteins, two critical transcription factors that regulate osteoblast differentiation. Initially, we used immunohistochemistry (IHC) to measure Osx in the tibiae and calvaria of wt and Atf4$^{-/-}$ mice with or without 28 d anabolic PTH treatment. As shown in Fig. 6, in wt-vehicle-treated tibiae, Osx-positive osteoblasts were only identified in the trabeculae and cortical endosteum close to the growth plate (Fig. 6A1, B1, and D1) and were almost undetectable in the same
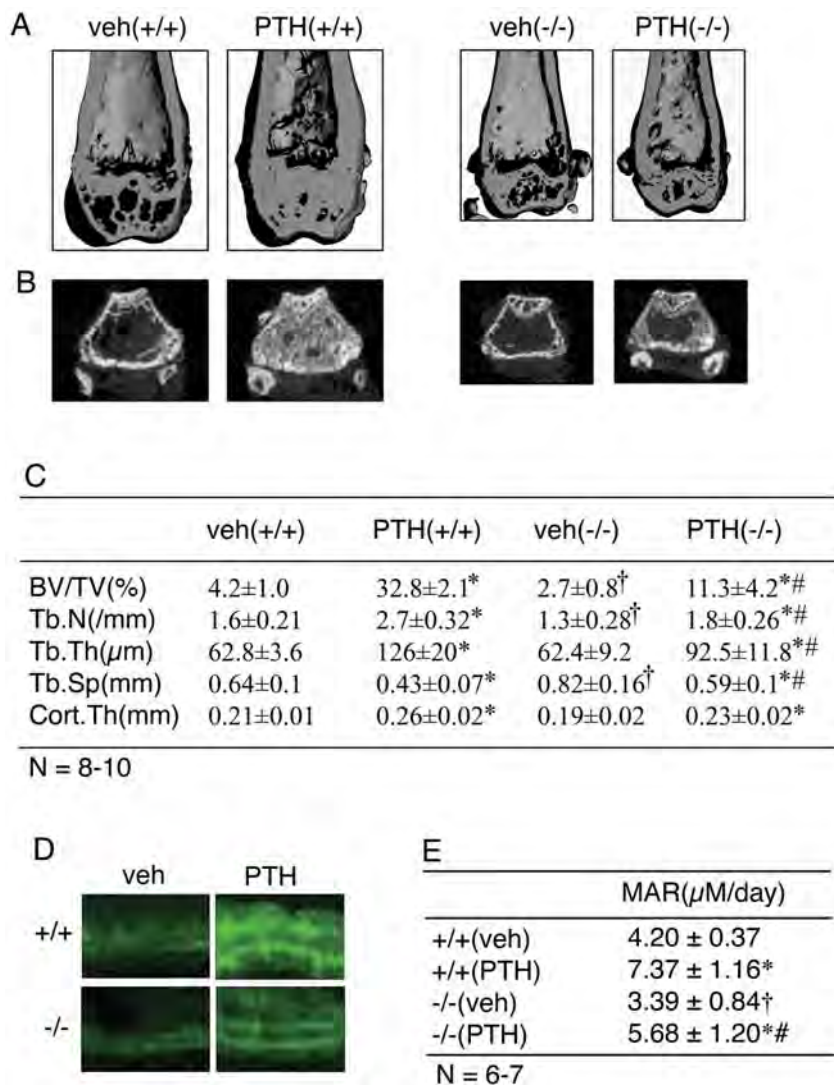
Figure 3. Effects of ATF4 deficiency on PTH stimulation in adult OVX bone. A, three-dimensional (3D) reconstruction from μCT scan of distal femurs of adult OVX mice. B, sagittal view of 2D distal femur at 1.7–2.0 mm from the chondro-osseous junction. C, BV/TV, Tb. N, Tb.Th, Tb.Sp, and Cort.Th. D, calcein double labeling of metaphyseal trabecular bone (magnification,x200). *$P<0.05$ (veh vs. PTH), † $P<0.05$ (wt-veh vs. $Atf4^{-/-}$-veh), #$P<0.05$ (PTH/veh-wt vs. PTH/veh-$Atf4^{-/-}$).
doi:10.1371/journal.pone.0007583.g003

regions close to the marrow (Fig. 6C1), indicating that cells in these areas are still in the immature (preosteoblast) state. In contrast, in the wt-PTH group, Osx-positive osteoblasts were identified on all surfaces of trabeculae and endosteum throughout the tibia. PTH increased the total number of Osx-positive cells per tibial section by 3.2-fold in wt mice (Panel 2). ATF4 deficiency reduced the numbers of Osx-positive cells by 50 percent (Panel 3). Strikingly, although PTH slightly increased bone volume in $Atf4^{-/-}$ bone (Fig. 1 and 2), it failed to elevate the numbers of Osx-positive cells in $Atf4^{-/-}$ tibiae. Similar results were obtained in calvariae (Fig. 6E). The IHC staining was highly specific since no signal was detected in the non-immune IgG control group (Panel 5). Consistent with IHC results, as shown in Fig. 6I, Western blot analysis using protein extracts showed that PTH dramatically elevated the level of Osx protein in wt tibiae. In contrast, Osx was not detected by Western blot in extracts from $Atf4^{-/-}$ animals (Fig. 6I). The level of Runx2 protein was slightly up-regulated by PTH in the wt group, but not in $Atf4^{-/-}$ group. Unlike Osx, the basal level of Runx2 was not reduced by ATF4 deficiency.

PTH1R protein, the major receptor for PTH and PTHrP signaling in osteoblasts, was expressed in endosteal osteoblasts of tibiae (Fig. 6F) and periosteal osteoblasts of calvariae and hypertrophic chrodrocytes in the growth plate area (unpublished data). The signal for PTH1R protein was weak in trabecular osteoblasts that actively form new bone (unpublished data). In contrast to results from a previous study showing that PTH1R is down-regulated by PTH in cultured osteoblasts [46], PTH1R was slightly increased by intermittent PTH treatment in vivo as measured by IHC and Western blot analysis. Importantly, ATF4 deficiency did not reduce the level of PTH1R (Fig. 6F and I). In addition, primary calvarial osteoblasts from wt and $Atf4^{-/-}$ mice displayed an identical cAMP accumulation curve in response to treatment of increasing concentrations of PTH in vitro. Taken together, these results indicate that the impaired anabolic response of skeleton to PTH observed in $Atf4^{-/-}$ animals cannot be explained by a reduction in the level of PTH1R and/or cAMP production. These results clearly demonstrate that: i) intermittent PTH stimulates the expression of Osx and, to a lesser extent,
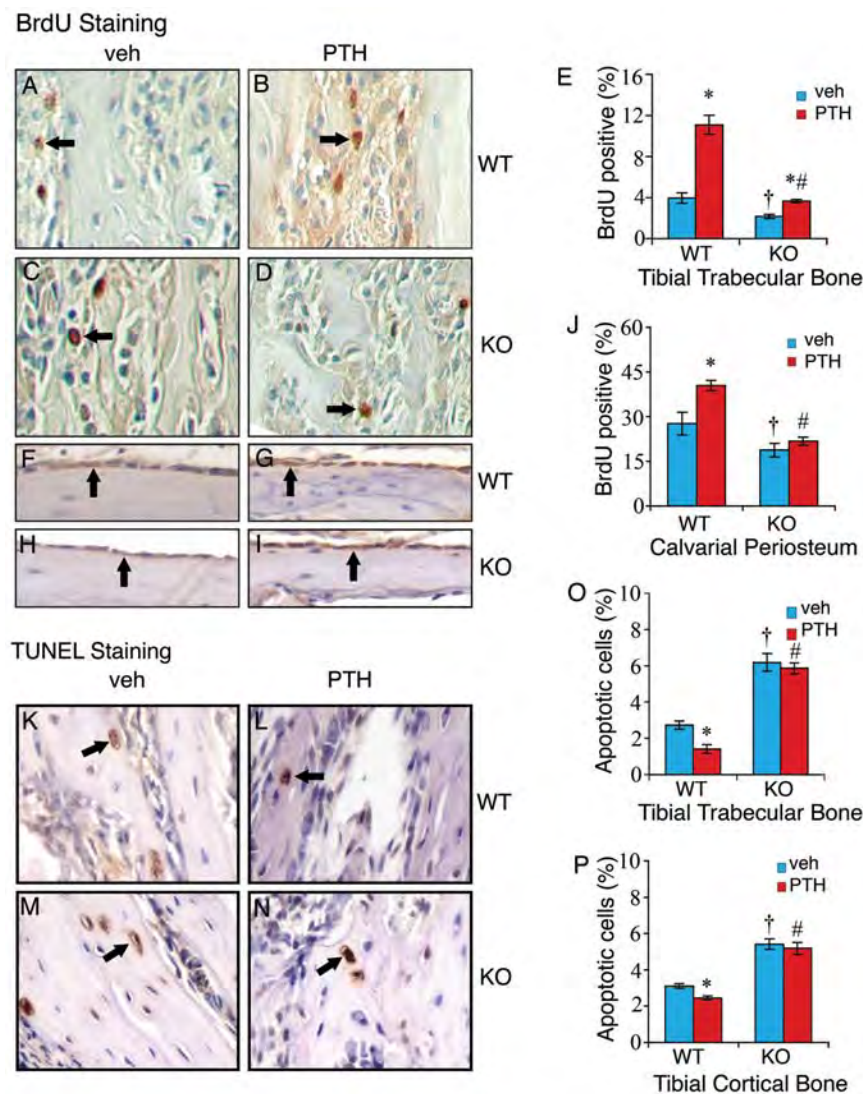
Figure 4. Effects of PTH on osteoblast proliferation and survival in wt and Atf4$^{-/-}$ bone. A–J, BrdU staining, sections of tibiae (A–D) and calvariae (F–I) were stained using a Zymed BrdU immunostaining kit. Proliferating cells were stained brown (arrows) and non-proliferating cells were stained blue. Proliferating cells on tibial trabecular surface or osteoid (E) or calvarial periosteal surface (J) were counted and normalized to total cells from the same area. K–P, TUNEL staining, sections of tibiae were stained using the ApopTag Peroxidase *In Situ* Apoptosis Detection Kit. Apoptotic osteoblasts and osteocytes (arrows) were stained brown and non-apoptotic cells were stained blue. Apoptotic osteoblasts and osteocytes in the trabecular (O) and cortical bone (P) of tibiae were counted and normalized to total osteoblasts and osteocytes from the same area. *P<0.05 (veh vs. PTH), † P<0.05 (wt-veh vs. *Atf4$^{-/-}$*-veh), #P<0.05 (PTH/veh-wt vs. PTH/veh-*Atf4$^{-/-}$*).
doi:10.1371/journal.pone.0007583.g004

Runx2, ii) PTH fails to stimulate Osx/Runx2 expression in the absence of ATF4, and iii) ATF4 is also required for basal level Osx expression.

Identification of a 132-bp ATF4-response element in proximal Osx promoter

Osx is not detected in *Runx2$^{-/-}$* mice [35], indicating that Runx2 functions upstream of this factor and is essential for Osx expression. However, the results described above showed that ATF4 deficiency dramatically reduced the level of Osx protein without decreasing Runx2, suggesting that Runx2 is not sufficient for the maximal expression of Osx and that ATF4 has an important role in Osx expression. To define the mechanism whereby ATF4 regulates Osx, we examined the effect of ATF4 overexpression on Osx expression in MC-4 preosteoblast cells. As shown in Fig. 7A, ATF4 dose-dependently increased levels of Osx

protein (top) and mRNA (bottom). We next examined whether ATF4 up-regulates Osx by increasing gene transcription by using a −1003/+68 mouse Osx promoter (Fig. 7 B). Using COS-7 cells, which lack detectable Runx2, ATF4 had comparable activity to Runx2 in terms of its ability to activate promoter activity (approx. 1.8-fold). Together, ATF4 and Runx2 maximally activated the *Osx* promoter (3.2-fold induction). To further define the region of the Osx promoter necessary for ATF4 responsiveness, several constructs containing various deletion mutants of the mouse *Osx* promoter were transiently transfected into COS-7 cells with and without an ATF4 expression plasmid. Results showed that luciferase activity of both control and ATF4-transfected groups decreased with progressively larger 5′ deletions. However, ATF4 stimulation was abrogated when a 132-bp region between bp −215 to −83 was deleted (Fig. 7C). A putative ATF4-binding sequence (CTTCCTCA) at −201/−194 bp was identified in this
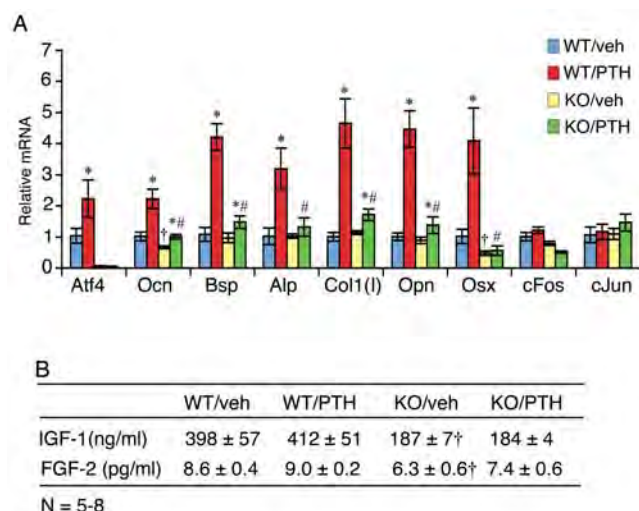
Figure 5. Effects of PTH on expression of osteoblast marker genes in wt and ATF4 deficient mice. A, quantitative real-time PCR, total RNAs were isolated from tibiae and analyzed by quantitative real-time RT-PCR using specific primers for *Atf4*, *Ocn*, *Bsp*, *Col 1(l)*, *ALP*, *Opn*, *Pthrp*, *c-Fos*, and *c-Jun* mRNAs, which were normalized to *Gapdh* mRNA. *$P<0.05$ (veh vs. PTH), #$P<0.05$ (wt-veh vs. *Atf4*$^{-/-}$-veh). B, plasma levels of IGF-1 and FGF-2 from mice using respective ELISA kits according to the manufacturer's instructions. *$P<0.05$ (veh vs. PTH), †$P<0.05$ (wt-veh vs. *Atf4*$^{-/-}$-veh), #$P<0.05$ (PTH/veh-wt vs. PTH/veh-*Atf4*$^{-/-}$).
doi:10.1371/journal.pone.0007583.g005

region by using a TRANSFAC retrieval program. Introduction of a 3-bp substitution mutation to this core sequence (from CTTCCTCA to CTTgtaCA) completely abolished ATF4 activation (Fig. 7D). As shown in Fig. 7E, a DNA oligo probe from the Osx promoter that contains the TTACATCA core sequence bound to a factor(s) in nuclear extracts from COS-7 cells transfected with an ATF4 expression vector. Importantly, this binding (see arrow) was dramatically reduced by the addition of a specific antibody against ATF4 but not by normal control IgG or antibodies against cFos (an AP1 family member) or ATF2.

PTH stimulation of Osx gene transcription requires an ATF4 response element

To study the mechanism whereby PTH regulates *Osx*, we next evaluated the effect of PTH on mouse $-1003/+68$ *Osx* promoter activity in MC-4 preosteoblast cells. As illustrated in Fig. 7F, PTH stimulated promoter activity in a dose-dependent manner with a detectable response seen at a PTH concentration of 10^{-10} M (significance at $P<0.01$). Measurable activation of the *Osx* promoter was observed 0.5 h after PTH addition with maximal induction occurring between 4–6 h (Fig. 7G). PTH-stimulated Osx protein expression was entirely blocked by PKA inhibition (Fig. 7H). The 132-bp ATF4-responsive element identified above was also required for PTH induction of promoter (Fig. 7I). Furthermore, the same 3-bp substitution mutation that abrogates ATF4 activation dramatically reduced PTH-dependent activation (Fig. 7J), indicating that this element is critical for the actions of PTH on this promoter.

ATF4 is recruited to the endogenous Osx promoter in a PTH-dependent manner

To determine whether ATF4 is associated with the endogenous *Osx* promoter in vivo, we performed chromatin immunoprecipi-

tation (ChIP) assays using MC-4 cells with and without PTH treatment. As shown in Fig. 7K and L, ATF4 specifically interacted with a chromatin fragment of the proximal *Osx* promoter that contains the ATF4-binding site identified above. This interaction was not detected in primary calvarial osteoblasts from *Atf4*$^{-/-}$ mice (data not shown). Furthermore, this interaction was dramatically stimulated by PTH treatment. Supporting our previous demonstration that the OSE1 site in the *mOG2* promoter mediates PTH induction of the gene [31,34], ATF4 also bound to an ATF4-binding site (OSE1)-containing chromatin fragment of the proximal *mOG2* promoter in a PTH-dependent manner (primers P3/P4). In contrast, ATF4 antibody failed to immuno-precipitate a 3′ chromatin fragment in the transcribed region of the *mOG2* gene that contains no ATF4-binding sites (primers P5/P6).

Discussion

Our goals in this study were: 1) to determine whether the bone-related transcription factor ATF4 plays a role in the anabolic effects of PTH in bone, and 2) if so, to define the relevant mechanisms. Our results clearly show that PTH-stimulated increases in osteoblast proliferation, volume of long bones, vertebrae, and calvariae as well as decreases in apoptosis are all dramatically reduced or completely abolished in *Atf4*-deficient mice. Equally importantly, PTH-induced bone in *Atf4*$^{-/-}$ mice cannot mature due to a severe defect in osteoblast differentiation as manifested by a defect in Osx expression. Therefore, this study establishes a critical role for ATF4 in the anabolic actions of PTH in bone.

In agreement with results from previous studies [14,47], we find that intermittent PTH dramatically increases trabecular and cortical bone volume. This PTH response is achieved at least in part by stimulating the proliferation of osteoblasts and preosteo-blasts and/or by inhibiting apoptotic death of osteoblasts and osteocytes in vivo [2,6,45,47]. Effects of PTH on osteoblast proliferation and survival can be reproduced in cultured osteoblasts [15,16,48]. Importantly, this study demonstrates that ATF4 plays a pivotal role in PTH stimulation of cell proliferation in osteoblasts and preosteoblasts and attenuation of apoptosis in osteoblasts and osteocytes in vivo. PTH can increase osteoblast proliferation at least in part through ATF4-mediated expression of cyclin D1 [33] because both factors are up-regulated by PTH in osteoblasts [15,34]. The mechanism whereby ATF4 blocks apoptosis in osteoblasts remains unknown. ATF4 deficiency also increases apoptosis in lens fiber cells in a p53-dependent manner. The embryonic lens in double homozygous *p53/Atf4*$^{-/-}$ mice does not undergo apoptosis, which suggests possible involvement of p53 in this process [49,50].

Accumulating evidence supports the concept that, in addition to increasing osteoblast cell number, intermittent PTH also stimulates osteoblast differentiation [4,51–53]. In agreement with these results, the present study clearly demonstrates that: i) PTH dramatically increases the in vivo expression of osteoblast differentiation marker genes, including *Ocn*, *Bsp*, *Alp*, *Opn*, and *Col1(I)*; and ii) PTH strikingly elevates the numbers of Osx-positive osteoblasts (i.e., mature or differentiating osteoblasts) and level of Osx protein as demonstrated by both IHC and Western blot analysis. Because PTH is able to stimulate the expression of many osteoblast differentiation marker genes in cultured osteoblast-like cells [12,30,31,54–57], it is likely that intermittent PTH also activates these genes in vivo via a similar molecular mechanism. Although part of the increased osteoblast activity in PTH-treated animals is likely explained by a PTH-dependent increase in
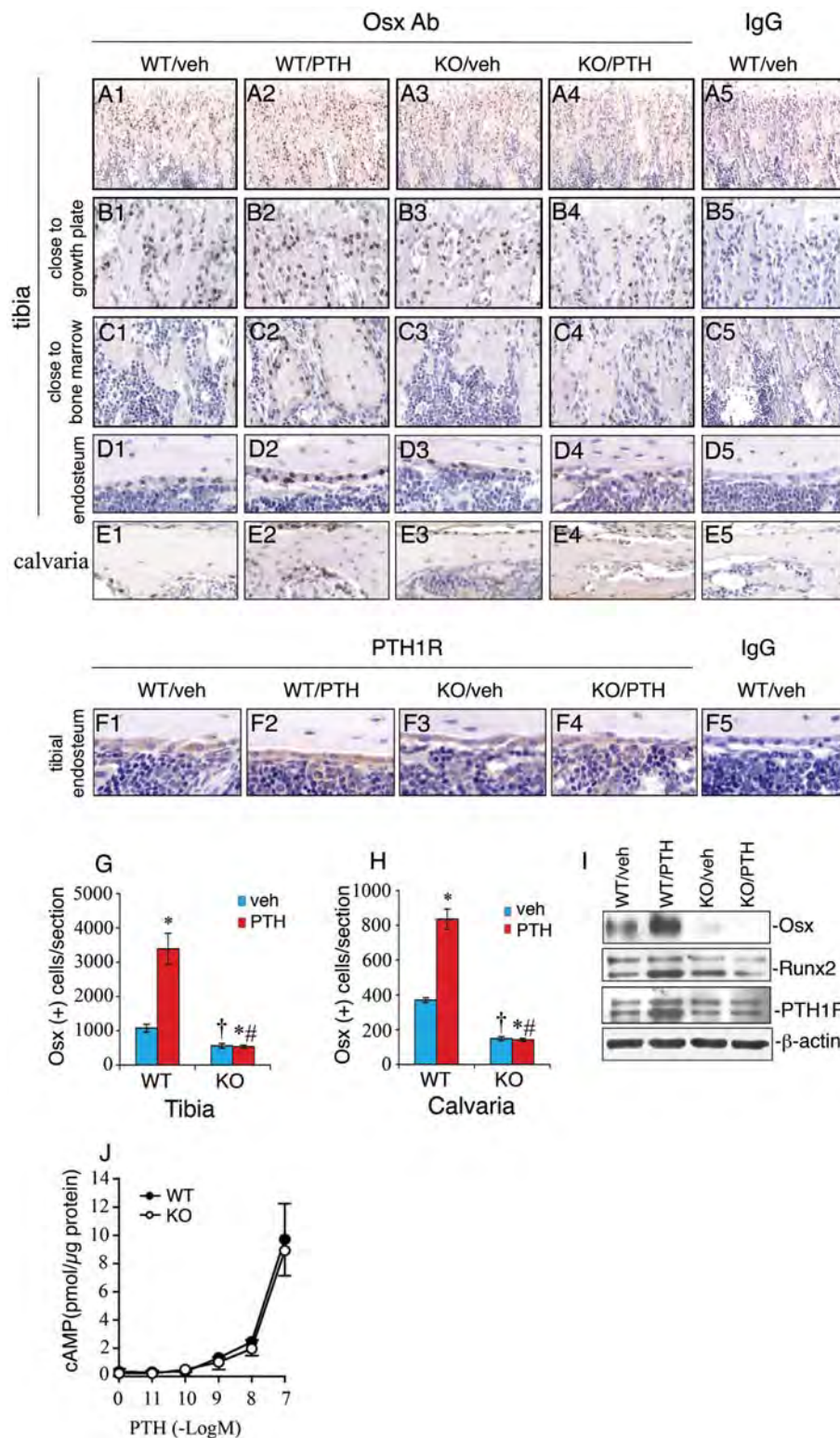
Figure 6. PTH fails to promote osteoblast maturation/differentiation in the absence of ATF4. A–E, IHC analysis of Osx expression, sections of tibiae (A–D) and calvariae (E) were immunohistochemically stained using a specific antibody against Osx protein. The nuclei of Osx-positive cells (i.e., osteoblasts) were stained brown. The nuclei of preosteoblasts and other cells are stained blue. The total numbers of Osx-positive osteoblasts per tibial (G) or calvarial (H) section were counted under microscope. F, sections of tibiae were stained using an antibody against PTH1R protein. I, Western blot analysis, protein extracts were isolated from tibiae and analyzed for Osx, Runx2, and PTH1R proteins. *P<0.05 (veh vs. PTH), † P<0.05 (wt-veh vs. Atf4⁻/⁻-veh), #P<0.05 (PTH/veh-wt vs. PTH/veh-Atf4⁻/⁻). J, cAMP assay, primary calvarial osteoblasts from 3-d-old wt or Atf4⁻/⁻ mice were isolated, seeded at density of 5×10^4 on 96-well plate, and treated with vehicle or increasing concentrations of human recombinant PTH(1-34) for 5 min followed by measurement of cAMP.
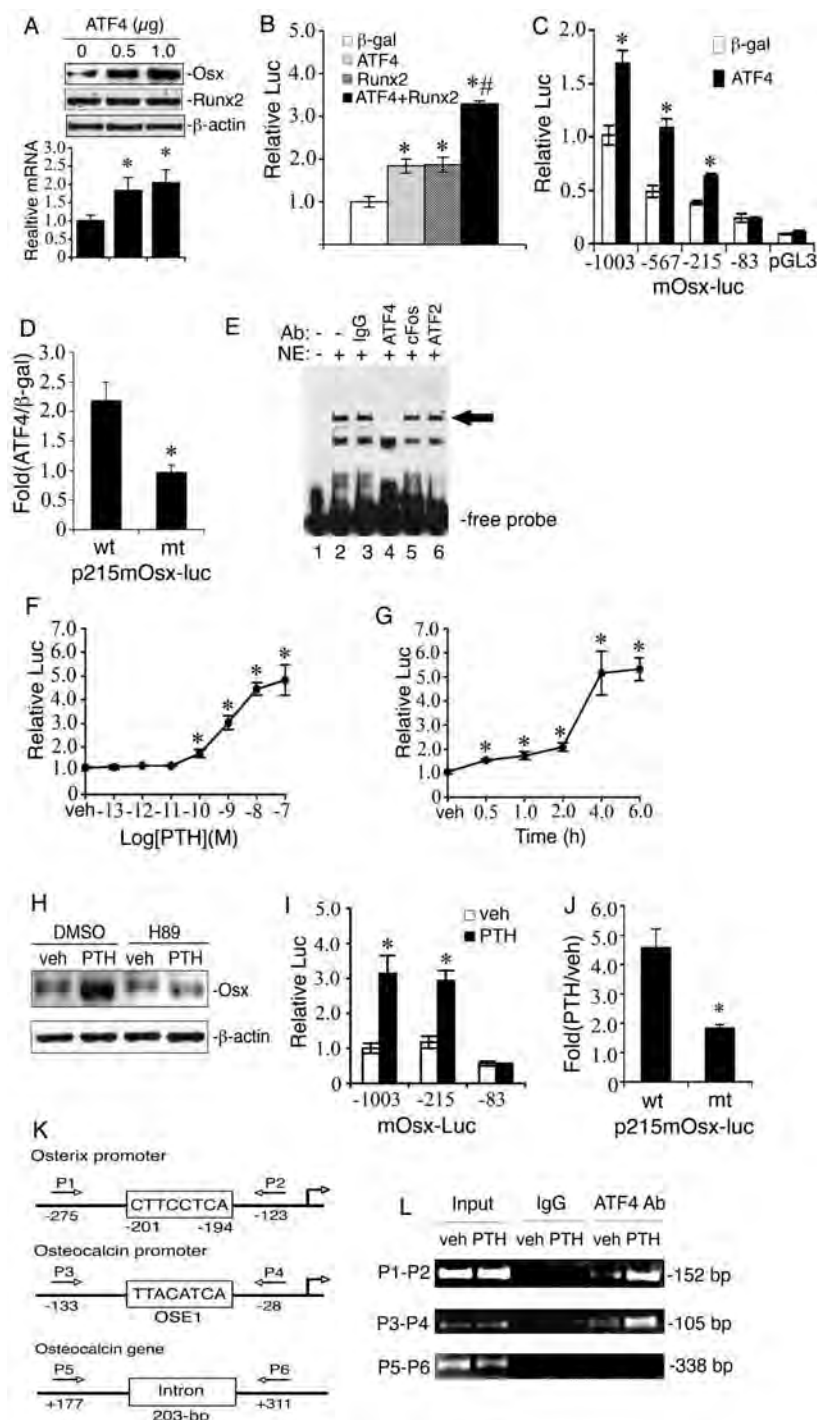doi:10.1371/journal.pone.0007583.g006

Figure 7. PTH activates Osx gene transcription via an ATF4-responsive element in the proximal Osx promoter. A, MC-4 cells were electroporated with indicated amount of ATF4 expression plasmid followed by Western blot. B, COS-7 cells were transfected with p1060mOsx-luc, pRL-SV40, and indicated expression vectors followed by dual luciferase assays. C, COS-7 cells were transfected with various deletion constructs and pRL-SV40 with and without ATF4 expression plasmid. D, COS-7 cells transfected with p215mOsx-luc or the same plasmid containing a 3-bp substitution mutation in the putative ATF4-binding site and pRL-SV40 with and without ATF4 expression plasmid. E, EMSA, labeled wild-type DNA probe was incubated with 2 μg nuclear extracts from COS-7 cells transfected with pCMV/ATF4 plasmid in the presence of normal control IgG (lane 3), ATF4 antibody (lane 4), cFos antibody (lane 5), and ATF2 antibody (lane 6). Experiments were repeated 3–4 times and qualitatively identical results were obtained. F and G, MC-4 cells transfected with p1003mOsx-luc and pRL-SV40 were treated with indicated concentration of PTH for 6 h (F) or with 10^{-7} M PTH for indicated times (G). H, MC-4 cells were treated with and without 10^{-7} M PTH in the presence and absence of 10 μM of H89 for 6 h. I, MC-4 cells transfected as in Fig. 7C were treated with and without 10^{-7} M PTH for 6 h. J, MC-4 cells transfected as in Fig. D were treated with and without 10^{-7} M PTH for 6 h. K, a schematic illustration of putative ATF4 binding sites in the 5′ flanking regions of the *Osx* and *osteocalcin* gene promoters and *osteocalcin* gene. L, ChIP assay of the *Osx* promoter in MC-4 cells treated with and without 10^{-7} M PTH for 6 h. *P<0.05 (β-gal vs. ATF4, Runx2, and ATF4 plus Runx2, or veh vs. PTH), #P<0.05 (ATF4 plus Runx2 vs. β-gal, ATF4, or Runx2).
doi:10.1371/journal.pone.0007583.g007

osteoblast proliferation and/or reduction of apoptosis, our studies suggest that PTH also increases osteoblast differentiation by rapidly up-regulating Osx.

Importantly, experiments from the current study show that effects of PTH on osteoblast differentiation are mediated by ATF4. Although PTH increased osteoblast proliferation in $Atf4^{-/-}$ animals as evidenced by significant increases in bone volume and nuclear BrdU labeling (Figs. 1–3), expression of osteoblast marker genes and numbers of Osx-positive osteoblasts were either dramatically reduced or completely abolished in $Atf4^{-/-}$ animals. Furthermore, since the basal levels of osteoblast differentiation markers are either slightly reduced or not changed at all in $Atf4^{-/-}$ animals, the impaired differentiation response to PTH cannot be explained by a nonspecific blockage in osteoblast differentiation associated with ATF4 deficiency. Instead, ATF4 appears to have a unique role in the PTH-dependent component of osteoblast differentiation.

Further support for the concept that PTH actions are mediated by ATF4 comes from mechanistic studies. Specifically, we showed that PTH is a potent inducer of Osx expression in vivo and this response is completely abolished by ATF4 deficiency. Furthermore, PTH directly activated Osx gene transcription in cultured osteoblast-like cells, a response that required an ATF4 response element located between −201 and −194 bp in the proximal mouse Osx promoter. Introduction of a 3-bp substitution mutation into this ATF4-binding site essentially eliminated the PTH response. ChIP assays demonstrated that ATF4 binds to an endogenous chromatin fragment near the putative ATF4-binding site in the proximal Osx promoter in MC-4 cells. Of particular significance, ATF4 binding to the Osx promoter is dramatically enhanced by PTH. Collectively, these studies establish a unique role for ATF4 in PTH-mediated induction of Osx and osteoblast differentiation.

Runx2 is absolutely required for Osx expression, osteoblast differentiation, and bone formation [35,58]. Nevertheless, ATF4 deficiency dramatically reduced the level of Osx protein without altering Runx2, suggesting that Runx2 is not sufficient for maximal Osx expression. ATF4 stimulated Osx gene transcription in COS-7 cells that lack Runx2 protein to an extent similar to that seen with Runx2. In addition, an ATF4 response element was identified in the proximal region of the mouse Osx promoter. These results demonstrate that both ATF4 and Runx2 are essential for the maximal expression of Osx and are reminiscent of our previous study showing cooperative interactions between these two factors in regulating the Ocn gene [59].

It should be noted that ATF4 deficiency did not completely block the anabolic actions of PTH since this hormone increased bone volume in both growing and adult OVX bones from $Atf4^{-/-}$ mice (Figs. 1–3). This suggests that other factors must be involved for the PTH response. c-Fos [3], cAMP response element binding protein (CREB) [16], a major downstream target for PTH/cAMP and calcium signals, cAMP-response element modulator (CREM)[60], and Runx2 [16,23], a master regulator of osteoblast differentiation and bone formation, have all been shown to mediate components of the PTH anabolic response. Interestingly, these factors are either structurally related to ATF4 (c-Fos and CREM) or can interact with this factor (Runx2 and c-Fos) [59,61–65]. Most recently, low-density lipoprotein-related protein 6 (LRP6)[66], a major component of the Wnt signaling pathway, has been implicated in the anabolic actions of PTH in bone. It would be interesting to determine whether ATF4 mediates the PTH anabolic response via interactions with these factors or signaling pathways.

PTH signaling may regulate ATF4 via several mechanisms. First, PTH up-regulates Atf4 gene expression in cultured osteoblasts as demonstrated by our recent study [34] as well as in vivo (Fig. 5). Second, PTH post-translationally activates ATF4 via PKA [34], a major route for PTH signaling in osteoblasts. PKA phosphorylation of ATF4 at its Ser254 residue mediates β-adrenergic induction of Rankl mRNA expression in osteoblasts [67]. ATF4 can also be directly phosphorylated and activated by RSK2 [26], a growth factor-regulated serine-threonine protein kinase activated by the Ras-Mitogen-Activated Protein Kinase (MAPK) pathway. This phosphorylation is critical for ATF4 activity as well as bone formation [26]. Because PTH signaling activates Erk/MAPK [48], an immediate upstream activator of RSK2, ATF4 can be activated via the PTH-MAPK-RSK2 signaling pathway. Lastly, PTH promotes ATF4-Runx2 interactions which are critical for osteoblast function and bone formation [59,61,63]. This notion is supported by the fact that PTH up-regulates both factors in osteoblasts [23,34].

Based on findings from this and other studies, we proposed a working model for ATF4 to mediate PTH stimulation of osteoblast function and bone formation (Fig. 8). Binding of PTH to its receptor, PTH1R, activates PKA and probably other intracellular signaling pathways, leading to up-regulation/activation of ATF4. ATF4 subsequently increases proliferation of osteoblasts and/or preosteoblasts via modulation of cyclin D1 protein, and attenuates apoptotic death in osteoblasts and osteocytes, resulting in a significant increase in the numbers of osteoblasts and/or osteocytes. At the same time, ATF4 together with Runx2 maximally activates Osx expression and increases osteoblast differentiation. The resulting increases in osteoblast number and
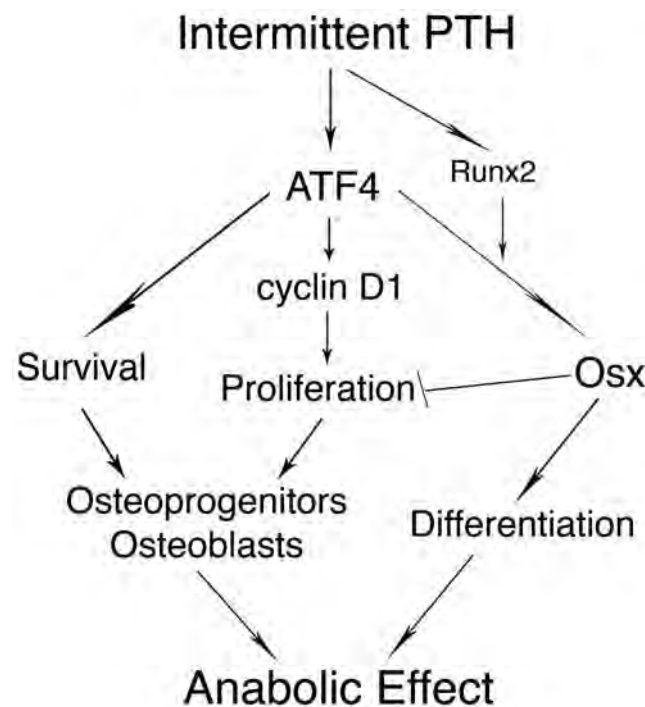

Figure 8. Proposed model for ATF4 mediation of PTH stimulation of bone formation. Binding of PTH to PTH1R activates PKA and leads to up-regulation of ATF4. ATF4 subsequently increases proliferation and survival of osteoblasts. At the same time, ATF4 together with Runx2 maximally activates Osx expression and increases osteoblast differentiation. These increases in osteoblast number and differentiation lead to massive bone formation. Osx also negatively regulates osteoblast proliferation, thus preventing excess bone formation.
doi:10.1371/journal.pone.0007583.g008

differentiation lead to bone formation. Osx also negatively regulates osteoblast proliferation, thus preventing excess bone formation [68].

Since ATF4 is known to regulate the expression of RANKL in osteoblasts and thereby osteoclast differentiation [67,69], it will be interesting to determine if ATF4 is also required for the catabolic actions of PTH in bone.

In summary, this study establishes a critical role for ATF4 in the anabolic actions of PTH in bone. ATF4 is necessary for PTH to increase both osteoblast numbers and differentiation. Therefore, ATF4 may provide a potential new therapeutic target for improving bone mass and for treating metabolic bone diseases such as osteoporosis.

Materials and Methods

Reagents

Tissue culture media and fetal bovine serum were obtained from HyClone (Logan, UT). H89, DMSO, PTH1R antibody, mouse monoclonal antibody against β-actin were purchased from Sigma (St Louis, MO). Other reagents were obtained from the following sources: antibodies against ATF4 (for Western blot), Runx2, normal control IgGs and horseradish peroxidase-conjugated mouse or goat IgG from Santa Cruz (Santa Cruz, CA), and Osterix antibody from Abcam Inc. (Cambridge, MA). ATF4 antibody used for EMSA was raised against epitope QETN-KEPPQTVNPIGHLPESLIK (St Louis, MO). All other chemicals were of analytical grade.

Atf4-deficient mice

Breeding pairs of *Atf4* heterozygous mice were described previously [34] and used to generate *Atf4* wild-type (wt) ($Atf4^{+/+}$), heterozygous ($Atf4^{+/-}$) and homozygous mutant ($Atf4^{-/-}$) mice for this study. All research protocols were approved by the Institutional Animal Care and Use Committee of the VA Pittsburgh Healthcare System, where this study was conducted.

In vivo PTH administration

For the "growing mouse model", five-day-old mice were given daily subcutaneous injections of vehicle (saline) or hPTH(1–34) (60 ng/g body weight, Bachem, Torrance, CA) for 28 d. For the "adult OVX mouse model", four-month-old female mice were anesthetized and ovariectomized as follows: A 1-cm midline incision was made through the skin. The "white line" will be visualized on the peritoneum and a second incision was made along the white line through the peritoneum. Using long, straight forceps, the left ovary was isolated and the connective tissue between the ovary and kidney was dissected away. Straight forceps with flat ends was used to pinch the uterine horn while another set of straight forceps was used to tear the ovary away from the uterine horn. The same was done on the right ovary. 6-0 PDS (Polydioxanone Sutures, 6/0) was used to tie around the uterine horn to provide hemostasis if necessary. 6-0 PDS was used to close the innermost layer. Sterile surgical staples were used to close the incision. Two months later mice were given daily subcutaneous injections of vehicle or hPTH(1-34) (100 ng/g body weight) for 28 d. Mice were euthanized 24 h after last PTH injection. The effects of these PTH dosing regimens on bone were determined by both biochemical and histomorphometric criteria.

Gross evaluation and serum biochemistry

Body weight was recorded every another day. The length of the femurs was measured using an electronic digital caliper. Faxitron X-ray analysis of femurs was conducted at 27 kv and 7.5 seconds (Faxitron X-Ray Corp., Wheeling, IL). Femurs were ashed at 800°C for 4 h and weighed. Serum calcium and Pi concentrations were determined using kits from Pointe Scientific, Inc (Canton, MI) following the manufacture's instructions (Sigma Diagnostics).

Bone morphometric analyses by micro-computerized tomography (μCT)

Upon termination of PTH or vehicle treatment, mice were sacrificed and femurs were isolated. Fixed non-demineralized femurs were used for μCT analysis at the Center for Bone Biology using a VIVACT40 (SCANCO Medical AG) following the standards of techniques and terminology recommended by American Society for Bone and Mineral Research [70]. For trabecular bone parameters, transverse CT slices were obtained in the region of interest in the axial direction from the trabecular bone 0.1 mm below the growth plate (bottom of the primary spongiosa) to the mid-femur. Contours were defined and drawn close to the cortical bone. The trabecular bone was then removed and analyzed separately. 3D analysis was then performed on trabecular bones slices. A 3-mm section was used to obtain mid-femoral cortical bone thickness. The analysis of the specimens involves the following bone measurements: bone volume fraction (BV/TV, %), trabecular number (Tb. N), trabecular thickness (Tb. Th), trabecular spacing (Tb. Sp), and cortical thickness (Cort.Th).

Histological evaluation

Tibiae, lumbar vertebrae (L5), and calvariae were fixed in PBS buffered 10% formalin at 4°C for 24 h, decalcified in 10% EDTA (pH 7.4) for 10–14 d, and embedded in paraffin. Longitudinal sections of tibiae and vertebrae were cut at 4 μm and stained with hematoxylin and eosin (H&E). Trabecular area of tibial sections was measured in the proximal metaphysis beginning immediately below the chondro-osseous junction to the mid-tibia. Calvariae were bisected perpendicular to the sagittal suture through the central portion of the parietal bones, parallel to lamboidal and coronal sutures, and embedded in paraffin to obtain sections of a standard area according to the method described by Zhao et al. [71]. Trabecular area versus total bone area was measured using an Image Pro Plus 6.2 software (Media Cybernetics, Inc, Bethesda, MD). The calvarial width was the average value from 20 random measurements of each calvaria (at least 6 samples per group) using a SPOT Advanced imaging software (provided with the purchase of the Olympus BX41 microscope).

Measurement of mineral apposition rate (MAR)

Mice were injected with calcein subcutaneously (20 mg/kg) at 6 and 2 d before sacrifice. Undecalcified tibia were fixed in 70% ethanol, embedded in methylmethacrylate and sectioned at 10 μm. Calcein labeling was visualized using a Nikon E800 fluorescence microscope. The metaphyseal trabecular bone projected into the marrow space was evaluated and the distance between the all double-labeled areas was measured at a magnification of 200x. MAR was calculated as mean distance between the double labels divided by the number of the days between the calcein injections. Histomorphometric analysis was performed using BioQuant image analysis software (R&M Bio Metrics, Nashville, TN, USA).

In vivo proliferation assay

Mice were injected intraperitoneally with 100 μg bromodeoxyuridine (BrdU)/12 μg fluorodeoxyuridine (FdU) per gram of body weight 12 h before sacrifice. After sacrifice, sections of tibiae and calvariae were obtained. To identify actively proliferating cells,

nuclei that have incorporated BrdU were detected using a Zymed BrdU immunostaining kit according to the manufacturer's instruction (Invitrogen, Carlsbad, CA). BrdU-positive cells (brown) on the calvarial periosteal surface or in the osteoid of tibiae were counted and normalized to the total numbers in the same area [33]. BrdU-positive hematopoietic cells in marrow were not counted.

In situ apoptosis detection

This assay is based on the classical TUNEL assay to examine apoptosis by detecting DNA fragmentation. 4-µm sections of tibiae were prepared and stained using the ApopTag Peroxidase *In Situ* Apoptosis Detection Kit according to the manufacturer's instruction (Millipore, Billerica, MA). Apoptotic osteoblasts and osteocytes in tibiae were counted and normalized to the total cells from the same area.

Immunohistochemistry (IHC)

Tibiae and calvariae were fixed, decalcified, and embedded in paraffin. Sections of tibiae and calvariae were stained with antibodies against Osx (Abcam Inc, Cambridge, MA) and PTH1R (Sigma, St. Louis, MO) using the EnVision$^+$System-HRP (DAB) kit (Dako North America, Inc, Carpinteria, CA) according to the manufacturer's instructions. Briefly, slides were baked at 55°C for 45 min, deparaffinized in three washes of xylene, and rehydrated in a decreasing ethanol gradient. Antigen retrieval was performed using 0.1% trypsin for 10 min at 37°C in a humidified chamber. Endogenous peroxidases were deactivated with 3% H_2O_2 in 1x PBS for 10 min, and sections were blocked in blocking solution for 30 min at room temperature. Sections were incubated with primary antibody (1:200 dilution for both osterix and PTH1R) in blocking solution for 2 hours at 4°C. Sections were washed in PBS three times and incubated with a donkey-anti-rabbit IgG-HRP secondary antibody solution for 30 min at room temperature. After washing with PBS three times, HRP activity was detected using a DAB substrate solution for 5 min at room temperature. Sections were counter-stained with a Mayer's hematoxylin solution.

Measurement of plasma levels of IGF-1 and FGF-2 by ELISA

Blood plasma samples were prepared from whole-blood samples from mice of each group and plasma levels of IGF-1 and FGF-2 were measured by using ELISA kits (human FGF basic Quantikine ELISA Kit, cat#: DFB50, and mouse IGF-I Quantikine ELISA Kit, cat#: MG100, both from R&D Systems Inc, Minnepolis, MN 55413) according to the manufacturer's instructions.

cAMP assay

Primary osteoblasts from calvariae of 3-d-old wt or $Atf4^{-/-}$ mice were isolated as described previously [72]. Cells were seeded at a desity of 5×10^4/well on 96-well plate and treated with vehicle or increasing concentrations of human recombinant PTH(1-34) for 5 min. Cells were then lysed with lysis reagent 1B and cell lysates used for cAMP assay using a cAMP Biotrak Enzyeimmunoassay (EIA) kit (cat #: RPN225, GE Healthcare Biosciences Corp, Piscataway, NJ) according to the manufacturer's instructions and the protein concentrations were measured using a BCA protein assay kit (Pierce). cAMP was normalized to total protein.

Quantitative real-time RT/PCR and Western blot analysis

RNA isolation, reverse transcription (RT), regular PCR, and quantitative real-time PCR analysis were performed as previously described [34]. The DNA sequences of mouse primers used for real-time PCR were summarized in Table 1. Western blot analysis was performed as previously described [33]. RNAs or protein extracts from at least six specimens in each group were used.

DNA constructs and site-directed mutagenesis, transfection

pCMV/β-gal, pCMV/ATF4, and pCMV/Runx2 were previously described [62]. mOsx-luc containing different mouse *Osx* promoter elements (−1003/+68, −567/+68, −215/+68, and −83/+68) driving a firefly luciferase reporter gene were constructed in the project laboratory by PCR subcloning promoter fragments using mouse tail DNA as a template into pGL3-luc vector (Promega, Madison, WI). Mutant p215mOsx-luc which contains a 3-bp substitution mutation in a putative ATF4-binding at positions −198, −197 and −196 (from CTTCCTCA to CTTgtaCA) was generated from the wild-type p215mOsx-luc by PCR amplification using a QuickChange^{TM} XL Site-Directed Mutagenesis Kit (Stratagene, La Jolla, CA) using the following primers: 5′-GGT ACC CCT CCC TCT CTC GCC TTg taC ATT GGA TCC GGA GTC TTC TCC GC-3′ (forward); 5′-GCG GAG AAG ACT CCG GAT CCA ATG tac AAG GCG AGA GAG GGA GGC GGT ACC-3′ (reverse). Sequence accuracy was confirmed by automatic DNA sequencing. For all transfection experiments, the amount of plasmid DNAs (reporter plasmid, 0.25 µg; normalization plasmid pRL-SV4, 10 ng; and expression plasmid, 1.0 µg) was balanced as necessary with β-galactosidase expression plasmid such that the total DNA was constant in each group. Experiments were performed in triplicates and repeated 3–4 times.

Nuclear extracts preparation and electrophoretic mobility shift assay (EMSA)

Nuclear extracts were prepared from COS-7 cells transfected with pCMV/ATF4 plasmids as previously described [73]. The DNA sequences of the oligonucleotides used for EMSA were as follows: GAT CCC TGC CTC CCT CTC TCG CCT TCC TCA TTG GAT CCG GAG TCT TCG. DNA oligonucleotide was labeled using a Biotin 3′ end DNA Labeling Kit (cat #: 89818, Pierce Biotechnology Inc., Rockford, IL). Two µg of nuclear extracts and 20 fmol biotin-labeled DNA probe were incubated in 1x binding buffer for 30 min at room temperature.

Table 1. real-time PCR primers.

Gene name	5′ primer	3′ primer
Alp	TCCCACGTTTTCACATTCGG	CCCGTTACCATATAGGATGGCC
Atf4	GAGCTTCCTGAACAGCGAAGTG	TGGCCACCTCCAGATAGTCATC
Bsp	AAGAGGAAGAAAATGAGAACGA	GCTTCTTCTCCGTTGTCTCC
cFos	AATGGTGAAGACCGTGTCAGGA	CCCTTCGGATTCTCCGTTTCT
cJun	GCCAACATGCTCAGGGAACAGGTG	GCCCCTCAGCCCTGACAGTCTG
Col I(1)	AGATTGAGAACATCCGCAGCC	TCCAGTACTCTCCGCTCTTCCA
Gapdh	CAGTGCCAGCCTCGTCCCGTAGA	CTGCAAATGGCAGCCCTGGTGAC
Ocn	TAGTGAACAGACTCCGGCGCTA	TGTAGGCGGTCTTCAAGCCAT
Opn	CCAATGAAAGCCATGACCACA	CGTCAGATTCATCCGAGTCCAC
Osx	AGAGGTTCACTCGCTCTGACGA	TTGCTCAAGTGGTCGCTTCTG
Pth1r	GATGCGGACGATGTCTTTACC	GGCGGTCAAATACCTCC

doi:10.1371/journal.pone.0007583.t001

Table 2. PCR primers used in ChIP assay.

Oligo name	Sequence
P1	CCCTCCCAGATCCCTTCTTT
P2	GGCTGCTCTCTGTCTGTAGGG
P3	CACAGCATCCTTTGGGTTTGAC
P4	TATCGGCTACTCTGTGCTCTCTGA
P5	TAGTGAACAGACTCCGGCGCTA
P6	TGTAGGCGGTCTTCA AGCCAT

doi:10.1371/journal.pone.0007583.t002

For supershift assay, 1 µg of IgG or indicated antibodies were first incubated with nuclear extracts prior to addition of DNA probe. Protein–DNA complexes were separated on 4% polyacrylamide gels in 1x TBE buffer, and transferred onto Biodyne B Nylon Membrane (cat #: 77016, Pierce). The membrane was blocked in 1x blocking buffer, washed five times with 1x wash buffer, and visualized by a Chemiluminescent Nucleic Acid detection Module (cat #: 89880, Pierce, Rockford, IL).

Chromatin immunoprecipitation (ChIP)

ChIP assays were performed using ATF4 antibody or control IgG as described previously [62]. PCR primer pairs (Table 2) were generated to detect DNA segments located near a putative ATF4-binding site (CTTCCTCAT) at −201/−193 (primers P1 and P2) determined by the TRANSFAC retrieval program in the 5′ flanking region of the *Osx* promoter, a previously identified ATF4-binding site (OSE1) in *osteocalcin* gene 2 (mOG2) promoter (primers 3 and 4), and a mOG2 gene region (+177/+311) that contains no ATF4-binding sites (primers P5 and P6) [62]. PCR products were run on 3% agarose gel and stained with ethidium bromide. Purified input chromatin was used to perform parallel PCRs with the respective primer pairs.

Statistical analysis

Data was analyzed with a GraphPad Prism software (4.0). A one-way ANOVA analysis was used followed by the Tukey test. Students' t test was used to test for differences between two groups of data as needed. Data of Figs. 1, 2, 4, and 5 and S1-2 were from growing mice and Figs. 3 and S3 from 7-month-old OVX mice. For H&E, IHC, BrdU, and TUNEL studies, two to three sections per specimen and at least six specimens in each group were used. Results were expressed as means ± standard deviation (SD). Differences with a $P<0.05$ was considered as statistically significant.

Supporting Information

Figure S1 Effects of PTH on animal growth, length and ash weight of femurs, and serum Pi and calcium concentrations and alkaline activity in wt and Atf4−/− mice. A, growth curve, B, length of femur, C, dry ash weight of femur, D, serum Pi, E, serum calcium. *$P<0.05$ (veh vs. PTH), † $P<0.05$ (wt-veh vs. Atf4-/--veh).
Found at: doi:10.1371/journal.pone.0007583.s001 (1.78 MB DOC)

Figure S2 Faxitron X-ray analysis of femurs from vehicle and PTH-treated growing wt, Atf4+/−, and Atf4-/− mice. Faxitron X-ray analysis was conducted at 27 kv and 7.5 seconds. Representative microradiographic images of femurs are shown.
Found at: doi:10.1371/journal.pone.0007583.s002 (1.45 MB TIF)

Figure S3 Effects of OVX surgery on bone parameters in wt and Atf4−/− mice. Four-month-old female mice were first ovariectomized. After two months, femurs were isolated for µCT analysis. *$P<0.05$ (sham vs. OVX), † $P<0.05$ (sham(+/+) vs. sham (−/−)).
Found at: doi:10.1371/journal.pone.0007583.s003 (0.16 MB DOC)

Acknowledgments

Author Contributions

Conceived and designed the experiments: SY JF JZ DR GX. Performed the experiments: SY ML DJ HC TGK YL KP KH GX. Analyzed the data: SY RF TGK DR GX. Wrote the paper: RF GX.

References

1. Neer RM, Arnaud CD, Zanchetta JR, Prince R, Gaich GA, et al. (2001) Effect of parathyroid hormone (1-34) on fractures and bone mineral density in postmenopausal women with osteoporosis. N Engl J Med 344: 1434–1441.
2. Miao D, He B, Karaplis AC, Goltzman D (2002) Parathyroid hormone is essential for normal fetal bone formation. J Clin Invest 109: 1173–1182.
3. Demiralp B, Chen HL, Koh AJ, Keller ET, McCauley LK (2002) Anabolic actions of parathyroid hormone during bone growth are dependent on c-fos. Endocrinology 143: 4038–4047.
4. Iida-Klein A, Zhou H, Lu SS, Levine LR, Ducayen-Knowles M, et al. (2002) Anabolic action of parathyroid hormone is skeletal site specific at the tissue and cellular levels in mice. J Bone Miner Res 17: 808–816.
5. Iida-Klein A, Lu SS, Kapadia R, Burkhart M, Moreno A, et al. (2005) Short-term continuous infusion of human parathyroid hormone 1-34 fragment is catabolic with decreased trabecular connectivity density accompanied by hypercalcemia in C57BL/J6 mice. J Endocrinol 186: 549–557.
6. Jilka RL, Weinstein RS, Bellido T, Roberson P, Parfitt AM, et al. (1999) Increased bone formation by prevention of osteoblast apoptosis with parathyroid hormone. J Clin Invest 104: 439–446.
7. Miyakoshi N, Kasukawa Y, Linkhart TA, Baylink DJ, Mohan S (2001) Evidence that anabolic effects of PTH on bone require IGF-I in growing mice. Endocrinology 142: 4349–4356.
8. Hurley MM, Okada Y, Xiao L, Tanaka Y, Ito M, et al. (2006) Impaired bone anabolic response to parathyroid hormone in Fgf2−/− and Fgf2+/− mice. Biochem Biophys Res Commun 341: 989–994.
9. Partridge NC, Alcorn D, Michelangeli VP, Kemp BE, Ryan GB, et al. (1981) Functional properties of hormonally responsive cultured normal and malignant rat osteoblastic cells. Endocrinology 108: 213–219.
10. McCauley LK, Koh AJ, Beecher CA, Cui Y, Decker JD, et al. (1995) Effects of differentiation and transforming growth factor beta 1 on PTH/PTHrP receptor mRNA levels in MC3T3-E1 cells. J Bone Miner Res 10: 1243–1255.
11. Swarthout JT, D'Alonzo RC, Selvamurugan N, Partridge NC (2002) Parathyroid hormone-dependent signaling pathways regulating genes in bone cells. Gene 282: 1–17.
12. Carpio L, Gladu J, Goltzman D, Rabbani SA (2001) Induction of osteoblast differentiation indexes by PTHrP in MG-63 cells involves multiple signaling pathways. Am J Physiol Endocrinol Metab 281: E489–499.
13. Swarthout JT, Doggett TA, Lemker JL, Partridge NC (2001) Stimulation of extracellular signal-regulated kinases and proliferation in rat osteoblastic cells by parathyroid hormone is protein kinase C- dependent. J Biol Chem 276: 7586–7592.
14. Calvi LM, Adams GB, Weibrecht KW, Weber JM, Olson DP, et al. (2003) Osteoblastic cells regulate the haematopoietic stem cell niche. Nature 425: 841–846.
15. Datta NS, Pettway GJ, Chen C, Koh AJ, McCauley LK (2007) Cyclin D1 as a Target for the Proliferative Effects of PTH and PTHrP in Early Osteoblastic Cells. J Bone Miner Res 22: 951–964.
16. Bellido T, Ali AA, Plotkin LI, Fu Q, Gubrij I, et al. (2003) Proteasomal Degradation of Runx2 Shortens Parathyroid Hormone-induced Anti-apoptotic

Signaling in Osteoblasts: A PUTATIVE EXPLANATION FOR WHY INTERMITTENT ADMINISTRATION IS NEEDED FOR BONE ANABOLISM. J Biol Chem 278: 50259–50272.

17. Chen HL, Demiralp B, Schneider A, Koh AJ, Silve C, et al. (2002) Parathyroid hormone and parathyroid hormone-related protein exert both pro- and anti-apoptotic effects in mesenchymal cells. J Biol Chem 277: 19374–19381.

18. Pearman AT, Chou WY, Bergman KD, Pulumati MR, Partridge NC (1996) Parathyroid hormone induces c-fos promoter activity in osteoblastic cells through phosphorylated cAMP response element (CRE)-binding protein binding to the major CRE. J Biol Chem 271: 25715–25721.

19. Gonzalez GA, Montminy MR (1989) Cyclic AMP stimulates somatostatin gene transcription by phosphorylation of CREB at serine 133. Cell 59: 675–680.

20. Selvamurugan N, Chou WY, Pearman AT, Pulumati MR, Partridge NC (1998) Parathyroid hormone regulates the rat collagenase-3 promoter in osteoblastic cells through the cooperative interaction of the activator protein-1 site and the runt domain binding sequence. J Biol Chem 273: 10647–10657.

21. McCauley LK, Koh AJ, Beecher CA, Rosol TJ (1997) Proto-oncogene c-fos is transcriptionally regulated by parathyroid hormone (PTH) and PTH-related protein in a cyclic adenosine monophosphate-dependent manner in osteoblastic cells. Endocrinology 138: 5427–5433.

22. McCauley LK, Koh-Paige AJ, Chen H, Chen C, Ontiveros C, et al. (2001) Parathyroid hormone stimulates fra-2 expression in osteoblastic cells in vitro and in vivo. Endocrinology 142: 1975–1981.

23. Krishnan V, Moore TL, Ma YL, Helvering LM, Frolik CA, et al. (2003) Parathyroid hormone bone anabolic action requires cbfa1/runx2-dependent signaling. Mol Endocrinol 17: 423–435.

24. Ducy P, Karsenty G (1995) Two distinct osteoblast-specific cis-acting elements control expression of a mouse osteocalcin gene. Mol Cell Biol 15: 1858–1869.

25. Ducy P, Zhang R, Geoffroy V, Ridall AL, Karsenty G (1997) Osf2/Cbfa1: a transcriptional activator of osteoblast differentiation [see comments]. Cell 89: 747–754.

26. Yang X, Matsuda K, Bialek P, Jacquot S, Masuoka HC, et al. (2004) ATF4 Is a Substrate of RSK2 and an Essential Regulator of Osteoblast Biology; Implication for Coffin-Lowry Syndrome. Cell 117: 387–398.

27. Banerjee C, Hiebert SW, Stein JL, Lian JB, Stein GS (1996) An AML-1 consensus sequence binds an osteoblast-specific complex and transcriptionally activates the osteocalcin gene. Proc Natl Acad Sci U S A 93: 4968–4973.

28. Banerjee C, McCabe LR, Choi JY, Hiebert SW, Stein JL, et al. (1997) Runt homology domain proteins in osteoblast differentiation: AML3/CBFA1 is a major component of a bone-specific complex. J Cell Biochem 66: 1–8.

29. Boudreaux JM, Towler DA (1996) Synergistic induction of osteocalcin gene expression: identification of a bipartite element conferring fibroblast growth factor 2 and cyclic AMP responsiveness in the rat osteocalcin promoter. J Biol Chem 271: 7508–7515.

30. Yu XP, Chandrasekhar S (1997) Parathyroid hormone (PTH 1-34) regulation of rat osteocalcin gene transcription [see comments]. Endocrinology 138: 3085–3092.

31. Jiang D, Franceschi RT, Boules H, Xiao G (2004) Parathyroid Hormone Induction of the Osteocalcin Gene: REQUIREMENT FOR AN OSTEOBLAST-SPECIFIC ELEMENT 1 SEQUENCE IN THE PROMOTER AND INVOLVEMENT OF MULTIPLE SIGNALING PATHWAYS. J Biol Chem 279: 5329–5337.

32. Yang X, Karsenty G (2004) ATF4, the osteoblast accumulation of which is determined post-translationally, can induce osteoblast-specific gene expression in non-osteoblastic cells. J Biol Chem 279: 47109–47114.

33. Zhang X, Yu S, Galson DL, Luo M, Fan J, et al. (2008) Activating transcription factor 4 is critical for proliferation and survival in primary bone marrow stromal cells and calvarial osteoblasts. J Cell Biochem 105: 885–895.

34. Yu S, Franceschi RT, Luo M, Zhang X, Jiang D, et al. (2008) Parathyroid hormone increases activating transcription factor 4 expression and activity in osteoblasts: requirement for osteocalcin gene expression. Endocrinology 149: 1960–1968.

35. Nakashima K, Zhou X, Kunkel G, Zhang Z, Deng JM, et al. (2002) The novel zinc finger-containing transcription factor osterix is required for osteoblast differentiation and bone formation. Cell 108: 17–29.

36. Otto F, Thornell AP, Crompton T, Denzel A, Gilmour KC, et al. (1997) Cbfa1, a candidate gene for cleidocranial dysplasia syndrome, is essential for osteoblast differentiation and bone development [see comments]. Cell 89: 765–771.

37. Mundlos S, Otto F, Mundlos C, Mulliken JB, Aylsworth AS, et al. (1997) Mutations involving the transcription factor CBFA1 cause cleidocranial dysplasia [see comments]. Cell 89: 773–779.

38. Komori T, Yagi H, Nomura S, Yamaguchi A, Sasaki K, et al. (1997) Targeted disruption of Cbfa1 results in a complete lack of bone formation owing to maturational arrest of osteoblasts [see comments]. Cell 89: 755–764.

39. Hock JM, Gera I, Fonseca J, Raisz LG (1988) Human parathyroid hormone-(1-34) increases bone mass in ovariectomized and orchidectomized rats. Endocrinology 122: 2899–2904.

40. Tanaka S, Sakai A, Tanaka M, Otomo H, Okimoto N, et al. (2004) Skeletal unloading alleviates the anabolic action of intermittent PTH(1-34) in mouse tibia in association with inhibition of PTH-induced increase in c-fos mRNA in bone marrow cells. J Bone Miner Res 19: 1813–1820.

41. Cole JA (1999) Parathyroid hormone activates mitogen-activated protein kinase in opossum kidney cells. Endocrinology 140: 5771–5779.

42. Dempster DW, Cosman F, Parisien M, Shen V, Lindsay R (1993) Anabolic actions of parathyroid hormone on bone. Endocr Rev 14: 690–709.

43. Calvi LM, Sims NA, Hunzelman JL, Knight MC, Giovannetti A, et al. (2001) Activated parathyroid hormone/parathyroid hormone-related protein receptor in osteoblastic cells differentially affects cortical and trabecular bone. J Clin Invest 107: 277–286.

44. Mosekilde L, Danielsen CC, Sogaard CH, McOsker JE, Wronski TJ (1995) The anabolic effects of parathyroid hormone on cortical bone mass, dimensions and strength—assessed in a sexually mature, ovariectomized rat model. Bone 16: 223–230.

45. Miao D, He B, Jiang Y, Kobayashi T, Soroceanu MA, et al. (2005) Osteoblast-derived PTHrP is a potent endogenous bone anabolic agent that modifies the therapeutic efficacy of administered PTH 1-34. J Clin Invest 115: 2402–2411.

46. Koh AJ, Beecher CA, Rosol TJ, McCauley LK (1999) 3′,5′-Cyclic adenosine monophosphate activation in osteoblastic cells: effects on parathyroid hormone-1 receptors and osteoblastic differentiation in vitro. Endocrinology 140: 3154–3162.

47. Jilka RL (2007) Molecular and cellular mechanisms of the anabolic effect of intermittent PTH. Bone 40: 1434–1446.

48. Chen C, Koh AJ, Datta NS, Zhang J, Keller ET, et al. (2004) Impact of the mitogen-activated protein kinase pathway on parathyroid hormone-related protein actions in osteoblasts. J Biol Chem 279: 29121–29129.

49. Tanaka T, Tsujimura T, Takeda K, Sugihara A, Maekawa A, et al. (1998) Targeted disruption of ATF4 discloses its essential role in the formation of eye lens fibres. Genes Cells 3: 801–810.

50. Hettmann T, Barton K, Leiden JM (2000) Microphthalmia due to p53-mediated apoptosis of anterior lens epithelial cells in mice lacking the CREB-2 transcription factor. Dev Biol 222: 110–123.

51. Wang YH, Liu Y, Buhl K, Rowe DW (2005) Comparison of the action of transient and continuous PTH on primary osteoblast cultures expressing differentiation stage-specific GFP. J Bone Miner Res 20: 5–14.

52. Schmidt IU, Dobnig H, Turner RT (1995) Intermittent parathyroid hormone treatment increases osteoblast number, steady state messenger ribonucleic acid levels for osteocalcin, and bone formation in tibial metaphysis of hypophysectomized female rats. Endocrinology 136: 5127–5134.

53. Kaback LA, Soung do Y, Naik A, Geneau G, Schwarz EM, et al. (2008) Teriparatide (1-34 human PTH) regulation of osterix during fracture repair. J Cell Biochem 105: 219–226.

54. Boguslawski G, Hale LV, Yu XP, Miles RR, Onyia JE, et al. (2000) Activation of osteocalcin transcription involves interaction of protein kinase A- and protein kinase C-dependent pathways. J Biol Chem 275: 999–1006.

55. Ogata Y, Nakao S, Kim RH, Li JJ, Furuyama S, et al. (2000) Parathyroid hormone regulation of bone sialoprotein (BSP) gene transcription is mediated through a pituitary-specific transcription factor-1 (Pit-1) motif in the rat BSP gene promoter. Matrix Biol 19: 395–407.

56. Wang BL, Dai CL, Quan JX, Zhu ZF, Zheng F, et al. (2006) Parathyroid hormone regulates osterix and Runx2 mRNA expression predominantly through protein kinase A signaling in osteoblast-like cells. J Endocrinol Invest 29: 101–108.

57. van der Horst G, Farih-Sips H, Lowik CW, Karperien M (2005) Multiple mechanisms are involved in inhibition of osteoblast differentiation by PTHrP and PTH in KS483 Cells. J Bone Miner Res 20: 2233–2244.

58. Karsenty G (2000) Role of Cbfa1 in osteoblast differentiation and function. Semin Cell Dev Biol 11: 343–346.

59. Xiao G, Jiang D, Ge C, Zhao Z, Lai Y, et al. (2005) Cooperative Interactions between Activating Transcription Factor 4 and Runx2/Cbfa1 Stimulate Osteoblast-specific Osteocalcin Gene Expression. J Biol Chem 280: 30689–30696.

60. Liu F, Lee SK, Adams DJ, Gronowicz GA, Kream BE (2007) CREM deficiency in mice alters the response of bone to intermittent parathyroid hormone treatment. Bone 40: 1135–1143.

61. Dobreva G, Chahrour M, Dautzenberg M, Chirivella L, Kanzler B, et al. (2006) SATB2 is a multifunctional determinant of craniofacial patterning and osteoblast differentiation. Cell 125: 971–986.

62. Yu S, Jiang Y, Galson DL, Luo M, Lai Y, et al. (2008) General transcription factor IIA-gamma increases osteoblast-specific osteocalcin gene expression via activating transcription factor 4 and runt-related transcription factor 2. J Biol Chem 283: 5542–5553.

63. Tominaga H, Maeda S, Hayashi M, Takeda S, Akira S, et al. (2008) CCAAT/Enhancer-binding Protein {beta} Promotes Osteoblast Differentiation by Enhancing Runx2 Activity with ATF4. Mol Biol Cell.

64. D'Alonzo RC, Selvamurugan N, Karsenty G, Partridge NC (2001) Physical interaction of the activator protein-1 factors, c-Fos and c-Jun, with Cbfa1 for collagenase-3 promoter activation. J Biol Chem 18: 18.

65. Hess J, Porte D, Munz C, Angel P (2001) AP-1 and Cbfa/runt physically interact and regulate parathyroid hormone-dependent MMP13 expression in osteoblasts through a new osteoblast-specific element 2/AP-1 composite element. J Biol Chem 276: 20029–20038.

66. Wan M, Yang C, Li J, Wu X, Yuan H, et al. (2008) Parathyroid hormone signaling through low-density lipoprotein-related protein 6. Genes Dev 22: 2968–2979.

67. Elefteriou F, Ahn JD, Takeda S, Starbuck M, Yang X, et al. (2005) Leptin regulation of bone resorption by the sympathetic nervous system and CART. Nature 434: 514–520.

68. Zhang C, Cho K, Huang Y, Lyons JP, Zhou X, et al. (2008) Inhibition of Wnt signaling by the osteoblast-specific transcription factor Osterix. Proc Natl Acad Sci U S A 105: 6936–6941.

69. Elefteriou F, Benson MD, Sowa H, Starbuck M, Liu X, et al. (2006) ATF4 mediation of NF1 functions in osteoblast reveals a nutritional basis for congenital skeletal dysplasiae. Cell Metab 4: 441–451.

70. Parfitt AM, Drezner MK, Glorieux FH, Kanis JA, Malluche H, et al. (1987) Bone histomorphometry: standardization of nomenclature, symbols, and units. Report of the ASBMR Histomorphometry Nomenclature Committee. J Bone Miner Res 2: 595–610.

71. Zhao W, Byrne MH, Wang Y, Krane SM (2000) Osteocyte and osteoblast apoptosis and excessive bone deposition accompany failure of collagenase cleavage of collagen. J Clin Invest 106: 941–949.

72. Ducy P, Starbuck M, Priemel M, Shen J, Pinero G, et al. (1999) A Cbfa1-dependent genetic pathway controls bone formation beyond embryonic development. Genes Dev 13: 1025–1036.

73. Xiao G, Cui Y, Ducy P, Karsenty G, Franceschi RT (1997) Ascorbic acid-dependent activation of the osteocalcin promoter in MC3T3-E1 preosteoblasts: requirement for collagen matrix synthesis and the presence of an intact OSE2 sequence. Mol Endocrinol 11: 1103–1113.
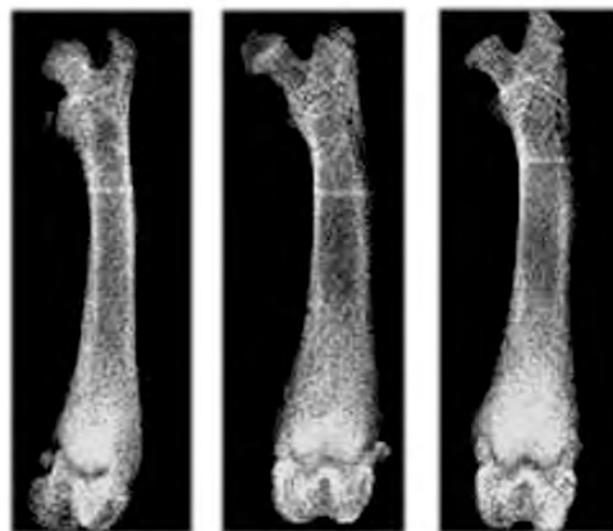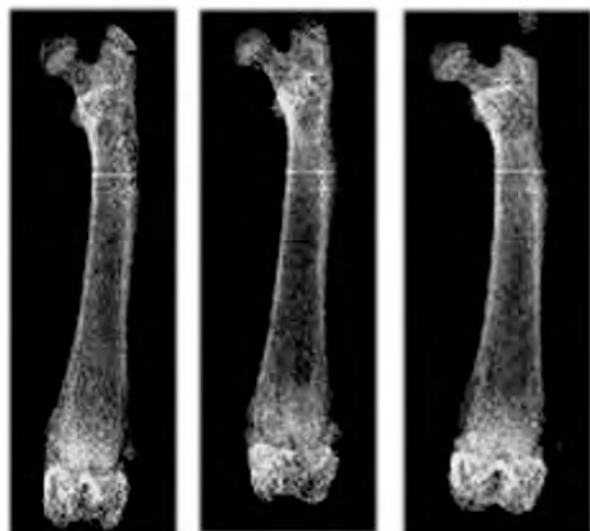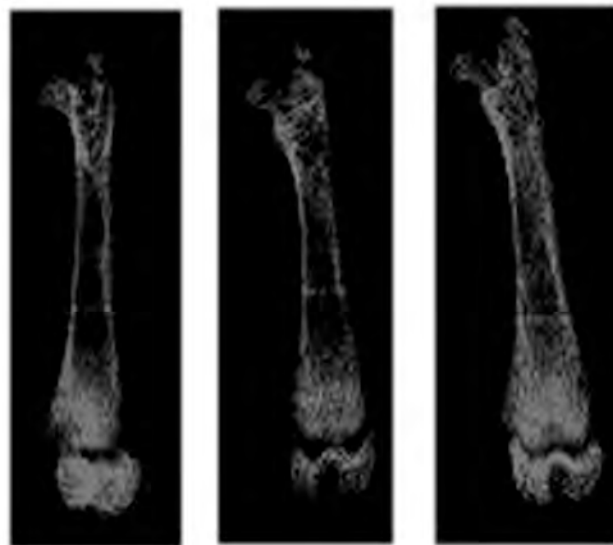
A

B

C

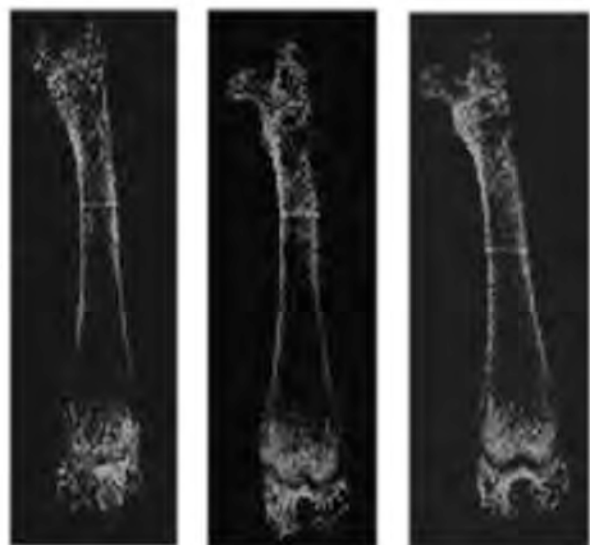D

E

F
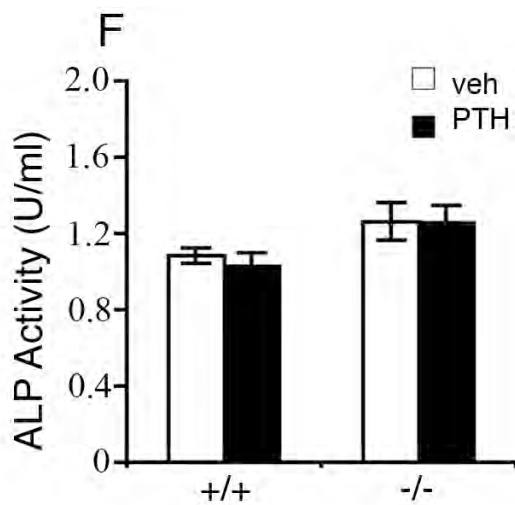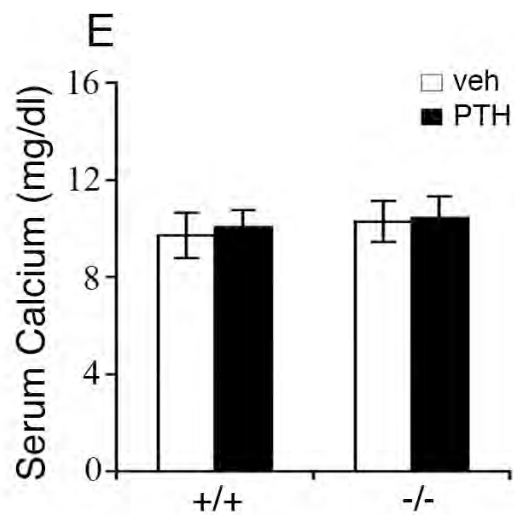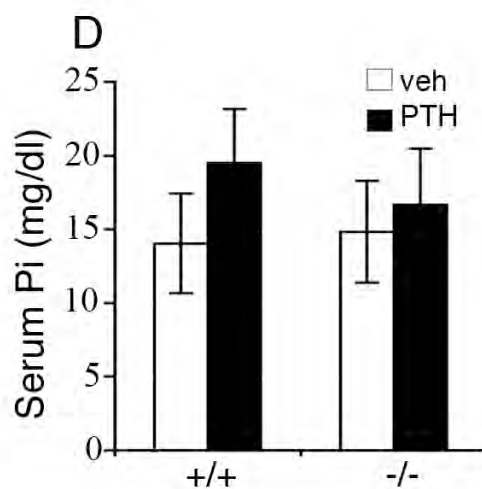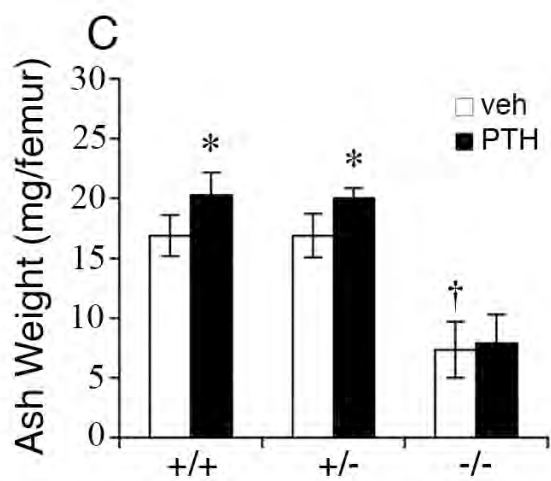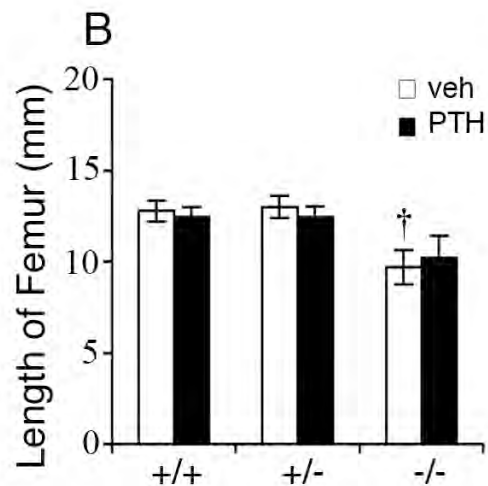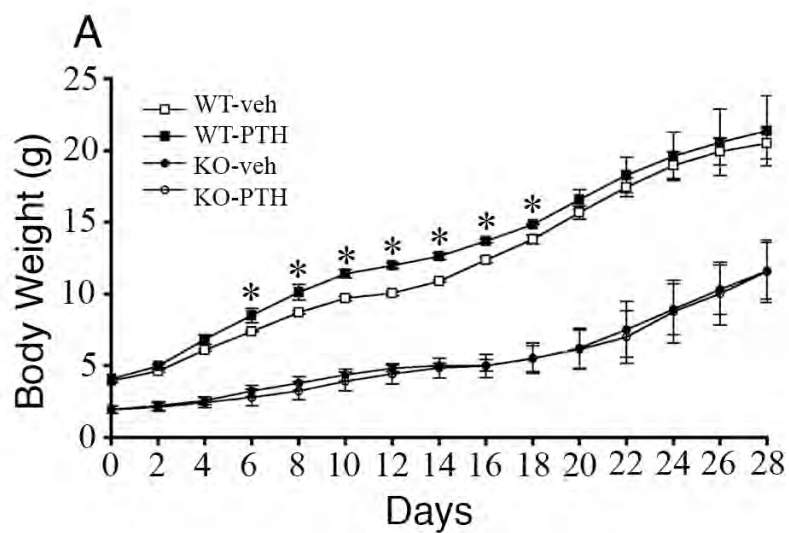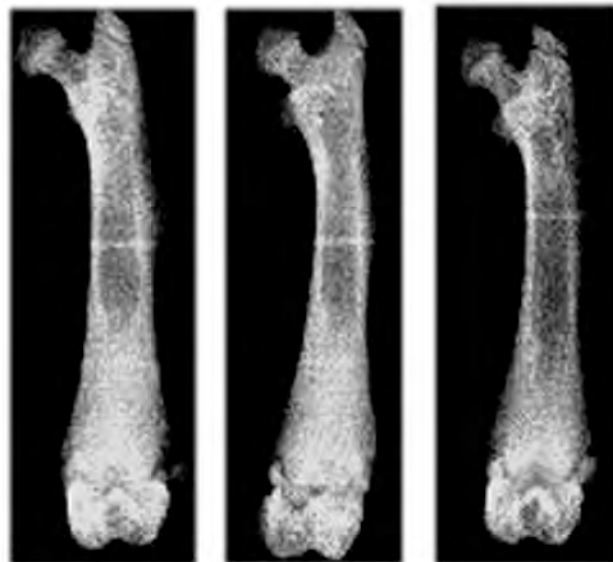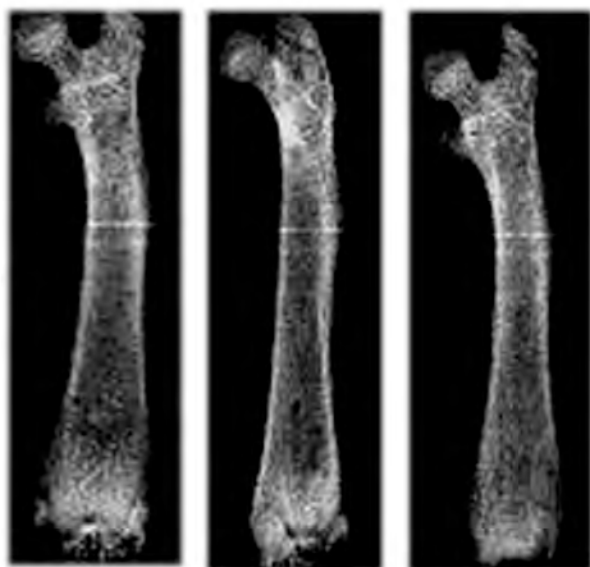
	Sham(+/+)	OVX(+/+)	Sham(-/-)	OVX(-/-)
BV/TV(%)	12±1.2	3.4±0.5*	1.8±0.08†	2.0±0.12
Tb.N(/mm)	2.2±0.24	1.5±0.06*	1.4±0.07†	1.3±0.01
Tb.Th(μm)	77.2±6.0	62.4±1.2*	59.3±11†	57.4±0.8
Tb.Sp(mm)	0.46±0.04	0.62±0.24*	0.71±0.03†	0.83±0.23
Cort.Th(mm)	0.2±0.05	0.21±0.01	0.17±0.01†	0.18±0.01

N = 3

Activating transcription factor 4 regulates osteoclast differentiation in mice

Huiling Cao,[1,2] Shibing Yu,[1] Zhi Yao,[2] Deborah L. Galson,[1] Yu Jiang,[3] Xiaoyan Zhang,[1,4] Jie Fan,[5] Binfeng Lu,[6] Youfei Guan,[4] Min Luo,[1] Yumei Lai,[3] Yibei Zhu,[6] Noriyoshi Kurihara,[1] Kenneth Patrene,[1] G. David Roodman,[1] and Guozhi Xiao[1,7]

[1]Department of Medicine, University of Pittsburgh, Pittsburgh, Pennsylvania, USA. [2]Department of Immunology, Key Laboratory of Educational Ministry of China, Tianjin Medical University, Tianjin, China. [3]Department of Pharmacology and Chemical Biology, University of Pittsburgh, Pittsburgh, Pennsylvania, USA. [4]Department of Physiology and Pathophysiology, Peking University Health Science Center, Beijing, China. [5]Department of Surgery and [6]Department of Immunology, University of Pittsburgh, Pittsburgh, Pennsylvania, USA. [7]College of Life Sciences, Nankai University, Tianjin, China.

Activating transcription factor 4 (ATF4) is a critical transcription factor for osteoblast (OBL) function and bone formation; however, a direct role in osteoclasts (OCLs) has not been established. Here, we targeted expression of ATF4 to the OCL lineage using the *Trap* promoter or through deletion of *Atf4* in mice. OCL differentiation was drastically decreased in *Atf4*−/− bone marrow monocyte (BMM) cultures and bones. Coculture of *Atf4*−/− BMMs with WT OBLs or a high concentration of RANKL failed to restore the OCL differentiation defect. Conversely, *Trap-Atf4-tg* mice displayed severe osteopenia with dramatically increased osteoclastogenesis and bone resorption. We further showed that ATF4 was an upstream activator of the critical transcription factor *Nfatc1* and was critical for RANKL activation of multiple MAPK pathways in OCL progenitors. Furthermore, ATF4 was crucial for M-CSF induction of RANK expression on BMMs, and lack of ATF4 caused a shift in OCL precursors to macrophages. Finally, ATF4 was largely modulated by M-CSF signaling and the PI3K/AKT pathways in BMMs. These results demonstrate that ATF4 plays a direct role in regulating OCL differentiation and suggest that it may be a therapeutic target for treating bone diseases associated with increased OCL activity.

Introduction

Skeletal integrity requires a delicate balance between bone-forming osteoblasts (OBLs) and bone-resorbing osteoclasts (OCLs). Abnormal osteoclastogenesis results in bone destruction, such as osteoporosis, metastatic osteolytic lesions, Paget disease of bone, and rheumatoid arthritis. In contrast, reduced osteoclastogenesis causes osteopetrosis, a disorder characterized by significantly increased skeletal mass and lack of a marrow space. Osteopetrosis is usually observed in animals or humans in which genes encoding cytokines, receptors, and signal transduction and transcription factors critical for OCL differentiation — such as RANKL; its receptor, RANK; the M-CSF receptor CSF1R (also known as c-Fms); TNF receptor–associated factor 6 (TRAF6); Src; PU.1, encoded by *Spi1*; p50/p52 NF-κb subunits; c-Fos; or v-ATPase V₀ subunit — are deleted or mutated (1–10). Defining the molecular mechanisms underlying osteoclastogenesis is essential to advance the understanding of the molecular basis for the pathogenesis of bone diseases with altered OCL activity. This knowledge will be important for the prevention and treatment of these diseases.

OCLs originate from cells in the monocyte/macrophage lineage (11). OCL formation and maturation are tightly regulated by OBL/stromal cell/hypertrophic chondrocyte-derived factors such as M-CSF, RANKL, and osteoprotegerin (OPG), a soluble decoy receptor that blocks RANKL binding to RANK and thereby inhibits OCL differentiation (12–15). M-CSF binds to its receptor, CSF1R, on early macrophage lineage cells and activates the *Rank* gene to generate OCL progenitors (16). The PI3K/AKT signaling pathways, which are strongly activated by M-CSF, play a critical role in activating OCL differentiation and bone resorption in nor-

mal and diseased states (17–24). However, little is known about the downstream molecular events that result from M-CSF–PI3K/AKT signaling and their relationship to osteoclastogenesis.

RANKL, a member of the TNF superfamily, binds to RANK on OCL precursors and recruits TRAF6, resulting in the activation of multiple signaling pathways including IKK complexes (IKKα, IKKβ, IKKγ, and NIK-IKKα) and MAPKs (Erk1/2, p38, and JNK) (2, 3, 25), which leads to activation of critical transcription factors such as NF-κB and c-Fos. RANKL activation of NF-κB and c-Fos results in induction of initial expression of the key transcription factor NFATc1 (also designated as NFAT2 or NFATc), which is activated by the Ca²⁺/calmodulin-regulated phosphatase calcineurin (3, 26–29). Eventually, calcium signaling occurs and activates the existing NFATc1, which triggers NFATc1 autoamplification (3, 30) required for further OCL differentiation. Inactivation of the *Nfatc1* gene in vivo is embryonic lethal due to a heart valve defect (31, 32). However, the lack of rescue of osteopetrosis in OCL-deficient *c-Fos*−/− mice by adoptive transfer of *Nfatc1*−/− (as opposed to *Nfatc1*+/−) hematopoietic stem cells provided evidence that NFATc1 is essential for osteoclastogenesis in vivo (33). Accordingly, transgenic overexpression of a constitutively active form of NFATc1 (caNFATc1) results in a skeletal phenotype of osteopenia associated with increased osteoclastogenesis and bone resorption (34). Importantly, overexpression of NFATc1 activates osteoclastogenesis in the absence of RANKL (29, 35, 36). In addition, ectopic NFATc1 can restore osteoclastogenesis in both the p50/p52 double knockout (37) and the c-Fos knockout mouse (38). These results suggest that the major OCL differentiation signals converge on NFATc1. However, the molecular mechanisms that control the expression of this key factor are not completely understood.

Critical roles for ATF4 in OBLs and bone formation are well established. ATF4 favors bone formation by promoting OBL-specific gene expression, amino acid import and the synthesis of type I
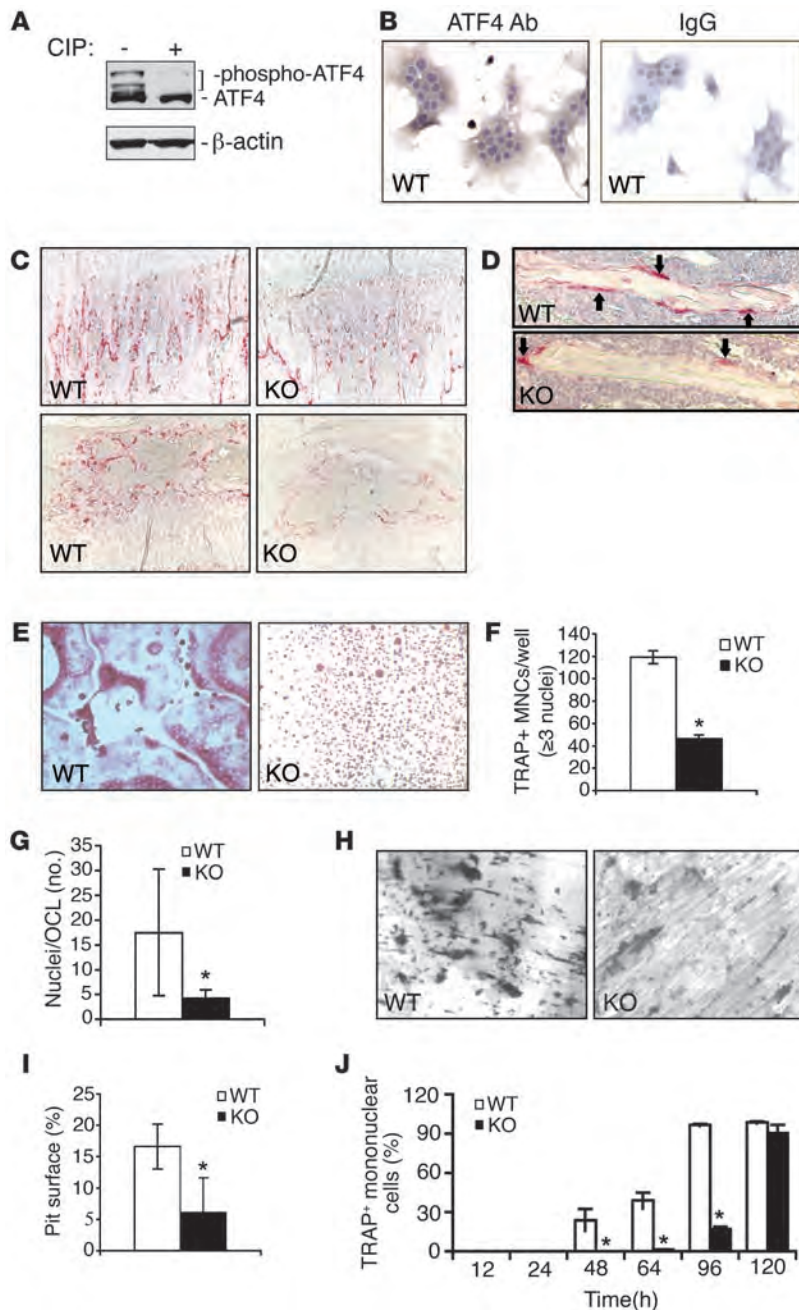
Figure 1
OCL differentiation is dramatically diminished in *Atf4−/−* BMM cultures and bones. (**A**) Western blot. Whole cell extracts (20 μg) from primary BMMs were incubated with or without 1 unit calf intestinal phosphatase (CIP) at room temperature for 30 minutes. (**B**) IHC. Differentiated BMMs were stained with an ATF4 antibody or control IgG. (**C**) Tibial sections were stained for TRAP activity for 30 minutes at 37°C. TRAP activity in both metaphyseal (top) and epiphyseal (bottom) regions of tibias is shown. (**D**) TRAP+ OCLs (arrows) on trabecular surfaces of WT and *Atf4−/−* tibiae. Oc.S/BS and Oc.Nb/BPm values for primary and secondary spongiosa are shown in Table 1. (**E**–**G**) WT and *Atf4−/−* BMMs were maximally differentiated for 9 days, followed by TRAP staining. TRAP+ MNCs (**F**) and the number of nuclei per OCL (**G**) were scored. (**H** and **I**) Bone resorption pit assay on dentin slices. BMMs were differentiated on dentin slices for 9 days. (**H**) Bone resorption pits were stained with hematoxylin solution. (**I**) Pit area versus total bone area on each dentin slice was measured as described in Methods. (**J**) Time course of TRAP+ mononuclear OCL differentiation. BMMs were differentiated for the indicated times followed by TRAP staining, and percent TRAP+ mononuclear cells was measured. *$P < 0.01$ versus WT. Original magnification, ×100 (**C**, **E**, and **H**), ×200 (**B** and **D**).

Using biochemical, cellular, and genetic approaches, the present study demonstrates that ATF4 is an osteoclastic transcription factor, which we believe to be novel, that is essential for OCL differentiation. We showed that both in vitro and in vivo OCL differentiation was severely impaired by lack of ATF4 in a cell-autonomous manner and increased by OCL-targeted transgenic ATF4 expression. Our results revealed that, mechanistically, ATF4 functioned as a direct upstream activator of the gene encoding the critical transcription factor NFATc1. Further, ATF4 modulated RANKL activation of MAPK pathways, a key molecular event in OCL differentiation. Additionally, we demonstrated that ATF4 was critical for M-CSF induction of RANK expression, a key step to generate OCL progenitors, and the level of ATF4 protein was largely modulated by M-CSF and the PI3K/AKT pathways in BMMs. Therefore, these results indicate that ATF4 has important OCL-intrinsic functions both upstream and downstream of RANKL signaling during OCL differentiation.

Results

Inactivation of the Atf4 gene severely impairs OCL differentiation in vitro and in vivo in a cell-autonomous manner. We first tested whether ATF4, a previously known OBL-enriched transcription factor (39), is expressed in OCL-like cells. As shown in Supplemental Figure 1 (supplemental material available online with this article; doi:10.1172/JCI42106DS1), the levels of ATF4 protein in primary mouse BMMs and RAW264.7 cells (a mouse monocyte/macrophage cell line) were comparable to those in OBL-like cells (mouse

collagen, and proliferation and survival of OBLs (39, 40). Furthermore, our most recent work showed that ATF4 is critical for osteoblastic responses to parathyroid hormone (PTH) to increase bone formation (41). Elefteriou and coworkers showed that ATF4 mediates β-adrenergic induction of *Rankl* mRNA expression via direct binding to the upstream OSE1 site in the *Rankl* promoter in OBLs (42). Work from the same group further showed that OBL-targeted expression of ATF4 increased osteoblastic *Rankl* expression and thereby OCL differentiation (43). Although these studies clearly demonstrate that increased OBL expression of ATF4 enhances OCL differentiation via RANKL production in OBLs, to our knowledge, the possibility of an OCL-intrinsic direct role for ATF4 in regulating OCL differentiation has not previously been addressed.

Table 1

Bone histomorphometry in WT and *Atf4*−/− tibiae

	WT	Atf4−/−
Primary spongiosa		
Oc.S/BS	8.4 ± 0.75	4.2 ± 0.48[A]
Oc.Nb/BPm	9.2 ± 0.96	5.1 ± 0.8[A]
Secondary spongiosa		
Oc.S/BS	8.5 ± 0.56	4.1 ± 0.55[A]
Oc.Nb/BPm	8.3 ± 0.91	4.3 ± 0.74[A]

Oc.S/BS and Oc.Nb/BPm in primary and secondary spongiosa of tibiae in Figure 1C were measured as described in Methods. [A]$P < 0.01$ versus WT.

MC-4 preosteoblastic cells, primary mouse bone marrow stromal cells [BMSCs], and rat UMR106-01 osteoblastic cells). As shown in Figure 1A, ATF4 protein was phosphorylated in primary mouse BMMs (note loss of upper bands with phosphatase treatment). Furthermore, a strong ATF4 signal was detected in the cytoplasm of the large multinuclear OCLs by immunohistochemical (IHC) staining using a specific ATF4 antibody (Figure 1B).

To determine whether ATF4 is required for osteoclastogenesis in vivo, the tibiae of 4-week-old WT and *Atf4*−/− mice were decalcified, and histological sections were stained for the OCL enzyme tartrate-resistant acid phosphatase (TRAP). We found that TRAP activity throughout the tibiae, including both the metaphyseal and the epiphyseal regions, was dramatically reduced in *Atf4*−/− compared with WT mice (Figure 1C). We next measured the effect of ATF4 deficiency on OCL differentiation in both primary and secondary spongiosa. OCL surface/bone surface (Oc.S/BS) and OCL number/bone perimeter (Oc.Nb/BPm) were reduced similarly in both primary and secondary spongiosa in *Atf4*−/− tibiae relative to WT tibiae (Figure 1D and Table 1). Given the dramatic decreases in Oc.S/BS and Oc.Nb/BPm in the *Atf4*−/− bone, we next determined whether ATF4 is intrinsically required in BMMs for OCL differentiation by assessing whether OCL differentiation was normal upon addition of exogenous RANKL to *Atf4*−/− compared with WT BMM cultures in vitro by measuring the number of TRAP+ multinucleated cells (MNCs; defined as having 3 or more nuclei per cell) generated by each. We found that TRAP+ MNCs in BMM cul-

tures from *Atf4*−/− mice were dramatically reduced compared with those from WT mice (Figure 1, E and F). Furthermore, the number of nuclei per MNC was decreased by 75% in *Atf4*−/− versus WT BMM cultures (Figure 1G), and the MNCs that formed in *Atf4*−/− BMM cultures were much smaller than those formed in WT cultures. Similar results were obtained in purified CD11b+ BMM cultures (Supplemental Figure 2, A and B). The ability to form TRAP+ MNCs was almost completely lost in BMM cultures from 15-month-old *Atf4*−/− mice (Supplemental Figure 2, C and D), which suggests that ATF4 is even more important for OCL differentiation in old animals. Furthermore, the resorption pit area on dentin slices was dramatically reduced in *Atf4*−/− versus WT BMM cultures (Figure 1, H and I). Although MNC number and size were both dramatically reduced in *Atf4*−/− BMM cultures relative to WT cultures, the ratio of total resorption pit area to total TRAP+ MNC area per slice was not significantly different in WT and *Atf4*−/− BMM cultures (WT, 0.46 ± 0.11; *Atf4*−/−, 0.56 ± 0.05), which suggests that the bone-resorbing activity of *Atf4*−/− TRAP+ MNCs is not impaired. Time-course experiments showed that the percentage of TRAP+ mononuclear OCLs was dramatically reduced in *Atf4*−/− versus WT BMM cultures in the first 4 days in OCL differentiation media. At day 5, this difference disappeared (Figure 1J), suggestive of a substantial delay rather than absolute decrease in early OCL differentiation. However, we noted that although the number of *Atf4*−/− and WT TRAP+ mononuclear cells was equivalent at day 5, the *Atf4*−/− cells did not go on to efficiently form MNCs at day 9 as described above (Figure 1, E–G). To further investigate the delayed early OCL differentiation, we assessed the in vitro formation of CFU-GMs, which are

Figure 2

ATF4 deficiency impairs OCL differentiation in a cell-autonomous manner. (**A** and **B**) CFU-GM assay. 2 × 10⁴ BMMs from WT and *Atf4*−/− mice (6 per group) were cultured in methylcellulose semisolid medium in 35-mm dishes in the presence of 1.0 ng/ml recombinant human GM-CSF for 10 days. The number of CFU-GM colonies was counted under an inverted microscope. Experiments were repeated 2 times. (**C** and **D**) OCL-OBL coculture. Primary calvarial OBLs from 3-day-old WT mice were cocultured with WT or *Atf4*−/− BMMs as described in Methods. (**E** and **F**) Effects of increased RANKL. Primary BMMs (**E**) and purified CD11b+ BMMs (**F**) from both genotypes were differentiated in the presence of increasing concentrations of RANKL for 7 days, and the number of TRAP+ MNCs per well was counted. *$P < 0.01$ versus WT. Original magnification, ×40 (**A**); ×200 (**C**).
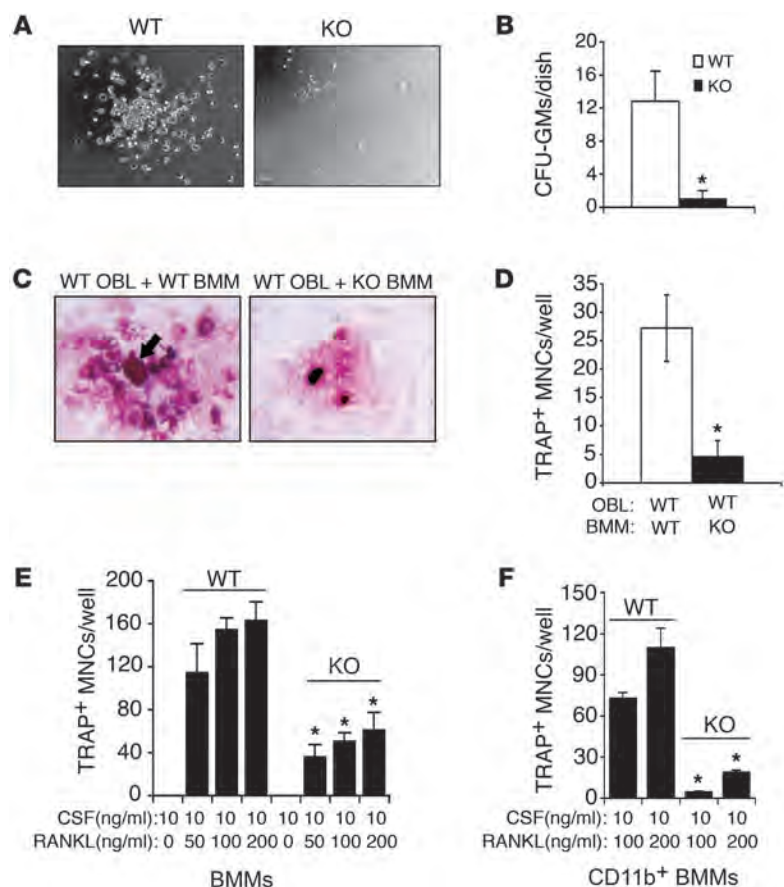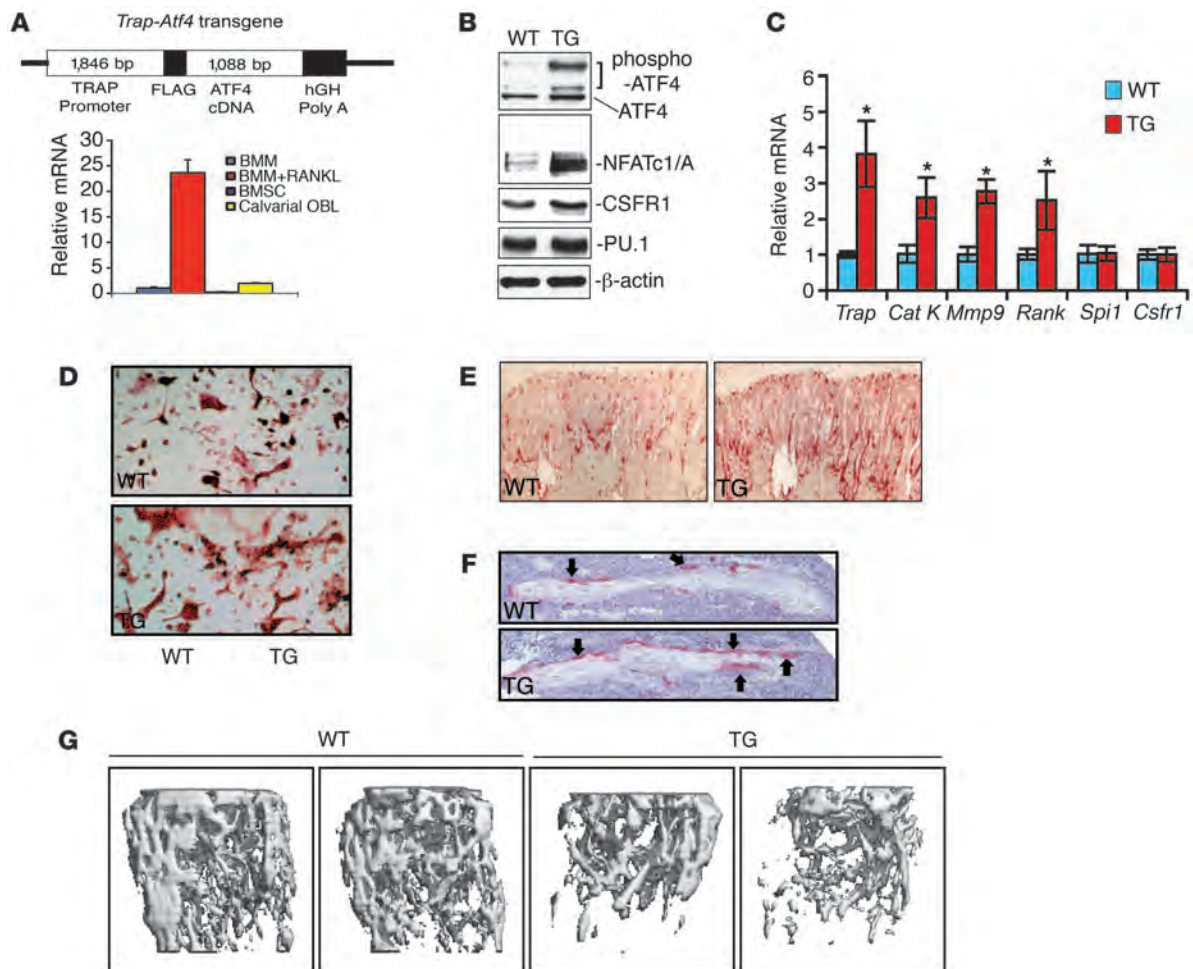
Figure 3
OCL-targeted transgenic overexpression of ATF4 dramatically increases OCL differentiation and bone resorption and results in a severe osteopenic phenotype. (**A**) Schematic representation of a transgene construct. An 1,846-bp fragment of the mouse *Trap* promoter was used to drive expression of full-length mouse ATF4 cDNA. *Atf4* transgene expression in RANKL-differentiated and undifferentiated BMMs, BMSCs, or calvarial OBLs was measured by quantitative real-time RT-PCR using transgene-specific primers as described in Methods. (**B**–**D**) In vitro OCL differentiation. BMMs from 4-week-old WT and *Trap-Atf4-tg* mice (founder no. 2360) were differentiated into OCLs for 5 days followed by (**B**) Western blot analysis of ATF4, NFATc1, PU.1, CSFR1, and β-actin for loading; (**C**) real-time RT-PCR analysis for *Trap*, *Cat K*, *Mmp9*, *Rank*, *Spi1*, and *Csfr1* mRNAs; and (**D**) TRAP staining of the BMM cultures. (**E**) TRAP staining. Tibial sections from 4-week-old WT and *Trap-Atf4-tg* mice were stained for TRAP activity. (**F**) TRAP⁺ OCLs (arrows) on trabecular surfaces of WT and *Trap-Atf4-tg* tibiae. Oc.S/BS and Oc.Nb/BPm values for primary and secondary spongiosa are shown in Table 2. (**G**) μCT analysis. Fixed nondemineralized femurs from 3-month-old male WT and *Trap-Atf4-tg* mice were used for μCT analysis as previously described (41). BV/TV, Tb.N, and Tb.Sp values are shown in Table 3. n = 3–7. *P < 0.01 versus WT. Original magnification, ×100 (**D** and **E**); ×200 (**F**).

known to contain the earliest OCL precursors (44), and found that it was severely compromised in *Atf4*⁻/⁻ BMMs (Figure 2, A and B). We next examined whether coculture with WT OBLs rescues the OCL formation of *Atf4*⁻/⁻ BMMs (Figure 2, C and D). As expected, cocultures of WT OBLs with WT BMMs significantly induced the formation of TRAP⁺ MNCs. Although WT OBLs did induce some TRAP⁺ mononuclear OCLs in coculture with *Atf4*⁻/⁻ BMMs, there were almost no TRAP⁺ MNCs observed. Furthermore, primary calvarial OBLs from 3-day-old *Atf4*⁻/⁻ mice failed to induce TRAP⁺ MNC formation when cocultured with either WT or *Atf4*⁻/⁻ BMMs (H. Cao and G. Xiao, unpublished observation), in support of the notion that osteoblastic ATF4 plays a role in OCL differentiation, probably via upregulation of RANKL expression (42). In addition,

high concentrations of RANKL (up to 200 ng/ml) did not restore the OCL differentiation defect in BMMs or purified CD11b⁺ BMMs of *Atf4*⁻/⁻ mice (Figure 2, E and F). Collectively, these findings suggest that ATF4 deficiency impairs osteoclastogenesis in a cell-autonomous manner.

OCL-targeted overexpression of ATF4 dramatically increases OCL differentiation and bone resorption and causes a severe osteopenic phenotype. To further examine the OCL-intrinsic role of ATF4 in regulating osteoclastogenesis in vivo, we developed transgenic mice in which the *Atf4* transgene is driven by an 1,846-bp mouse *Trap* promoter that selectively expresses ATF4 in OCLs (referred to herein as *Trap-Atf4-tg* mice; Figure 3A). This promoter has been successfully used to target OCL expression of many transgenes (45–47). *Atf4*

Table 2

Bone histomorphometry in WT and *Trap-Atf4-tg* tibiae

	WT	*Trap-Atf4-tg*
Primary spongiosa		
Oc.S/BS	9.1 ± 0.36	16 ± 0.71[A]
Oc.Nb/BPm	9.2 ± 1.2	16 ± 0.94[A]
Secondary spongiosa		
Oc.S/BS	9.2 ± 0.51	16.5 ± 0.72[A]
Oc.Nb/BPm	9.3 ± 1.03	16.6 ± 1.3[A]

Oc.S/BS and Oc.Nb/BPm in both primary and secondary spongiosa of tibiae in Figure 3E were measured as described in Methods. [A]$P < 0.01$ versus WT.

transgene mRNA was highly expressed in RANKL-differentiated BMMs, but was minimal in undifferentiated BMMs, calvarial OBLs, or BMSCs (Figure 3A). As shown in Figure 3B, the level of ATF4 protein was dramatically increased in RANKL-differentiated BMM cultures from *Trap-Atf4-tg* mice compared with BMM from the control littermates. Transgenic ATF4 dramatically increased the protein levels of NFATc1/A, but not of PU.1 or CSFR1, in differentiated BMM cultures. The levels of OCL differentiation marker gene mRNAs (*Trap*, *Rank*, *Cat K*, and *Mmp9*) were all dramatically elevated in differentiated BMM cultures from *Trap-Atf4-tg* mice compared with those from WT mice. In contrast, like the proteins, the levels of *Spi1* and *Csfr1* mRNAs were not increased by transgenic ATF4 (Figure 3C). Using BMMs from 3 different transgenic lines, we found that OCL-targeted overexpression of ATF4 dramatically increased the number of TRAP+ MNCs in vitro (WT, 56 ± 11 TRAP+ MNCs/well; *Trap-Atf4-tg*, 270 ± 17 TRAP+ MNCs/well; $P < 0.01$; Figure 3D). We found a similar effect of transgenic ATF4 expression in vivo. TRAP activity was markedly increased in *Trap-Atf4-tg* compared with WT tibiae (Figure 3E). Oc.S/BS and Oc.Nb/BPm in both primary and secondary spongiosa of tibiae were dramatically increased in *Trap-Atf4-tg* versus WT mice ($P < 0.01$; Figure 3F and Table 2). The serum level of C-telopeptide (CTX), an indicator of in vivo OCL activity, was elevated 2.4-fold in *Trap-Atf4-tg* mice relative to WT mice (WT, 19.5 ± 3.7; *Trap-Atf4-tg*, 46 ± 3.3; $P < 0.01$). Quantitative μCT analysis of femur histomorphometric parameters showed that *Trap-Atf4-tg* mice had a significant reduction in bone volume/tissue volume (BV/TV) and trabecular number (Tb.N), as well as a marked increase in trabecular space (Tb.Sp), compared with WT littermates ($P < 0.01$, all comparisons; Figure 3G and Table 3). Results from these experiments demonstrated that osteoclastic ATF4 overexpression increased OCL differentiation and bone resorption, resulting in a severe osteopenic phenotype.

ATF4 is an upstream activator of the Nfatc1 gene. We next examined whether deletion of *Atf4* reduces expression of NFATc1, a master regulator of OCL differentiation. Results from quantitative real-time RT-PCR analysis showed that the level of *Nfatc1* mRNA relative to *Gapdh* mRNA was greatly decreased in *Atf4*−/− BMM cultures compared with WT cells (Figure 4A and Supplemental Figure 3). The expression of *Cat K*, a well-known NFATc1 downstream target gene, was almost abolished in *Atf4*−/− cells compared with WT control cells. Western blot analysis confirmed that NFATc1/A protein, the major isoform of NFATc1 expressed in OCLs, was drastically reduced by ATF4 deficiency (Figure 4B). In contrast, the levels of TRAF6 and c-Fos, both critical factors for OCL differentiation and NFATc1 induction (7, 8, 48, 49), were not decreased by ATF4

deficiency. Likewise, the mRNA and protein levels of PU.1 and CSFR1, both critical factors for early OCL lineage commitment and development, were not reduced by the lack of ATF4 (Figure 4, A and B), in accordance with their observed lack of increase by overexpression of ATF4 (Figure 3, B and C). As expected, the level of *Atf4* mRNA was minimal in *Atf4*−/− BMM cultures (Figure 4A). IHC staining of differentiated BMM cultures using a specific antibody for NFATc1 showed a strong signal in MNCs of WT cultures that was drastically reduced in *Atf4*−/− cultures, although there were some mononuclear OCLs that were NFATc1+ in *Atf4*−/− cultures (Figure 4C). Similarly, in vivo, a strong NFATc1 signal was identified on all surfaces of trabeculae throughout WT tibiae, where OCLs are usually located (Figure 4D). In contrast, the majority of the trabecular surfaces of *Atf4*−/− tibiae were negative for NFATc1. Adenoviral ATF4 overexpression in BMMs increased the level of NFATc1 protein in a dose-dependent manner (Figure 4E). ATF4 activated –847/+66 *Nfatc1* P1 promoter–pGL3–luciferase reporter activity in a dose-dependent manner, but failed to stimulate a 2.8-kb mouse *Runx2* promoter (Figure 4F). In contrast, the *Nfatc1* P1 promoter was not activated by Runx2 (Supplemental Figure 4). As shown in Figure 4G, introduction of a 4-bp substitution mutation to the known AP1 binding site located at –644/–637 (from TGACTTCA to TGCGAACA) decreased ATF4 activation by 50% without affecting basal promoter activity, which indicates that this site is critical for ATF4 regulation. ChIP assays showed that RANKL induced ATF4 interaction with a chromatin fragment of the proximal *Nfatc1* promoter in RAW264.7 OCL-like cells (Figure 4H). Consistent with results from previous studies (33, 38), both c-Fos and NFATc1 itself were also recruited to the same region of the *Nfatc1* promoter in a RANKL-dependent manner. These data demonstrate that ATF4 is a critical upstream activator of the *Nfatc1* gene and indicate that ATF4 not only regulates the number of OCL progenitors, but also has a direct role in activating genes downstream of RANK signaling.

We next examined whether NFATc1 can rescue the defective OCL differentiation of *Atf4*−/− BMMs. WT and *Atf4*−/− BMMs were infected with increasing amounts of retrovirus expressing a constitutively active form of NFATc1 (50) and differentiated for 7 days, followed by TRAP staining. Although caNFATc1 dose-dependently increased the number of TRAP+ MNCs in *Atf4*−/− BMM cultures (Figure 4I), surprisingly, at even the highest dose, it only slightly increased the number of nuclei per MNC (WT plus empty virus, 24 ± 3.8; WT plus NFATc1 virus, 32.6 ± 5.5; $P < 0.01$; KO plus empty virus, 3.3 ± 0.42; KO plus NFATc1 virus, 4.8 ± 0.71; $P < 0.01$).

ATF4 modulates RANKL activation of MAPKs, but not IκBα pathways, in OCL progenitors. Because activation of the MAPK and IκBα/NF-κB pathways by RANKL is crucial for NFATc1 expression and OCL differentiation, we next examined whether ATF4 deficiency affects

Table 3

Quantitative μCT analysis of WT and *Trap-ATF4-tg* femur histomorphometric parameters

	WT	*Trap-ATF4-tg*
BV/TV (%)	21 ± 3.0	12 ± 3.8[A]
Tb.N (per mm)	3.4 ± 0.37	2.3 ± 0.07[A]
Tb.Sp (mm)	0.30 ± 0.03	0.45 ± 0.01[A]

Fixed nondemineralized femurs from 3-month-old male WT and *Trap-Atf4-tg* animals were used for μCT analysis as previously described (41).
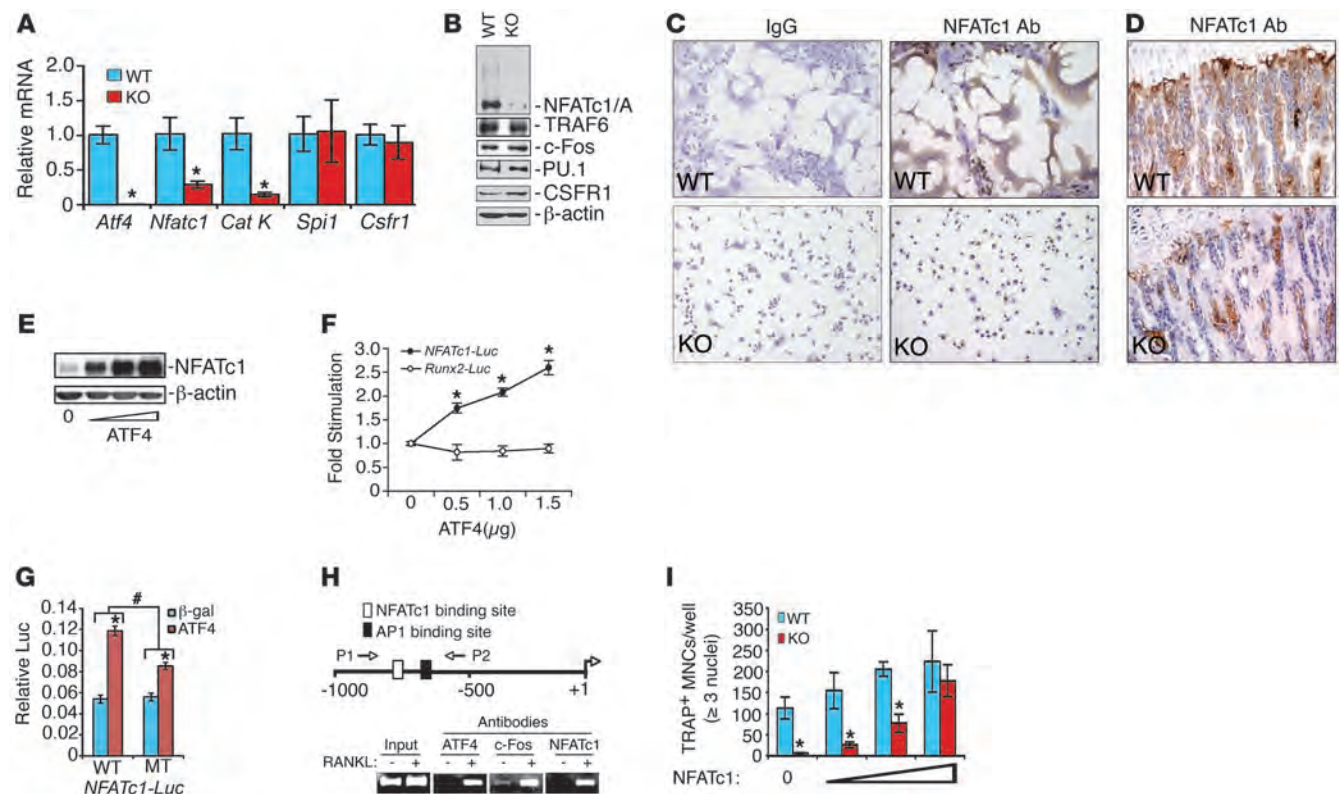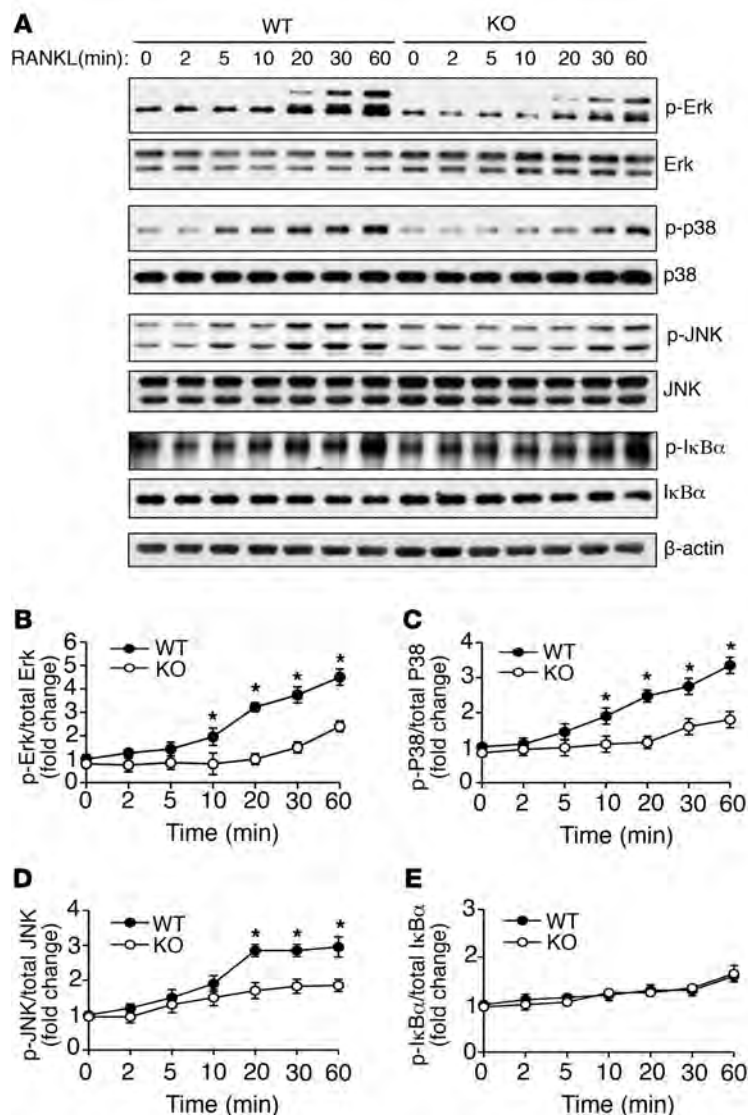
Figure 4
ATF4 regulates NFATc1 expression in BMM cultures and bones. (**A** and **B**) Total RNAs and protein lysates from differentiated WT and *Atf4*−/−
BMMs were used for real-time RT/PCR analysis (**A**) and Western blot (**B**). (**C** and **D**) Differentiated BMMs and tibial sections were subjected to
IHC staining for NFATc1. (**E**) WT BMMs were infected with increasing amounts of ATF4 adenovirus, then switched to differentiation medium for
72 hours, followed by Western blot for NFATc1. (**F**) ATF4 activates the *Nfatc1* P1 promoter. COS-7 cells were transfected with 0.8-kb *Nfatc1*-luc
or 2.8-kb mouse *Runx2*-luc constructs and pRL-SV40 with the indicated amounts of ATF4 expression plasmid. After 30 hours, cells were har-
vested for the dual luciferase assay. *P < 0.01 versus 0 μg ATF4. (**G**) COS-7 cells transfected with 0.8-kb *Nfatc1*-luc (WT) or the same plasmid
containing a 4-bp substitution mutation (MT) in the putative ATF4-binding site and pRL-SV40 with or without ATF4 expression plasmid. *P < 0.05
versus β-gal; #P < 0.05, WT versus MT ATF4/β-gal. (**H**) ChIP assay. A schematic representation of the relevant region of the mouse *Nfatc1* P1
promoter is shown. P1 and P2 indicate PCR primers used to analyze ChIP DNAs. RAW264.7 cells were treated with or without 50 ng/ml RANKL
for 24 hours. ChIP assays were performed using antibodies against ATF4, c-Fos, or NFATc1. (**I**) WT and *Atf4*−/− BMMs were cultured and infected
with increasing amounts of retrovirus expressing caNFATc1, and switched to differentiation medium for 7 days. The number of TRAP+ MNCs
per well was counted. *P < 0.01 versus WT. Original magnification, ×100.

RANKL activation of these important pathways in OCL progeni-
tors. As shown in Figure 5, RANKL rapidly induced the phos-
phorylation of Erk1/2 in a time-dependent manner, which was
delayed and reduced in *Atf4*−/− cells. ATF4 deficiency also slightly
reduced the basal phosphorylation level of Erk1/2. Lack of ATF4
similarly compromised RANKL activation of p38 and JNK with-
out markedly affecting their basal levels. In contrast, no difference
was seen in RANKL-induced phosphorylation of IκBα in cells of
the 2 genotypes. Collectively, lack of ATF4 reduced the ability of
RANKL to activate the Erk1/2, p38, and JNK MAPK pathways in
OCL progenitors.

We next determined whether ATF4 deficiency affects M-CSF–
dependent signaling in BMMs. As shown in Supplemental Figure 5,
M-CSF rapidly stimulated the phosphorylation of AKT and JNK in
WT cells, which was slightly reduced in *Atf4*−/− cells. The levels of
both phosphorylated and total Src were similar in WT and *Atf4*−/−
cells with or without M-CSF. In contrast to RANKL, M-CSF simi-
larly activated Erk1/2 and p38 in WT and *Atf4*−/− cells. Thus, ATF4
deficiency did not dramatically impact M-CSF signaling in BMMs.

*Levels of ATF4 protein in BMMs are modulated by M-CSF and PI3K/
AKT, and ATF4 is required for M-CSF induction of RANK expression.*
To determine whether ATF4 is regulated by M-CSF in early OCL
differentiation, BMMs were cultured in the presence and absence
of 30 ng/ml M-CSF for 0, 6, 12, 24, and 48 hours, followed by
Western blot for ATF4. The results showed that the level of ATF4
protein was dramatically reduced in the absence of M-CSF in a
time-dependent manner. However, this reduction was completely
prevented by M-CSF (Figure 6A). M-CSF did not alter the level of
Atf4 mRNA (Figure 6B), which suggests that a posttranscriptional
mechanism is involved in this regulation.

To define the signaling pathways through which M-CSF regulates
ATF4, BMMs were treated with and without inhibitors or activa-
tors for various pathways in the presence of M-CSF for 24 hours. As
shown in Figure 6C, LY294002, a specific inhibitor of the PI3K/AKT
pathway, dramatically reduced total and phosphorylated ATF4. In
contrast, the p38 inhibitor SB209580, the Erk1/2 inhibitor U0126,
the PKA inhibitor H89, the PKC inhibitor GF109203X, and the
PKA activator FSK did not markedly decrease or increase ATF4 or
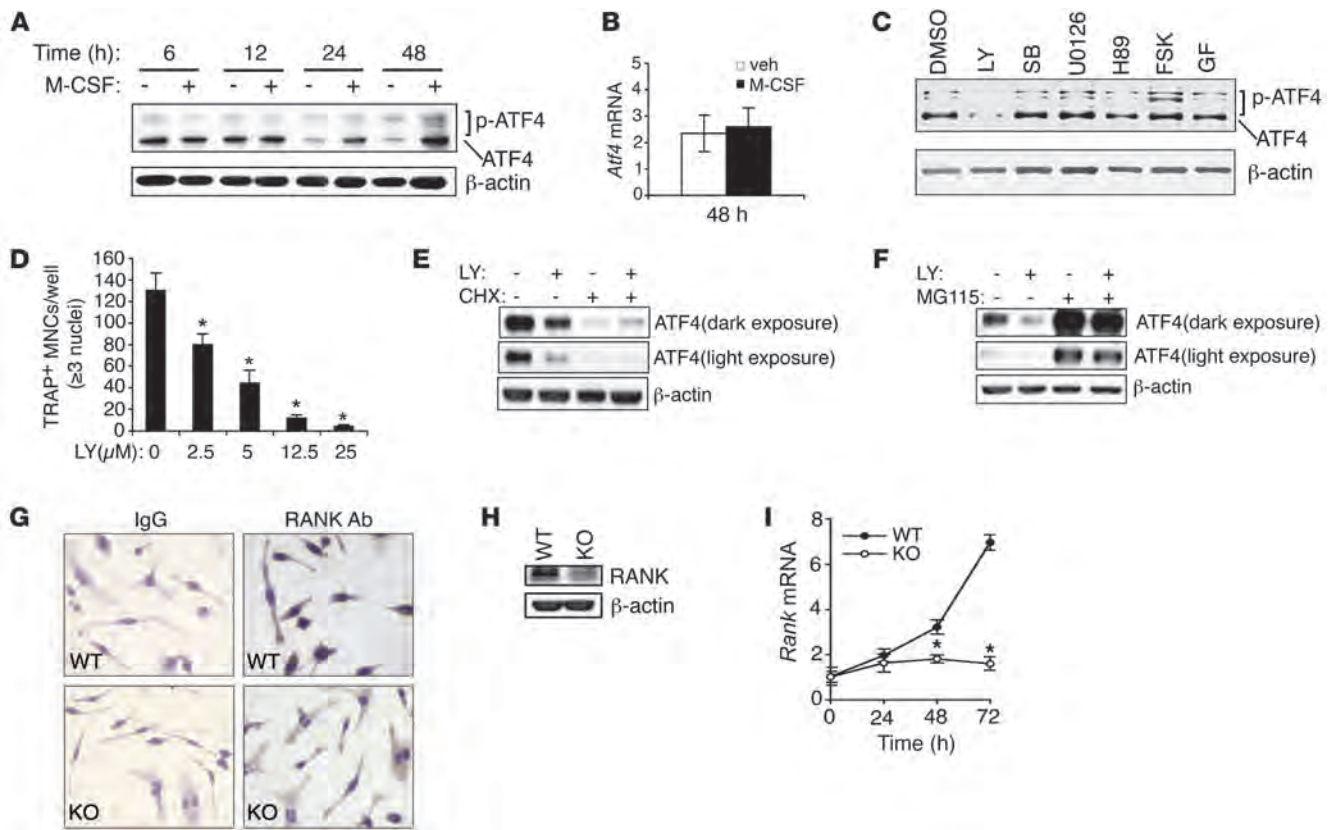
A

B

C

D

E

specific antibodies. M-CSF time-dependently induced *Rank* mRNA expression in WT BMM cultures (Figure 6I), consistent with results from a previous study (16). However, this induction was dramatically reduced in *Atf4*^{−/−} cells. Taken together, these results suggest that ATF4 regulates early OCL differentiation at least in part by facilitating M-CSF induction of the *Rank* gene.

ATF4 deficiency results in increased CD11b^{+} *cells in bone marrow and spleen and reduced CD3*^{−}*CD45R*^{−}*CD11b*^{−/lo} *c-kit*^{+}*CD115*^{hi} *cells in bone marrow.* Because OCLs and macrophages share the same precursor, we next determined whether lack of ATF4 affects monocyte/macrophage precursors by measuring the CD11b^{+} cell population in splenocytes and bone marrow from WT and *Atf4*^{−/−} mice. In 5 independent experiments, the percentage of CD11b^{+} cells was dramatically increased in *Atf4*^{−/−} splenocytes compared with WT cells, as measured by flow cytometry (WT, 3.04% ± 0.64%; KO, 9.6% ± 2.1%; $P < 0.01$; Figure 7A). This increase in CD11b^{+} cells was specific, because the percentages of both T lymphocytes (CD3^{+}; Figure 7A) and dendritic cells (CD11c^{+}; Supplemental Figure 6, A and B) were not increased by ATF4 deficiency (WT, 27.63% ± 1.9% CD3^{+}, 1.59% CD11c^{+}; KO, 21.04% ± 4.1% CD3^{+}, 1.52% CD11c^{+}; $P > 0.05$). Likewise, in bone marrow, the number of CD11b^{+} cells was similarly increased in *Atf4*^{−/−} mice (WT, 41.5% ± 0.08%; KO, 63.6% ± 3.4%; $P < 0.01$), but the number of CD3^{+} cells (WT, 1.04% ± 0.2%; KO, 0.8% ± 0.06%; $P > 0.05$) and CD11c^{+} cells (Supplemental Figure 6C) was not. At the same time, the percentage of CD11b^{−/lo} cells, the osteoclastogenic population in the bone marrow, was dramatically reduced in *Atf4*^{−/−} marrow and spleen. Since the CD3^{−}CD45R^{−}CD11b^{−/lo}c-kit^{+}CD115^{hi} population (approximately 2% of fresh murine bone marrow preparations) contains the highest in vitro osteoclastogenic activity (55), we next determined whether *Atf4* inactivation affects this OCL precursor population in bone marrow cells and splenocytes. In 5 independent experiments, the percentage of this cell population was slightly but significantly reduced in bone marrow cells by ATF4 deficiency (WT, 2.3% ± 0.11%; KO, 2.0% ± 0.02%; $P = 0.01$; Figure 7A). However, the percentage of this cell population in splenocytes was much lower than in bone marrow (approximately 0.25%) and was not significantly changed by ATF4 deficiency. It should be noted that although *Atf4*^{−/−} bones are smaller and thinner than WT bones, total nucleated bone marrow cells per bone were not reduced in *Atf4*^{−/−} compared with WT mice (Supplemental Figure 6D). ATF4 deficiency did not alter the proliferation and survival of CD11b^{+} BMMs (Figure 7, B–E). Therefore, the lack of

alter its phosphorylation. Importantly, exposure to LY294002 for only 24 hours prior to the addition of differentiation media inhibited in vitro OCL differentiation in a dose-dependent manner (Figure 6D). The concentrations of the inhibitors or activators used in this study are in the ranges previously reported to selectively affect the relevant pathways (51–54), or were as suggested by the respective manufacturers. We found no evidence of cell toxicity using these experimental conditions. Interestingly, the decrease in ATF4 in COS-7 cells induced by LY294002 was completely abolished by cycloheximide (CHX) and dramatically reduced by the proteasome inhibitor MG115 (Figure 6, E and F). These results suggest that regulation of ATF4 by LY294002 involves de novo protein biosynthesis as well as modulation of protein stability.

M-CSF–induced RANK expression is essential for generating OCL progenitors. We next evaluated whether ATF4 is required for this regulation. To this end, highly purified CD11b^{+} BMMs were cultured in M-CSF–containing medium for 72 hours and stained with an anti-RANK antibody or control IgG. As shown in Figure 6, G and H, the RANK signal was dramatically decreased in *Atf4*^{−/−} relative to WT cells, as measured by both IHC and Western blot using

Figure 6
ATF4 is upregulated by M-CSF and PI3K/AKT and is required for M-CSF induction of RANK expression in BMMs. (**A** and **B**) Effects of M-CSF on ATF4 in BMMs. Cells were cultured with or without 30 ng/ml M-CSF for the indicated times, followed by Western blot (**A**) or real-time RT-PCR (**B**) for ATF4. (**C**) Effects of various inhibitors or activators on the level of ATF4 in BMMs. Cells were cultured in M-CSF–containing medium with and without the indicated inhibitors or activators (10 μM) for 24 hours. LY, LY294002; SB, SB209580; GF, GF109203X. (**D**) Effect of PI3K/AKT inhibition on OCL differentiation. BMMs were seeded in proliferation medium for 3 days and treated with increasing concentrations of LY294002 for 24 hours. Inhibitor was then removed by switching cells to differentiation medium for 5 days, followed by TRAP staining. *$P < 0.01$ versus 0 μm. (**E** and **F**) COS-7 cells were transfected with 1.0 μg pCMV/ATF4 expression plasmid. After 24 hours, cells were treated with or without 10 μM LY294002 as well as with or without 10 μg/ml CHX (**E**) or 10 μM MG115 (**F**) for another 24 hours. (**G**) IHC. Purified CD11b+ BMMs were seeded in proliferation medium for 72 hours, followed by IHC with an anti-RANK antibody or control IgG. (**H**) Western blot. Primary BMMs were seeded in 35-mm dishes in proliferation medium for 72 hours. (**I**) Real-time RT-PCR. WT and *Atf4*−/− BMMs were cultured in proliferation medium for 3 days and switched to 2% FBS α-MEM without M-CSF overnight. Cells were then treated with 10 ng/ml M-CSF for the indicated times. *$P < 0.01$, WT versus KO. Original magnification, ×200.

ATF4 causes a lineage shift between OCLs and macrophages, resulting in an increase in macrophages. Interestingly, a similar increase in macrophages was observed in mice lacking c-Fos, whose deficiency also reduces NFATc1 and OCL differentiation (7–9).

Discussion

The results of our present study establish, for the first time to our knowledge, that ATF4, a transcription factor previously shown to be important in OBLs, also plays a direct and critical role in regulating OCL differentiation both in vitro and in bones. Drastically reduced OCL differentiation in BMM cultures from *Atf4*−/− animals was not rescued by coculture with WT OBLs or high concentrations of RANKL, which suggests that ATF4 plays an intrinsic role in OCLs that is indispensable for RANKL-induced OCL differentiation. Dramatic reduction in the formation of CFU-GMs in *Atf4*−/− BMM cultures suggests that ATF4 deficiency impairs the formation of OCL precursors. To examine the in vivo actions of ATF4 in OCLs, this study used the mouse *Trap* promoter to drive expression of ATF4 in OCLs. Using this approach, ATF4 was shown to stimulate expression of NFATc1 and other OCL-specific genes and OCL differentiation in BMM cultures. Of particular significance, *Trap-Atf4-tg* animals displayed a striking in vivo effect on OCL differentiation and bone resorption, resulting in a severe osteopenic phenotype. Because the *Trap* promoter is not active in OBLs, we were able to discriminate between the effects of ATF4 in OCLs and those in OBLs or BMSCs (i.e., via ATF4-dependent production of RANKL). Furthermore, as shown in Figure 1C and Figure 3E, TRAP activity in hypertrophic chondrocytes close to primary spongiosa was very weak, which suggests that the *Trap* promoter is not active in these cells. Therefore, *Atf4* transgene expression driven by this promoter should be low in the hypertrophic chondrocytes; consequently, the potential contribution of the *Atf4* transgene expression in these cells to the observed bone phenotype in *Trap-Atf4-tg* mice (i.e., osteopenia, increased OCL differentiation, and bone resorption) should be minimal.
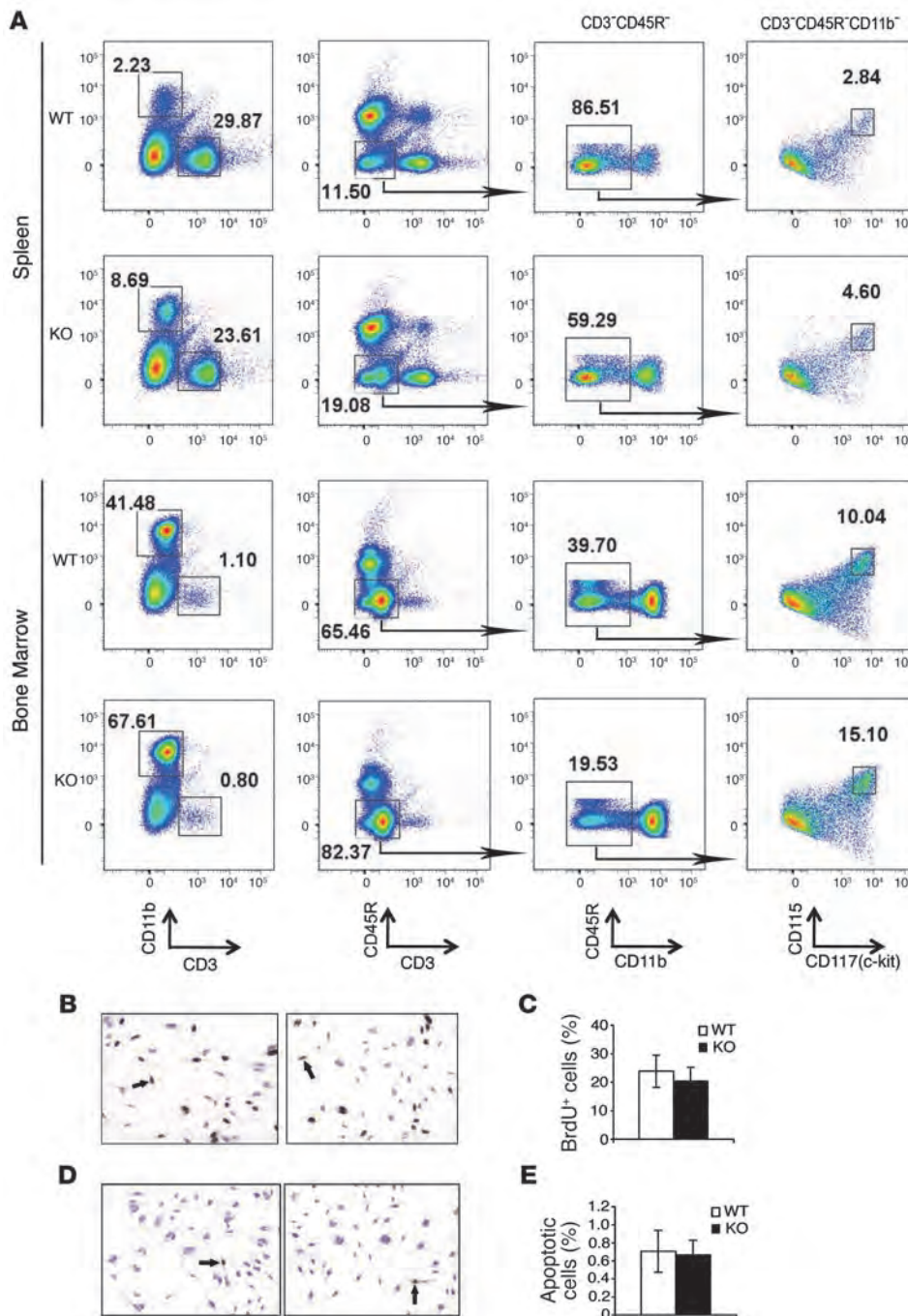
Figure 7
ATF4 deficiency increases CD11b+ cells in bone marrow and spleen and reduces CD3–CD45R–CD11b–/lo c-kit+CD115hi cells in bone marrow. (**A**) Flow cytometry. Splenocytes and bone marrow cells from WT and *Atf4−/−* mice were stained with bio-strep-PB–conjugated CD11b, FITC-conjugated CD3, PE-conjugated CD45R, Pecy5-conjugated c-kit (CD117), and APC-conjugated CD115 antibodies and analyzed with flow cytometry as described in Methods. The percentage of CD3–CD45R–CD11b–/lo c-kit+CD115hi cells in bone marrow cells or splenocytes was calculated by multiplying the percentages of gated populations as indicated. A representative experiment is shown; values in Results were averaged over 5 independent experiments. 1 WT and 1 *Atf4−/−* mouse were used in each experiment. (**B** and **C**) BrdU staining. Purified CD11b+ BMMs were cultured in 8-well chambers (5 × 10⁵ cells/well) in proliferation medium for 72 hours, followed by BrdU staining as described previously (40, 41). Arrows indicate BrdU+ (i.e., proliferating) cells. (**D** and **E**) TUNEL staining. CD11b+ BMMs were treated as in **B**, followed by TUNEL staining as described previously (40, 41). Arrows indicate apoptotic cells. Original magnification, ×100.

One striking result in the present study, which we believe to be novel, is the finding that ATF4 is a direct upstream activator of the *Nfatc1* gene, a master regulator of OCL differentiation. Levels of NFATc1 were drastically reduced in *Atf4−/−* OCLs and bones. Conversely, OCL-specific expression of ATF4 in transgenic mice greatly increased the expression of NFATc1 and its downstream target genes as well as OCL differentiation. ATF4 activated *Nfatc1* gene transcription via interaction with the P1 promoter. Interestingly, a previously known AP1 binding site located at –644/–637 was critical for ATF4 activation of the *Nfatc1* P1 promoter, which suggests that ATF4 directly binds to this site and/or functions

via interactions with AP1 factors. Future study will differentiate among these possibilities. Of particular significance, ATF4 interaction with the P1 promoter was stimulated by RANKL. In addition to its direct regulation, ATF4 may also indirectly increase NFATc1 expression by promoting RANKL-RANK signaling. This notion is supported by our findings that (a) M-CSF induction of RANK, the receptor for RANKL in OCL precursors, was severely impaired in *Atf4−/−* BMMs; and (b) RANKL activation of the Erk1/2, JNK, and p38 MAPK pathways in OCL progenitors, which is crucial for the subsequent expression of NFATc1, was greatly compromised by the lack of ATF4. Although ATF4 is essential for its expression,

retroviral transduction of NFATc1 cDNA into BMM only partially rescued the OCL differentiation defect in *Atf4*^{-/-} BMM cultures, as large OCLs were still not formed. Possible explanations include: (a) the magnitude and duration of NFATc1 expression was inappropriate for full rescue; and (b) other OCL differentiation–related genes and/or factors are also regulated by ATF4.

Our results established that ATF4 is a critical downstream target of M-CSF–PI3K/AKT signaling in early OCL differentiation. The level of ATF4 protein was largely dependent upon the presence of M-CSF and the PI3K/AKT pathway in BMMs. M-CSF upregulated ATF4 at least in part by stabilizing its protein, which involves the PI3K/AKT pathway. Strikingly, short-term pharmacologic inhibition of the PI3K/AKT pathway dramatically reduced the level of ATF4 protein in undifferentiated BMMs and subsequent OCL differentiation. These results strongly suggest that the M-CSF–PI3K/AKT–ATF4 axis identified in the present study plays a crucial role in regulating early OCL differentiation. PI3K/AKT signaling has been implicated in OCL activation and bone resorption in neurofibromatosis type I (NF1), a congenital disorder resulting from loss of function of the tumor suppressor gene *NF1*, which encodes neurofibromin, a GTPase-activating protein for Ras. NF1 patients have a significantly higher incidence of osteoporosis and osteopenia (21–23). Recent studies showed that increased OCL activity and osteoporosis is caused by increased AKT signaling in OCLs in murine and human *NF1* haploinsufficiency (18, 19). It would be interesting to test whether ATF4 plays a role in the AKT-induced OCL differentiation and bone resorption in NF1 patients. Notably, mice selectively lacking NF1 in OBLs displayed increased OCL activity, probably via upregulation of ATF4 in OBLs, and thereby exhibited increased RANKL expression (43).

Results from the present study demonstrated that ATF4 is not required for early OCL lineage commitment and development. First, CSFR1 and PU.1 expression, which is required for the generation of the common progenitors for both macrophages and OCLs, was not altered in *Atf4*^{-/-} BMMs or bones. Second, M-CSF activation of AKT and MAPKs was not markedly different in WT and *Atf4*^{-/-} BMMs. Third, both proliferation and survival of highly purified CD11b^{+} BMMs of the 2 genotypes were similar. Finally, the number of macrophages was increased in *Atf4*^{-/-} animals. Therefore, ATF4 deficiency impairs OCL, but not macrophage, differentiation, and the OCL differentiation defect in *Atf4*^{-/-} mice occurs later than in *Spi1*- or *Csfr1*-deficient mice.

Although ATF4 is crucial for OCL differentiation, *Atf4*^{-/-} mice did not display an osteopetrotic phenotype, which is often observed in mice and humans in which genes encoding key OCL-regulating factors — such as CSF1R, RANK, RANKL, TRAF6, Src, PU.1, NF-κB (p50/p52 double knockout), and c-Fos — are inactivated or mutated (1–9). Lack of osteopetrosis in *Atf4*^{-/-} mice could be explained, at least in part, by the fact that ATF4 is also important for OBL function and bone formation (39, 40, 56). Therefore, it is expected that *Atf4*^{-/-} mice have a low–bone turnover osteoporosis.

ATF4 can be specifically regulated by different signal transduction factors in OBLs and OCLs. For examples, ATF4 is directly phosphorylated and activated by RSK2 in OBLs, which is critical for ATF4 activity as well as bone formation (56). Furthermore, PTH — via its receptor, PTH1R, which is expressed in OBLs — upregulates *Atf4* gene expression and activity, which is required for this hormone to induce *osteocalcin* gene expression as well as bone formation (41, 53). PKA phosphorylation of ATF4 at its Ser254 residue mediates β-adrenergic induction of *Rankl* mRNA expression in OBLs (42). Additionally, ATF4 increases OBL function and bone

formation through interactions with the OBL-specific transcription factor Runx2 (57–60). In contrast, in OCLs, ATF4 is regulated by M-CSF and the PI3K/AKT pathway, mediates M-CSF induction of RANK, and facilitates RANKL induction of MAPKs and expression of NFATc1. In contrast to the effects of M-CSF and PI3K/AKT on ATF4 protein levels in BMMs and OCLs, both RSK2 and PKA do not affect the ATF4 protein level in OBLs (42, 56). Furthermore, ATF4[Ser219] and ATF4[Ser224] phosphorylation is involved in binding to βTrCP ubiquitin ligase, thus increasing proteolytic degradation in HeLa cells (61, 62), whereas the activation of AKT in BMMs enhances ATF4 stability. This suggests that ATF4 is modulated by differential phosphorylations in OBLs and OCLs and/or that M-CSF–PI3K/AKT signaling regulates a protein that modulates ATF4 protein stability in BMMs/OCLs. Therefore, it should be possible to design therapeutic agents that selectively inhibit ATF4 in OCLs.

The results of the present study establish a direct and important role for ATF4 in regulating multiple steps in OCL differentiation and suggest that manipulation of ATF4 in OCLs may be a strategy for increasing bone mass in diseased states.

Methods

Reagents. Tissue culture media and FBS were obtained from Thermo Scientific HyClone. LY294002, SB209580, U0126, H89, FSK, GF109203X, and DMSO were purchased from Sigma-Aldrich. Calf intestinal phosphatase was purchased from Promega. All other chemicals were of analytical grade.

Atf4-deficient and Trap-Atf4-tg mice. Breeding pairs of *Atf4*-heterozygous mice (Swiss black), as described previously (40, 53), were used to generate WT *Atf4*^{+/+}, heterozygous *Atf4*^{+/-}, and homozygous mutant *Atf4*^{-/-} mice for this study. 4- to 8-week-old mice were sacrificed for BMMs. Mice selectively expressing ATF4 in OCLs were developed at the Transgenic & Chimeric Mouse Facility of the University of Pittsburgh using an 1,846-bp mouse *Trap* promoter, provided by S. Reddy (Medical University of South Carolina, Charleston, South Carolina, USA; ref. 63). We identified 17 positive animals by PCR of tail DNA using a 5′ primer in the *Atf4* cDNA sequence (5′-ATGACCCACCTGGAGTTAGTTTGACA-3′) and a 3′ primer in the *hGH-PoyA* sequence (5′-GCACTGGGGAGGGGTCACA-3′). Expression of *Atf4* transgene was measured by Western blot analysis using ATF4 antibody. 5 founders (animal no. 2330, 2333, 2358, 2359, and 2360) were found to express *Atf4* transgene at different levels. These transgenic animals were in C57BL/6 background. All research protocols were approved by the Institutional Animal Care and Use Committee of the VA Pittsburgh Healthcare System, where this study was conducted.

In vitro OCL assays and serum CTX assay. Nonadherent BMMs were isolated from total bone marrow cells cultured on tissue culture dishes for 48 hours. CD11b^{+} or CD11c^{+} cells were isolated from BMMs using the CD11b or CD11c microbeads and the LS columns according to the manufacturer's instructions (Miltenyi Biotec Inc). For differentiation, cells were first cultured in proliferation medium (α-MEM containing 10% FBS and 10 ng/ml human recombinant M-CSF) for 3 days, then switched to differentiation medium (proliferation medium plus 50 ng/ml human recombinant RANKL) for 4–9 days. The TRAP[+] MNCs were scored using an inverted microscope. For Pit assay, BMMs (5×10^5 cells/well) were seeded on dentin slices in 24-well plates in proliferation medium for 3 days and switched to differentiation medium for 9 days. Bone resorption pits were stained with hematoxylin solution. Pit area versus total bone area and pit area versus TRAP[+] MNC area of each dentin slice were measured using Image Pro Plus 6.2 software (Media Cybernetics Inc). Coculture experiments were performed as previously described (64). Briefly, primary calvarial OBLs (3.2×10^4 cells/well) were seeded in 24-well plates and cultured in α-MEM containing 10% FBS and 50 μg/ml ascorbic acid. BMMs (4×10^5 cells/well) were seeded on top of the OBLs. The medium was

supplemented with 10 ng/ml M-CSF and 10^{-8} M 1,25 dihydroxyvitamin D$_3$. OCLs were identified by TRAP staining and counted. Serum levels of CTX, degradation products from type I collagen during osteoclastic bone resorption, were measured using the RatLaps EIA Kit according to the manufacturer's instruction (Immunodiagnostic Systems Limited).

Histological evaluation, bone histomorphometry, and IHC. WT and *Atf4*$^{-/-}$ mice were euthanized, and tibiae were fixed in 10% formalin at 4°C for 24 hours, decalcified in 10% EDTA (pH 7.4) for 10–14 days, and embedded in paraffin. Sections of tibiae from WT and *Atf4*$^{-/-}$ mice were used for TRAP staining as described previously (65). Bone histomorphometry, such as Oc.S/BS and Oc.Nb/BPm, in both primary and secondary spongiosa of tibiae was measured using Image Pro Plus 6.2 software (Media Cybernetics Inc.) as previously described (43, 66). Cells cultured in 8-well culture chambers (Nalgene Nunc), or 5-μm sections of tibiae, were subjected to IHC staining with antibodies against ATF4, NFATc1, or RANK (Santa Cruz Biotechnology) using the EnVision⁺System-HRP (DAB) kit (Dako North America Inc.) as described previously (41). Fixed nondemineralized femurs were used for μCT analysis at the Center for Bone Biology using VIVACT40 (SCANCO Medical AG), as previously described (41).

Cell proliferation and TUNEL staining. BrdU staining was used to measure cell proliferation as previously described (40, 41). Cell survival was evaluated using the ApopTag Peroxidase In Situ Apoptosis Detection Kit according to the manufacturer's instruction (Millipore).

Quantitative RT-PCR. RNA isolation and RT were previously described (53). Quantitative real-time RT-PCR analysis was performed to measure relative mRNA levels using SYBR Green kit (Bio-Rad Laboratories Inc.). Samples were normalized to *Gapdh* expression. The DNA sequences of mouse primers used for real-time PCR are summarized in Supplemental Table 1.

Western blot analysis. Western blot analysis was performed as previously described (53, 58). Antibodies used were as follows: antibodies against NFATc1, c-Fos, TRAF6, RANK, and CSFR1 and anti-rabbit or anti-mouse antibodies conjugated with horseradish peroxidase from Santa Cruz Biotechnology Inc.; antibodies recognizing phosphorylated and total ERK1/2, p38 MAPK, JNK, AKT, Src, IκBα, and PU.1 from Cell Signaling Technology Inc.; and mouse monoclonal antibody against β-actin from Sigma-Aldrich.

DNA constructs, transfection, adenovirus, and retrovirus. pCMV/β-gal, pCMV/ATF4, and pCMV/Runx2 were described previously (41, 57, 58, 67). *NFATc1*-luc, containing a mouse *Nfatc1* promoter element (–847/+66) driving a firefly luciferase reporter gene, was constructed in the project laboratory by PCR subcloning promoter fragment using mouse tail DNA as a template into pGL3-luc vector (Promega). Mutant *Nfatc1*-luc, which contains a 4-bp substitution mutation in the AP1 binding site located at –644/–637 (from TGACTTCA to TGCGAACA), was generated from WT *Nfatc1*-luc (–847/+66) by PCR amplification using a QuickChange XL Site-Directed Mutagenesis Kit (Stratagene) with the following primers: forward, 5′-GGGAAGCCTGC-GATTTTACATAATGCGAACAGCATGCAAGGCGTCTCGGCACCC-3′; reverse, 5′-GGGTGCCGAGACGCCTTGCATGCTGTTCGCATTATGTA-AAATCGCAGGCTTCCC-3′. Sequence accuracy was confirmed by automatic DNA sequencing. *Runx2*-luc was provided by P. Ducy (Columbia University, New York, New York, USA; ref. 68). For all transfection experiments, the amount of plasmid DNAs (0.125 μg reporter plasmid, 1.0 ng normalization

plasmid pRL-SV4, and 0.5–1.5 μg expression plasmid) was balanced as necessary with β-gal expression plasmid such that the total DNA was constant in each group. Experiments were performed in triplicate and repeated 3–4 times. Adenoviruses expressing ATF4 and β-gal were described previously (57). Retrovirus expressing caNFATc1 and its control empty retrovirus were described previously (38). The amount of adenovirus or retrovirus was balanced as necessary with a control adenovirus expressing β-gal or an empty retrovirus such that the total amount was constant in each group.

ChIP. ChIP assays were performed as described previously (41, 58). The equivalent of 10 μg DNA was used as starting material (input) in each ChIP reaction with 2 μg of the appropriate antibody (ATF4, c-Fos, or NFATc1). Fractions of the purified ChIP DNA (5%) or inputs (0.02%–0.05%) were used for PCR analysis. The reaction was performed with AmpliTaq Gold DNA Polymerase (Applied Biosystems) for 35 cycles of 60 seconds at 95°C, 90 seconds at 58°C, and 120 seconds at 68°C. A PCR primer pair (P1, CCGGGAC-GCCCATGCAATCGTTAGTAATT; P2, GCGGGTGCCCTGAGAAAGC-TACTCTCCCTT) was generated to detect DNA segments located near the AP-1–binding site at –644/–637 and 2 NFATc1-binding sites at –689/–684 (TTTTCC) and –680/–676 (TTTTCC), respectively, in mouse *Nfatc1* proximal promoter (33). The PCR products were separated on 3% agarose gels and visualized with ultraviolet light. All ChIP assays were repeated at least 3 times.

Flow cytometry. Cell surface fluorescence was determined using FITC-conjugated CD3, bio-strep-PB– or APC-conjugated CD11b, Pecy5-conjugated c-kit (i.e., CD117), PE-conjugated CD45R, APC-conjugated CD115, and FITC-conjugated CD11c with appropriate isotype controls (eBioscience Inc.). For flow cytometry samples, erythrocytes were first removed by lysis. BMMs or splenocytes from WT and *Atf4*$^{-/-}$ mice were then stained with the appropriate antibody. Between 5,000 and 10,000 events were collected from samples using a BD FACScan (BD Biosciences), and analysis was performed using Cell Quest (BD Biosciences).

Statistics. Data were analyzed with GraphPad Prism software, version 4.0. A 1-way ANOVA analysis was used, followed by the Tukey test. Results are expressed as mean ± SD. Differences with a *P* value less than 0.05 were considered statistically significant.

Address correspondence to: Guozhi Xiao, Rm 2E-107, VA Pittsburgh Healthcare System, 151-U, Pittsburgh, Pennsylvania 15240, USA. Phone: 412.360.3036; Fax: 412.360.6960; E-mail: xiaog@upmc.edu.

1. Roodman GD. Regulation of osteoclast differentiation. *Ann N Y Acad Sci.* 2006;1068:100–109.
2. Yavropoulou MP, Yovos JG. Osteoclastogenesis - Current knowledge and future perspectives. *J Musculoskelet Neuronal Interact.* 2008;8(3):204–216.
3. Asagiri M, Takayanagi H. The molecular understanding of osteoclast differentiation. *Bone.* 2007; 40(2):251–264.
4. Kobayashi T, et al. TRAF6 is a critical factor for dendritic cell maturation and development. *Immu-*
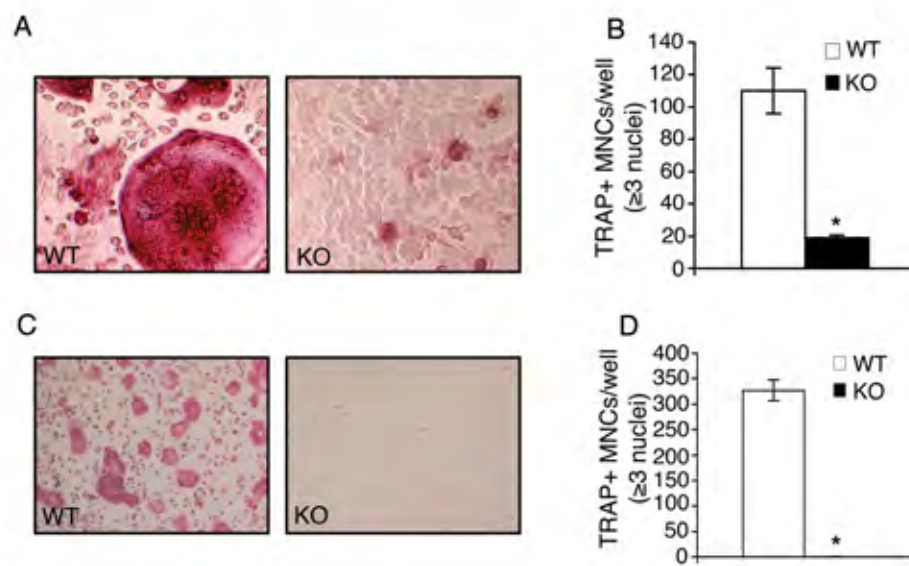*nity.* 2003;19(3):353–363.
5. Kong YY, et al. OPGL is a key regulator of osteoclastogenesis, lymphocyte development and lymph-node organogenesis. *Nature.* 1999;397(6717):315–323.
6. Kim N, Odgren PR, Kim DK, Marks SC Jr, Choi Y. Diverse roles of the tumor necrosis factor family member TRANCE in skeletal physiology revealed by TRANCE deficiency and partial rescue by a lymphocyte-expressed TRANCE transgene. *Proc Natl Acad Sci U S A.* 2000;97(20):10905–10910.
7. Wang ZQ, Ovitt C, Grigoriadis AE, Mohle-Steinlein U, Ruther U, Wagner EF. Bone and haematopoietic defects in mice lacking c-fos. *Nature.* 1992;360(6406):741–745.
8. Johnson RS, Spiegelman BM, Papaioannou V. Pleiotropic effects of a null mutation in the c-fos proto-oncogene. *Cell.* 1992;71(4):577–586.
9. Grigoriadis AE, et al. c-Fos: a key regulator of osteoclast-macrophage lineage determination and bone remodeling. *Science.* 1994;266(5184):443–448.

10. Lee SH, et al. v-ATPase V0 subunit d2-deficient mice exhibit impaired osteoclast fusion and increased bone formation. *Nat Med*. 2006;12(12):1403–1409.

11. Ash P, Loutit JF, Townsend KM. Osteoclasts derived from haematopoietic stem cells. *Nature*. 1980;283(5748):669–670.

12. Lacey DL, et al. Osteoprotegerin ligand is a cytokine that regulates osteoclast differentiation and activation. *Cell*. 1998;93(2):165–176.

13. Yasuda H, et al. Osteoclast differentiation factor is a ligand for osteoprotegerin/osteoclastogenesis-inhibitory factor and is identical to TRANCE/RANKL. *Proc Natl Acad Sci U S A*. 1998;95(7):3597–3602.

14. Simonet WS, et al. Osteoprotegerin: a novel secreted protein involved in the regulation of bone density. *Cell*. 1997;89(2):309–319.

15. Usui M, et al. Murine and chicken chondrocytes regulate osteoclastogenesis by producing RANKL in response to BMP2. *J Bone Miner Res*. 2008; 23(3):314–325.

16. Arai F, et al. Commitment and differentiation of osteoclast precursor cells by the sequential expression of c-Fms and receptor activator of nuclear factor kappaB (RANK) receptors. *J Exp Med*. 1999; 190(12):1741–1754.

17. Chang H, Hamilton JA, Scholz GM, Masendycz P, Macaulay SL, Elsegood CL. Phosphatidylinositol-3 kinase and phospholipase C enhance CSF-1-dependent macrophage survival by controlling glucose uptake. *Cell Signal*. 2009;21(9):1361–1369.

18. Yan J, et al. Rac1 mediates the osteoclast gains-in-function induced by haploinsufficiency of Nf1. *Hum Mol Genet*. 2008;17(7):936–948.

19. Yang FC, et al. Hyperactivation of p21ras and PI3K cooperate to alter murine and human neurofibromatosis type 1-haploinsufficient osteoclast functions. *J Clin Invest*. 2006;116(11):2880–2891.

20. Takeshita S, et al. SHIP-deficient mice are severely osteoporotic due to increased numbers of hyperresorptive osteoclasts. *Nat Med*. 2002;8(9):943–949.

21. Kuorilehto T, Poyhonen M, Bloigu R, Heikkinen J, Vaananen K, Peltonen J. Decreased bone mineral density and content in neurofibromatosis type 1: lowest local values are located in the load-carrying parts of the body. *Osteoporos Int*. 2005;16(8):928–936.

22. Lammert M, et al. Decreased bone mineral density in patients with neurofibromatosis 1. *Osteoporos Int*. 2005;16(9):1161–1166.

23. Illes T, Halmai V, de Jonge T, Dubousset J. Decreased bone mineral density in neurofibromatosis-1 patients with spinal deformities. *Osteoporos Int*. 2001;12(10):823–827.

24. Kawamura N, et al. Akt1 in osteoblasts and osteoclasts controls bone remodeling. *PLoS ONE*. 2007;2(10):e1058.

25. Boyle WJ, Simonet WS, Lacey DL. Osteoclast differentiation and activation. *Nature*. 2003; 423(6937):337–342.

26. Hogan PG, Chen L, Nardone J, Rao A. Transcriptional regulation by calcium, calcineurin, and NFAT. *Genes Dev*. 2003;17(18):2205–2232.

27. Crabtree GR. Generic signals and specific outcomes: signaling through Ca2+, calcineurin, and NF-AT. *Cell*. 1999;96(5):611–614.

28. Crabtree GR, Olson EN. NFAT signaling: choreographing the social lives of cells. *Cell*. 2002;109 suppl:S67–S79.

29. Ishida N, et al. Large scale gene expression analysis of osteoclastogenesis in vitro and elucidation of NFAT2 as a key regulator. *J Biol Chem*. 2002; 277(43):41147–41156.

30. Shinohara M, Takayanagi H. Novel osteoclast signaling mechanisms. *Curr Osteoporos Rep*. 2007; 5(2):67–72.

31. de la Pompa JL, et al. Role of the NF-ATc transcription factor in morphogenesis of cardiac valves and septum. *Nature*. 1998;392(6672):182–186.

32. Ranger AM, et al. The transcription factor NF-ATc is essential for cardiac valve formation. *Nature*. 1998;392(6672):186–190.

33. Asagiri M, et al. Autoamplification of NFATc1 expression determines its essential role in bone homeostasis. *J Exp Med*. 2005;202(9):1261–1269.

34. Ikeda F, Nishimura R, Matsubara T, Hata K, Reddy SV, Yoneda T. Activation of NFAT signal in vivo leads to osteopenia associated with increased osteoclastogenesis and bone-resorbing activity. *J Immunol*. 2006;177(4):2384–2390.

35. Takayanagi H, et al. Induction and activation of the transcription factor NFATc1 (NFAT2) integrate RANKL signaling in terminal differentiation of osteoclasts. *Dev Cell*. 2002;3(6):889–901.

36. Hirotani H, Tuohy NA, Woo JT, Stern PH, Clipstone NA. The calcineurin/nuclear factor of activated T cells signaling pathway regulates osteoclastogenesis in RAW264.7 cells. *J Biol Chem*. 2004; 279(14):13984–13992.

37. Yamashita T, et al. NF-kappaB p50 and p52 regulate receptor activator of NF-kappaB ligand (RANKL) and tumor necrosis factor-induced osteoclast precursor differentiation by activating c-Fos and NFATc1. *J Biol Chem*. 2007;282(25):18245–18253.

38. Matsuo K, et al. Nuclear factor of activated T-cells (NFAT) rescues osteoclastogenesis in precursors lacking c-Fos. *J Biol Chem*. 2004;279(25):26475–26480.

39. Yang X, Karsenty G. ATF4, the osteoblast accumulation of which is determined post-translationally, can induce osteoblast-specific gene expression in non-osteoblastic cells. *J Biol Chem*. 2004; 279(45):47109–47114.

40. Zhang X, et al. Activating transcription factor 4 is critical for proliferation and survival in primary bone marrow stromal cells and calvarial osteoblasts. *J Cell Biochem*. 2008;105(3):885–895.

41. Yu S, et al. Critical role of activating transcription factor 4 in the anabolic actions of parathyroid hormone in bone. *PLoS One*. 2009;4(10):e7583.

42. Elefteriou F, et al. Leptin regulation of bone resorption by the sympathetic nervous system and CART. *Nature*. 2005;434(7032):514–520.

43. Elefteriou F, et al. ATF4 mediation of NF1 functions in osteoblast reveals a nutritional basis for congenital skeletal dysplasiae. *Cell Metab*. 2006; 4(6):441–451.

44. Menaa C, Kurihara N, Roodman GD. CFU-GM-derived cells form osteoclasts at a very high efficiency. *Biochem Biophys Res Commun*. 2000;267(3):943–946.

45. Ikeda F, et al. Critical roles of c-Jun signaling in regulation of NFAT family and RANKL-regulated osteoclast differentiation. *J Clin Invest*. 2004; 114(4):475–484.

46. Hentunen TA, et al. Immortalization of osteoclast precursors by targeting Bcl-XL and Simian virus 40 large T antigen to the osteoclast lineage in transgenic mice. *J Clin Invest*. 1998;102(1):88–97.

47. Kurihara N, et al. Mutation of the sequestosome 1 (p62) gene increases osteoclastogenesis but does not induce Paget disease. *J Clin Invest*. 2007; 117(1):133–142.

48. Wong BR, et al. TRANCE, a TNF family member, activates Akt/PKB through a signaling complex involving TRAF6 and c-Src. *Mol Cell*. 1999; 4(6):1041–1049.

49. Lomaga MA, et al. TRAF6 deficiency results in osteopetrosis and defective interleukin-1, CD40, and LPS signaling. *Genes Dev*. 1999;13(8):1015–1024.

50. Porter CM, Clipstone NA. Sustained NFAT signaling promotes a Th1-like pattern of gene expression in primary murine CD4+ T cells. *J Immunol*. 2002; 168(10):4936–4945.

51. Jiang D, Franceschi RT, Boules H, Xiao G. Parathyroid hormone induction of the osteocalcin gene: requirement for an osteoblast-specific element 1 sequence in the promoter and involvement of multiple signaling pathways. *J Biol Chem*. 2004;279(7):5329–5337.

52. Xiao G, Jiang D, Gopalakrishnan R, Franceschi RT. Fibroblast growth factor 2 induction of the osteocalcin gene requires MAPK activity and phosphorylation of the osteoblast transcription factor, Cbfa1/Runx2. *J Biol Chem*. 2002; 277(39):36181–36187.

53. Yu S, et al. Parathyroid hormone increases activating transcription factor 4 expression and activity in osteoblasts: requirement for osteocalcin gene expression. *Endocrinology*. 2008;149(4):1960–1968.

54. Selvamurugan N, Pulumati MR, Tyson DR, Partridge NC. Parathyroid hormone regulation of the rat collagenase-3 promoter by protein kinase A-dependent transactivation of core binding factor alpha1. *J Biol Chem*. 2000;275(7):5037–5042.

55. Jacquin C, Gran DE, Lee SK, Lorenzo JA, Aguila HL. Identification of multiple osteoclast precursor populations in murine bone marrow. *J Bone Miner Res*. 2006;21(1):67–77.

56. Yang X, et al. ATF4 Is a Substrate of RSK2 and an Essential Regulator of Osteoblast Biology; Implication for Coffin-Lowry Syndrome. *Cell*. 2004; 117(3):387–398.

57. Xiao G, et al. Cooperative Interactions between Activating Transcription Factor 4 and Runx2/Cbfa1 Stimulate Osteoblast-specific Osteocalcin Gene Expression. *J Biol Chem*. 2005;280(35):30689–30696.

58. Yu S, et al. General transcription factor IIA-gamma increases osteoblast-specific osteocalcin gene expression via activating transcription factor 4 and runt-related transcription factor 2. *J Biol Chem*. 2008; 283(9):5542–5553.

59. Dobreva G, et al. SATB2 is a multifunctional determinant of craniofacial patterning and osteoblast differentiation. *Cell*. 2006;125(5):971–986.

60. Tominaga H, et al. CCAAT/enhancer-binding protein {beta} promotes osteoblast differentiation by enhancing Runx2 activity with ATF4. *Mol Biol Cell*. 2008;19(12):5373–5386.

61. Lassot I, et al. ATF4 degradation relies on a phosphorylation-dependent interaction with the SCF(betaTrCP) ubiquitin ligase. *Mol Cell Biol*. 2001; 21(6):2192–2202.

62. Pons J, Evrard-Todeschi N, Bertho G, Gharbi-Benarous J, Benarous R, Girault JP. Phosphorylation-dependent structure of ATF4 peptides derived from a human ATF4 protein, a member of the family of transcription factors. *Peptides*. 2007;28(12):2253–2267.

63. Reddy SV, Kuzhandaivelu N, Acosta LG, Roodman GD. Characterization of the 5'-flanking region of the human tartrate-resistant acid phosphatase (TRAP) gene. *Bone*. 1995;16(5):587–593.

64. Mak KK, et al. Hedgehog signaling in mature osteoblasts regulates bone formation and resorption by controlling PTHrP and RANKL expression. *Dev Cell*. 2008;14(5):674–688.

65. Liu B, Yu SF, Li TJ. Multinucleated giant cells in various forms of giant cell containing lesions of the jaws express features of osteoclasts. *J Oral Pathol Med*. 2003;32(6):367–375.

66. Parfitt AM, et al. Bone histomorphometry: standardization of nomenclature, symbols, and units. Report of the ASBMR Histomorphometry Nomenclature Committee. *J Bone Miner Res*. 1987;2(6):595–610.

67. Singha UK, et al. Rapamycin inhibits osteoblast proliferation and differentiation in MC3T3-E1 cells and primary mouse bone marrow stromal cells. *J Cell Biochem*. 2008;103(2):434–446.

68. Zambotti A, Makhluf H, Shen J, Ducy P. Characterization of an osteoblast-specific enhancer element in the CBFA1 gene. *J Biol Chem*. 2002; 277(44):41497–41506.

A

WT   KO

B

TRAP+ MNCs/well (≥3 nuclei)
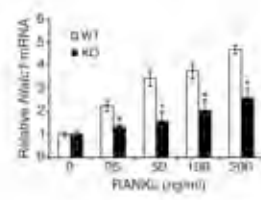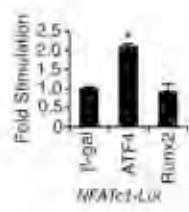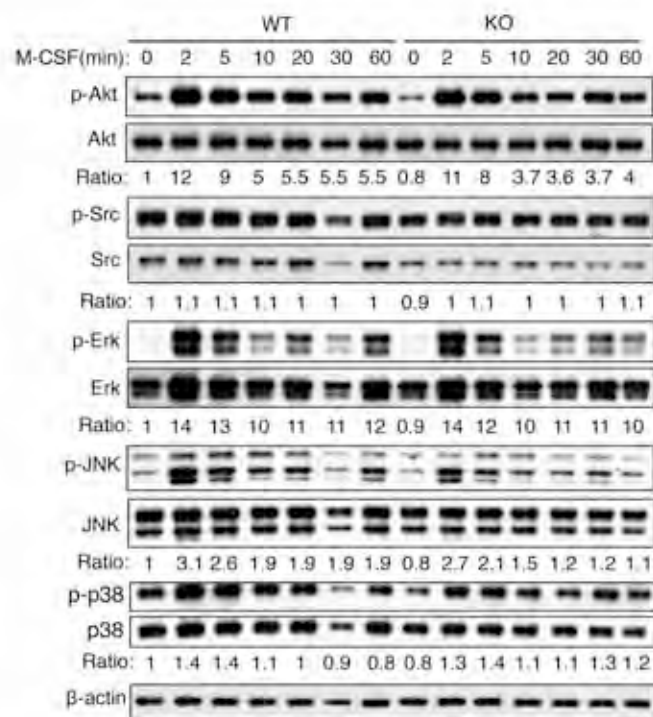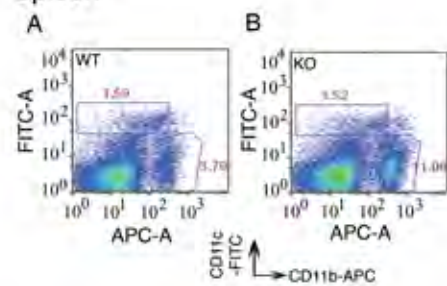
□ WT
■ KO

*

C

WT   KO

D

TRAP+ MNCs/well (≥3 nuclei)

□ WT
■ KO

*

Figure S4

Spleen

Bone Marrow
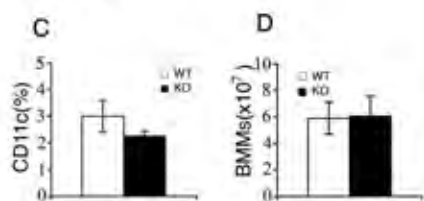
Table S1: real-time PCR primers

Name	5' primer	3' primer
Atf4	GAGCTTCCTGAACAGCGAAGTG	TGGCCACCTCCAGATAGTCATC
Cat K	AATACGTGCAGCAGAACGGAGGC	CTCGTTCCCCACAGGAATCTCTCTGTAC
c-Fms	CCTCCTCTGGTCCTGCTGCTGG	GCTCACACATCGCAGGGTCACC
Gapdh	CAGTGCCAGCCTCGTCCCGTAGA	CTGCAAATGGCAGCCCTGGTGAC
Mmp9	TGCCCTGGAACTCACACGACATCTTC	TGCCCTGGAACTCACACGACATCTTC
Nfatc1	CCCCATCCGCCAGGCTACA	GGTTGTCTGCACTGAGCCAACTCC
PU.1	CTCCAGGTGTACCCCCCAGAGG	CTCCAGGGCGGGGCTGTC
Rank	AGAGGGGAGCCTCAGGGTCC	AAGTTCATCACCTGCCCGCTAGA
Trap	CACTCCCACCCTGAGATTTGTG	ACGGTTCTGGCGATCTCTTTG

Legends for Supplementary Figures:

Fig. S1. ATF4 is expressed in OCL-like cells. Mouse MC-4 preosteoblastic cells, rat UMR106-01 osteoblastic cells, primary mouse bone marrow stromal cells (BMSCs), RAW264.7 cells (a mouse monocyte/macrophage cell line), and primary mouse bone marrow-derived monocytes (BMMs) were cultured in 10%FBS media for 24 h. Whole cell extracts were used for Western blot analysis for ATF4.

Fig. S2. TRAP staining in CD11b$^+$ BMMs and BMMs from aged mice. (A) TRAP staining. Purified CD11b$^+$ BMMs from 4-week-old wt and *Atf4$^{-/-}$* mice were differentiated for 5d followed by TRAP staining and TRAP-positive multinucleated cells (MNCs) were scored. (**B**) Statistical analysis of TRAP staining in (A). Magnification: 100X. **(C**) TRAP staining. Primary BMMs from 15-month-old wt and *Atf4$^{-/-}$* mice were differentiated for 5d followed by TRAP staining. (**D**) Statistical analysis of TRAP staining in (C). Magnification: 40X.

Fig. S3. RANKL induction of *Nfatc1* mRNA expression in wt and *Atf4$^{-/-}$* BMMs (dose-response). Wt and *Atf4$^{-/-}$* BMMs were treated with indicated concentrations of RANKL (25-200 ng/ml) for 7d followed by quantitative real-time RT/PCR for *Nfatc1* mRNA. *Gapdh* mRNA was used for loading. *$P<0.01$ wt vs. *Atf4$^{-/-}$*).

Fig. S4. ATF4 but not Runx2 activates the *Nfatc1 P1* promoter. COS-7 cells were

transfected with 0.125 µg 0.8-kb *Nfatc1*-luc and 1.0 ng pRL-SV40 with 1.0 µg

expression plasmid for ATF4 or Runx2. *P<0.01 (β-gal vs. ATF4).

Figure S5. Effects of M-CSF on activation of the AKT, Src, and MAPKs pathways

in wt and *Atf4^-/-* BMMs. Wt and *Atf4^-/-* BMMs were cultured in proliferation medium for 3

d and switched to 2% FBS α-MEM without M-CSF overnight. Cells were then exposed

to 30 ng/ml M-CSF for the indicated times. Cells were then lysed, fractionated by

SDS–PAGE, and analyzed by Western blot analysis using antibodies recognizing

phosphorylated and total ERK1/2, p38, JNK, AKT, and Src. β-actin served as the

loading control. Similar results were obtained from three independent experiments.

Fig. S6. *Atf4^-/-* mice display an increase in macrophage. (**A-B**) Flow cytometry.

Splenocytes from wt and *Atf4^-/-* mice were stained with CD11b-APC and CD11c-FITC

antibodies and analyzed with flow cytometry as described in Experimental Procedures.

(**C**) CD11c^+ cells were purified and counted from wt and *Atf4^-/-* BMMs as described in

Experimental Procedures. (**D**) Total nucleated bone marrow cells were counted from

long bones (two femurs and two tibias) from 6-week-old wt and *Atf4^-/-* mice (6 mice per

group).

ATF4 Is Required for the Anabolic Actions of PTH on Bone in vivo

S. Yu[1], M. Luo[1], R. T. Franceschi[2, 3], D. Jiang[2], J. Zhang[1], K. Patrene[1], K. Hankenson[4], G. D. Roodman[1], G. Xiao[1]. [1]Division of Hematology/Oncology, Department of Medicine, University of Pittsburgh, Pittsburgh, PA 15240, [2]Department of Periodontics and Oral Medicine, University of Michigan School of Dentistry, Ann Arbor, MI 48109, [3]Department of Biological Chemistry, University of Michigan School of Medicine, Ann Arbor, MI 48109, [4]Department of Animal Biology, School of Veterinary Medicine, University of Pennsylvania, Philadelphia, PA 19104-6010,

Parathyroid hormone (PTH) is a potent stimulator of bone formation and a proven anabolic agent for the treatment of osteoporosis. However, the mechanism whereby PTH increases bone formation remains poorly understood. Activating transcription factor 4 (ATF4) is a critical factor for bone formation during development and throughout postnatal life. This study examined if ATF4 is required for the anabolic actions of PTH on bone using an $Atf4^{-/-}$ mouse model. Five-day-old w*t* and $Atf4^{-/-}$ mice were given daily subcutaneous injections of vehicle (saline) or hPTH(1-34) (0.04 µg/g body weight) for 28 days. In *wt* mice, µCT analyses of femurs show that this PTH regimen significantly increased bone volume/tissue volume (BV/TV, 4.3-fold), trabecular thickness (Tb.Th, 50%), trabecualr numbers (Tb.N, 1.5-fold), cortical thickness (Cort.Th, 77%), and cross sectional area (CSA, 24%) and decreased trabecular spacing (Tb.Sp, 1.7-fold). These PTH effects were dramatically reduced or completely abolished in the absence of ATF4. Histological analyses show that PTH displayed potent anabolic effects on tibiae, vertebrae, and calvariae, which were significantly reduced in $Atf4^{-/-}$ mice. At the molecular level, PTH markedly increased levels of osteocalcin (*Ocn*) and bone sialoprotein (*Bsp*) mRNA of long bones as measured by quantitative real-time RT/PCR. This increase was completely abolished in the absence of ATF4. This study demonstrates that ATF4 is required for the anabolic actions of PTH on bone *in vivo* and also suggested that modulation of the levels and activity of ATF4 may have therapeutic significance for the treatment of metabolic bone diseases such as osteoporosis.

TFIIA, ATF4, and Runx2 Synergistically Activate Osteoblast-specific Osteocalcin Gene Expression

S. Yu[1], Y. Jiang[2], M. Luo[1], Y. Lu[1], J. Zhang[1], G. D. Roodman[1], G. Xiao[1,] [1]Division of Hematology/Oncology, Department of Medicine, University of Pittsburgh, Pittsburgh, PA 15240, [2]Department of Pharmacology, University of Pittsburgh, Pittsburgh, PA 15240

Runx2, a member of the runt homology domain family of transcription factors, is a master regulator of osteoblast function and bone formation. Mice lacking Runx2 have no mineralized skeleton due to a complete lack of mature osteoblasts. The expression level of Runx2 protein is regulated by a number of factors including BMPs, FGF-2, IGF-1, TNF-α, TGF-β, and PTH, all of which play important roles in osteoblasts and bone both *in vitro* and *in vivo*. In addition, the activity of Runx2 protein is positively or negatively modulated through protein-protein interactions. Activating transcription factor 4 (ATF4) is an osteoblast-enriched factor which regulates the terminal differentiation and function of osteoblasts. ATF4 knock-out mice have reduced bone mass and bone mineral density (severe osteoporosis) throughout their life. To identify proteins interacting with Runx2, we used a yeast two-hybrid system and identified TFIIA, a general transcriptional factor, as a Runx2-interacting factor. While pull-down assays confirmed that TFIIA physically interacted with Runx2 when both factors were coexpressed in COS-7 cells, surprisingly, it did not activate or inhibit Runx2-dependent transcriptional activity. In contrast, TFIIA unexpectedly activated ATF4, which we recently identified as a Runx2-interacting protein, in a dose-dependent manner. Deletion analysis found that this activation required the presence of the C-terminal 15 amino acid residues of ATF4 molecule. Finally, TFIIA, ATF4, and Runx2 synergistically stimulated the 0.657-kb mOG2 (mouse osteocalcin gene 2) promoter activity and endogenous osteocalcin mRNA expression. In summary, this study demonstrates a novel mechanism through which bone-specific transcription factors and general transcription factors cooperate in regulating osteoblast-specific gene expression.

Role of ATF4 in Osteoblast Proliferation and Survival

X. Zhang[1,3], S. Yu[1], D.L. Galson, M. Luo[1], J. Fan[2], J. Zhang[1], G. Guan[3], G. Xiao[1]. Department of Medicine[1], and Surgery[2], University of Pittsburgh, Pittsburgh, PA 15240, [3]Department of Physiology and Pathophysiology, Peking (Beijing) University Health Science Center, Beijing 100083, China

ATF4 (activating transcription factor 4) is essential for bone formation. However, the mechanism of its actions in bone is poorly understood. The present study examined the role for ATF4 in the regulation of proliferation and survival of primary mouse bone marrow stromal cells (BMSCs) and osteoblasts. Results showed that $Atf4^{-/-}$ cells display a severe proliferative defect as measured by multiple cell proliferation assays. Cell cycle progression of $Atf4^{-/-}$ BMSCs was largely delayed with a significant G1 arrest. Expression of cyclins A1, D1, and D3 was dramatically decreased both at the mRNA and protein level. A similar proliferation defect was observed in $Atf4^{-/-}$ calvarial periosteal osteoblasts in vivo. Knocking down $Atf4$ mRNA by small interfering RNA in MC3T3-E1 subclone 4 preosteoblasts markedly reduced expression of the cyclins and cell proliferation. In contrast, overexpression of ATF4 increased cyclin D1 expression as well as cell proliferation. In addition, apoptosis was significantly increased in cultured $Atf4^{-/-}$ BMSCs and calvarial periosteal osteoblasts in vivo relative to wt controls. Taken together, this study demonstrates that ATF4 is a critical regulator of proliferation and survival in primary BMSCs and osteoblasts.

Activating Transcription Factor 4 Mediates the Anabolic Actions of Parathyroid Hormone in Bone S. Yu[1], R.T. Franceschi[4,5], M. Luo[1], J. Fan[2], D. Jiang[4], H. Cao[1], Y. Lai[3], J. Zhang[1], K. Patrene[1], K. Hankenson[6], G. D. Roodman[1], G. Xiao[1].

Department of Medicine[1], Surgery[2], and Pharmacology and Chemical Biology[3], University of Pittsburgh, Pittsburgh, PA 15240; [4]Department of Periodontics and Oral Medicine, School of Dentistry, [5]Department of Biological Chemistry, School of Medicine, University of Michigan, Ann Arbor, MI 48109; [6]Department of Animal Biology, School of Veterinary Medicine, University of Pennsylvania, Philadelphia, PA 19104-6010.

Parathyroid hormone (PTH) is a potent anabolic agent for the treatment of osteoporosis. However, its mechanism of action in osteoblast and bone is not completely understood. In this study, we show that the anabolic actions of PTH in bone are severely impaired in both growing and adult ovariectomized mice lacking bone-related activating transcription factor 4 (ATF4). Our study demonstrates that inactivation of the *Atf4* gene in mice i) suppresses PTH-stimulated osteoblast proliferation and survival; and ii) abolishes PTH-induced osteoblast differentiation, which, together, compromise the anabolic response. We further demonstrate that intermittent PTH increases osteoblast differentiation in vivo at least in part through an ATF4-dependent up-regulation of Osterix (Osx). ATF4 stimulates Osx expression by activating Osx gene transcription. PTH activates Osx transcription through an ATF4 responsive element in the proximal promoter. ATF4 binds to an endogenous Osx promoter in a PTH-dependent manner. Taken together these experiments establish a novel role for ATF4 in the regulation of the anabolic response of osteoblast and bone to PTH.

CRITICAL ROLE OF ACTIVATING TRANSCRIPTION FACTOR 4 IN PARATHYROID HORMONE-MEDIATED BONE FORMATION

Guozhi Xiao

University of Pittsburgh Medical Center

Background and Objectives: Parathyroid hormone (PTH) is a potent stimulator of bone formation and a proven anabolic agent for the treatment of osteoporosis. However, the mechanism whereby PTH increases bone formation remains poorly understood. The objective of this study was to test our hypothesis that activating transcription factor 4 (ATF4) mediates the anabolic response of skeleton to intermittent PTH.

Materials and Methods: Five-day-old wt and Atf4-/- mice were given daily subcutaneous injections of vehicle (saline) or hPTH(1–34) (60 ng/g body weight) for 28 days. Mice were euthanized 24 hours after the last injection. The effects of this PTH-dosing regimen on long bones (femurs and tibiae), vertebrae, and calvariae were determined by both biochemical and histomorphometric criteria.

Results: Quantitative uCT analysis of femurs showed that Atf4-/- mice had a significant reduction in bone volume/tissue volume (BV/TV), trabecular number (Tb.N), and cortical thickness (Cort.Th) and a marked increase in trabecular space (Tb.Sp) compared with the wt or Atf4+/- littermates. In wt femurs, intermittent PTH increased BV/TV, Tb.N, and trabecular thickness (Tb.Th) by 4.4-fold, 1.7-fold, and 50%, respectively, and decreased Tb.Sp by 1.5-fold. PTH-stimulated bone formation were dramatically reduced (BV/TV, Tb.N, Tb.Sp) or completely abolished (Cort.Th and Tb.Th) in Atf4-/- mice relative to wt mice. Histological analyses show that PTH displayed potent anabolic effects on tibiae, vertebrae, and calvariae, which were markedly reduced in Atf4-/- mice. ATF4 deficiency resulted in a drastic reduction in osteoprogenitors in bone marrow, which impairs the anabolic response of skeleton to PTH. This is probably related to the ability of ATF4 to promote proliferation of osteoblasts/osteoprogenitors as well as survival of osteoblasts and osteocytes, two critical steps for intermittent PTH to increase bone formation. In addition, ATF4 is required for PTH stimulation of osteoblast differentiation.

Conclusion and Impact: This study demonstrates that ATF4 is required for the anabolic actions of PTH in bone and suggests that modulation of the levels and activity of ATF4 may have therapeutic significance for the treatment of metabolic bone diseases such as osteoporosis.

Abstract Center

Abstracts   Sponsorship

My Abstracts > **Abstract Submission** > Step 6. Preview
Title: Critical Role of ATF4 in Regulating Osteoclast Differentiation and Bone Resorption ID: A11005902

Preview

Verify the information entered in this abstract.

Critical Role of ATF4 in Regulating Osteoclast Differentiation and Bone Resorption

Categories

- **Option 1:** Osteoclasts
- **Option 2:** --
- **Option 3:** --
- **Poster Cluster:** Osteoclasts: Differentiation

Award Consideration(s)

- Young Investigator Award
- Young Investigator Annual Meeting Travel Grant

Abstract Body

Activating Transcription Factor 4 (ATF4) has a critical role in regulating osteoblast differentiation and bone formation. However, its direct role in osteoclasts differentiation has not been addressed yet. In order to define the role of ATF4 in osteoclasts, we deleted ATF4 expression in mice or targeted expression of ATF4 to the osteoclast lineage using the tartrate-resistant acid phosphatase (TRAP) promoter. Osteoclast differentiation was severely impaired in primary bone marrow monocyte (BMM) cultures and bones from Atf4-/- mice. Coculture with wt osteoblasts or a high concentration of receptor activator of NF-kappaB ligand (RANKL) failed to restore the osteoclast differentiation defect in Atf4-/- BMM cultures. Conversely, Trap-ATF4-tg mice display a severe osteopenia with dramatically increased osteoclastogenesis and bone resorption. We further demonstrated that ATF4 is a novel upstream activator of the critical transcription factor nuclear factor of activated T cells c1 (NFATc1) gene and is critical for RANKL activation of multiple MAPK pathways in osteoclast precursors. Further more, ATF4 is crucial for M-CSF induction of receptor activator of NF-kappaB (RANK) expression on BMMs, and lack of ATF4 caused a shift in osteoclast precursors to macrophages, thereby increasing macrophages. Finally, ATF4 is largely modulated by M-CSF signaling and the PI3K/AKT pathways in BMMs. These results for the first time demonstrate that ATF4 plays a critical direct osteoclast-intrinsic role in regulating osteoclast differentiation and suggest that it may be a therapeutic target for treating bone diseases associated with increased osteoclast activity.

Keywords

ATF4, NFATc1, RANK

Attachments

--

Authors

Name	Presenting
Huiling Cao, University of Pittsburgh School of Medicine, USA	✓
Shibing Yu, University of Pittsburgh Medical Center, USA	
Zhi Yao, Tianjin Medical University, China	

Instructions

Use this page to review your abstract. Use the drop-down box at the top to go back to a step and fix any errors.

You will **NOT** be able to change your abstract after the submission deadline.

Status

- Your abstract is ready for submittal.
- Your abstract is complete.

Deborah L. Galson, University of Pittsburgh School of Medicine, USA

Yu Jiang, University of Pittsburgh, USA

Xiaoyan Zhang, Peking Univerisity, China

Jie Fan , University of Pittsburgh, USA

Binfeng Lu, University of Pittsburgh, USA

Youfei Guan, Peking University, China

Min Luo, University of Pittsburgh, USA

Yumei Lai, University of Pittsburgh, USA

Noriyoshi Kurihara, Center for Bone Biology, University of Pittsburgh, USA

Kenneth Patrene, University of Pittsburgh, USA

G. David Roodman, VA Pittsburgh Healthcare System (646), USA

Guozhi Xiao, University of Pittsburgh School of Medicine, USA

Sponsor

Name	Response
Huiling Cao	Accepted

Scheduling Conflicts

--

Continue   Exit

Preview

Foxo1 Mediates IGF1/Insulin Regulation of Osteocalcin Expression by Antagonizing Runx2 in osteoblasts

Categories

Option 1: Osteoblasts
Option 2: --
Option 3: --
Poster Cluster: Osteoblasts: Gene Expression and Transcription Factors

Award Consideration(s)

Young Investigator Award

Abstract Body

In this study, we determined the molecular mechanisms whereby forkhead transcription factor Foxo1, a key downstream signaling molecule of insulin-like growth factor 1 (IGF1)/insulin actions, regulates Runx2 activity and expression of the mouse osteocalcin gene 2 (Bglap2) in osteoblasts in vitro. We showed that Foxo1 inhibited Runx2-dependent transcriptional activity and osteocalcin mRNA expression and Bglap2 promoter activity in MC-4 preosteoblasts. Co-immunoprecipitation assay showed that Foxo1 physically interacted with Runx2 via its C-terminal region in osteoblasts or when coexpressed in COS-7 cells. Electrophoretic mobility shift assay demonstrated that Foxo1 suppressed Runx2 binding to its cognate site within the Bglap2 promoter. IGF1 and insulin prevented Foxo1 from inhibiting Runx2 activity by promoting Foxo1 phosphorylation and nuclear exclusion. In contrast, a neutralizing anti-IGF1 antibody decreased Runx2 activity and osteocalcin expression in osteoblasts. Chromatin immunoprecipitation assay revealed that IGF1 increased Runx2 interaction with a chromatin fragment of the proximal Bglap2 promoter in a PI3K/AKTdependent manner. Conversely, knockdown of Foxo1 decreased Runx2 interaction with the promoter. This study establishes that Foxo1 is a novel negative regulator of osteoblastspecific transcription factor Runx2 and modulates IGF1/insulin-dependent regulation of osteocalcin expression in osteoblasts.

Keywords

Runx2, Foxo1, Osteoblast, IGF1/Insulin

Attachments

--

Authors

Name	Presenting
Shengyong Yang, USA	✔
Haiyan Xu, Rhode Island Hospital, Brown Medical School, USA	
Shibing Yu, University of Pittsburgh Medical Center, USA	
Huiling Cao, University of Pittsburgh School of Medicine, USA	
Jie Fan, University of Pittsburgh School of Medicine, USA	

Chunxi Ge, University of Michigan School of Dentistry, USA

Dr. Renny T. Franceschi, University of Michigan, USA

Henry Dong, Children's Hospital of Pittsburgh, University of Pittsburgh, USA

Guozhi Xiao, University of Pittsburgh School of Medicine, USA

Sponsor

Name	Response
Shengyong Yang	Accepted

Scheduling Conflicts

--

X Close Window